AD-A191 273 MULTICHANNEL 2-D POWER SPECTRAL ESTIMATION AND APPLICATIONS(U) NAVAL POSTGRADUATE SCHOOL MONTEREY CA H T EL-SHAMER DEC 87 1/4

UNCLASSIFIED F/G 12/3 NL

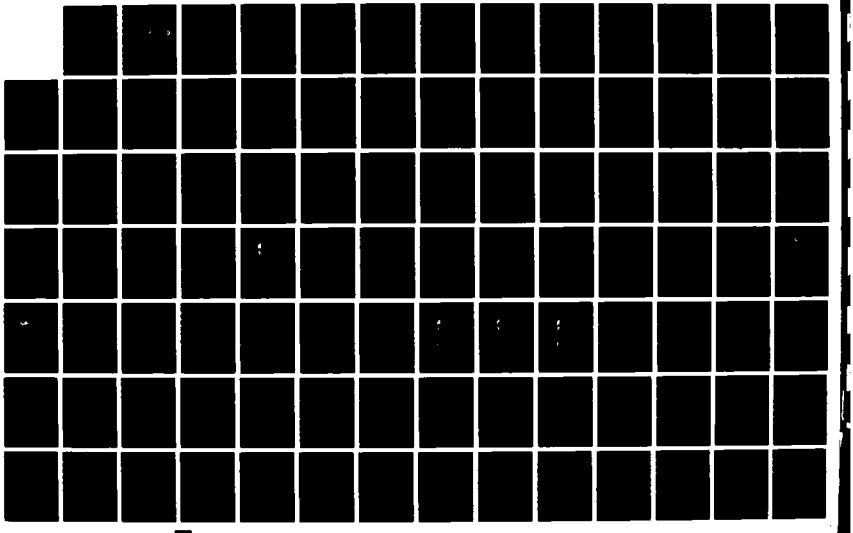

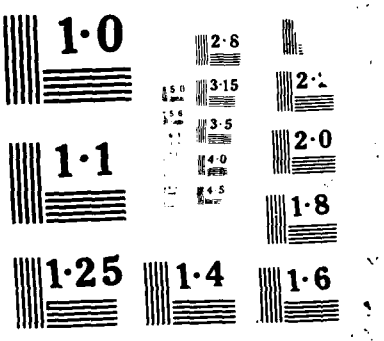
1·0
1·1
1·25
1·4
1·6
1·8
2·0
2·5
2·8
3·15
3·5
4·0
4·5
5·0
5·6

(2)

NAVAL POSTGRADUATE SCHOOL
Monterey, California

THESIS

MULTICHANNEL 2-D POWER SPECTRAL ESTIMATION AND APPLICATIONS

by

Hamdy Taha M. El-Shaer

December 1987

Dissertation Supervisor: C.W. Therrien

Approved for public release; distribution is unlimited

A191 273

SECURITY CLASSIFICATION OF THIS PAGE

REPORT DOCUMENTATION PAGE

1a REPORT SECURITY CLASSIFICATION UNCLASSIFIED	1b RESTRICTIVE MARKINGS
2a SECURITY CLASSIFICATION AUTHORITY	3 DISTRIBUTION / AVAILABILITY OF REPORT Approved for public release; distribution is unlimited
2b DECLASSIFICATION / DOWNGRADING SCHEDULE	
4 PERFORMING ORGANIZATION REPORT NUMBER(S)	5 MONITORING ORGANIZATION REPORT NUMBER(S)
6a NAME OF PERFORMING ORGANIZATION Naval Postgraduate School	6b OFFICE SYMBOL (If applicable) 62
7a NAME OF MONITORING ORGANIZATION Naval Postgraduate School	
6c ADDRESS (City, State, and ZIP Code) Monterey, California 93943-5000	7b ADDRESS (City, State, and ZIP Code) Monterey, California 93943-5000
8a NAME OF FUNDING / SPONSORING ORGANIZATION	8b OFFICE SYMBOL (If applicable)
9 PROCUREMENT INSTRUMENT IDENTIFICATION NUMBER	
8c ADDRESS (City, State, and ZIP Code)	10 SOURCE OF FUNDING NUMBERS PROGRAM ELEMENT NO / PROJECT NO / TASK NO / WORK UNIT ACCESSION NO

11 TITLE (Include Security Classification)
MULTICHANNEL 2-D POWER SPECTRAL ESTIMATION AND APPLICATIONS

12 PERSONAL AUTHOR(S)
El-Shaer, Hamdy T.M.

13a TYPE OF REPORT	13b TIME COVERED	14 DATE OF REPORT (Year Month Day)	15 PAGE COUNT
Ph.D. Dissertation	FROM ____ TO ____	1987 November	304

16 SUPPLEMENTARY NOTATION

17 COSATI CODES		
FIELD	GROUP	SUB-GROUP

18 SUBJECT TERMS (Continue on reverse if necessary and identify by block number)
Signal Modeling, Linear Prediction, Image Coding, AR Models, Maximum Likelihood Method, Spectral Estimation

19 ABSTRACT (Continue on reverse if necessary and identify by block number)

Spectral estimation for *multiple* 2-D signals by model-based methods is developed. The procedures compute the entire spectral matrix of autospectra and cross spectra for the set of 2-D signals. Spectral analysis by autoregressive (AR) modeling is studied extensively. Specific differences between AR models for this problem and those for lower dimensional problems are highlighted. An extension of the Jackson-Chien method for combining estimates with single quadrant support is proposed and a method is developed for estimating the model parameters directly from the data (i.e. without prior estimation of a correlation matrix). A measure of the similarity of two spectral estimates based on the statistical *divergence* is proposed and used to compare various spectral estimates. A comprehensive set of experimental studies are presented

20 DISTRIBUTION / AVAILABILITY OF ABSTRACT	21 ABSTRACT SECURITY CLASSIFICATION
☐ UNCLASSIFIED/UNLIMITED ☐ SAME AS RPT ☐ DTIC USERS	UNCLASSIFIED
22a NAME OF RESPONSIBLE INDIVIDUAL Prof. C.W. Therrien	22b TELEPHONE (Include Area Code) (408) 646-2032 / 22c OFFICE SYMBOL 62Ti

DD FORM 1473, 84 MAR 83 APR edition may be used until exhausted
All other editions are obsolete

SECURITY CLASSIFICATION OF THIS PAGE
UNCLASSIFIED

showing the performance of the methods in estimating the autospectra and magnitude and phase of the cross spectra. The Maximum Likelihood Method (MLM) of spectral estimation is extended to the multichannel 2-D case. The properties are compared experimentally with the autoregressive methods. The Improved Maximum Likelihood Method (IMLM) is also developed for the multichannel case. Finally applications of multichannel 2-D spectral analysis models to image coding are presented.

Approved for public release; distribution is unlimited

Multichannel 2-D Power Spectral Estimation and Applications

by

Hamdy Taha M. El-Shaer
Colonel, Egypt Army
B.S., Elec. Eng., M.T.C., Egypt, 1972
M.S., Elec. Eng., Ain Shams University, Egypt, 1980

Submitted in partial fulfillment of the
requirements for the degree of

DOCTOR OF PHILOSOPHY IN ELECTRICAL ENGINEERING

from the

NAVAL POSTGRADUATE SCHOOL
December 1987

Author: Hamdy T. El-Shaer
Hamdy Taha M. El-Shaer

Approved by:

H. Fredricksen
Professor of Mathematics

P.A.W. Lewis
Professor of Operations Research

P.H. Moose
Professor of Elec. & Comp. Eng.

L.J. Ziomek
Professor of Elec. & Comp. Eng.

C.W. Therrien
Professor of Elec. & Comp. Eng.
Dissertation Supervisor

Approved by:

John P. Powers, Chairman, Dept. of Elec. & Comp. Eng.

Approved by:

Kneale T. Marshall, Acting Academic Dean

ABSTRACT

Spectral estimation for *multiple* 2-D signals by model-based methods is developed. The procedures compute the entire spectral matrix of autospectra and cross spectra for the set of 2-D signals. Spectral analysis by autoregressive (AR) modeling is studied extensively. Specific differences between AR models for this problem and those for lower dimensional problems are highlighted. An extension of the Jackson-Chien method for combining estimates with single quadrant support is proposed and a method is developed for estimating the model parameters directly from the data (i.e. without prior estimation of a correlation matrix). A measure of the similarity of two spectral estimates based on the statistical *divergence* is proposed and used to compare various spectral estimates. A comprehensive set of experimental studies are presented showing the performance of the methods in estimating the autospectra and magnitude and phase of the cross spectra. The Maximum Likelihood Method (MLM) of spectral estimation is extended to the multichannel 2-D case. The properties are compared experimentally with the autoregressive methods. The Improved Maximum Likelihood Method (IMLM) is also developed for the multichannel case. Finally applications of multichannel 2-D spectral analysis models to image coding are presented.

TABLE OF CONTENTS

LIST OF TABLES

LIST OF FIGURES

ACKNOWLEDGEMENTS

The author wishes to express his appreciation and sincere thanks to his advisor Professor Charles W. Therrien for his supervision and valuable comments during the progress of this work. The efforts made by Professor C.W. Therrien for development and presentation of this work, his valuable discussions and guidance, also his encouragement and support at every stage of this work makes me very grateful to him.

I wish also to thank all doctoral committee members: H. Fredricksen Professor of Mathematics, P.A.W. Lewis Professor of Operations Research, P.H. Moose Professor of Electrical and Computer Engineering, and L.J. Ziomek Professor of Electrical and Computer Engineering for their valuable comments and interest in this work. I have to mention also my thanks to Mrs. Rosalie Johnson in Computer Science department for her assistance with the computer simulations and data transmission needed for the image coding work.

I thank all the members of Electrical and Computer Engineering department for their help during these years.

Finally I would like to thank Professor R.A. McGonigal, International Education Coordinator for his assistance with various aspects of my program at the Naval Postgraduate School.

Some of the figures in this thesis were computed using the APL GRAFSTAT package from the IBM Research Laboratories. This package has been made available at the Naval Postgraduate School under a test bed agreement with IBM Research. We thank Dr. P.D. Welch for his efforts in this regard.

I. INTRODUCTION

Model-based methods of spectrum estimation have received considerable attention over the last fifteen or twenty years because of their ability to provide high resolution with limited data and potentially more accurate estimates. A lot of work has been done for model-based methods of spectrum estimation of one dimensional (1-D) random processes with the development of methods such as maximum entropy, autoregressive (AR), and maximum likelihood. A review of the model-based methods of spectral analysis in the 1-D case can be found in the references (Childers,1978; Kesler,1986; Kay and Marple,1981; Nuttal,1976; Proc. of RADC Spectrum Estimation Workshop,1978; Robinson,1982; Dudgeon and Mersereau,1977; Marple,1987). Unfortunately much of the work done in 1-D spectral estimation does not extend easily to the two-dimensional (2-D) case. This is true in particular for the maximum entropy and AR spectral estimates which are identical in the 1-D case but may be significantly different in the 2-D case. Indeed, while a 2-D AR spectral estimate can be computed from *any* estimated correlation function, the corresponding maximum entropy spectral estimate may not even *exist*. McClellan (1982) gives a review of methods of multidimensional power spectrum estimation. Lang and McClellan (1982, 1983) focus attention on 2-D maximum entropy power spectrum estimation and show the specific differences between the 2-D and the 1-D case.

This thesis addresses the problem of spectrum estimation for *multiple* 2-D signals. We refer to the set of signals as a *multichannel* 2-D signal. Multichannel 2-D signals can be viewed as several planes of correlated 2-D data (see Fig. 1.1). For instance, a digital color image may be considered as a sample function of a discrete three-channel 2-D random signal consisting of three registered components representing red, green, and blue intensities. Other examples of multichannel 2-D signals can be found in array processing, in certain radar applications, and in the set of images received from a satellite multispectral scanner.

The spectrum estimation methods that will be applied to these signals compute the entire spectral matrix. That is, estimates for the 2-D autospectra and magnitude and

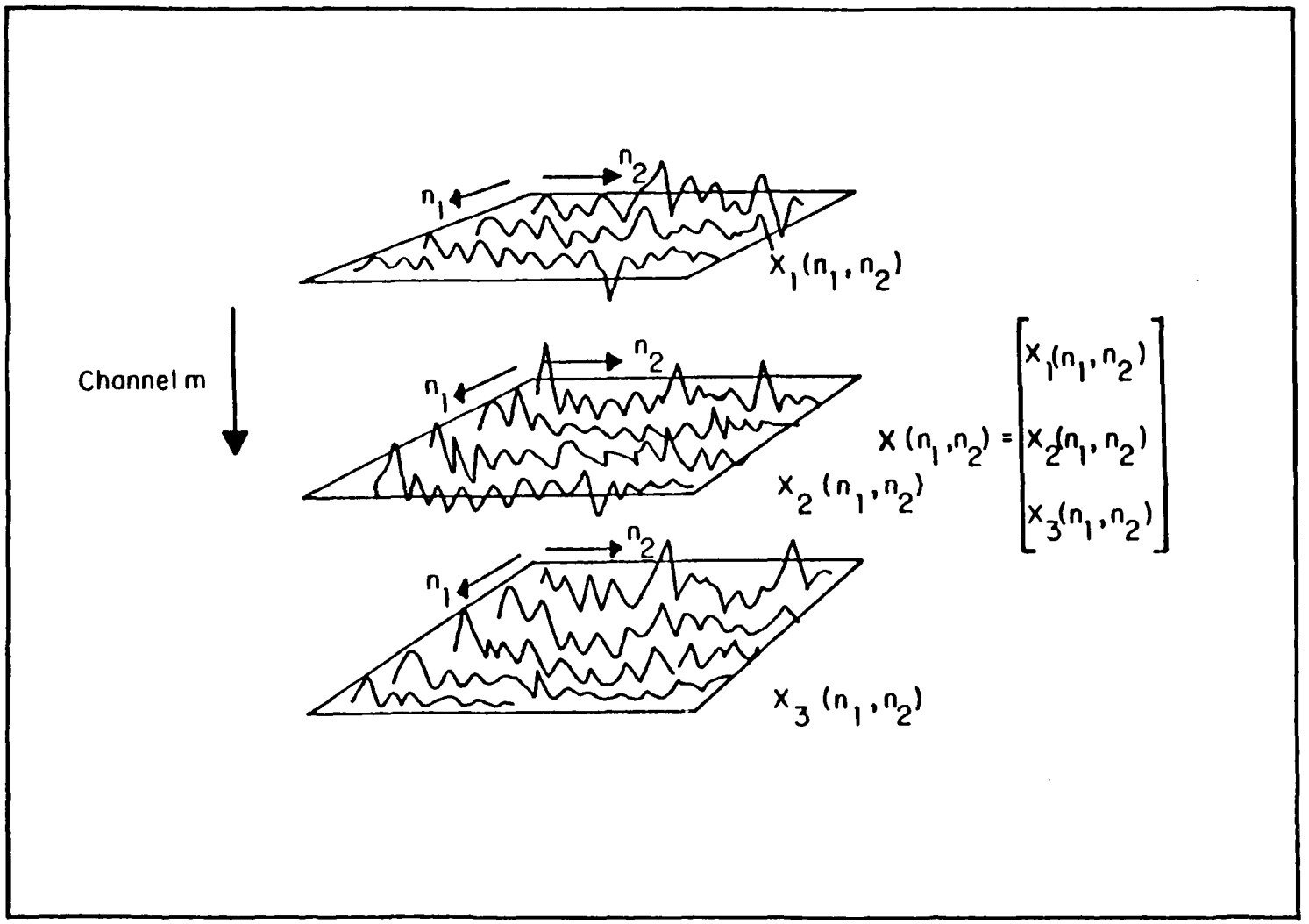

Fig. 1.1 Multichannel 2-D signal (M=3).

phase of the cross spectra are produced all at once. This thesis describes some methods of spectrum estimation that are model-based and can provide better resolution than conventional Fourier transform methods. It will be seen that the methods we describe have characteristics of both 1-D multichannel problems and 2-D single channel problems and so are considerably different from 3-D spectrum estimation procedures. The latter are almost identical to 2-D single channel problems.

In this chapter we define the problem of spectral analysis for multiple 2-D random signals and outline our approach to this problem. We give a brief description of linear prediction as it relates to spectral estimation, and an outline of some previous work in spectral estimation for single 2-D signals. We also indicate how the models we develop can be applied to other applications such as coding.

The main contributions of the thesis are as follows: First, the multichannel 2-D AR model and specific differences from single channel models are described. Models with quadrant plane and nonsymmetric half plane support and their forward and backward forms are defined. It is shown that unlike lower-dimensional cases the forward and backward models produce *different* spectral estimates. Secondly, an estimate for the spectral matrix based on a combination of models with first and second quadrant support is presented and a method for estimating the model parameters directly from the data (i.e. without prior estimation of a correlation function) is given. Third, a measure for comparing spectral estimates based on the statistical divergence is proposed and used to compare various spectral estimates. Fourth, a comprehensive set of experimental studies of the spectral estimation procedures is presented. Fifth, the Maximum Likelihood Method and Improved Maximum Likelihood Method of spectral estimation are extended to the multichannel 2-D case and results are compared experimentally to power spectral estimation results based on AR modeling.

Finally, although the main goal of this thesis was multichannel 2-D spectral analysis a large part of the work had to deal with modeling of multichannel 2-D random processes. These models have applications to signal processing problems other than spectral analysis. To illustrate this versatility we have applied the models and devoted one chapter of the thesis to the problem of image coding. The results show that efficient

coding of color images can be obtained using general models that have been derived from analysis of several different types of color images.

A. SIGNAL MODELING AND LINEAR PREDICTION

A large class of methods for spectral analysis deals with modeling the signal as a linear filter driven by a known noise source (usually white noise). One class of modeling for which a considerable amount of work has been done is the AR or "all-pole" model. In this case the random signal is considered as the output of a 2-D purely recursive and stable linear filter which is driven by white noise. Sometimes this model is called the synthesis model since it may be thought of as a random signal generator. The inverse of the filter used in the AR model, which is also causal, is a 2-D FIR filter that whitens the random process. This filter is thus known as the whitening filter.

Another class of models is defined by applying linear prediction techniques. The random signal sample is predicted from a linear combination of the previous N samples weighted by a set of filter coefficients. The difference between the actual data sample and the predicted one is known as the prediction error and is minimized in the mean square sense. This linear predictive model is also called a minimum mean square error (MMSE) model. (Jain,1981)

The distinction between the AR model and linear predictive model lies in the fact that linear prediction does not always produce white noise. The AR and linear predictive models are identical only when the process is truly described by an AR model with the support region used for linear prediction. In this case a white noise prediction error is obtained. Fortunately a close AR representation for most 2-D random processes can be obtained by choosing a linear predictive model with sufficiently large nonsymmetric half plane support. Theoretical results (Ekstrom and Woods,1976; Marzetta, 1978) show that NSHP support is sufficient to represent any 2-D random process but in general the support will be infinite.

The idea of linear prediction is therefore to determine a causal filter that (approximately) whitens a given random process. There are two classes of linear prediction problems. In one case we are given a finite set of samples from the random process, and we want to estimate the causal linear predictive whitening filter. We refer to this

problem as the AR model fitting problem. In this case the whitening filter is modeled as an FIR filter.

In the second class of linear prediction problems we are given the actual power density spectrum of the process, and the idea is to derive from it the causal whitening filter. This problem is called spectral factorization (Marzetta, 1978). We concentrate in this thesis on problems in the first class.

The two most popular methods of AR model fitting are the autocorrelation method, and the Burg algorithm. In the first method estimation of the model parameters is based on prior estimation of the correlation function. In the second method the model parameters are estimated directly from the data.

In 1-D an important representation of the linear predictive filter is the lattice structure. In this case the system is represented by so-called reflection coefficients. Various attempts have been made to extend the lattice to 2-D. One approach was suggested by Marzetta (1979). He defined a set of 2-D reflection coefficients and a corresponding 2-D lattice implementation of the linear predictive filter. The polynomial representation of the 2-D minimum phase filter corresponding to the given finite set of reflection coefficients will have a finite region of support. Unfortunately the converse of this statement is not true. If the polynomial representation is defined on a finite region of support, the corresponding lattice structure representation will be in general finite in one direction and infinite in the other direction. In either case the stability of the corresponding IIR filter is guaranteed if the magnitude of the reflection coefficients is less than one.

In another approach Parker and Kayran (1984) suggested a different extension of 1-D lattice AR modeling to the 2-D case. Although the resulting 2-D filter has some interesting characteristics, it is neither a whitening filter nor a minimum mean square error prediction filter.

B. SPECTRAL ESTIMATION METHODS

Power spectrum estimation has progressed through several stages since the turn of the century. The first estimation methods used extensively were based on the Fourier transform. They are known as *classical* or *conventional* methods (Kay and Marple,1981; Oppenheim and Schafer,1975; Priestley,1981) and can be classified into correlelogram

and periodogram methods. The correlelogram method developed by Blackman and Tukey involves estimating the autocorrelation function from the observed data, windowing the autocorrelation estimate in an appropriate manner, and then Fourier transforming the windowed autocorrelation function to obtain the estimated power spectrum. In the periodogram method the spectral estimate can be obtained by taking the Fourier transform of the observed data and squaring its magnitude. Modified periodogram methods were also developed that use window functions. A main disadvantage of these methods is the relatively poor resolution when the data length is short.

More recently, model-based methods have become available to estimate spectra with increased resolution. Examples of model-based methods are the maximum likelihood method (MLM), autoregressive or AR method, maximum entropy method (MEM), and the Pisarenko method. (Burg,1975; Cadzow and Ogino,1981; Capon,1969; Childers,1978; Dowla and Lim,1983,1984,1985; Dudgeon and Mersereau,1984; Efron and Tufts,1986; Ekstrom,1984; Jackson and Chien,1979; Jain,1981; Kay and Marple,1981; Kesler,1986; Lang and McClellan,1980,1982,1983; Lim and Malik,1981,1982; Marple,1987; Marzetta,1978; McClellan,1982; Nuttal,1976; Papoulis,1981; Parker and Kayran,1984; Robinson,1982; Strand,1977; Woods,1976)

Among the various model-based methods cited, MEM is particularly interesting. In 1-D the method is theoretically equivalent to the AR method for Gaussian random processes. In conventional methods the power spectrum estimate obtained from a given autocorrelation sequence assumes no values of the sequence outside the given range; actually the values outside this range are considered to be zero. The effect of this truncation is overcome by using a window function. MEM retains all the estimated values of the correlation sequence without modification, and at the same time extends the values of the autocorrelation function outside the given range. The spectral estimate in this case is the most random or has the maximum entropy of any power spectrum whose correlation function matches that of the given data. (Burg,1967,1968,1975)

In 1-D linear prediction the minimum phase property of the prediction error filter (PEF) insures the stability of its inverse. This guarantees, among other things, that a stable AR model exists for the data. In addition, an AR model of order N matches the N+1 given values of the correlation function and extends it in the maximum entropy

sense. The computation of the prediction error filter involves solution of a Toeplitz system of Normal equations. The equations can be solved by the Levinson algorithm which leads to a prediction error variance and a set of reflection coefficients to represent the filter. In 1-D therefore, there is a one-to-one correspondence between the given values of the correlation function, the parameters of the linear predictive filter that appear in the Normal equations, and the set of reflection coefficients and prediction error variance.

In the 2-D case the linear prediction problem is more complicated than in the 1-D case. Further in 2-D the autocorrelation matching property does not always hold and a positive definite extension may not exist (Ekstrom and Woods,1976; Lang and McClellan,1980,1982,1983; Marzetta,1978). In contrast to the 1-D case the 2-D AR filter is not always stable and the ME spectral estimate and the AR spectral estimate are not necessarily the same. Finally there is no assurance that a 2-D ME spectral estimate exists (Dickinson,1980; Jain,1981; McClellan,1982). Woods (1976) proved that the maximum entropy spectral estimate exists and is unique provided that the known autocorrelation coefficients are actually part of a valid autocorrelation function, but Dickinson (1980) pointed out that 2-D spectrum estimates based on a *finite* segment of the autocorrelation function or on estimated autocorrelation data do not always exist.

Spectral factorization in 1-D is obtained by dividing the spectral density function (SDF) of the random process into two factors. One factor contains all its poles and zeros inside the unit circle and is called the causal or minimum phase factor. The other factor contains all its poles and zeros outside the unit circle and is called the anticausal or maximum phase factor. The causal factor can be written in the form of a difference equation such that the random process generated by driving this difference equation with white noise has the given SDF. The AR model is obtained when the difference equation is purely recursive i.e. the system function has only poles. Also the difference equation can be interpreted as a linear predictor, where a sample of the random process is predicted from the linear combination of previous samples, such that the mean square of a prediction error is minimized.

In 2-D the spectral factorization problem is more complicated. Marzetta (1978) tried to approach the spectral factorization problem by extending the results of 1-D prediction theory to 2-D. He proved that the exact solution can be obtained by solving an

infinite set of linear equations. Using a finite set of linear equations gives an approximate solution. Ekstrom and Woods (1976) and subsequently others looked at the 2-D spectral factorization problem directly. Their results show that while 2-D spectral factorization is indeed possible, the resulting white noise-driven filter required to model the process may have infinite NSHP support in general.

MLM was originally developed by Capon (1969) for seismic array frequency wavenumber analysis. The MLM spectral estimate may be derived by solving a classical optimal filtering problem. The filter is designed to pass the power in a narrow band about the signal frequency of interest and minimize the power due to interfering spectral components such as noise. From a computational view point, MLM is straightforward. It has a closed form solution and requires only the inversion of a non-singular covariance matrix. However a major disadvantage is that it has poorer resolution than other methods (such as AR method and MEM). Burg (1972) showed that there exists a simple, exact relationship between maximum entropy spectra and maximum likelihood spectra when the correlation function is known at uniform intervals of lag for the 1-D case. He proved that the reciprocal of the maximum likelihood spectrum is equal to the average of the reciprocals of the maximum entropy spectra obtained from predictors of order one to P, where P represents the order of the MLM filter. Lim and Dowla (1984) showed a similar relationship between MLM and AR spectral estimates for m-D signals sampled nonuniformly or uniformly. They proposed a new method for 2-D spectral estimation called improved MLM (IMLM) (1985). This method is based on the relationship between the MLM and AR model. The IMLM has a computational requirement similar to that of the MLM, but has a resolution property which is considerably better than that of MLM. Lagunas *et al* (1985), and Baggeroer (1975) reported separately on how to include general concepts of the 1-D MLM procedure in a two-channel problem of cross spectrum estimation. Their algorithms treat cross spectral estimation separately from autospectral estimation and do not consider the full multichannel spectral estimation problem. Up to this point no counterpart to IMLM appears to have been developed for cross spectral estimation.

While spectral estimation for single channel 2-D signals leads to a number of interesting and surprising results, spectral estimation for *multichannel* 2-D signals leads to still more interesting phenomena. The spectrum estimation methods that will be applied to these signals in this thesis compute the entire spectral matrix. That is, estimates for the 2-D autospectra and magnitude and phase of the cross spectra are produced all at once. As mentioned earlier, the methods have characteristics of both 1-D multichannel methods and 2-D single channel methods. However properties sometimes exist that are found in neither the 1-D multichannel or the 2-D single channel case. For example, it will be shown that unlike either of the other two cases, the forward and backward forms of the 2-D AR models produce theoretically *different* spectral estimates.

C. APPLICATION OF SPECTRAL ANALYSIS MODELS TO IMAGE CODING

Data compression is the conversion of a train of data into a train of low rate data for purposes of storage or communication over a digital communication channel. Theory and application of data compression for images and speech has become very important due to increased demand for availability of these data in data bases and in integrated network environments. Images and speech are probably the currently most important applications of data compression. (Gibson,1980; Goodman and Gersho,1974; Jain,1981; Jayant,1974,1976,1984; Margos,Schafer and Mersereau,1984; Netravali,1980)

Due to the conversion of high rate data to low rate data there is a loss of fidelity or an increase in the distortion. The aim of data compression is to obtain the best possible fidelity for the given data rate or to minimize the rate required for a given fidelity.

Waveform coding techniques have become popular because of their simplicity and generally good performance. Waveform coding can be classified into the following major categories: pulse code modulation (PCM), predictive coding, transform coding, interpolative, and extrapolative coding. Each of these classes can be further divided into fixed and adaptive methods.

In PCM the signal sampling generally occurs at the Nyquist rate, and the sampling amplitude is represented by some number of quantization levels. In linear predictive or differential PCM (DPCM) the sample to be encoded is predicted from the encoded values of the previously transmitted samples and only the prediction error is quantized for

transmission. Such an approach can be made adaptive either by changing the prediction or quantization or by not transmitting the prediction error whenever it is below a certain threshold. In transform coding, an alternative representation of the signal is made first by taking linear combinations of samples (called coefficients) in a block of data and then quantizing the coefficients. Transform coders can be made adaptive by changing the type of transformation of the coefficients. Interpolative and extrapolative coders attempt to send certain samples to the receiver and either interpolate or extrapolate all the rest. Adaptation can be incorporated by changing the criterion for selection of the samples to be sent and/or the procedure for interpolating or extrapolating the remaining samples. Predictive and transform coding can also be combined resulting in hybrid coding. All of these techniques share a fundamental property: the actual quantization or coding is done on scalars. (Jayant,1974,1976,1984; Zetterberg, Ericsson and Brusewitz,1982)

Recently vector quantization (VQ) has evolved as a new and powerful speech and image coding technique. The data to be encoded is divided into small blocks and then encoded block by block. The idea is to identify a list of reconstruction levels of possible blocks of data which represent the encoded information. We refer to the reconstruction levels in VQ as the *codebook*. The algorithm most often used for generating this codebook is named as the Linde-Buzo-Gray (LBG) algorithm and seeks to develop centers or clusters of the data in a multidimensional metric space which can serve as reconstruction levels. (Cuperman and Gersho,1985; Goldberg, Boucher and Shilien,1986; Gray and Linde,1982; Gray,1984; Hang and Woods,1985; Linde, Buzo and Gray,1980; Makhoul, Roucos and Gish,1985)

In our work we concentrate on linear predictive coding for color images. The coder is based on the multichannel linear predictive models developed in the thesis and the error residual is coded at two or three levels for each channel. Methods involving specific linear predictive models for each image to be transmitted are compared to methods involving use of an "average" (non-optimal) set of coefficients for the prediction error filter.

D. AN OUTLINE OF THE DISSERTATION

The purpose of this dissertation is to introduce and analyze some new algorithms for multichannel 2-D linear prediction and power spectrum estimation (the linear predictive models used in the spectrum estimation are also applied to the coding of color images). The thesis is organized as follows:

In Chapter II we briefly review some of the existing results on single channel 2-D spectral estimation. The 2-D AR model and its specific differences from 1-D models are described. Two specific 2-D AR models are considered here namely the nonsymmetric half plane (NSHP) model and quadrant plane (QP) model. Spectral estimation experimental results are compared with results of the Fourier transform techniques. We also review in this chapter the lattice structure and a proposed 2-D Burg algorithm.

In addition, some original results are presented in Chapter II that are later extended to the 2-D multichannel case. We develop a method of parameter estimation that allows the model parameters to be estimated directly from the data without prior estimation of a correlation function. This method is based on the close relation between the single channel 2-D linear prediction problem and the multichannel 1-D linear prediction problem. We refer to the method as a *direct* method. Secondly we propose a quantitative measure for comparing the similarity of two single channel 2-D spectral estimates based on the statistical *divergence* and use it to compare the spectral estimates generated by various 2-D models.

Chapter III deals with the representation and statistical characterization of multichannel 2-D signals. We discuss multichannel 2-D linear prediction theory using both NSHP and QP models. The multichannel 2-D AR model and specific differences from single channel models are described. The concept of forward and backward forms of linear prediction and their related AR models are introduced. It is shown that unlike the single channel 2-D case, the forward and backward models are not identical. We also define the four possible QP models and discuss their differences. Relations between 2-D multichannel problems and higher order 1-D multichannel problems are then discussed. These results are used to formulate a direct method for estimation of the 2-D multichannel model parameters (i.e. without explicit prior estimation of the correlation function).

The divergence measure used for comparing spectral estimates of single channel 2-D random processes in Chapter II is then developed for the multichannel case.

Chapter IV is concerned with multichannel 2-D spectral estimation based on AR models. Here the problem is to obtain accurate spectral estimates given a finite number of data samples. We begin by summarizing the spectral estimation models, and show that since the NSHP forward and backward models have distinctly different model parameters, in general this leads to different spectral estimates. Similarly it is shown that in general none of the four possible multichannel 2-D QP models give the same estimate for the spectral matrix. This suggests a generalization of the procedure used by Jackson and Chien for combining multiple quadrant based spectral estimates into a single combined spectral estimate. We call this procedure the combined quadrant (CQ) method, and it can be used effectively with the *direct* method of parameter estimation developed in Chapter III.

A comprehensive set of experimental studies for estimating the spectral matrix for 2-channel 2-D random processes is presented. The estimate includes the 2-D autospectrum for each channel and magnitude and phase of the cross spectra. The estimates compared correspond to NSHP, CQ, and direct CQ models.

In Chapter V we review the 2-D single channel Maximum Likelihood Method (MLM) of spectral estimation and describe extensions of the MLM method to cross spectrum estimation. We then develop the MLM method specifically for the 2-D multichannel case, and compare our results to the earlier results where the components of the spectral matrix are computed individually. We discuss the differences in the methods and show experimentally that our algorithm gives results very close to those for the single channel MLM algorithm and the extended cross spectrum MLM estimation technique.

Since MLM estimates generally have significantly poorer resolution than those based on AR models, we consider the so-called Improved MLM (IMLM) of Lim and Dowla and develop it for the multichannel case. This method retains the computational simplicity of the MLM, but gives better resolution. We carry out an experiment to compare the amplitude and phase of cross spectra of AR, MLM and IMLM techniques. Finally, in this chapter we measure and compare the resolution properties of the estimate experimentally as a function of signal-to-noise ratio and as a function of the model order.

Chapter VI applies the 2-D spectral analysis models developed earlier to the problem of image coding. We are concerned here with predictive coding i.e. linear prediction followed by quantization of the prediction error. We begin by summarizing the two types of quantization namely scalar quantization and vector quantization.

In our experimental procedure in this chapter we compare two methods initially, in the first, the whole frame of the image is divided into subframes; the predictor coefficients are then computed separately for each subframe. In the second, the predictor coefficients are obtained for the whole frame of the image. Both of these methods have the disadvantage that the linear prediction coefficients matrices must be computed in real time, and transmitted to the receiver as side information. This greatly increases complexity of the coding system. As an alternative we consider using a fixed set of prediction matrices, i.e. one that does not depend on the specific image being coded. In this way both receiver and transmitter have the linear prediction matrices and no side information has to be transmitted. Such prediction matrices can be generated by various averaging methods discussed in the chapter. We compare the results of this coding to that resulting from the previous two methods.

The last chapter, VII, concludes the thesis. It briefly summarizes our most important results and cites areas for further research.

II. SINGLE CHANNEL 2-D SPECTRAL ESTIMATION

A. INTRODUCTION

Two-dimensional (2-D) digital signal processing is concerned with the processing of discrete signals which can be represented on 2-D lattice. For instance, a digital image is a 2-D array of real numbers representing intensity as a function of spatial position. Geological data and other sampled waveforms received from an array of sensors can also be considered as 2-D or higher dimensional discrete signals. Since 2-D signals can be deterministic or stochastic the mathematical characterization of 2-D signals can be deterministic or statistical. In the deterministic representation, each value of the 2-D sequence is uniquely determined by a mathematical expression. In statistical representation a signal is specified by the average properties such as the mean, correlation, and power spectrum. Many 2-D signals can be considered as a sample function of a 2-D discrete, wide sense stationary (or homogeneous) random field, which is described in terms of its mean and covariance function.

An important topic in stationary 2-D random process analysis is power spectrum estimation. The problem of spectral estimation is considerably more complex in the 2-D case than in the 1-D case (Cadzow and Ogino,1981; Dudgeon,1984; Ekstrom,1984; Ekstrom and Woods,1976; Jain,1977,1978,1981; Lang and McClellan,1980,1982,1983; Lim and Malik,1981; Marzetta,1978,1979,1980; McClellan,1982; Nikias and Raghuveer,1983; Woods,1976). The spectral estimation problem may be stated briefly in the following way. Given samples of a stationary and homogeneous random field $x(n_1,n_2)$, specified by its second order statistics, estimate its power spectrum.

There are many different techniques that can be used to estimate the 2-D power spectrum (McClellan,1982). Conventional methods based on the discrete Fourier transform (DFT) generalize from 1-D time series analysis in a straightforward manner when the sampling is uniform. However the more recent high resolution model-based methods such as MEM (Lang and McClellan,1982; Lim and Malik,1981,1982; Roucos and Childers,1979,1980; Wernecke and D'Addario,1977), and AR-modeling (Dudgeon

and Mersereau,1984; Ekstrom,1984; Jackson and Chien,1979; Lacoume,1983; Sharma and Chellappa,1986), take on a different and more complicated form.

In this chapter we briefly review some of the existing results on single channel 2-D spectral estimation. The 2-D AR model and its specific differences from 1-D models are described. Two specific 2-D AR models are considered here namely the nonsymmetric half plane (NSHP) model and quadrant plane (QP) model. Some AR model-based spectral estimation experimental results are given and compared with results of classical Fourier transform techniques. We also review in this chapter the lattice structure for the 2-D AR model developed by Marzetta and a proposed 2-D Burg algorithm.

Some original results are also presented in this chapter that are later extended to the 2-D multichannel case. We develop a method of parameter estimation that allows the model parameters to be estimated directly from the data without prior estimation of a correlation function. This method is based on the close relation between the single channel 2-D linear prediction problem and the multichannel 1-D linear prediction problem. We refer to the method as a *direct method.* In addition we propose a quantitative measure for comparing the similarity of two single channel 2-D spectral estimates based on the divergence and use it to compare the spectral estimates generated by various 2-D models.

B. REVIEW OF CLASSICAL METHODS

Historically, methods based on the Fourier transform have been widely used for spectral estimation (Jenkins and Watts,1968; Oppenheim and Schafer,1975; Priestley,1981; Robinson,1982). The advent of the Fast Fourier Transform (FFT) algorithm helped to make these techniques very attractive. Although many variations exist, there are fundamentally only two distinct estimators of the Fourier type. One is the correlelogram method which is based on the fact that the power spectrum and the autocorrelation function form a Fourier transform pair. The other is the periodogram estimate and its various smoothed versions. The use of these estimators in the multidimensional case is virtually identical to the use in the 1-D case.

1. Correlelogram Method of Spectral Estimation

We define the power spectrum of a random process $x(n_1,n_2)$ as the Fourier transform of the autocorrelation function $R_x(k_1,k_2)$

$$S_x(\omega_1,\omega_2) = \sum_{k_1=-\infty}^{\infty} \sum_{k_2=-\infty}^{\infty} R_x(k_1,k_2) \, . \, e^{-j\omega_1 k_1} e^{-j\omega_2 k_2} \tag{2.1}$$

where:

$$R_x(k_1,k_2) = E\Big[x(n_1,n_2)\, x(n_1-k_1,n_2-k_2) \Big] \tag{2.2}$$

and E [.] denotes the expectation over the ensemble of the random process. Hence, given a finite number of data samples on a rectangular lattice $\Big\{ x(n_1,n_2),\ (1,1) \le (n_1,n_2) \le (N_1,N_2) \Big\}$ the estimate for the autocorrelation can be made only on a finite range $\Big\{ \hat{R}(k_1,k_2),\ -(P_1,P_2) \le (k_1,k_2) \le (P_1,P_2) \Big\}$, and the power spectrum estimate can be formed as :

$$S(\omega_1,\omega_2) = \sum_{k_1=-P_1}^{P_1} \sum_{k_2=-P_2}^{P_2} \hat{R}(k_1,k_2) \, . \, e^{-j\omega_1 k_1} e^{-j\omega_2 k_2} \tag{2.3}$$

Since with most methods for estimating the correlation function fewer data samples enter into estimation of covariances at larger lags, the reliability of the estimates decreases with increasing lag. This necessitates application of a window to the estimated correlations to reduce the contribution of correlations at larger lags to the power spectral estimation. A typical windowed correlelogram estimate is of the form

$$S(\omega_1,\omega_2) = \sum_{k_1=-P_1}^{P_1} \sum_{k_2=-P_2}^{P_2} C(k_1,k_2)\, \hat{R}(k_1,k_2)\, e^{-j\omega_1 k_1} e^{-j\omega_2 k_2} \tag{2.4}$$

where $C(k_1,k_2)$ is the window function. This multiplication of the estimated autocorrelation sequence by a window function is equal to the convolution of the true power spectrum with the transform of the window function. In the 1-D case, the triangular window or other windows such as, the raised cosine may be used. Harris (1978) provides a

summary of various windows applied for spectral analysis computation. In the 2-D case, windows are most often generated either by taking the outer product of two 1-D windows to generate a 2-D window with rectangular region of support or by sampling a circularly rotated 1-D window function to generate a 2-D window with circular region of support (Dudgeon and Mersereau,1984).

2. Power Spectrum Estimation Using Periodogram Methods

As mentioned earlier, several different estimates of the 2-D autocorrelation are possible. If the estimated autocorrelation function $\hat{R}(k_1,k_2)$ of the random process $x(n_1,n_2)$ given on a finite range $0 \le n_1 < N_1$; $0 \le n_2 < N_2$ is taken as

$$\hat{R}(k_1,k_2) = \frac{1}{N_1 N_2} \sum_{n_1=0}^{N_1-|k_1|-1} \sum_{n_2=0}^{N_2-|k_2|-1} x(n_1,n_2)x(n_1-k_1,n_2-k_2) \qquad (2.5)$$

$$|k_1| \le N_1-1 \; ; \; |k_2| \le N_2-1$$

then the estimated power spectrum of the random process can be given by the Fourier transform of the estimated autocorrelation function

$$S(\omega_1,\omega_2) = \sum_{k_1=-(N_1-1)}^{N_1-1} \sum_{k_2=-(N_2-1)}^{N_2-1} \hat{R}(k_1,k_2) \, . \, e^{-j\omega_1 k_1} e^{-j\omega_2 k_2} \qquad (2.6)$$

Since the Fourier transform of the finite data segment $x(n_1,n_2)$, $(0 \le n_1 < N_1 \; ; \; 0 \le n_2 < N_2)$ is

$$X(e^{j(\omega_1,\omega_2)}) = \sum_{n_1=0}^{N_1-1} \sum_{n_2=0}^{N_2-1} x(n_1,n_2) e^{-j\omega_1 n_1} e^{-j\omega_2 n_2} \qquad (2.7)$$

it is easy to show that

$$S(\omega_1,\omega_2) = \frac{1}{N_1 N_2} \left| \sum_{n_1=0}^{N_1-1} \sum_{n_2=0}^{N_2-1} x(n_1,n_2) \, . \, e^{-j\omega_1 n_1} e^{-j\omega_2 n_2} \right|^2$$

$$= \frac{1}{N_1 N_2} \left| X(e^{j(\omega_1,\omega_2)}) \right|^2 \qquad (2.8)$$

This is called the periodogram. Thus in the periodogram method the estimated power spectrum $S(\omega_1,\omega_2)$ can be obtained by taking the 2-D Fourier transform of the given data set $x(n_1,n_2)$ and squaring its magnitude. We can generalize the periodogram estimate by slightly to form the modified periodogram $S(\omega_1,\omega_2)$ by multiplying the data by a 2-D window function $C'(n_1,n_2)$.

$$S(\omega_1,\omega_2) = \frac{1}{N_1 N_2} \left| \sum_{n_1=0}^{N_1-1} \sum_{n_2=0}^{N_2-1} C'(n_1,n_2)\, x(n_1,n_2)\, e^{-j\omega_1 n_1} e^{-j\omega_2 n_2} \right|^2 \qquad (2.9)$$

The window C appearing in Eqn. (2.4) is then the 2-D convolution of the window C' with itself.

The periodogram is known to be a poor estimate of the power spectrum of the process. Bartlett suggested a modification of the periodogram to obtain a statistically more reliable spectral estimate. In this case the signal is divided into L-blocks, and the periodogram of each block is computed. The individual periodograms are then averaged to obtain the spectral estimate.

$$S(\omega_1,\omega_2) = \frac{1}{L} \sum_{l=0}^{L-1} S_l(\omega_1,\omega_2) \qquad (2.10)$$

Where $S_l(\omega_1,\omega_2)$ represents the periodogram power spectral estimate of the block l. In this case the variance is reduced, but at the expense of a reduction in the frequency resolution. Welch (1967) proposed dividing the data record into either overlapping or nonoverlapping segments. Each data segment is windowed before computing its periodogram. The resulting periodograms are then averaged as above (see Eqn. (2.10)). The resulting estimate is asymptotically unbiased and has lower variance than the Bartlett method. (Oppenheim and Schafer,1975; Priestley,1981)

The disadvantage of both Fourier methods, is the resolution limit. Longer data sets provide better resolution but result in increased variance. For this reason the Fourier methods have met with limited success and much recent research has been directed at deriving high resolution estimators. The remainder of this chapter will be devoted to some of these other techniques.

C. AUTOREGRESSIVE (AR) SPECTRAL ESTIMATION

Power spectral estimation methods based on the Fourier transform are known also as "conventional" or classical methods. The computational efficiency of FFT algorithms makes these methods simple and easy to implement. On the other hand the low resolution afforded by these methods is due in part to the fact that, the data is given on a finite range and is assumed to be zero outside this range Modern spectrum estimation techniques give higher resolution than the conventional methods. These methods have also been called data adaptive methods or high resolution spectral estimation techniques. The various modern spectral estimation techniques that exist in the literature may be based on different principles, but all strive towards a common goal: to improve the resolution of the power spectral estimate beyond the Fourier limit by explicitly or implicitly providing an extrapolation of the data outside it's known extent. Since most of the modern spectral estimation techniques are model-based, they are usually parameteric in nature.

Since the theory for 1-D parametric spectral estimation techniques is well understood, a natural intermediate step in the development of 2-D spectral estimators was the extension of 1-D spectral estimators to the 2-D problem. A method of spectral estimation which has attracted much attention in 1-D signal analysis is the technique of Maximum Entropy (ME) proposed by Burg (1967,1968,1975). This method was shown to be equivalent to AR modeling (Childers,1978; Nuttall,1976) in 1-D. The success of the ME method in 1-D has led researchers to explore this problem in 2-D. Unfortunately, the simplicity and elegance of this method is lost in two and higher dimensions.

The ME spectrum parameters for the 2-D case are in general different from the those for spectral estimation by the AR technique. Maximum entropy requires the solution of a nonlinear optimization problem (McClellan,1982), and there is no known closed form solution. The method requires one to maximize the entropy subject to a correlation matching constraint. Malik and Lim (1981) suggested an iterative algorithm for solving the 2-D ME problem.

A more fundamental problem for the ME method is that the ME spectral estimate may not exist. Woods (1972,1976) has shown the existence and uniqueness of a 2-D discrete Markov random field which agrees with given correlation values on an array of nearest neighbors. The resulting power spectrum estimate is the 2-D ME spectrum. He

suggested an iterative algorithm to evaluate the Markov spectral estimation for a regularly spaced array. However Dickinson (1980) pointed out that the 2-D Markov spectrum estimates based on estimated autocorrelation data may not always exist. Thus Woods results apply only when existence of the estimate is known.

A power spectrum estimate of a 2-D random process can also be developed using an AR model. In this case the random process $x(n_1,n_2)$ is represented by an AR model defined over some region α.

$$x(n_1,n_2) = - \sum_{\substack{(i_1,i_2)\in\alpha \\ (i_1,i_2)\neq(0,0)}} a_{i_1 i_2} x(n_1-i_1,n_2-i_2) + w(n_1,n_2) \tag{2.11}$$

Where $a_{i_1 i_2}$ are the filter coefficients and $w(n_1,n_2)$ is 2-D white noise. Although the parameters of this model are most often generated by considering the 2-D linear prediction problem with region of support α and formulating and solving a set of Normal equations, this method is strictly valid only when an AR representation of the 2-D random process is known to exist. That is, the linear prediction model is the same as the AR model only when the process is truly described by a model with the postulated form of support. In this case the error produced by the linear prediction is white and the original random process can be generated by inverse filtering.

The linear prediction model is sometimes refered to as the minimum mean-square error model (Jain,1981). It differs in general from the AR or white noise driven model in that the error residuals are not guaranteed to be white.

In practice, when a NSHP model of sufficiently large size is used, the error residuals are found to be nearly uncorrelated so that the distinction between the two types of models is not so important. In general, this will not be true for models with quadrant support and so single quadrant AR models (as will be seen) tend to produce poor spectral estimates. Nevertheless, combinations of the quadrant-based models, while lacking a theoretical justification, tend to produce reasonably well behaved spectral estimates.

In the NSHP model the linear prediction model and the AR model become identical when we have an infinite region of support (Ekstrom and Woods,1976; Jain,1981; Marzetta,1978,1979,1980). In this case the spectrum of the process is given by

$$S(\omega_1,\omega_2) = \frac{\sigma_\varepsilon^2}{|H(\omega_1,\omega_2)|^2} \tag{2.12}$$

where

$$H(\omega_1,\omega_2) = \sum_{(n_1,n_2)\varepsilon\alpha} a_{n_1n_2} e^{-j\omega_1 n_1} e^{-j\omega_2 n_2} \quad , \quad a_{00}=1 \tag{2.13}$$

and σ_ε^2 is the prediction error variance. Since infinite NSHP support can not be used in practical applications formula (2.12) is used with a finite region α. Experimental results show that NSHP support of modest size is adequate to obtain a good spectral estimate.

Although models with support in only a single quadrant are seldom adequate to represent a general 2-D random process, it has been mentioned that quadrant support is useful for spectrum estimation if two or more quadrant models are combined. The two types of AR models, QP and NSHP, are discussed in more detail below.

1. <u>Quadrant Plane (QP) Model</u>

Generally the region α of an AR model can take many different forms. Let α be the rectangular region shown in Fig. 2.1. In this case the region α consists of $P_1 \times P_2$ points and L_1 and L_2 are chosen to be within the range $-P_1 < L_1 \leq 0$, $-P_2 < L_2 \leq 0$.

First quadrant support can be considered as a special case of rectangular support where $L_1 = L_2 = 0$. In this case the region of support α for the first quadrant plane will be $\left[0, P_1-1\right] \times \left[0, P_2-1\right]$. In this thesis we define an N^{th} order first quadrant plane model to be one with $P_1 - 1 = P_2 - 1 = N$. When P_1 and P_2 are not equal we can refer to the order as (P_1-1, P_2-1).

Now let $x(n_1,n_2)$ represent a zero-mean stationary 2-D random signal. Then the estimated value $\hat{x}(n_1,n_2)$ using first quadrant linear prediction model can be written in the following form :

$$\hat{x}(n_1,n_2) = -\sum_{i_1=0}^{P_1-1} \sum_{i_2=0}^{P_2-1} a_{i_1 i_2} x(n_1-i_1, n_2-i_2) \quad , \quad (i_1,i_2) \neq (0,0) \tag{2.14}$$

If we define the matrix 2-D correlation function as

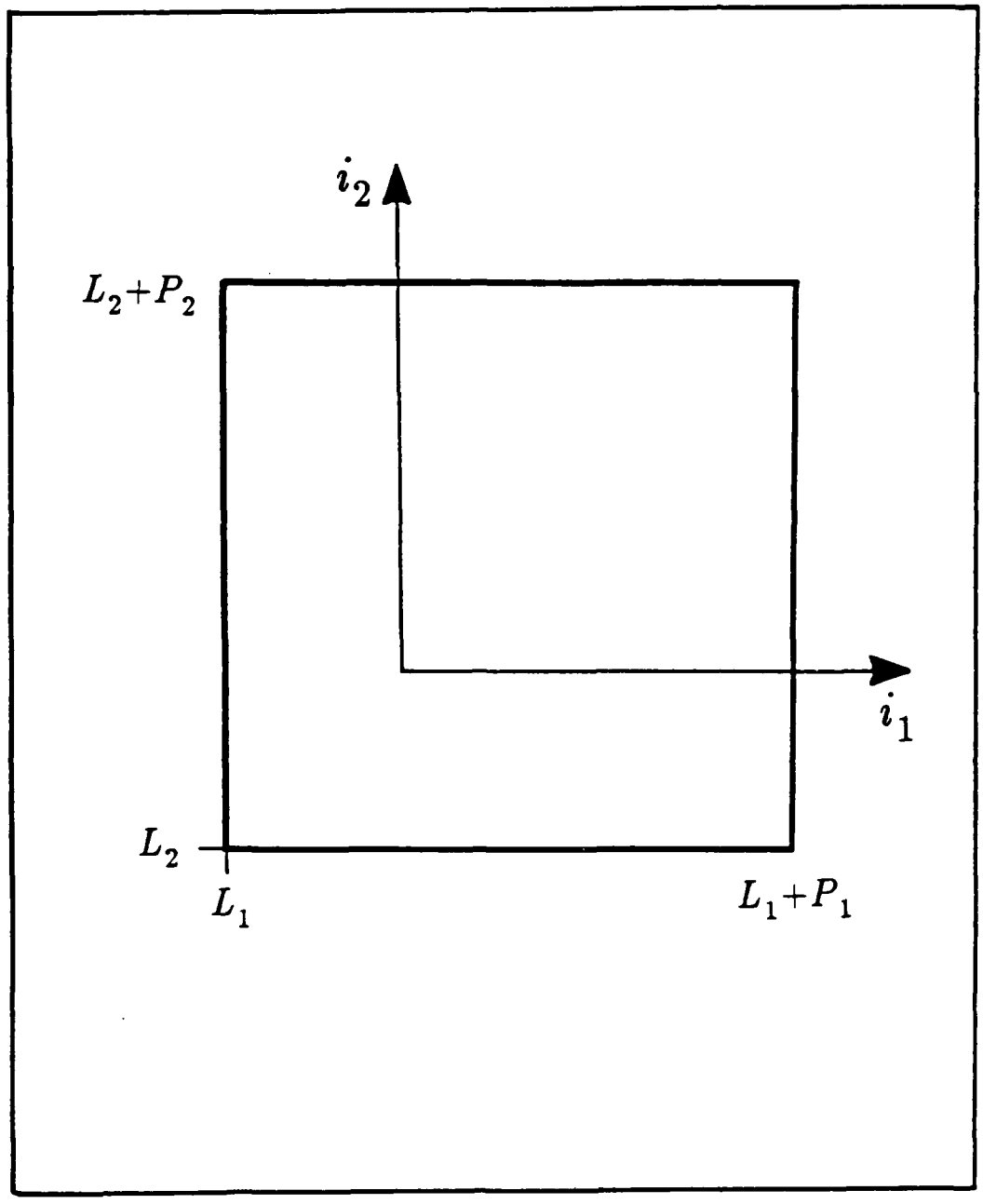

Fig. 2.1 Rectangular region of support

$$R(k_1,k_2) = R(-k_1,-k_2) = E\left[x(n_1,n_2)x(n_1-k_1,n_2-k_2)\right] \tag{2.15}$$

then the Normal equations of the first quadrant plane model have the form

$$\mathbf{R} \,.\, \mathbf{A} = \mathbf{S} \tag{2.16}$$

where **R** represents the correlation matrix, **A** is the filter coefficient vector and **S** is the error variance vector. The Normal equations (2.16) in this case have the specific form :

$$\begin{bmatrix} \mathbf{R}(0) & \mathbf{R}(-1) & \ldots & \mathbf{R}(-P_1+1) \\ \mathbf{R}(1) & \mathbf{R}(0) & \ldots & \mathbf{R}(-P_1+2) \\ . & . & & . \\ . & . & & . \\ . & . & & . \\ \mathbf{R}(P_1-1) & \mathbf{R}(P_1-2) & \ldots & \mathbf{R}(0) \end{bmatrix} \begin{bmatrix} \mathbf{A}^{(0)} \\ \mathbf{A}^{(1)} \\ . \\ . \\ . \\ \mathbf{A}^{(P_1-1)} \end{bmatrix} = \begin{bmatrix} \mathbf{S}^{(0)} \\ \mathbf{0} \\ . \\ . \\ . \\ \mathbf{0} \end{bmatrix} \tag{2.17}$$

where

$$\mathbf{R}(k) = \mathbf{R}(-k) = \begin{bmatrix} R(k,0) & R(k,-1) & \ldots & R(k,-P_2+1) \\ R(k,1) & R(k,0) & \ldots & R(k,-P_2+2) \\ . & . & & . \\ . & . & & . \\ . & . & & . \\ R(k,P_2-1) & R(k,P_2-2) & \ldots & R(k,0) \end{bmatrix} \tag{2.18a}$$

$$\mathbf{A}^{(k)} = \begin{bmatrix} a_{k,0} \\ a_{k,1} \\ . \\ . \\ . \\ a_{k,P_2-1} \end{bmatrix} \tag{2.18b}$$

$$\mathbf{S}^{(0)} = \begin{bmatrix} \sigma_1^2 \\ 0 \\ \cdot \\ \cdot \\ \cdot \\ 0 \end{bmatrix} \tag{2.18c}$$

and where

$$a_{0,0} = 1 \tag{2.18d}$$

$$\sigma_1^2 = E\left[(x(n_1,n_2) - \hat{x}(n_1,n_2))^2 \right] \tag{2.18e}$$

Note that σ_1^2 is the prediction error variance. The spectral estimate yielded by the first QP model is given by:

$$S_1(\omega_1,\omega_2) = \frac{\sigma_1^2}{|H_1(\omega_1,\omega_2)|^2} \tag{2.19}$$

where

$$H_1(\omega_1,\omega_2) = \sum_{n_1=0}^{P_1-1} \sum_{n_2=0}^{P_2-1} a_{n_1 n_2} e^{-j\omega_1 n_1} e^{-j\omega_2 n_2} \quad , \quad a_{00}=1 \tag{2.20}$$

Naturally, it is possible to develop a model assuming other regions of support for the filter coefficients. If we set up the problem assuming that the second quadrant is our region of support, we will get a different answer. Specifically, in terms of Fig. 2.1, let $L_1 = -P_1$ and $L_2 = 0$. Then the second quadrant prediction equation can be written as

$$\hat{x}(n_1,n_2) = -\sum_{j_1=0}^{P_1-1} \sum_{j_2=0}^{P_2-1} b_{j_1 j_2} x(n_1+j_1, n_2-j_2) \quad , \quad (j_1,j_2) \neq (0,0) \tag{2.21}$$

and the Normal equations take the form :

$$\mathbf{R} \,.\, \mathbf{B} = \mathbf{S}_b \tag{2.22}$$

where :

$$\mathbf{B} = \begin{bmatrix} \mathbf{B}^{(0)} \\ \mathbf{B}^{(1)} \\ \cdot \\ \cdot \\ \cdot \\ \mathbf{B}^{(P_1-1)} \end{bmatrix} \tag{2.23a}$$

$$\mathbf{B}^{(i)} = \begin{bmatrix} b_{i,P_2-1} \\ b_{i,P_2-2} \\ \cdot \\ \cdot \\ \cdot \\ b_{i,0} \end{bmatrix} \qquad b_{0,0} = 1 \tag{2.23b}$$

$$\mathbf{S}_b = \begin{bmatrix} \mathbf{S}_b^{(0)} \\ \mathbf{0} \\ \cdot \\ \cdot \\ \cdot \\ \mathbf{0} \end{bmatrix} \tag{2.23c}$$

and

$$\mathbf{S}_b^{(0)} = \begin{bmatrix} 0 \\ \cdot \\ \cdot \\ \cdot \\ 0 \\ \sigma_2^2 \end{bmatrix} \tag{2.23d}$$

and where σ_2^2 is the prediction error variance of the second quadrant model.

The resulting spectral estimate of the second quadrant is

$$S_2(\omega_1,\omega_2) = \frac{\sigma_2^2}{|H_2(\omega_1,\omega_2)|^2} \tag{2.24}$$

where

$$H_2(\omega_1,\omega_2) = \sum_{n_1=0}^{P_1-1} \sum_{n_2=0}^{P_2-1} b_{n_1 n_2} e^{j\omega_1 n_1} e^{-j\omega_2 n_2} \quad , \quad b_{00}=1 \tag{2.25}$$

and is not equal to the spectral estimate of the first quadrant $S_1(\omega_1,\omega_2)$. Jackson and Chien (1979) observed that, in typical cases of estimating sinusoids in noise the spectral estimates of each quadrant were skewed. This is not surprising since the prediction geometry of quadrant plane causal models is too restrictive. To remove the skewness, they suggested designing two quadrant plane models with support on different quadrants and combining them. Their combined estimate can be written as :

$$S(\omega_1,\omega_2) = \frac{1}{\frac{1}{S_1(\omega_1,\omega_2)} + \frac{1}{S_2(\omega_1,\omega_2)}} \tag{2.26}$$

and tends to produce a more symmetric spectral estimate. The specific form (2.26) is important, since Jackson and Chien showed that other symmetric combinations of S_1 and S_2 did not have desirable properties. We will call this model a combined quadrant (CQ) model.

2. Nonsymmetric Half Plane (NSHP) Model

The NSHP model is a very important form, since it is always possible to factor an arbitrary 2-D spectral density into factors with infinite extent NSHP support. While it is not practical in spectral modeling to use very large support regions, NSHP support of modest size has been found to give reasonable results. The infinite region of support α for the general NSHP linear prediction model (also called a causal model) is shown in Fig. 2.2a.

We define an N^{th} order NSHP model to be one with N points above, below, and to the right of the refrence point (i,j) = (0,0). That is, $P_1-1 = P_2-1 = N$ as shown in Figure 2.2b. When $P_1 \neq P_2$ we may also refer to the order of the filter as (P_1-1,P_2-1) order.

Now we consider the problem of finding a NSHP linear prediction model of finite order. Let $x(n_1,n_2)$ represent a stationary zero-mean random process. The linear prediction equation takes the form :

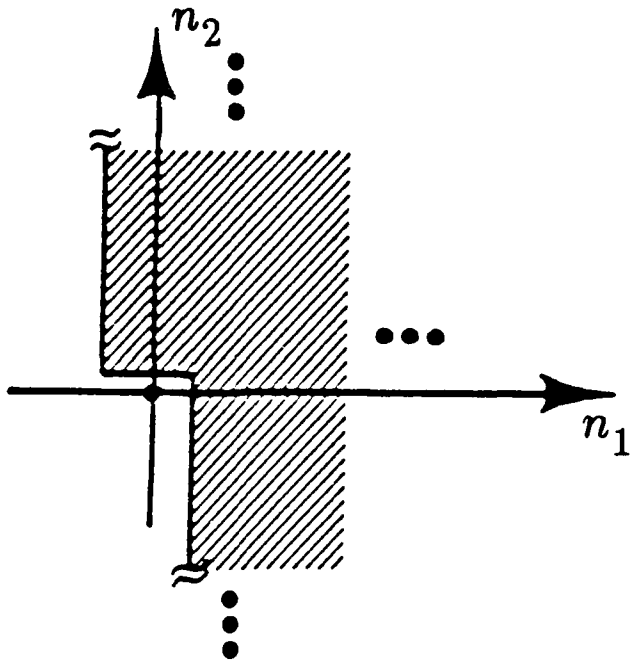

(a) Causal prediction region

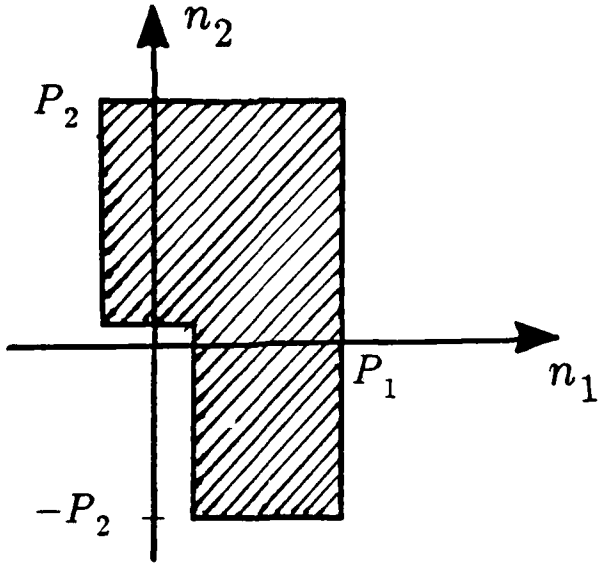

(b) Region of finite support

Fig. 2.2 NSHP region of support .

$$\hat{x}(n_1,n_2) = -\sum_{i_2=1}^{P_2-1} a_{0i_2}\, x(n_1,n_2-i_2) - \sum_{i_1=1}^{P_1-1}\sum_{i_2=-(P_2-1)}^{P_2-1} a_{i_1i_2}\, x(n_1-i_1,n_2-i_2) \qquad (2.27)$$

The corresponding Normal equation is :

$$\mathbf{R} \,.\, \mathbf{A} = \mathbf{S} \qquad (2.28)$$

where **R** represents the correlation matrix, **A** is the filter coefficient vector and **S** is the error variance vector. In this case the Normal equation has the specific form:

$$\begin{bmatrix} \mathbf{R}'(0) & \mathbf{R}'(-1) & \cdots & \mathbf{R}'(-P_1+1) \\ \mathbf{R}'(1) & \mathbf{R}(0) & \cdots & \mathbf{R}(-P_1+2) \\ \cdot & \cdot & & \cdot \\ \cdot & \cdot & & \cdot \\ \cdot & \cdot & & \cdot \\ \mathbf{R}'(P_1-1) & \mathbf{R}(P_1-2) & \cdots & \mathbf{R}(0) \end{bmatrix} \begin{bmatrix} \mathbf{A}'^{(0)} \\ \mathbf{A}^{(1)} \\ \cdot \\ \cdot \\ \cdot \\ \mathbf{A}^{(P_1-1)} \end{bmatrix} = \begin{bmatrix} \mathbf{S}'^{(0)} \\ \mathbf{0} \\ \cdot \\ \cdot \\ \cdot \\ \mathbf{0} \end{bmatrix} \qquad (2.29)$$

where

$$\mathbf{R}(k) = \mathbf{R}(-k) = \begin{bmatrix} R(k,0) & R(k,-1) & \cdots & R(k,-2P_2+1) \\ R(k,1) & R(k,0) & \cdots & R(k,-2P_2+2) \\ \cdot & \cdot & & \cdot \\ \cdot & \cdot & & \cdot \\ \cdot & \cdot & & \cdot \\ R(k,2P_2-1) & R(k,2P_2-2) & \cdots & R(k,0) \end{bmatrix} \qquad (2.30a)$$

$$\mathbf{A}^{(k)} = \begin{bmatrix} a_{k,-P_2+1} \\ a_{k,-P_2+2} \\ \cdot \\ a_{k,0} \\ \cdot \\ a_{k,P_2-1} \end{bmatrix} \quad , \quad k \neq 0 \qquad (2.30b)$$

$$\mathbf{R}'(k) = \mathbf{R}'(-k) = \begin{bmatrix} R(k,P_2-1) & R(k,P_2-2) & \cdots & R(k,-P_2+1) \\ R(k,P_2) & R(k,0) & \cdots & R(k,-P_2+2) \\ \cdot & \cdot & & \cdot \\ \cdot & \cdot & & \cdot \\ \cdot & \cdot & & \cdot \\ R(k,2P_2-1) & R(k,2P_2-2) & \cdots & R(k,0) \end{bmatrix} \tag{2.30c}$$

and

$$\mathbf{R}'(0) = \begin{bmatrix} R(0,0) & R(0,-1) & \cdots & R(0,-P_2+1) \\ R(0,1) & R(0,0) & \cdots & R(0,-P_2+2) \\ \cdot & \cdot & & \cdot \\ \cdot & \cdot & & \cdot \\ \cdot & \cdot & & \cdot \\ R(0,P_2-1) & R(0,P_2-2) & \cdots & R(0,0) \end{bmatrix} \tag{2.30d}$$

$$\mathbf{A}'^{(0)} = \begin{bmatrix} a_{0,0} \\ a_{0,1} \\ \cdot \\ \cdot \\ \cdot \\ a_{0,P_2-1} \end{bmatrix} \tag{2.30e}$$

$$\mathbf{S}'^{(0)} = \begin{bmatrix} \sigma_\varepsilon^2 \\ \mathbf{0} \\ \cdot \\ \cdot \\ \cdot \\ \mathbf{0} \end{bmatrix} \tag{2.30f}$$

and where

$$a_{0,0} = 1 \tag{2.30g}$$

$$\sigma_\varepsilon^2 = E\left[(x-\hat{x})^2\right] \tag{2.30h}$$

Note that $R(k_1,k_2)$ is the 2-D autocorrelation function for the data defined by Eqn. (2.15) and σ_ε^2 is the prediction error variance. The spectral estimate resulting from the NSHP model is given by:

$$S(z_1,z_2) = \frac{\sigma_\varepsilon^2}{|H(z_1,z_2)|^2} \tag{2.31}$$

where

$$H(z_1,z_2) = 1 + \sum_{i_2=1}^{P_2-1} a_{0i_2} z_2^{-i_2} + \sum_{i_1=1}^{P_1-1} \sum_{i_2=-(P_2-1)}^{P_2-1} a_{i_1 i_2} z_1^{-i_1} z_2^{-i_2} \tag{2.32}$$

It is of interest to study the behaviour of the AR spectral estimation algorithms, and compare the results with those of Fourier transform techniques. A sinusoidal signal plus white noise $w(n_1,n_2)$ has been investigated as a test example. Assume our process is :

$$x(n_1,n_2) = \sum_{i=1}^{L} \cos(n_1\omega_{i1} + n_2\omega_{i2}) + w(n_1,n_2) \tag{2.33}$$

where $w(n_1,n_2)$, is a zero mean independent white noise signal, and L represents the number of sinusoids. Estimates were computed for a dataset size of 16×16 with L=2, $\omega_{11}=\omega_{12}=\frac{\pi}{2}$, and $\omega_{21}=\omega_{22}=\frac{\pi}{3}$. Figure 2.3 shows the NSHP and CQ spectral estimates. The location of the peaks are in the correct place and there is good resolution. Fig. 2.4 shows the result of power spectral estimation on the same data applying both correlelogram and periodogram techniques. Comparison of Figs. 2.3 and 2.4, shows that the NSHP and CQ models have significantly higher resolution than the Fourier transform techniques.

D. LATTICE STRUCTURE

The key step in parametric spectral estimation is the computation of the parameters of the model. Least square estimation of model parameters (in the AR case) is one approach and requires the solution of a set of linear equations involving the sample covariance matrix. Another approach that has many advantages in 1-D is to represent the

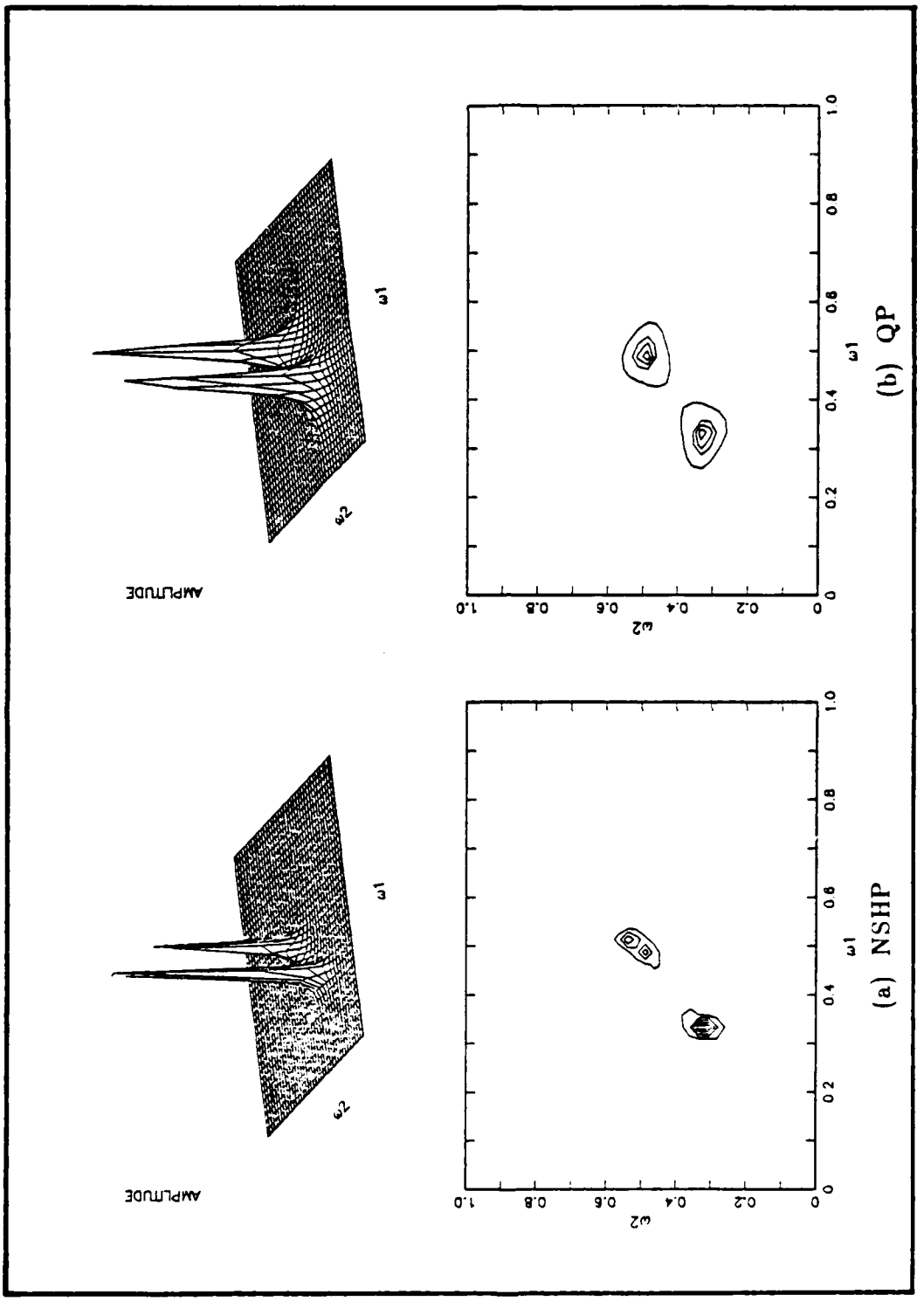

Fig. 2.3 Power spectral estimation of two sinusoids (NSHP, QP)

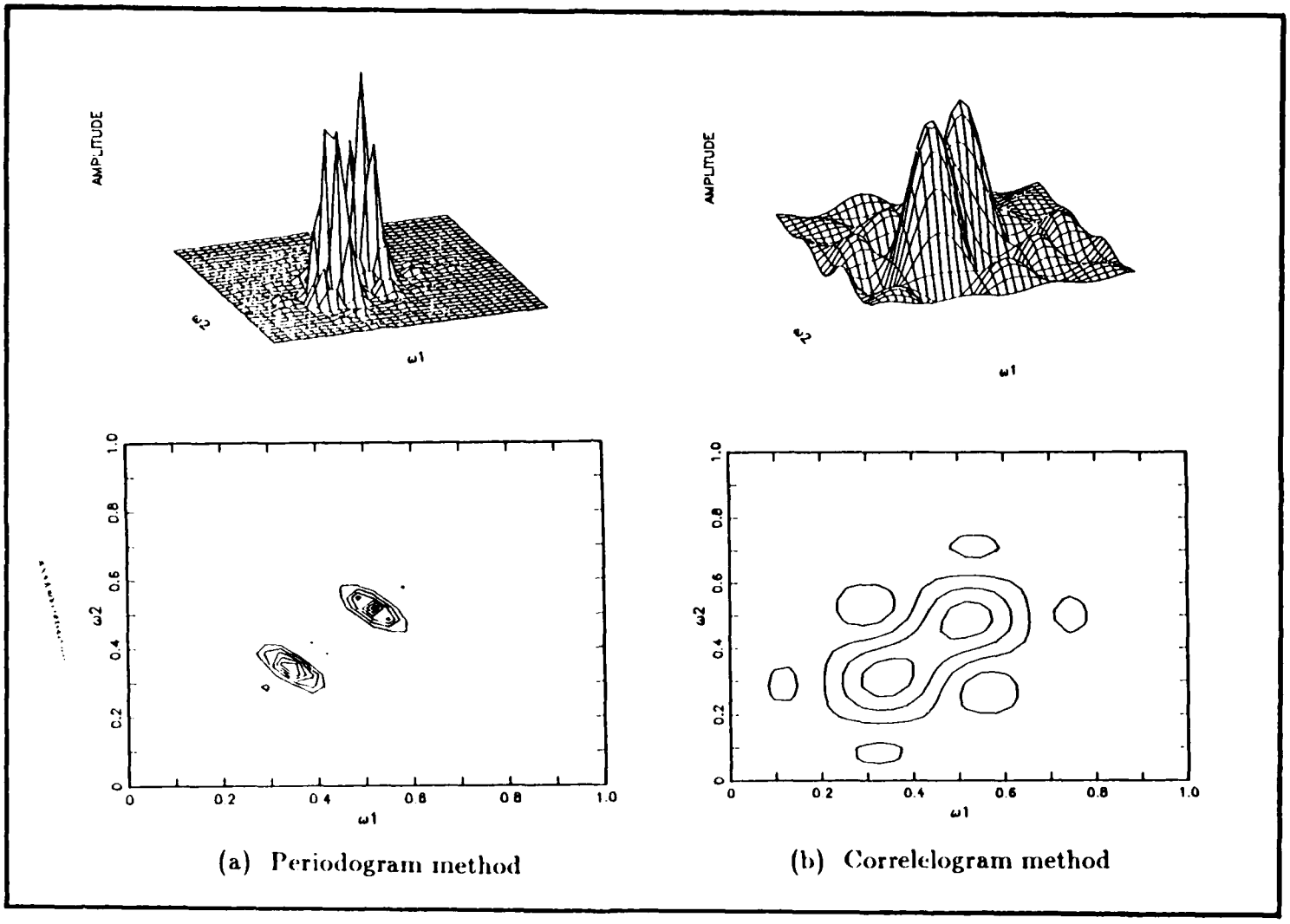

(a) Periodogram method

(b) Correlelogram method

Fig. 2.4 Power spectral estimation of two sinusoids (conventional methods).

model in terms of a finite number of reflection coefficients which are chosen to obtain a good fit between the whitening filter model and the data. The realization of the filter is then in the form of a lattice structure.

In 2-D there has been no direct counterpart to the lattice structure of the prediction filter that exists in 1-D. Marzetta (1978), however developed a set of 2-D reflection coefficients. In his approach the available data is used to estimate the 2-D autocorrelation function to a finite lag, and then the estimated autocorrelation function is used to compute the reflection coefficients which determine the whitening filter $\hat{H}(z_1,z_2)$. This is similar to what is done in 1-D.

Given a lattice structure in 2-D, another approach for choosing the reflection coefficients is analogous to the Burg algorithm. Estimates of the filter parameters as obtained directly from the data, and the lattice structure can be formed from the forward and backward predictions. Fig. 2.5 depicts L lattice sections connected in cascade. The input to the system is $x(n_1,n_2)$ and the two outputs equal forward and backward prediction errors at step L. The initial values of the forward and backward prediction errors of model order (0,0) are given by:

$$x(n_1,n_2) = e^{(0,0)}(n_1,n_2) = e^{\prime(0,0)}(n_1,n_2) \tag{2.34}$$

Parker and Kayran (1984) developed a different kind of lattice representation in 2-D. Their initial development was done for quadrant-based models but since their representation is neither a true whitening filter nor an optimal least squares prediction filter, we will not pursue it further here. Marzetta's method is outlined briefly below.

1. 2-D Levinson Algorithm (Marzetta)

Marzetta proposed a 2-D Levinson algorithm for the 2-D case which has the same structure as 1-D Levinson recursion. Suppose that we have a positive definite autocorrelation sequence : $\left\{ R(k,l);\ (0,0)\leq(k,l)\leq(N,M) \right\}$ and assume that we know the solution to the Normal equations for : $H^{(n,m-1)}(z_1,z_2)$ and the optimum mean square error $P^{(n,m-1)}$ for the order (n,m-1). Then the solution for $H^{(n,m)}(z_1,z_2)$ and $P^{(n,m)}$ are given by (Marzetta,1978,1979,1980):

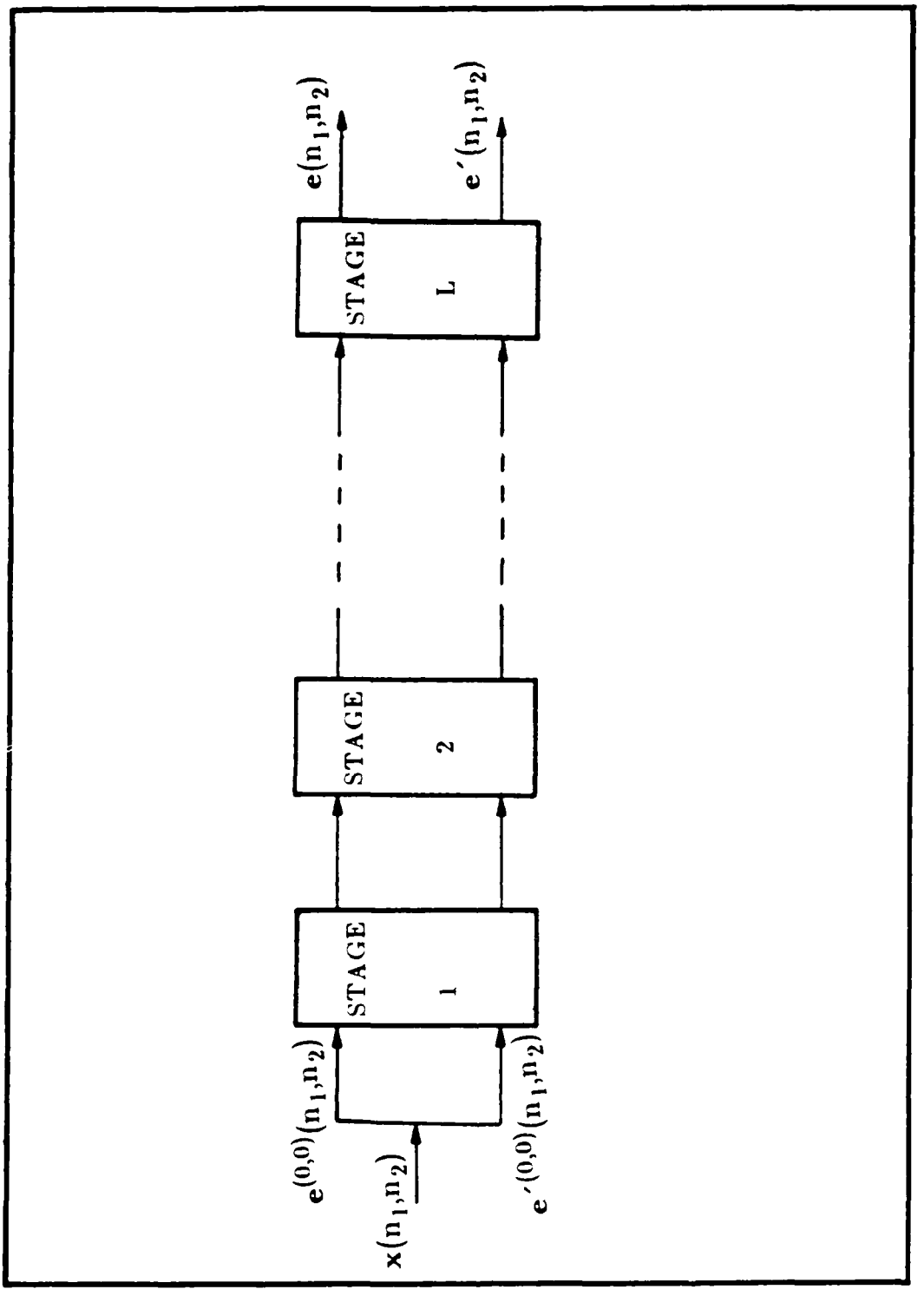

Fig. 2.5 2-D Lattice structure.

$$H^{(n,m)}(z_1,z_2) = H^{(n,m-1)}(z_1,z_2) - K^{(n,m)}.z_1^{-n}.z_2^{-m}.H^{(n,m-1)}(z_1^{-1},z_2^{-1}) \qquad (2.35)$$

and :

$$P^{(n,m)} = P^{(n,m-1)}\left[1 - \left[K^{(n,m)}\right]^2\right] \qquad (2.36)$$

where $K^{(n,m)};(n=0,\ 1\le m\le M),\ (1\le n\le N,\ -M\le m\le M)$ is the 2-D reflection coefficient sequence, and where N and M are positive integers that represent the order of the filter. The 2-D reflection coefficients are defined by

$$K^{(n,m)} = \frac{1}{P^{(n,m-1)}} E\left\{\left[x(n_1,n_2) - \sum_{(k_1,k_2)}\sum a^{(n,m-1)}(k_1,k_2)x(n_1-k_1,n_2-k_2)\right]\right.$$

$$\left.\left[x(n_1-n,n_2-m) - \sum_{(k_1,k_2)}\sum a^{(n,m-1)}(k_1,k_2)\,x(n_1-n+k_1,n_2-m+k_2)\right]\right\}$$

$$= \frac{1}{P^{(n,m-1)}}\left[R(n,m) - \sum_{(k_1,k_2)}\sum a^{(n,m-1)}(k_1,k_2)\,R(n-k_1,m-k_2)\right] \qquad (2.37)$$

The idea of a 2-D Levinson algorithm is to get the prediction error filter $H^{(N,M)}(z_1,z_2)$ from these reflection coefficients by recursively computing a sequence of 2-D finite order prediction error filters, $H^{(n,m)}(z_1,z_2)$.

Marzetta (1978) defined a 2-D stable, linear, shift-invariant filter to be one whose unit sample response is absolutely summable and defined a 2-D minimum phase filter to be a 2-D, causal, stable, linear shift-invariant filter which has a causal, stable inverse. In this case he proved that if $H^{(n,m-1)}(z_1,z_2)$ is analytic minimum phase, then $H^{(n,m)}(z_1,z_2)$ as defined by Eqn. (2.35) is also analytic minimum phase. He defined a 2-D filter to be analytic minimum phase if the filter is minimum phase and also analytic in some neighborhood of the unit bicircle.

2. Marzetta Approach and Burg Algorithm

Marzetta's (1979) approach to designing the 2-D all pole recursive filter, is to represent the denominator polynomial of the filter in terms of a finite set of 2-D reflection coefficients which are chosen to provide a good estimate of the desired power spectrum.

His algorithm is simply the 2-D Levinson algorithm, used under the assumption that the true reflection coefficient sequence $K^{(n,m)}$, vanishes for : $\left\{0 \le n \le N-1,\ |m| > M\right\}$ and $\left\{n = N,\ m < -M\right\}$. He showed that to preserve the minimum phase property required an infinite set of reflection coefficients defined on the " *continuous support* " region shown in Figure 2.6. Let $\left\{a(n_1,n_2),\ 0 \le n_1 \le N,\ 0 \le n_2 \le M,\ (n_1,n_2) \ne (0,0)\right\}$ be a set of 2-D FIR filter coefficients, for a NSHP filter with finite support. Then

$$H^{(N,M)}(z_1,z_2) = 1 - \sum_{n_1=0}^{N} \sum_{n_2=0}^{M} a(n_1,n_2)\, z_1^{-n_1} z_2^{-n_2} \quad , \quad (n_1,n_2) \ne (0,0) \tag{2.38}$$

Marzetta showed that although a finite-extent sequence $\left\{a(n_1,n_2)\right\}$ results in an infinite sequence of reflection coefficients, fortunately the converse of this result is not true. If a polynomial is defined by a finite sequence of reflection coefficients $K^{(n,m)}$, that polynomial will still have finite degree. Furthermore, if $|K^{(n,m)}| < 1$ for all (n,m), that polynomial will have minimum phase. The polynomial can be found from the reflection coefficients $K^{(n,m)}$ by means of the following recursion: Starting with the n=0 column, and with the initial condition:

$$H^{(0,0)}(z_1,z_2) = 1 \tag{2.39}$$

then $H^{(n,m)}(z_1,z_2)$ for $(1 \le m \le M)$ can be written as

$$H^{(n,m)}(z_1,z_2) = H^{(n,m-1)}(z_1,z_2) - K^{(n,m)}\, z_1^{-n}\, z_2^{-m} H^{(n,m-1)}(z_1^{-1},z_2^{-1}) \tag{2.40}$$

Then shifting to the next column i.e. $(n > 0,\ -M \le m \le M)$ and starting with the boundary condition:

$$H^{(n,-(M+1))}(z_1,z_2) = H^{(n-1,M)}(z_1,z_2) \tag{2.41}$$

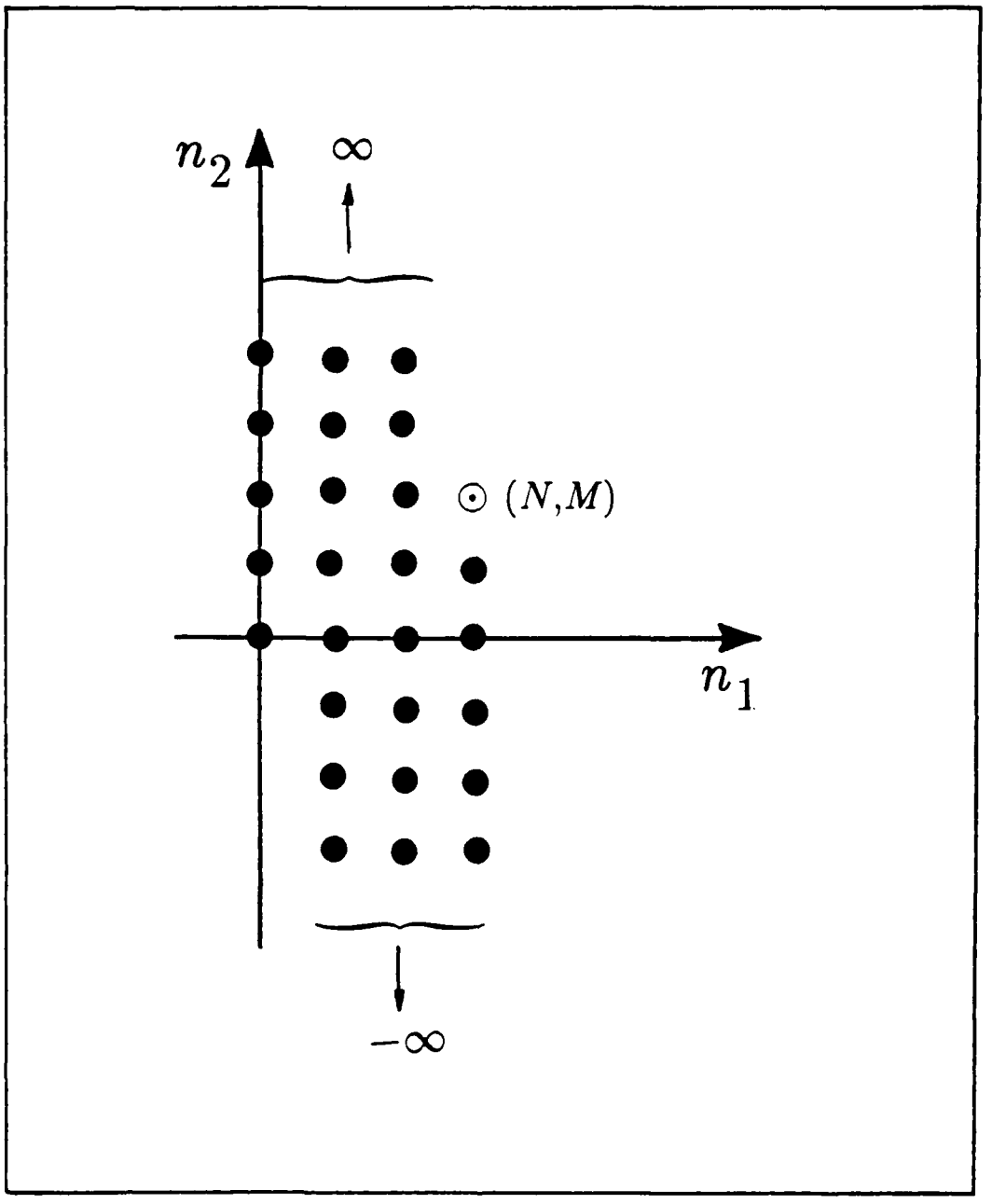

Fig. 2.6 Region of continous support.

this recursion is repeated for all values of (n,m) for which $K^{(n,m)} \neq 0$. It can be shown (Marzetta,1978) that the value of $K^{(n,m)}$ which minimizes the new prediction error, $P^{(n,m)}$ is :

$$K^{(n,m)} = \frac{1}{P^{(n,m-1)}} \left[R(n,m) - \sum_{(k_1,k_2)} \sum h^{*2(n,m-1)}(k_1,k_2) R(n-k_1, m-k_2) \right] \quad (2.42)$$

where :

$$H^{2(n,m-1)}(z_1,z_2) = 1 - \sum_{(k_1,k_2)} \sum h^{*2(n,m-1)}(k_1,k_2) z_1^{-k_1} z_2^{-k_2} \quad (2.43)$$

The new prediction error is then :

$$P^{(n,m)} = P^{(n,m-1)} \left[1 - \left[K^{(n,m)} \right]^2 \right] \quad (2.44)$$

It can further be shown that the magnitude of $K^{(n,m)}$ is always less than one.

Burg developed an algorithm for estimating 1-D prediction coefficients directly from the data (Burg,1967,1968,1975). Burg makes no assumption about the univariate data except that the signal is treated as a stationary random process. No estimation of the autocorrelation function is required in this algorithm.

Marzetta made the suggestion to extend the 1-D Burg algorithm to 2-D (details are given in Appendix A) but so far no one in the literature has tried to test the 2-D Burg algorithm. We have done this however and we will illustrate here an example to study the behaviour of the estimating algorithm. In this example the estimated power spectrum is computed by combining forward and backward estimates in a manner similar to the combined quadrant technique. Consider a signal consisting of sinusoids in additive noise as given in Equation (2.33). The results are shown for the cases of one sinusoid and two sinusoids. In case of one sinusoid (L=1) the estimated power spectrum is given for a dataset size of 64×64 and frequency values of $\omega_{11} = \omega_{12} = \pi/2$. A third order model is used. Figure 2.7a shows the results of the forward NSHP model, while the backward NSHP model results are shown in Figure 2.7b. It is clear that using either the forward or the backward NSHP models alone results in a spreading of the peak in one direction.

The combined estimate using both forward and backward models gives a more accurate result as shown in Fig. 2.7c.

In the second example the results are shown for the case of two-sinusoids (L=2), with $\omega_{11} = \omega_{12} = \omega_{22} = \pi/2$ and $\omega_{21} = \pi/5$. This results are compared with the results of the AR (NSHP) model for the same test case. Figure 2.8a shows the results of the combined forward and backward NSHP Burg technique, while Fig. 2.8b shows the results of the AR model. A third order model is used in both cases. This example shows the high resolution properties of the AR relative to Burg technique. We have examined many different examples, with different choices of the peak positions, we observed that AR model has consistently better resolution properties than Burg algorithm.

E. 2-D DIRECT METHOD OF SPECTRAL ESTIMATION

Therrien (1981) pointed out that, there exists a close relation between 2-D linear prediction problems and multichannel 1-D linear prediction problems. He suggested a procedure for solving 2-D normal equation by relating the 2-D linear prediction problem to a multichannel linear prediction problem and applying the multichannel Levinson recursion. These results can be used to formulate a method for estimating the 2-D model parameters without explicit prior estimation of the correlation function and we will refer to it as a *direct* method. The procedure can be summarized briefly as follows: Consider a 2-D stationary zero-mean random process $x(n_1,n_2)$ defined over a rectangular support region. The linear prediction equation is of the form:

$$\hat{x}(n_1,n_2) = -\sum_{i_1=0}^{P_1-1}\sum_{i_2=0}^{P_2-1} a_{i_1 i_2} x(n_1-i_1,n_2-i_2) \quad , \quad (i_1,i_2)\neq(0,0) \tag{2.45}$$

The corresponding Normal equation is given by Eqn. (2.17) but repeated here for convenience

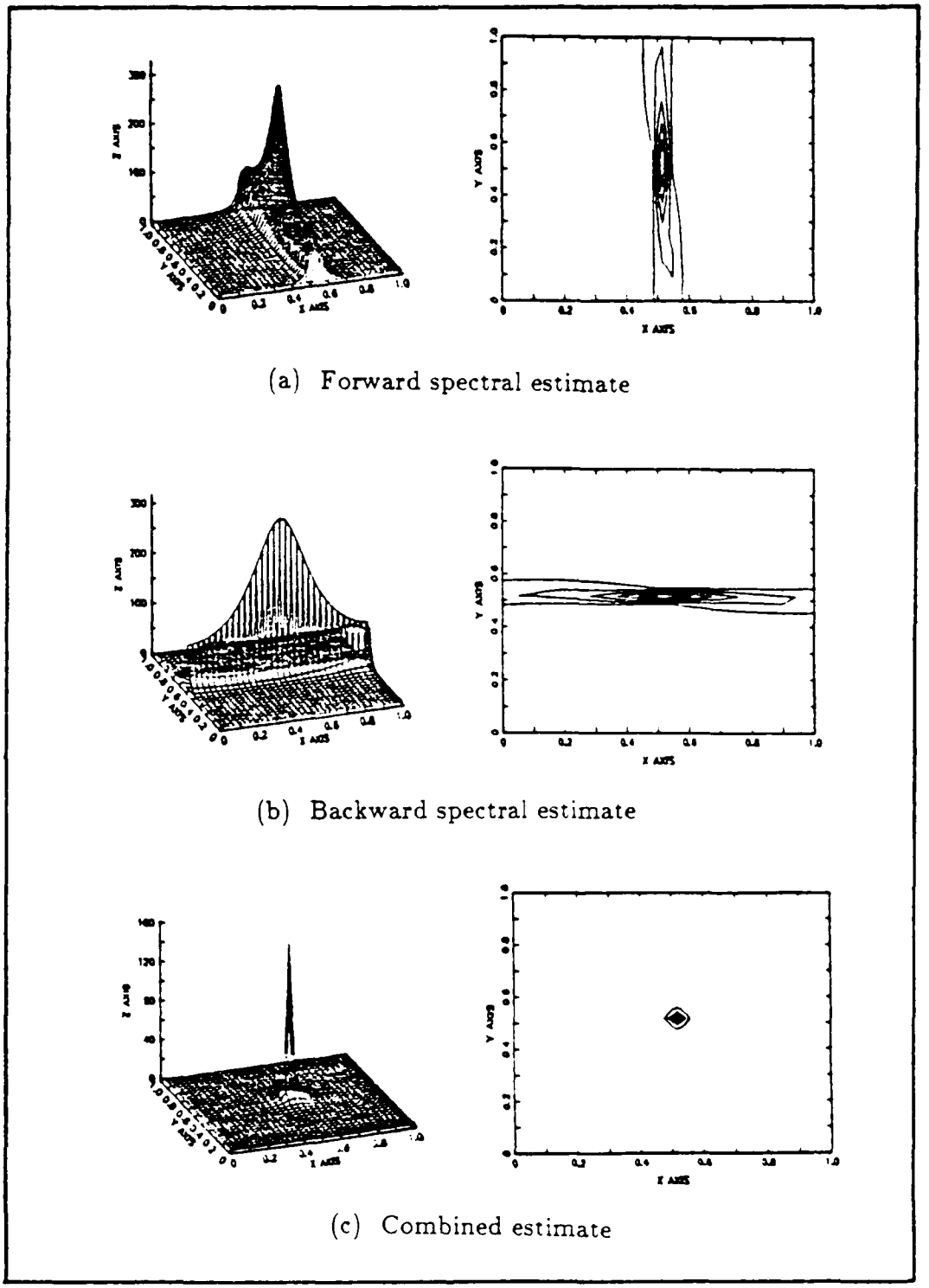

(a) Forward spectral estimate

(b) Backward spectral estimate

(c) Combined estimate

Fig. 2.7 Forward, backward, and combined spectral estimates applying 2-D Burg technique.

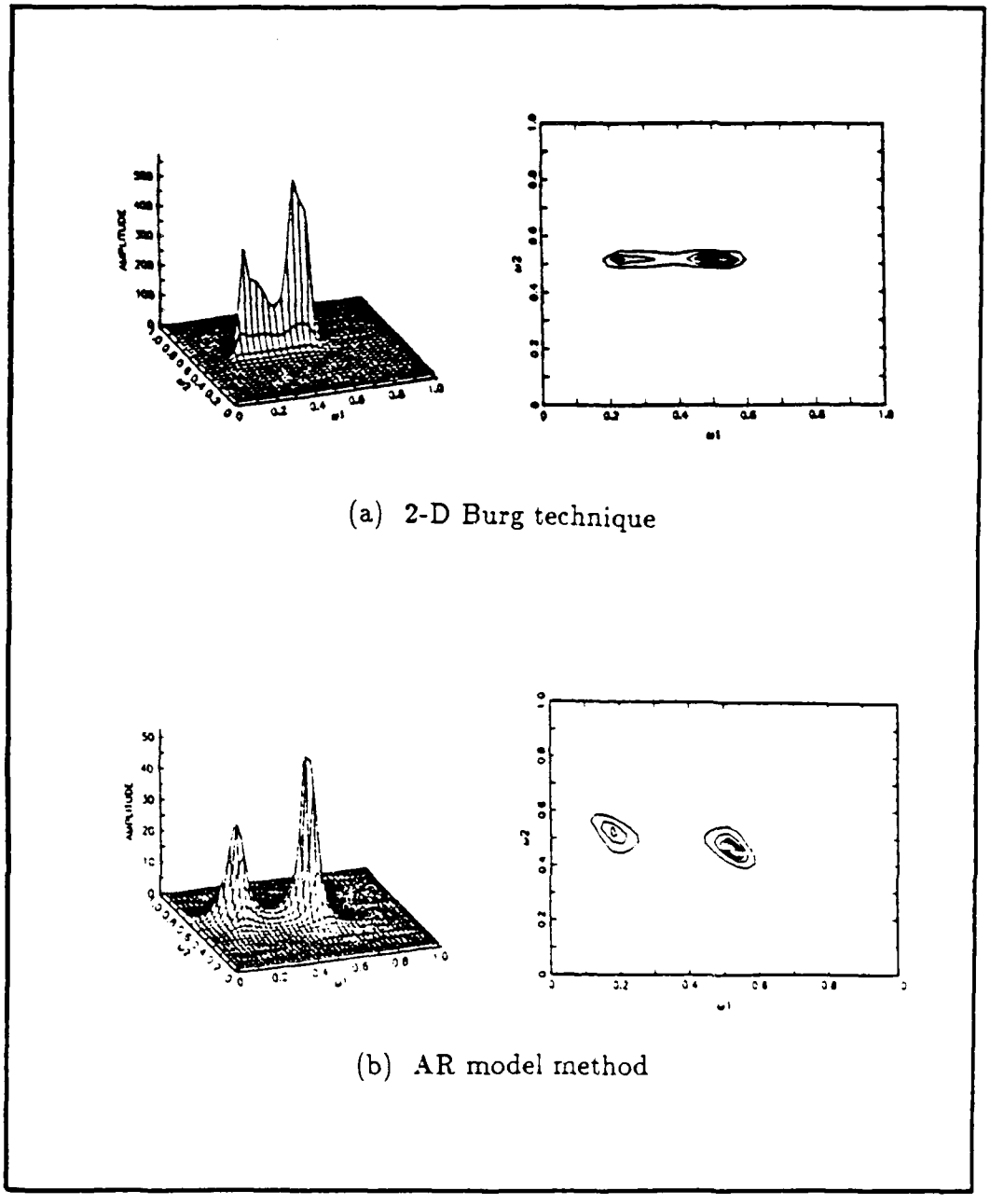

(a) 2-D Burg technique

(b) AR model method

Fig. 2.8 Estimation of two-sinusoids in noise (Burg.AR).

$$\begin{bmatrix} \mathbf{R}(0) & \mathbf{R}(-1) & \cdots & \mathbf{R}(-P_1+1) \\ \mathbf{R}(1) & \mathbf{R}(0) & \cdots & \mathbf{R}(-P_1+2) \\ \cdot & \cdot & & \cdot \\ \cdot & \cdot & & \cdot \\ \cdot & \cdot & & \cdot \\ \mathbf{R}(P_1-1) & \mathbf{R}(P_1-2) & \cdots & \mathbf{R}(0) \end{bmatrix} \begin{bmatrix} \mathbf{A}^{(0)} \\ \mathbf{A}^{(1)} \\ \cdot \\ \cdot \\ \cdot \\ \mathbf{A}^{(P_1-1)} \end{bmatrix} = \begin{bmatrix} \mathbf{S}^{(0)} \\ \mathbf{0} \\ \cdot \\ \cdot \\ \cdot \\ \mathbf{0} \end{bmatrix} \tag{2.46}$$

where

$$\mathbf{A}^{(k)} = \begin{bmatrix} a_{k,0} \\ a_{k,1} \\ \cdot \\ \cdot \\ \cdot \\ a_{k,P_1-1} \end{bmatrix} \tag{2.47a}$$

and where

$$\mathbf{S}^{(0)} = \begin{bmatrix} \sigma^2 \\ \mathbf{0} \\ \cdot \\ \cdot \\ \cdot \\ \mathbf{0} \end{bmatrix} \tag{2.47b}$$

where σ^2 represents the variance of the error resulting from optimal linear prediction.

If the data is represented as a vector

$$\mathbf{x_n} = \begin{bmatrix} x(n,0) \\ x(n,1) \\ \cdot \\ \cdot \\ \cdot \\ x(n,P_2-1) \end{bmatrix} \tag{2.48}$$

then the vector $\mathbf{x_n}$ can be considered as consisting of the components of a 1-D *multichannel* random process evolving in the n direction. A corresponding 1-D P_2- channel linear prediction problem can be written as

$$\hat{\mathbf{x}}_n = -\sum_{i=1}^{P_1-1} \left[\boldsymbol{\alpha}^i\right]^T \mathbf{x}_{n-i} \tag{2.49}$$

where $\boldsymbol{\alpha}^{(i)}$ are a set of matrix coefficients.

$$\boldsymbol{\alpha}^{(i)} = \begin{bmatrix} \alpha_{00}^{(i)} & \alpha_{01}^{(i)} & \cdots & \alpha_{0,P_2-1}^{(i)} \\ \alpha_{10}^{(i)} & \alpha_{11}^{(i)} & \cdots & \alpha_{1,P_2-1}^{(i)} \\ \cdot & \cdot & & \cdot \\ \cdot & \cdot & & \cdot \\ \cdot & \cdot & & \cdot \\ \alpha_{P_2-1,0}^{(i)} & \alpha_{P_2-1,1}^{(i)} & \cdots & \alpha_{P_2-1,P_2-1}^{(i)} \end{bmatrix} \tag{2.50}$$

The values of the $\boldsymbol{\alpha}^{(i)}$ are found by solving a set of Normal equations

$$\begin{bmatrix} \mathbf{R}(0) & \mathbf{R}(-1) & \cdots & \mathbf{R}(-P_1+1) \\ \mathbf{R}(1) & \mathbf{R}(0) & \cdots & \mathbf{R}(-P_1+2) \\ \cdot & \cdot & & \cdot \\ \cdot & \cdot & & \cdot \\ \cdot & \cdot & & \cdot \\ \mathbf{R}(P_1-1) & \mathbf{R}(P_1-2) & \cdots & \mathbf{R}(0) \end{bmatrix} \begin{bmatrix} \mathbf{I} \\ \boldsymbol{\alpha}^{(1)} \\ \cdot \\ \cdot \\ \cdot \\ \boldsymbol{\alpha}^{(P_1-1)} \end{bmatrix} = \begin{bmatrix} \mathbf{E}_{P_1} \\ \mathbf{0} \\ \cdot \\ \cdot \\ \cdot \\ \mathbf{0} \end{bmatrix} \tag{2.51}$$

where $\mathbf{E}_{P_1}$ is the error covariance of the optimal estimate.

$$\mathbf{E}_{P_1} = E\left[(\mathbf{x}_n - \hat{\mathbf{x}}_n)(\mathbf{x}_n - \hat{\mathbf{x}}_n)^T\right] \tag{2.52}$$

By comparing Equation (2.46) and Equation (2.51) we note that if we define $\mathbf{S}^{(0)}$ such that

$$\mathbf{S}^{(0)} = \mathbf{E}_{P_1} \mathbf{A}^{(0)} \tag{2.53a}$$

then the 2-D coefficients can be computed from

$$\mathbf{A}^{(i)} = \boldsymbol{\alpha}^{(i)}\,\mathbf{A}^{(0)} \quad , \quad i=1,2, \cdots P_1-1 \tag{2.53b}$$

The multichannel Levinson recursion (see Appendix B) can be used to solve for the $\boldsymbol{\alpha}^{(i)}$ and $\mathbf{E}_{P_1}$. Then Eqn. (2.53) can be used to solve for $\mathbf{A}^{(i)}$ and σ^2. That is, one first solves Eqn. (2.53a) for $\mathbf{A}^{(0)}$ and $\mathbf{S}^{(0)}$, then applies Eqn. (2.53b) to compute the remaining $\mathbf{A}^{(i)}$. The multichannel Levinson recursion computes both the calculation of the *forward and backward* multichannel linear prediction parameters simultaneously. The backward parameters relate to the second quadrant 2-D filter parameters in a similar manner and thus can be computed from equations analogous to Eqn. (2.53). The parameters of the first and third quadrant filters are identical. The second and fourth filter parameters are also identical.

Now instead of using the covariance matrix in the multichannel Levinson recursion to solve for the $\boldsymbol{\alpha}^{(i)}$ and $\mathbf{E}_{P_1}$, we apply the multichannel form of the Burg technique to calculate the parameters directly from the given data. Explicit forms of the Burg method for the 1-D multichannel case were developed separately by Nuttall (1976) and Strand (1977) and the procedure is sometimes called the Nuttal-Strand algorithm (Appendix C). Then application of Eqn. (2.53) gives a method for estimating the 2-D parameters directly from the data.

The power spectral estimation results of this technique are compared with the results of estimation by first estimating the correlation function. Our method for estimating the model parameters is as follows. Suppose we are given an array of 2-D data of size N_1 - columns and N_2 - rows as shown in Fig. 2.9a. Suppose this array is divided into L-sectors, each sector is a subarray of size M by N_1 ($M = P_2$), as shown in Fig. 2.9b. The 2-D data set $x(n_1,n_2)$ is mapped into a 1-D M-channel data vector $\mathbf{x}(k)$ by concatenating the sectors as shown in Fig. 2.9c.

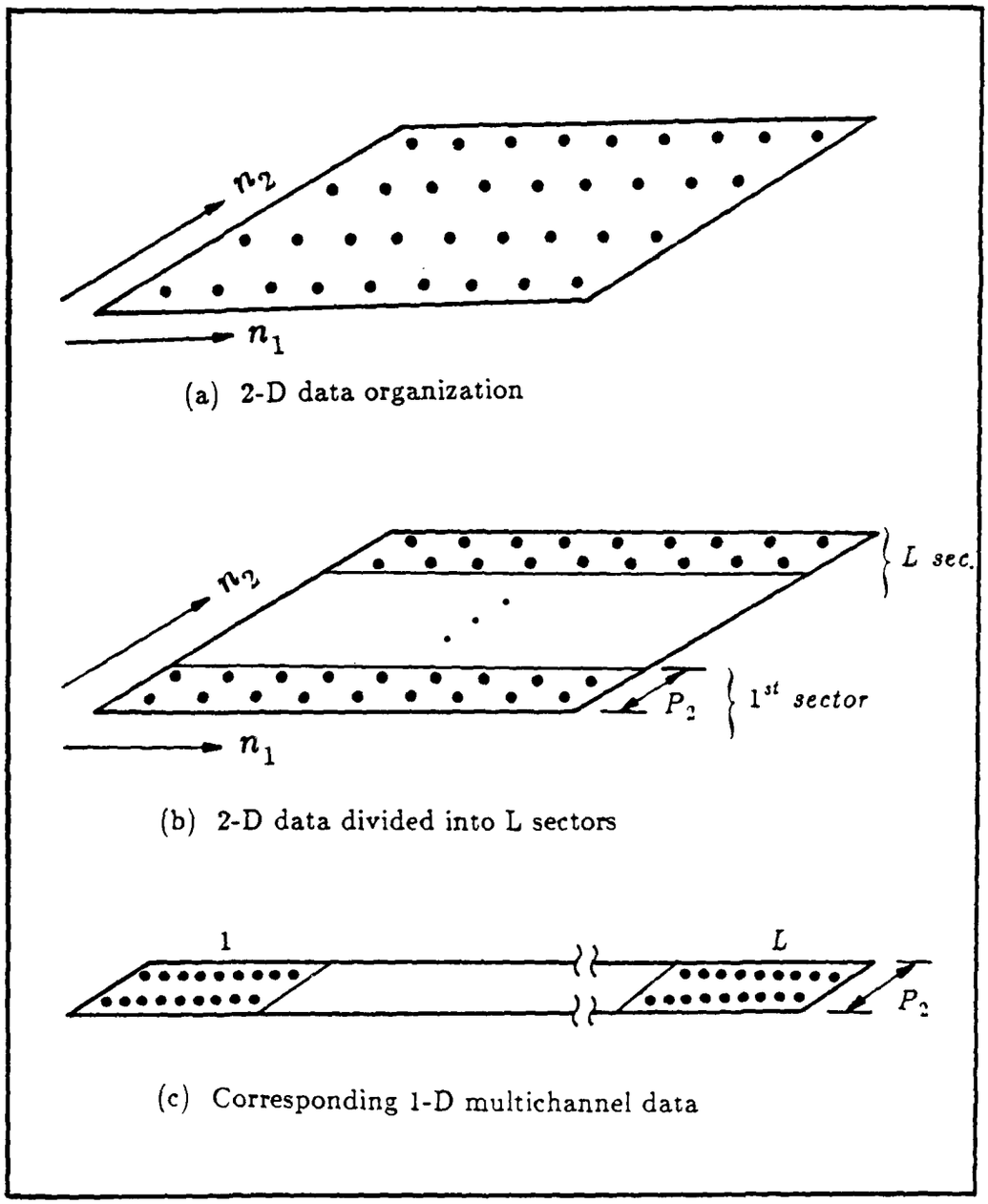

Fig. 2.9 Sectioning 2-D data for the direct method.

$$\mathbf{x}(k) = \begin{bmatrix} x_1(k) \\ x_2(k) \\ \cdot \\ \cdot \\ \cdot \\ x_M(k) \end{bmatrix} \tag{2.54}$$

Discontinuities of course exist at the points of concatenation but in practice these are not troublesome. By applying the multichannel Burg algorithm (Appendix C) to this 1-D multichannel data set we compute the estimated values of the filter coefficients $\alpha^{(i)}$ and also the error covariance matrix $\mathbf{E}_{P_1}$. Then the 2-D parameters ($\mathbf{A}^{(i)}$ and σ^2) can be obtained from Equations (2.53a) and (2.53b).

Since the method estimates both the forward and backward multichannel parameters we have the 2-D filter coefficients for first and second quadrant model and we can finally estimate these power spectra as

$$S_1(\omega_1,\omega_2) = \frac{\sigma_1^2}{|H_1(\omega_1,\omega_2)|^2} \tag{2.55a}$$

and

$$S_2(\omega_1,\omega_2) = \frac{\sigma_2^2}{|H_2(\omega_1,\omega_2)|^2} \tag{2.55b}$$

where the parameters are defined as in section C. Then the CQ power spectrum estimate can be obtained by using Equation (2.26). We called this method the *direct* CQ method.

It is of interest to study the behaviour of the CQ algorithm when the model parameters are obtained by estimating the correlation function and solving the Normal equations, and compare the results with the case where the parameters are obtained directly from the given data by using the new algorithm. The performance of the two algorithms for two sinusoids in white noise has been investigated. Suppose a 2-D random process $x(n_1,n_2)$ is defined by

$$x(n_1,n_2) = \sum_{i=1}^{2} C_i \cos(n_1\omega_{i_1} + n_2\omega_{i_2}) + w(n_1,n_2) \qquad (2.56)$$

A dataset of (64×64) data points is considered here, with the parameters $\omega_{11} = \omega_{12} = \frac{\pi}{2}$, $\omega_{21} = \omega_{22} = \frac{\pi}{3}$, and $C_1 = C_2 = 4$. Two methods are used to compute the power spectral estimation. In the first case the 1-D multichannel filter parameters are computed from the prior estimated autocorrelation function, while in the second case the parameters are computed directly from the data (CQ direct method).

The effect of model order is also illustrated here, by considering three different filter orders. First order model results are shown in Fig. 2.10. In both techniques the resolution of the first order model is poor and only one peak appears. Fig. 2.11 shows the results of computed spectra for the second order model; the resolution in this case increases and the two peaks appear. Finally Fig. 2.12 shows the results of power spectral estimation using third order models. It is clear that the resolution is high and the peaks are very close to the correct peak locations. Comparing the results of the two techniques, we find that somewhat better resolution results are obtained for direct CQ technique. It will be seen later that this is consistently true for the direct method. Also we observe that, generally for both techniques, the resolution increases with increasing order of the filter.

F. DISTANCE MEASURES BETWEEN RANDOM PROCESSES

In problems of communication and radar, the optimum signals (for purposes of detection) are those that minimize the probability of error. However in many cases, direct minimization of the probability of error to determine an optimum signal set is impossible. Since an explicit analytical expression for the error probability may be too difficult to find it is useful to search for signal selection criteria that although weaker than the error probability are easier to evaluate and manipulate. In the search for suitable criteria, the notion of a distance between two probability distributions is quite useful. One such

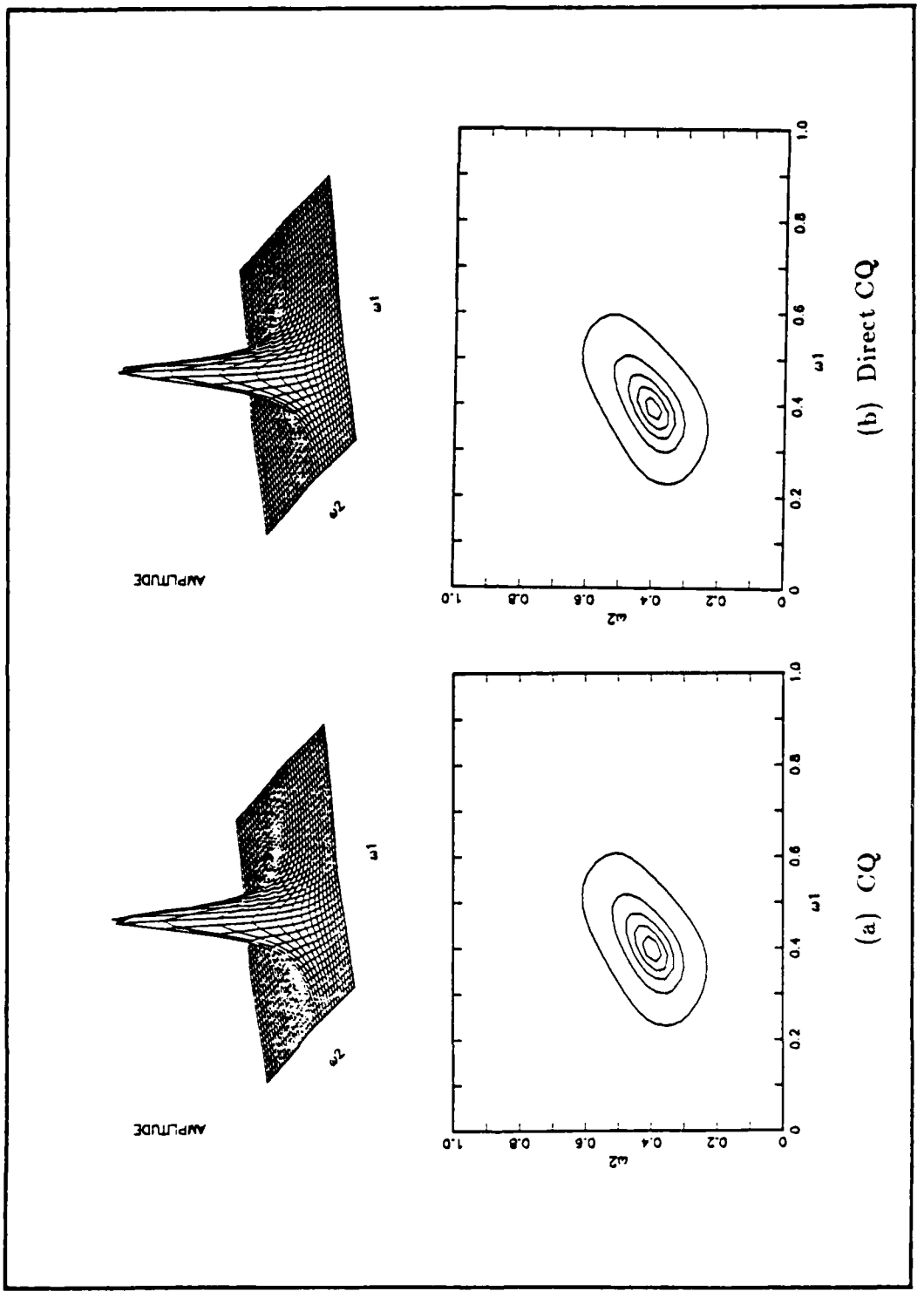

(a) CQ (b) Direct CQ

Fig. 2.10 Spectral estimation of two sinusoids (first order).

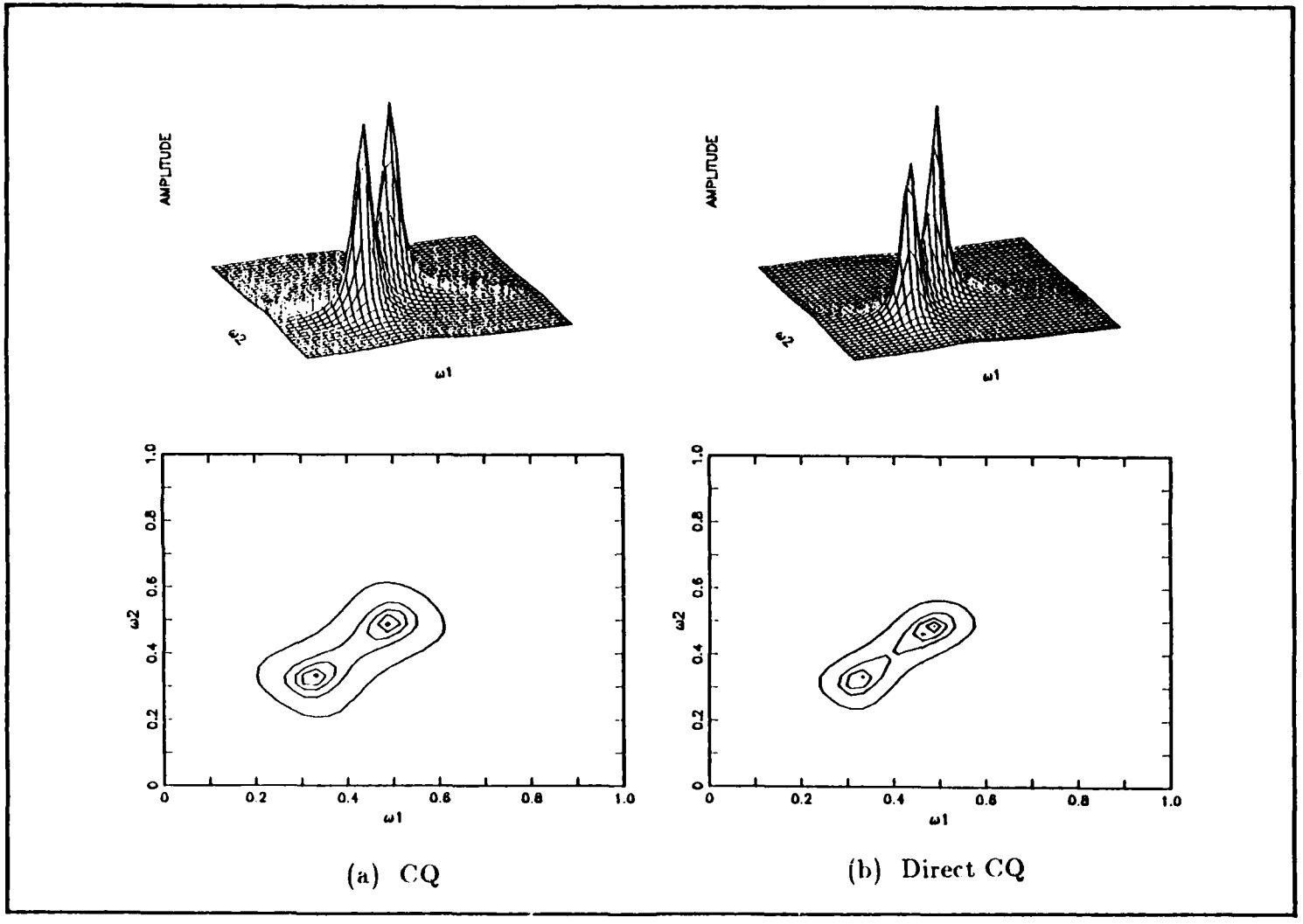

Fig. 2.11 Spectral estimation of two sinusoids (second order).

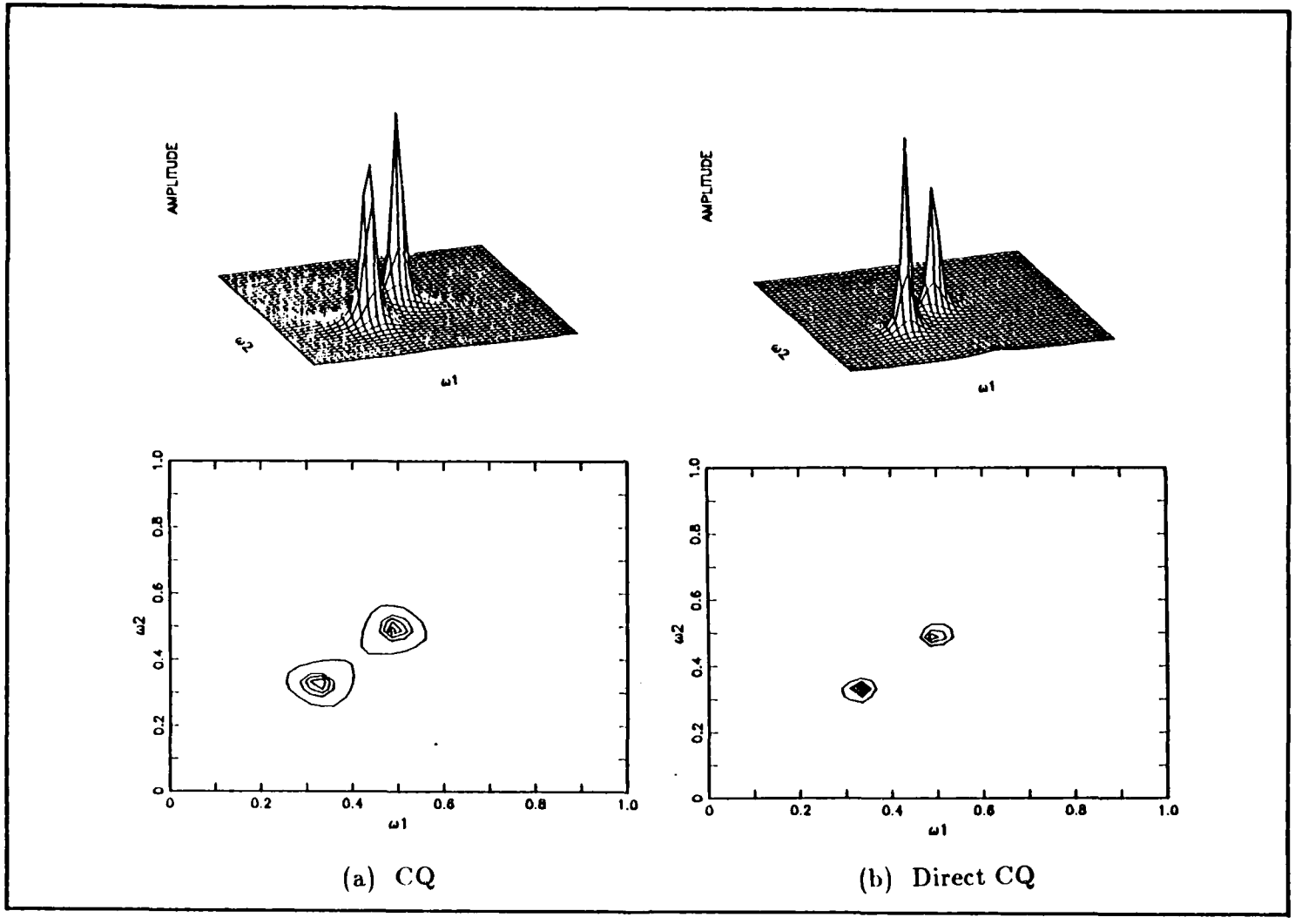

Fig. 2.12 Spectral estimation of two sinusoids (third order).

measure is the statistical *divergence*. (Grettenberg,1963; Hartwig,1972; Hingorani and Hancock,1965; Kailath,1967; Kazakos and Papantoni-Kazakos,1980; Marill and Green,1963; Schweppe,1967)

Let $f_1(x)$ and $f_2(x)$ represent the probability density functions of two random processes that we wish to discriminate by means of a statistical hypothesis test. By defining the logarithm of the likelihood ratio $\Lambda_{1,2}$ as

$$\Lambda_{1,2} = \log \frac{f_1(x)}{f_2(x)} \tag{2.57}$$

then the mean information I(1,2) is defined as:

$$I(1,2) = E_1\left[\Lambda_{1,2}\right] \tag{2.58}$$

where $E_1[\,.\,]$ represents the expectation under the distribution f_1. The divergence was first introduced by Jeffreys (1946). It is defined as the difference in the mean values of the log likelihood ratio under the two hypotheses H_1 and H_2. That is

$$J(1,2) = I(1,2) + I(2,1) \tag{2.59}$$

where:

$$I(2,1) = -E_2\left[\Lambda_{1,2}\right] \tag{2.60}$$

and $E_2[\,.\,]$ denotes the expectation under f_2.

Since spectral estimation involves building a model for the random process under consideration, it is reasonable to use the divergence measurement to compare the spectral estimates. The divergence in this case measures the ability to discriminate between the random processes produced by two alternative models. Therefore it measures the closeness of the distributions of the random processes and the closeness of two corresponding spectral estimates.

Since J increases with each additional sample of the random process one needs to specify the number of observations of the random process to compute the divergence. Alternatively one can consider the *change* in divergence that occurs with each new observation. For a homogeneous process with AR model this increase in divergence is constant and is called the *"incremental divergence"* ΔJ.

In the 1-D multichannel case, the incremental divergence $\Delta J(1,2)$, for a stationary Gaussain random AR processes with zero mean can be expressed (Fishman, Jones, and Therrien, 1981,1983) either in terms of the filter parameters, or in terms of the estimated power spectra. The results for 1-D random processes can be straightforwardly extended to the 2-D case. The results can be summarized as follows:

1. In terms of filter parameters:

$$\Delta J(1,2) = \frac{1}{2}\left[tr\ \mathbf{A}_2 \mathbf{R}_1 \mathbf{A}_2^T (\sigma_2^2)^{-1} + tr\ \mathbf{A}_1 \mathbf{R}_2 \mathbf{A}_1^T (\sigma_1^2)^{-1} \right] - 1 \qquad (2.61)$$

where: $\mathbf{A}_k$ are the set of filter coefficients of the process k, (k=1,2). $\mathbf{R}_k$ represents the entire covariance matrix of the process k, and σ_k^2 is the corresponding error covariance of the process k (equations for $\mathbf{A}_k$, $\mathbf{R}_k$, and σ_k^2 are given in section C and are defined by Eqns. (2.16-2.18)).

2. In terms of spectral estimates:

$$\Delta J(1,2) = \frac{1}{8\pi^2}\left[\int_{-\pi}^{\pi} \frac{S_1(\omega)}{S_2(\omega)} d\omega + \int_{-\pi}^{\pi} \frac{S_2(\omega)}{S_1(\omega)} d\omega \right] - 1 \qquad (2.62)$$

where $S_k(\omega)$ denotes the power spectral of the process k.

In this section, we illustrate two different examples to measure the incremental divergence between two random processes. In the first example the incremental divergence was measured by estimating the filter parameters while in the second example the measurement was computed from the estimated power spectra.

Example (1):

In this example we measure the incremental divergence between the first and second quadrant models as a function of model order, calculated from the filter parameters.

Consider a signal consisting of two-sinusoids in additive noise, as given in Equation (2.56), with the same parameters, except $C_1 = C_2 = 1$. The incremental divergence in this

example is calculated from Eqn. (2.61). Fig. 2.13 shows the incremental divergence between the first and second quadrant for different values of the model order. The value of incremental divergence at first decreases with increasing model order. This implies that the first and second quadrants spectral estimates tend to get closer to each other as the model order increases. Beyond order 4 the divergence increases then decreases again. Since the quadrant models are not sufficient for modeling the random process, this increase in divergence with order is not necessarily unexpected.

Example (2):

In this example we make a comparison between the nonsymmetric half plane and the quadrant-based models. Also we measure the incremental divergence between quadrant plane AR models and CQ model.

Consider the previous example with the same parameters. The comparisons are made for these models by numerically integrating the computed power spectral estimates to obtain the incremental divergence for different model orders. Table 2.1a shows the results of comparing NSHP spectral estimate with the quadrant-based model estimates, while Table 2.1b shows the results of comparisons between the CQ model and first and second quadrant plane models. The tables shows closeness between NSHP model and the CQ model, as we expect, while the difference between the NSHP and the individual quadrant plane models is high. Also the tables indicates that in general the spectral estimates tend to be closer as the model order increases.

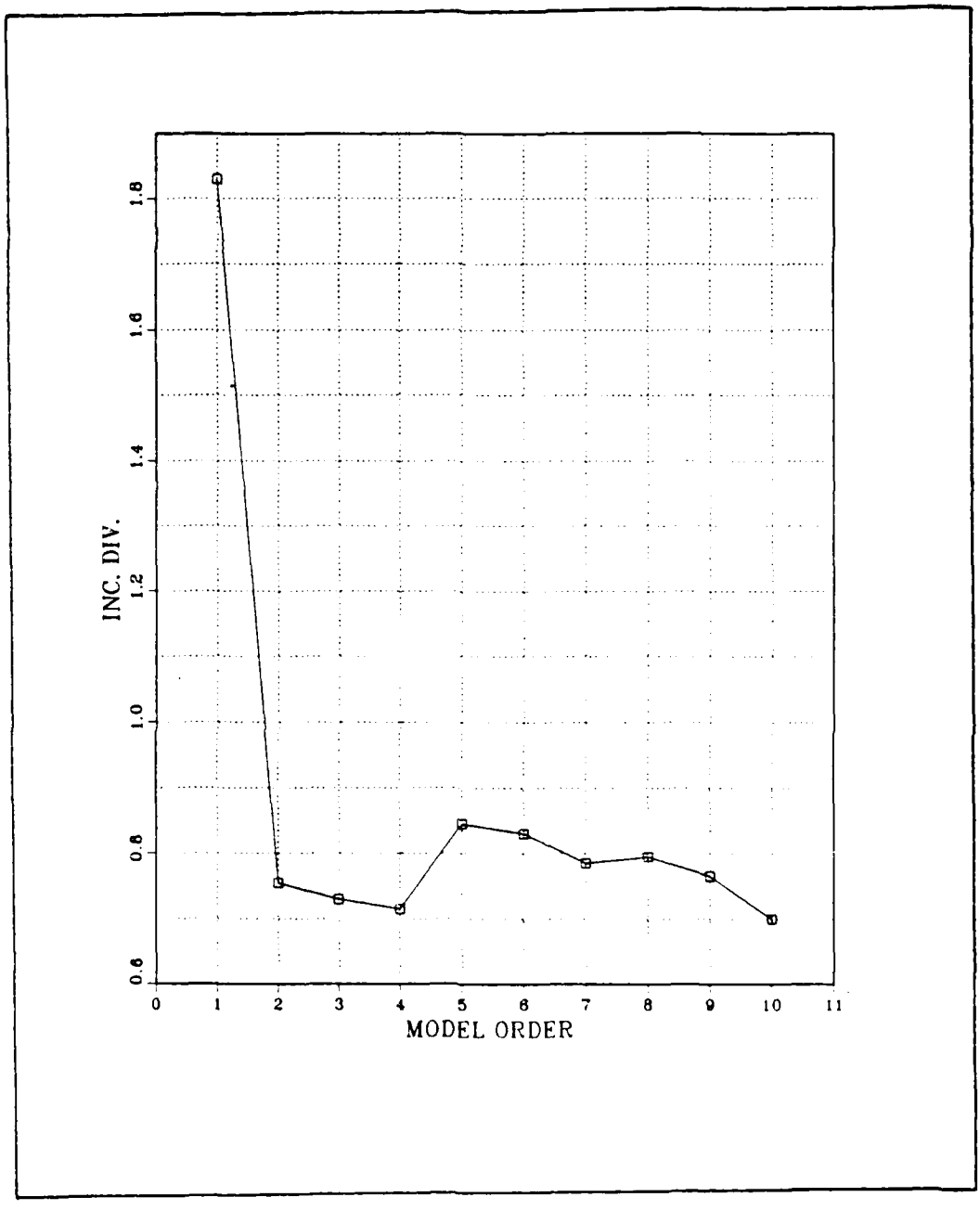

Fig. 2.13 Incremental divergence.

TABLE 2.1 INCREMENTAL DIVERGENCE MEASUREMENT

(a) Quadrant vs NSHP models

Incremental Divergence (ΔJ)			
Method	Model Order		
	1	2	3
1^{st} QP	0.6827	0.4054	0.4004
2^{nd} QP	0.7171	0.5332	0.5287
CQ	0.1248	0.0373	0.0348

(b) Quadrant vs CQ models

Incremental Divergence (ΔJ)			
Method	Model Order		
	1	2	3
1^{st} QP	1.1574	0.5188	0.4964
2^{nd} QP	1.1474	0.5099	0.5043

III. MULTICHANNEL 2–D SIGNAL MODELS FOR SPECTRAL ANALYSIS

A. FORM OF THE DATA

Multichannel 2-D signals will be represented by a vector valued quantity such as $\mathbf{x}(n_1,n_2)$ where n_1 and n_2 are integer-valued time or space indices and the dimension M of $\mathbf{x}$ is equal to the number of channels. The notation $\mathbf{x}(n_1,n_2)$ used to represent multichannel 2-D signals may refer either to the *function* $\mathbf{x}$ or to the *value* of the function $\mathbf{x}$ at a specific point (n_1,n_2) for all the given channels. The meaning will normally be clear from the context. An example of $\mathbf{x}(n_1,n_2)$ is sketched in Fig. 3.1, which shows that multichannel 2-D signals can be viewed as M-planes of correlated 2-D data

$$\mathbf{x}(n_1,n_2) = \begin{bmatrix} x_1(n_1,n_2) \\ x_2(n_1,n_2) \\ \\ \\ \\ x_M(n_1,n_2) \end{bmatrix} \tag{3.1}$$

Each plane $x_k(n_1,n_2)$ (k = 1, 2, ..., M) of the vector represents a 2-D signal existing in one of the channels.

Suppose that the multichannel 2-D signal is represented over a finite rectangular region of support $0 \le n_1 < N_1$ and $0 \le n_2 < N_2$. If the vector valued signals at point (n_1,n_2) are organized first by row then by column into a larger vector, then the multichannel 2-D signal can be represented by the vector

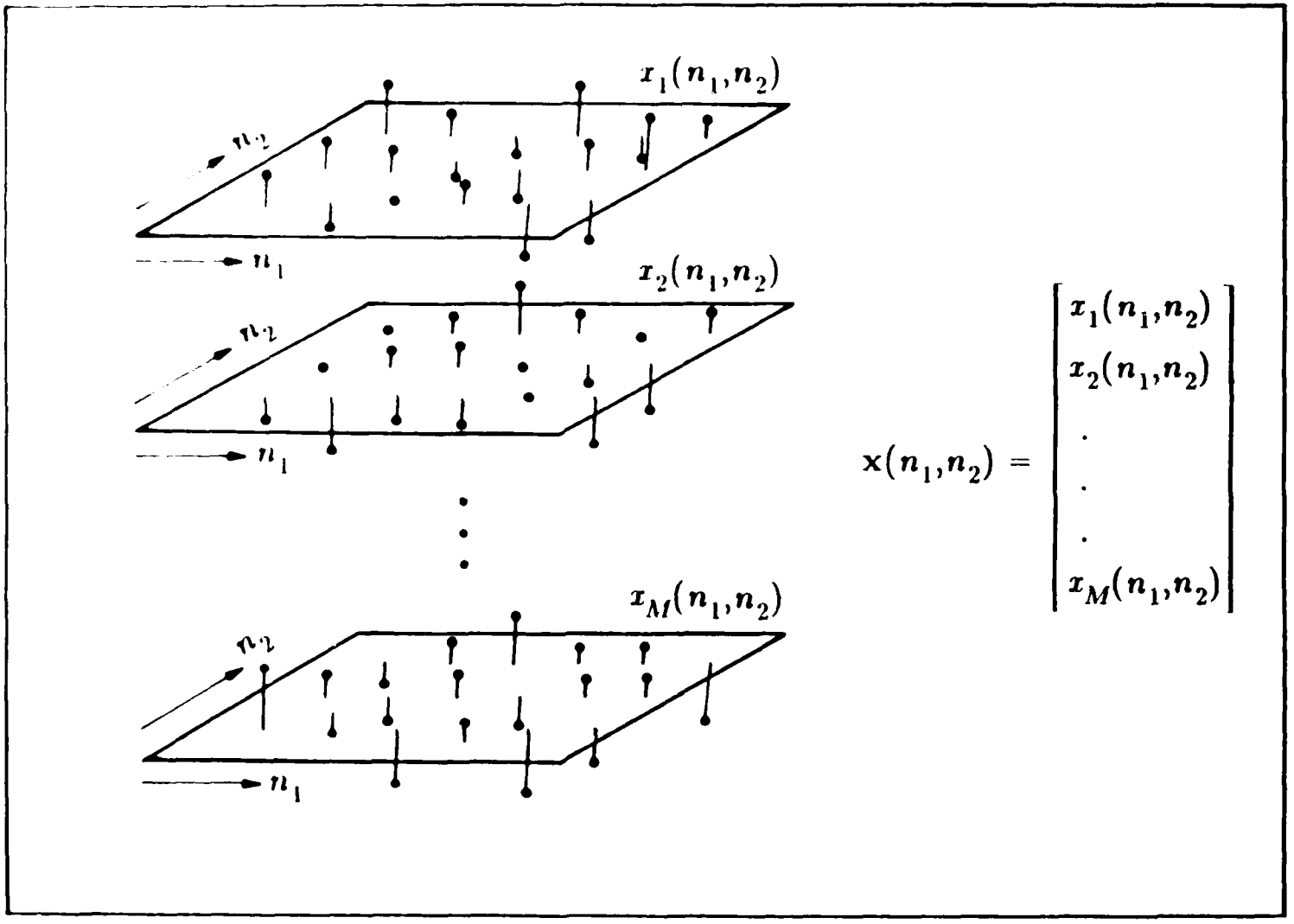

Fig. 3.1 Discrete multichannel 2-D signal.

$$\mathbf{x} = \begin{bmatrix} \mathbf{x}_0 \\ \mathbf{x}_1 \\ . \\ . \\ . \\ \mathbf{x}_{N_1-1} \end{bmatrix} \tag{3.2a}$$

where

$$\mathbf{x}_{n_1} = \begin{bmatrix} \mathbf{x}(n_1,0) \\ \mathbf{x}(n_1,1) \\ . \\ . \\ . \\ \mathbf{x}(n_1,N_2-1) \end{bmatrix} \tag{3.2b}$$

This idea is illustrated in Fig. 3.2 for the case M=2.

B. ESTIMATION OF THE CORRELATION FUNCTION

Let $\mathbf{x}(n_1,n_2)$ be a multichannel 2-D stationary random signal. Thus the mean is a vector quantity independent of n_1 and n_2 and defined by

$$\mathbf{m}_x = E\left[\mathbf{x}(n_1,n_2)\right] \tag{3.3}$$

and the correlation and covariance are $M \times M$ matrix functions defined (respectively) by

$$\mathbf{R}(k_1,k_2) = E\left[(\mathbf{x}(n_1,n_2)\,\mathbf{x}^T(n_1-k_1,n_2-k_2)\right] \tag{3.4a}$$

and

$$\mathbf{C}(k_1,k_2) = E\left[\left[\mathbf{x}(n_1,n_2)-\mathbf{m}_x\right]\left[\mathbf{x}(n_1-k_1,n_2-k_2)-\mathbf{m}_x\right]^T\right] \tag{3.4b}$$

From their definitions it is clear that the correlation and covariance functions have the following symmetry properties

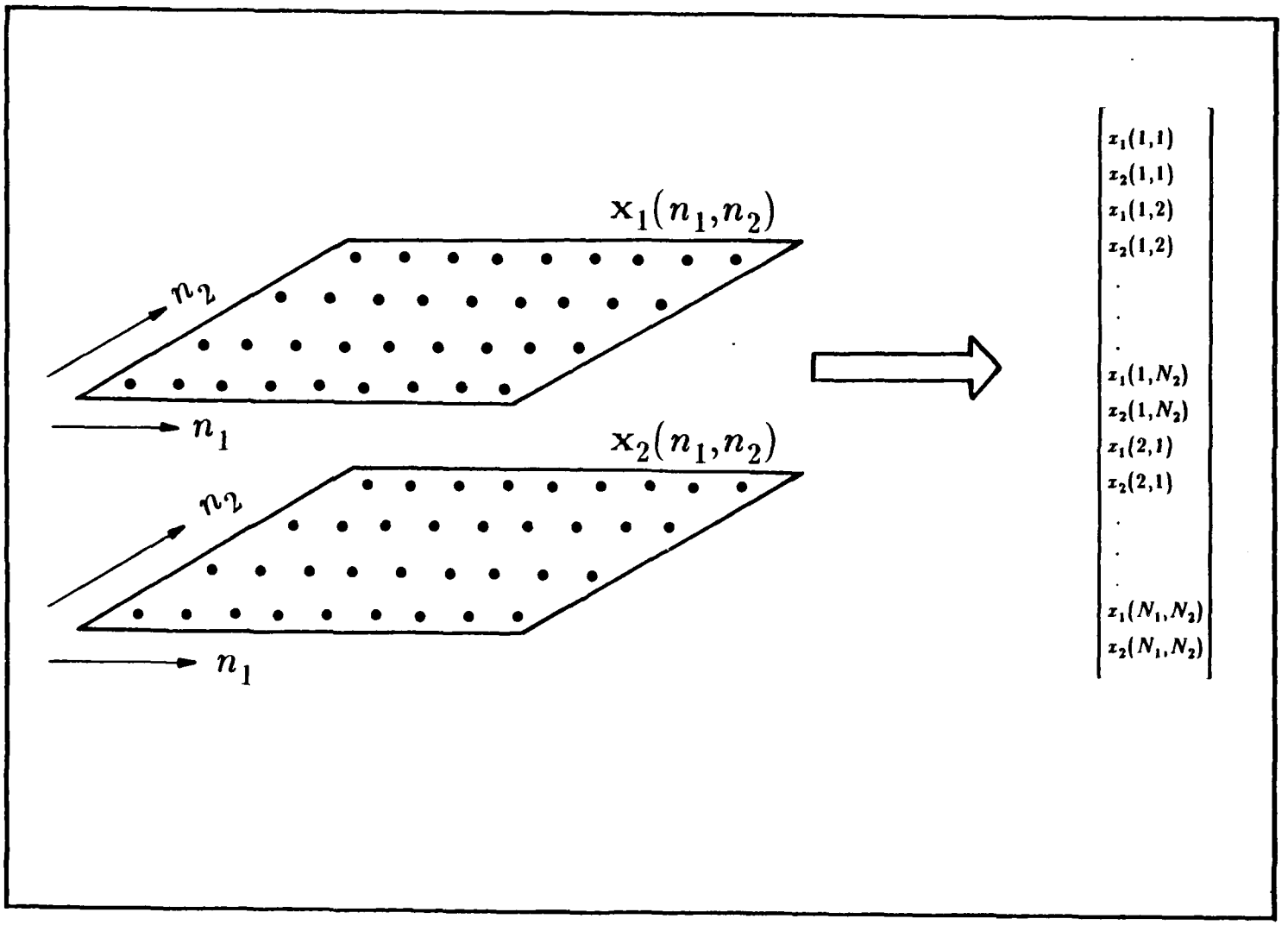

Fig. 3.2 Data formation.

$$\mathbf{R}(k_1,k_2) = \mathbf{R}^T(-k_1,-k_2) \tag{3.5a}$$

$$\mathbf{C}(k_1,k_2) = \mathbf{C}^T(-k_1,-k_2) \tag{3.5b}$$

Spectral estimation techniques are based on the assumption that the correlation sequence is available. Therefore, to apply these techniques it is necessary to estimate the correlation from the available data. The spectral estimate can differ significantly, depending on the method by which the correlation sequence is estimated.

Suppose we are given (N_1,N_2) multichannel 2-D data points and our main interest is in estimating the autocorrelation function. As a preliminary step, we must first estimate the mean $\mathbf{m}_x$. The usual estimate, namely the sample mean,

$$\hat{\mathbf{m}}_x = \frac{1}{N_1 N_2} \sum_{n_1=1}^{N_1} \sum_{n_2=1}^{N_2} \mathbf{x}(n_1,n_2) \tag{3.6}$$

provides an unbiased and consistent estimate of $\mathbf{m}_x$.

Now assume we have a stationary multichannel 2-D random process with zero mean; i.e.,

$$\mathbf{m}_x = \mathbf{0} \tag{3.7}$$

then the autocovariance sequence is

$$\mathbf{C}(k_1,k_2) = E\Big[\mathbf{x}(n_1,n_2)\,\mathbf{x}^T(n_1-k_1,n_2-k_2)\Big] \tag{3.8}$$

which is also equal to the correlation sequence $\mathbf{R}(k_1,k_2)$. One estimate for the autocorrelation sequence is

$$\hat{\mathbf{R}}(k_1,k_2) = \frac{1}{(N_1-|k_1|)(N_2-|k_2|)} \sum_{n_1=0}^{N_1-|k_1|-1} \sum_{n_2=0}^{N_2-|k_2|-1} \mathbf{x}(n_1,n_2)\mathbf{x}^T(n_1-|k_1|,n_2-|k_2|) \tag{3.9}$$

where $|k_1|<N_1$ and $|k_2|<N_2$. It can easily be shown that $\hat{\mathbf{R}}(k_1,k_2)$ is an unbiased estimate of $\mathbf{R}(k_1,k_2)$. An alternate estimate for the autocorrelation sequence is

$$\hat{\mathbf{R}}'(k_1,k_2) = \frac{1}{N_1 N_2} \sum_{n_1=0}^{N_1-|k_1|-1} \sum_{n_2=0}^{N_2-|k_2|-1} \mathbf{x}(n_1,n_2)\mathbf{x}^T(n_1-|k_1|,n_2-|k_2|) \qquad (3.10)$$

which differs from Eq. (3.9) only in the multiplying factor in the front of the sum. Comparing Eqns. (3.9) and (3.10) we find that

$$\hat{\mathbf{R}}'(k_1,k_2) = \left[\frac{N_1-|k_1|}{N_1}\right]\left[\frac{N_2-|k_2|}{N_2}\right]\hat{\mathbf{R}}(k_1,k_2) \qquad (3.11)$$

Consequently, $\hat{\mathbf{R}}'(k_1,k_2)$ is a biased estimate of the autocorrelation sequence, although it is asymptotically unbiased. The Fourier transform of the biased estimate is guaranteed to be non-negative definite but that of the unbiased estimate is not; for this reason the biased estimator is used more often.

In our work, we are dealing with statistical properties of multichannel 2-D random signals. The signal vectors defined in Eqn. (3.2) can be characterized by mean vectors and correlation matrices. These quantities are defined by

$$\mathbf{m} = E\left[\mathbf{x}\right] \qquad (3.12a)$$

$$\mathbf{R} = E\left[\mathbf{x}\mathbf{x}^T\right] \qquad (3.12b)$$

Note that for stationary random processes the vector $\mathbf{m}$ will consist of N_1N_2 M-dimensional subvectors all equal to the signal mean $\mathbf{m}_x$. The elements of $\mathbf{m}_x$ however are not in general all equal.

The correlation matrix for stationary multichannel 2-D random processes has a specific structure and symmetry at its various levels of partitioning (Therrien,1986). These properties are shown in Figure 3.3. Figure 3.4 shows the detailed structure of the correlation matrix $\mathbf{R}$ for $N_1 = 3, N_2 = 4$, and M = 2. The scalar elements r_{ij}^{kl} are given by

$$r_{ij}^{kl} = E\left[x_i(n_1,n_2)x_j(n_1-k,n_2-l)\right] \qquad (3.13)$$

which represent the element in the i^{th} row and the j^{th} column of the correlation function $\mathbf{R}(k,l)$. (Recall that $\mathbf{R}(k,l)$ is an M×M matrix).

Signal Vector

$$\mathbf{x} = \begin{bmatrix} \mathbf{x}_0 \\ \mathbf{x}_1 \\ . \\ . \\ . \\ \mathbf{x}_{N_1-1} \end{bmatrix} \quad \textit{where} \quad \mathbf{x}_{n_1} = \begin{bmatrix} \mathbf{x}(n_1,0) \\ \mathbf{x}(n_1,1) \\ . \\ . \\ . \\ \mathbf{x}(n_1,N_2-1) \end{bmatrix}$$

Correlation Matrix

$$\mathbf{R} = E\left[\mathbf{x}\mathbf{x}^T\right] = \begin{bmatrix} \mathbf{R}(0) & \mathbf{R}(1) & \cdots & \mathbf{R}(N_1-1) \\ \mathbf{R}(-1) & \mathbf{R}(0) & \cdots & \mathbf{R}(N_1-2) \\ . & . & & . \\ . & . & & . \\ . & . & & . \\ \mathbf{R}(-N_1+1) & \mathbf{R}(-N_1-2) & \cdots & \mathbf{R}(0) \end{bmatrix}$$

(BLOCK TOEPLITZ WITH $N_2M \times N_2M$ BLOCKS)

where

$$\mathbf{R}(k) = E\left[\mathbf{x}_n \mathbf{x}_{n-k}^T\right] = \begin{bmatrix} R(k,0) & R(k,1) & \cdots & R(k,N_2-1) \\ R(k,-1) & R(k,0) & \cdots & R(k,N_2-2) \\ . & . & & . \\ . & . & & . \\ . & . & & . \\ R(k,-N_2+1) & R(k,-N_2+2) & \cdots & R(k,0) \end{bmatrix}$$

(BLOCK TOEPLITZ WITH $M \times M$ BLOCKS)

where

$$R(k_1,k_2) \quad R^T(\ k_1,\ k_2) \quad E[\mathbf{x}(n_1,n_2)\mathbf{x}^T(n_1\ \ k_1,n_2-k_2)] \quad \textit{(NOT TOEPLITZ)}$$

Fig. 3.3 The correlation matrix (figure taken from Therrien,1986).

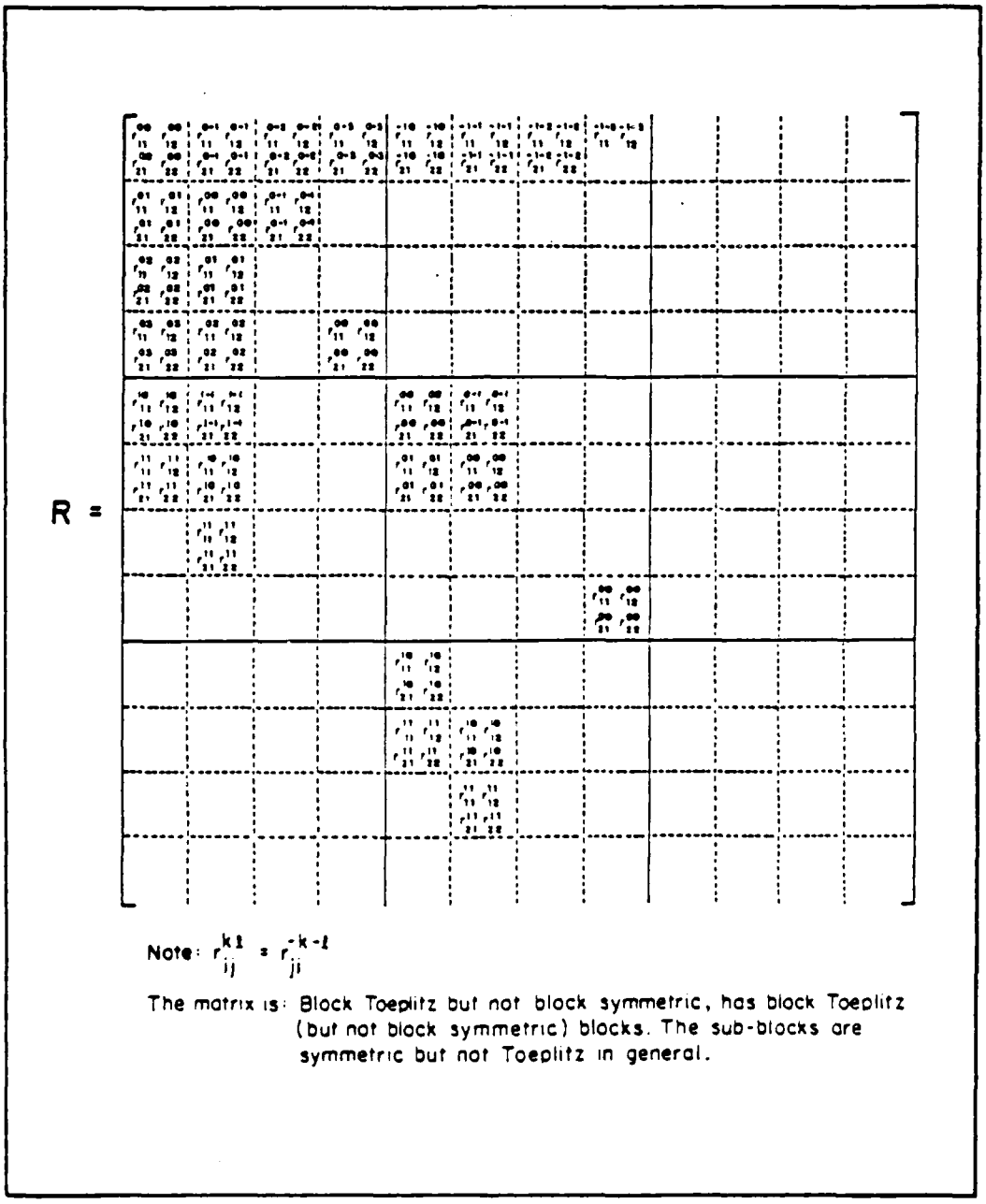

Fig. 3.4 Correlation matrix for $N_1=3$, $N_2=4$,and $M=2$ (figure taken from Therrien,1986).

C. ESTIMATION IN THE FREQUENCY DOMAIN

Stationary random signals are characterized in the frequency domain by their power spectral density. The power spectral density (or simply the power spectrum) matrix for a multichannel 2-D random process is defined by:

$$\mathbf{S}(\omega_1,\omega_2) = \sum_{k_1,k_2=-\infty,-\infty}^{\infty,\infty} \mathbf{R}(k_1,k_2)\, e^{-j\omega_1 k_1} e^{-j\omega_2 k_2} \tag{3.14}$$

where $\mathbf{R}(k_1,k_2)$ is the true autocorrelation function. In case of a two-channel (M=2) random process the spectral matrix is given by

$$\mathbf{S}(\omega_1,\omega_2) = \begin{bmatrix} S_{11}(\omega_1,\omega_2) & S_{12}(\omega_1,\omega_2) \\ S_{21}(\omega_1,\omega_2) & S_{22}(\omega_1,\omega_2) \end{bmatrix} \tag{3.15}$$

where $S_{11}(\omega_1,\omega_2)$ and $S_{22}(\omega_1,\omega_2)$ represent the autospectrum components corresponding to the two channels while $S_{12}(\omega_1,\omega_2)$ and $S_{21}(\omega_1,\omega_2)$ represent the cross spectrum components (between channels). The autospectrum components are always real and nonnegative, while the cross spectrum components are generally complex. For the case of a real random process the cross spectrum components are equal in magnitude and opposite in phase. Sometimes the 2-D *magnitude squared coherency* (MSC) is used instead of the magnitude of the cross spectrum. This quantity (κ^2) is defined by

$$\kappa^2(\omega_1,\omega_2) = \frac{|S_{12}(\omega_1,\omega_2)|^2}{S_{11}(\omega_1,\omega_2)S_{22}(\omega_1,\omega_2)} \tag{3.16}$$

D. MULTICHANNEL 2-D RANDOM PROCESS AND LINEAR PREDICTION

The methods of 2-D AR spectrum estimation discussed in Chapter II can be extended to the multichannel case. Consider a stationary multichannel 2-D signal $\mathbf{x}(n_1,n_2)$. The linear prediction problem is to predict the current value of the vector $\mathbf{x}(n_1,n_2)$ on the basis of all "past" values of the signal in a region α. The estimated value

takes the form

$$\hat{\mathbf{x}}(n_1,n_2) = - \sum_{\substack{(i_1,i_2)\varepsilon\alpha \\ (i_1,i_2)\neq(0,0)}} \mathbf{A}_{i_1 i_2}^T \mathbf{x}(n_1-i_1,n_2-i_2) \tag{3.17}$$

where the parameters $\mathbf{A}_{i_1 i_2}$ are M×M matrix coefficients. Let us define

$$\mathbf{A}_{00} = \mathbf{I} \tag{3.18}$$

where $\mathbf{I}$ is the identity matrix. Then the remaining values of the predictive filter coefficients $\mathbf{A}_{i_1 i_2}$ $(i_1,i_2\varepsilon\alpha)$ are chosen such that the mean square values of the components of the prediction error

$$\begin{aligned} \varepsilon(n_1,n_2) &= \mathbf{x}(n_1,n_2) - \hat{\mathbf{x}}(n_1,n_2) \\ &= \sum_{(i_1,i_2)\varepsilon\alpha} \mathbf{A}_{i_1 i_2}^T \mathbf{x}(n_1-i_1,n_2-i_2) \end{aligned} \tag{3.19}$$

are minimized. Fig. 3.5 depicts the interrelationships. The correlation function of the error evaluated at lag (0,0) is the M×M prediction error covariance matrix Σ_ε.

$$\Sigma_\varepsilon = E\left[\varepsilon(n_1,n_2)\varepsilon^T(n_1,n_2) \right] = \mathbf{R}_\varepsilon(0,0) \tag{3.20}$$

The mean-squared error is given by

$$E\left[|\varepsilon(n_1,n_2)|^2 \right] = E\left[\varepsilon^T(n_1,n_2)\varepsilon(n_1,n_2) \right] = tr\,\Sigma_\varepsilon \tag{3.21}$$

It is known from the orthogonality principle (Papoulis,1981) that the prediction error of the signal must be orthogonal to all the past values of the signal used to estimate the present value.

$$E\left[\mathbf{x}(n_1-i_1,n_2-i_2)\varepsilon^T(n_1,n_2) \right] = \left[\mathbf{O} \right] \quad (i_1,i_2)\varepsilon\alpha, \quad (i_1,i_2)\neq(0,0) \tag{3.22}$$

It further follows from Equations (3.19), (3.20) and (3.22) that

$$\Sigma_\varepsilon = E\left[\mathbf{x}(n_1,n_2)\varepsilon^T(n_1,n_2) \right] \tag{3.23}$$

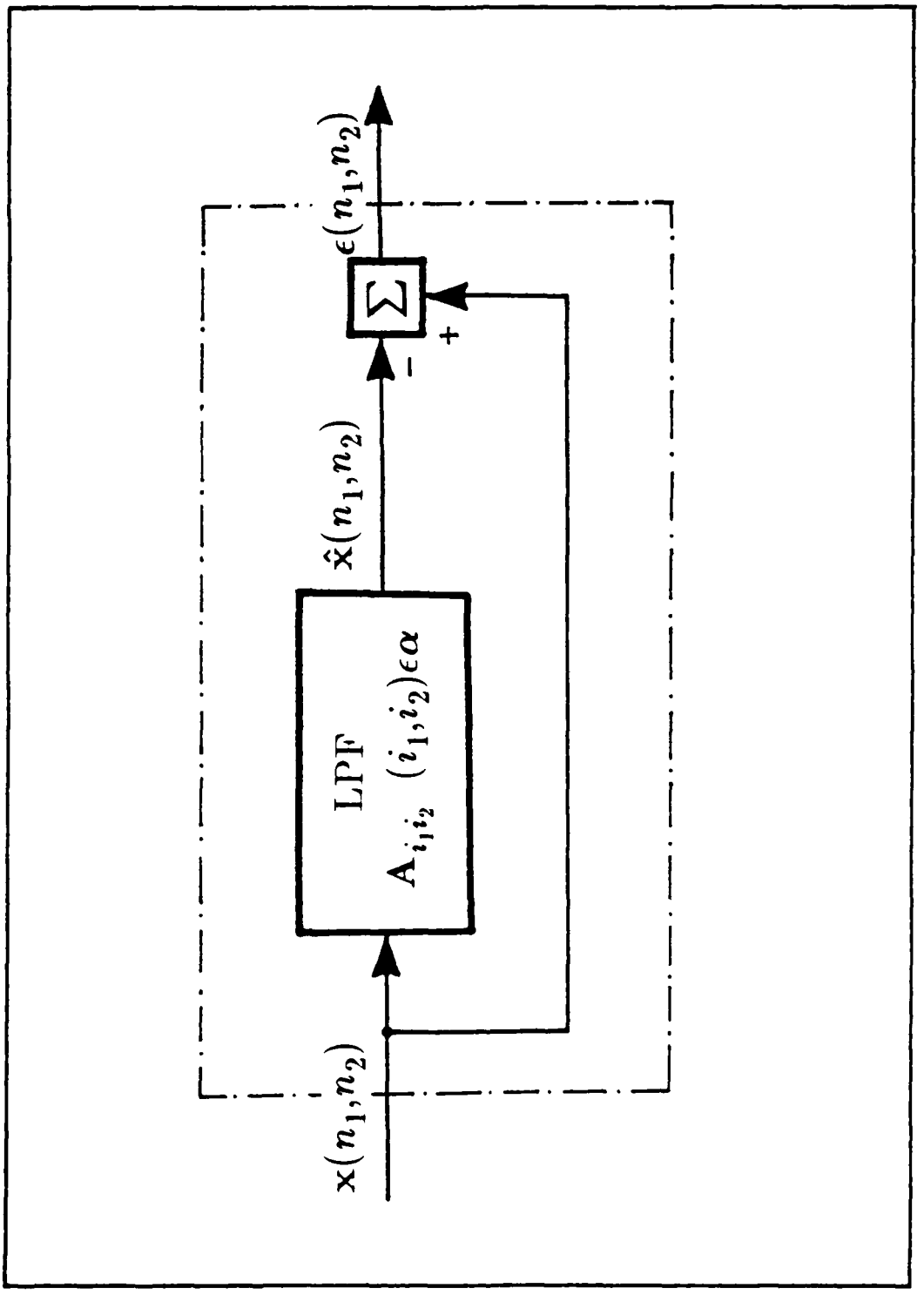

Fig. 3.5 Block diagram of prediction operation.

These last two equations can thus be written as

$$E\left[\mathbf{x}(n_1-i_1,n_2-i_2)\varepsilon^T(n_1,n_2)\right] = \Sigma_\varepsilon \delta(i_1,i_2) \quad (i_1,i_2)\varepsilon\alpha \tag{3.24}$$

Equation (3.19) can be put in a matrix form as follows

$$\varepsilon(n_1,n_2) = \mathbf{A}^T\, \mathbf{x}_{n_1n_2} \tag{3.25}$$

where $\mathbf{x}_{n_1n_2}$ is an vector of the ordered values $\mathbf{x}(n_1-i_1,n_2-i_2)$ appearing in Eqn. (3.19) and **A** is a correspondingly ordered matrix with blocks equal to the $\mathbf{A}_{i_1i_2}$ for $(i_1,i_2)\varepsilon\alpha$. Substituting into Equation (3.24) we have

$$E\left[\mathbf{x}_{n_1n_2}\,.\,\varepsilon^T(n_1,n_2)\right] = E\left[\mathbf{x}_{n_1n_2}\,.\,\mathbf{x}^T_{n_1n_2}\,.\,\mathbf{A}\right]$$

$$= E\left[\mathbf{x}_{n_1n_2}\,.\,\mathbf{x}^T_{n_1n_2}\right]\,.\,\mathbf{A} = \mathbf{S} \tag{3.26}$$

or

$$\mathbf{R}\,.\,\mathbf{A} = \mathbf{S} \tag{3.27}$$

where **R** is the correlation matrix of $\mathbf{x}_{n_1n_2}$ and **S** is matrix of size corresponding to the matrix **A** with blocks defined as follows:

$$\mathbf{S} = \begin{bmatrix} \mathbf{S}^{(0)} \\ \mathbf{0} \\ \cdot \\ \cdot \\ \cdot \\ \mathbf{0} \end{bmatrix} \tag{3.28a}$$

$$S^{(0)} = \begin{bmatrix} \Sigma_w \\ 0 \\ \cdot \\ \cdot \\ \cdot \\ 0 \end{bmatrix} \tag{3.28b}$$

We will refer to Eqn. (3.27) as the Normal equations for 2-D multichannel linear prediction. The error covariance matrix and the filter coefficients are obtained from the solution of these Normal equations. Specific examples of these equations are considered in the next section.

E. LINEAR PREDICTION MODELS

Let $\mathbf{x}(n_1,n_2)$ be an arbitrary zero-mean random process and let $\hat{\mathbf{x}}(n_1,n_2)$ denote a prediction estimate of the random variable $\mathbf{x}(n_1,n_2)$. Two different linear prediction models are considered here, namely the quadrant plane model (QP) and non-symmetric half plane (NSHP) model.

1. Analysis of Quadrant Plane Models

The estimated prediction error filter coefficients, and the prediction error covariance can be evaluated for the quadrant plane model as follows, assuming the size of the region of support α is $P_1 \times P_2$ points. Eqn. (3.19) can be written in the form

$$\varepsilon(n_1,n_2) = \sum_{i_1=0}^{P_1-1} \sum_{i_2=0}^{P_2-1} \mathbf{A}_{i_1 i_2}^T \mathbf{x}(n_1-i_1,n_2-i_2) \tag{3.29}$$

This model is called a first quadrant model since the impulse response of this filter has support in only the first quadrant of the 2-D plane. The signal data needed in Eqn. (3.19) is in the range n_1-P_1+1 to n_1 and n_2-P_2+1 to n_2 as shown in Fig. 3.6, where the solid dots denote prediction error samples which have been computed, and the crosses represent samples that remain to be computed. For this particular case of a quadrant plane model the vector $\mathbf{x}_{n_1,n_2}$ is defined by

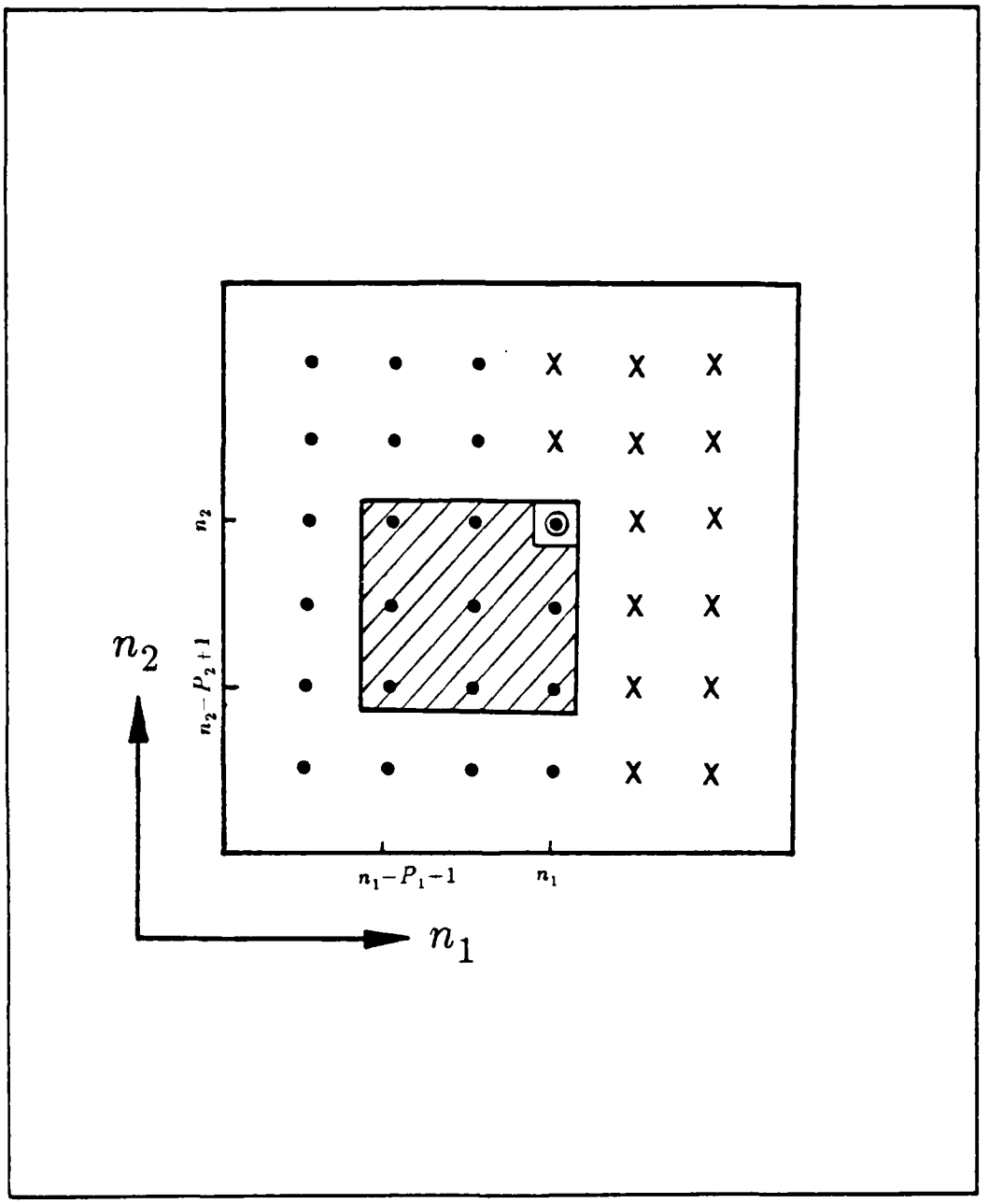

Fig. 3.6 Predictor of first quadrant support.

$$\mathbf{x}_{n}$$

$$\mathbf{x}_{n}$$

$$\mathbf{x}_{n\ n_2} = \qquad (3.31)$$

$$\mathbf{x}_{n\ P_2}$$

where

$$\mathbf{x}_{n_1-i} = \begin{bmatrix} \mathbf{x}(n_1-i,n_2) \\ \mathbf{x}(n_1-i,n_2-1) \\ \\ \\ \\ \mathbf{x}(n_1-i,n_2-P_2+1) \end{bmatrix} \qquad i=0,1,\quad P_1-1 \qquad (3.3)$$

The prediction error is given by Eqn. (3.25)

where **A** now has the specific form

$$\mathbf{A} = \begin{bmatrix} \mathbf{A}^{(0)} \\ \mathbf{A}^{(1)} \\ \\ \\ \\ \mathbf{A}^{(P_1-1)} \end{bmatrix} \qquad (3.32a)$$

and

$$\mathbf{A}^{(i)} = \begin{bmatrix} \mathbf{A}_{i,0} \\ \mathbf{A}_{i,1} \\ \\ \\ \\ \mathbf{A}_{i,P_2-1} \end{bmatrix} \qquad (3.32b)$$

The Normal equations for this region of support can be viewed as follows. We have a set

of $P_1 \times P_2$ points as shown in Fig. 3.7a and a correlation matrix $\mathbf{R}$ is formed for the $P_1 \times P_2$ points. The terms of the correlation function appearing in the matrix are shown in Fig. 3.7b. The Normal equations have the general form of Eqn. (3.27). The specific structure in this case is as follows

$$\begin{bmatrix} \mathbf{R}(0) & \mathbf{R}(-1) & \cdots & \mathbf{R}(-P_1+1) \\ \mathbf{R}(1) & \mathbf{R}(0) & \cdots & \mathbf{R}(-P_1+2) \\ & & \cdots & \\ \mathbf{R}(P_1-1) & \mathbf{R}(P_1-2) & \cdots & \mathbf{R}(0) \end{bmatrix} \begin{bmatrix} \mathbf{A}^{(0)} \\ \mathbf{A}^{(1)} \\ \cdots \\ \mathbf{A}^{(P_1-1)} \end{bmatrix} = \begin{bmatrix} \mathbf{S}^{(0)} \\ \mathbf{0} \\ \cdots \\ \mathbf{0} \end{bmatrix} \tag{3.33a}$$

where

$$\mathbf{R}(k_1) = \mathbf{R}^T(-k_1) = \begin{bmatrix} \mathbf{R}(k_1,0) & \mathbf{R}(k_1,-1) & \cdots & \mathbf{R}(k_1,-P_2+1) \\ \mathbf{R}(k_1,1) & \mathbf{R}(k_1,0) & \cdots & \mathbf{R}(k_1,-P_2+2) \\ & & \cdots & \\ \mathbf{R}(k_1,P_2-1) & \mathbf{R}(k_1,P_2-2) & \cdots & \mathbf{R}(k_1,0) \end{bmatrix} \tag{3.33b}$$

$$\mathbf{S}^{(0)} = \begin{bmatrix} \boldsymbol{\Sigma}_\varepsilon \\ \mathbf{0} \\ \cdots \\ \mathbf{0} \end{bmatrix} \tag{3.33c}$$

and where

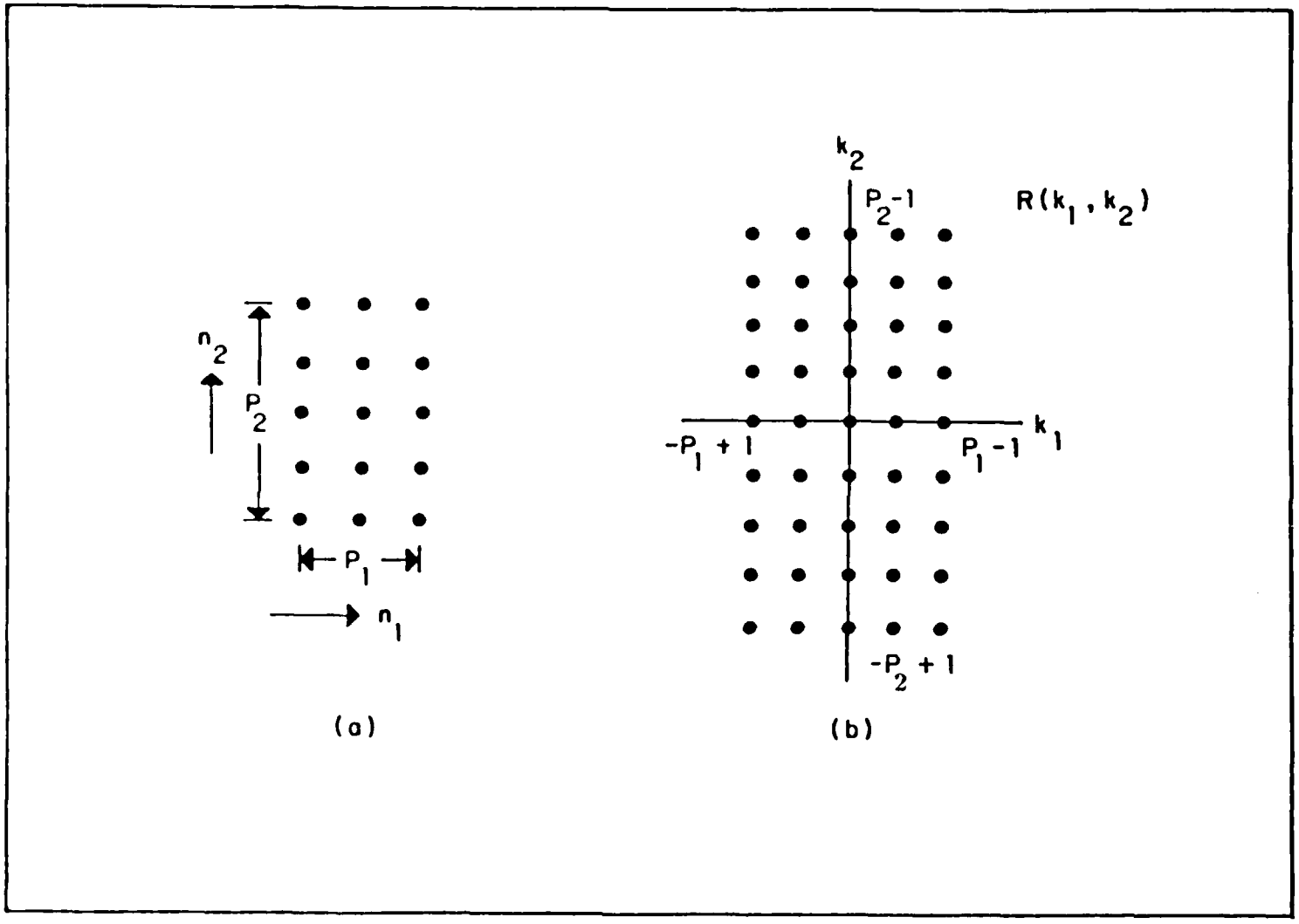

Fig. 3.7 Linear prediction with quadrant support.

$$\mathbf{R}(k_1,k_2) = \mathbf{R}^T(-k_1,-k_2) = E\left[\mathbf{x}(n_1,n_2)\mathbf{x}^T(n_1-k_1,n_2-k_2)\right] \tag{3.33d}$$

$$= \begin{bmatrix} r_{11}(k_1,k_2) & r_{12}(k_1,k_2) & \cdots & r_{1M}(k_1,k_2) \\ r_{21}(k_1,k_2) & r_{22}(k_1,k_2) & \cdots & r_{2M}(k_1,k_2) \\ \cdot & \cdot & & \cdot \\ \cdot & \cdot & & \cdot \\ \cdot & \cdot & & \cdot \\ r_{M1}(k_1,k_2) & r_{M2}(k_1,k_2) & \cdots & r_{MM}(k_1,k_2) \end{bmatrix}$$

$$\mathbf{A}_{0,0} = \mathbf{I} \tag{3.33e}$$

$$\Sigma_\varepsilon = E\left[(\mathbf{x}-\hat{\mathbf{x}})(\mathbf{x}-\hat{\mathbf{x}})^T\right] \tag{3.33f}$$

$$= \begin{bmatrix} \sigma_{11}^2 & \sigma_{12}^2 & \cdots & \sigma_{1M}^2 \\ \sigma_{21}^2 & \sigma_{22}^2 & \cdots & \sigma_{2M}^2 \\ \cdot & \cdot & & \cdot \\ \cdot & \cdot & & \cdot \\ \cdot & \cdot & & \cdot \\ \sigma_{M1}^2 & \sigma_{M2}^2 & \cdots & \sigma_{MM}^2 \end{bmatrix}$$

As mentioned before $\mathbf{R}$ is an $MP_1P_2 \times MP_1P_2$ matrix and $\mathbf{A}$ and $\mathbf{S}$ are each $MP_1P_2 \times M$ matrices. Note that the matrix $\mathbf{R}$ defined in Eqn. (3.33) differs from that in Fig. 3.3 in that the first level partitions are block transposed. This results from the particular ordering of the vector $\mathbf{x}_{n_1,n_2}$ (Eqn. (3.30)) which is used to define the 2-D multichannel linear prediction problem.

The previous analysis was derived for the case where the filter coefficients $\mathbf{A}_{k_1,k_2}$ had first quadrant support. If we set up the problem assuming second quadrant support In this case the prediction error filter is given by

$$\varepsilon(n_1,n_2) = \sum_{i_1=0}^{P_1-1}\sum_{i_2=0}^{P_2-1} \mathbf{B}_{i_1 i_2}^{T}\mathbf{x}(n_1+i_1,n_2-i_2) \tag{3.34}$$

where $\mathbf{B}_{i_1 i_2}$ represent the backward predictive filter coefficients. The filter is actually similar to that of Fig. 3.6 except it predicts the point in the upper left corner and we get a different set of filter coefficients. We can set up a matrix equation similar to Eqn. (3.27), but now the matrix **B** reflects the second quadrant support

$$\mathbf{R}\,\mathbf{B} = \mathbf{S}_b \tag{3.35}$$

where **R** is the same matrix as (3.27) and **B** is defined by

$$\mathbf{B} = \begin{bmatrix} \mathbf{B}^{(0)} \\ \mathbf{B}^{(1)} \\ \\ \\ \mathbf{B}^{(P_1-1)} \end{bmatrix} \tag{3.36a}$$

$$\mathbf{B}^{(\cdot)} = \begin{bmatrix} \mathbf{B}_{(\cdot,P_2-1)} \\ \mathbf{B}_{(\cdot,P_2-2)} \\ \\ \\ \mathbf{B}_{(\cdot,0)} \end{bmatrix} \qquad \mathbf{B}_{0,0} = \mathbf{I} \tag{3.36b}$$

$$\mathbf{S}_{(\cdot)}$$

$$\mathbf{0}$$

$$\mathbf{S}_{(\cdot)}$$

$$\mathbf{0}$$

$$S_b^{(0)} = \begin{bmatrix} \mathbf{0} \\ \mathbf{0} \\ \\ \\ \Sigma_{\varepsilon_b} \end{bmatrix} \tag{3.36d}$$

The third and fourth quadrant filters for predicting the bottom left and bottom right points are also distinct. Their Normal equations differ from the Normal equations of the first and second quadrant filters in that the innermost blocks $\mathbf{R}(k_1,k_2)$ of the matrix $\mathbf{R}$ are replaced by their transposes. This is a difference from the single channel 2-D case where the first and third and the second and fourth quadrant filters are identical

2. Analysis of Non-Symmetric Half Plane Model

As we discussed in Chapter II, the NSHP model is an important form of predictor because of the ability to factor arbitrary spectra into terms with forward and backward NSHP support. Also we mentioned that models with NSHP support of modest sizes have been found to give reasonable results in spectral estimation

Now we consider the problem of finding a finite order NSHP model as sketched in Fig. 3.8a, given covariances on a finite window as shown in Fig. 3.8b. The prediction equation for a (P_1,P_2) order NSHP model is

[illegible]

[illegible]

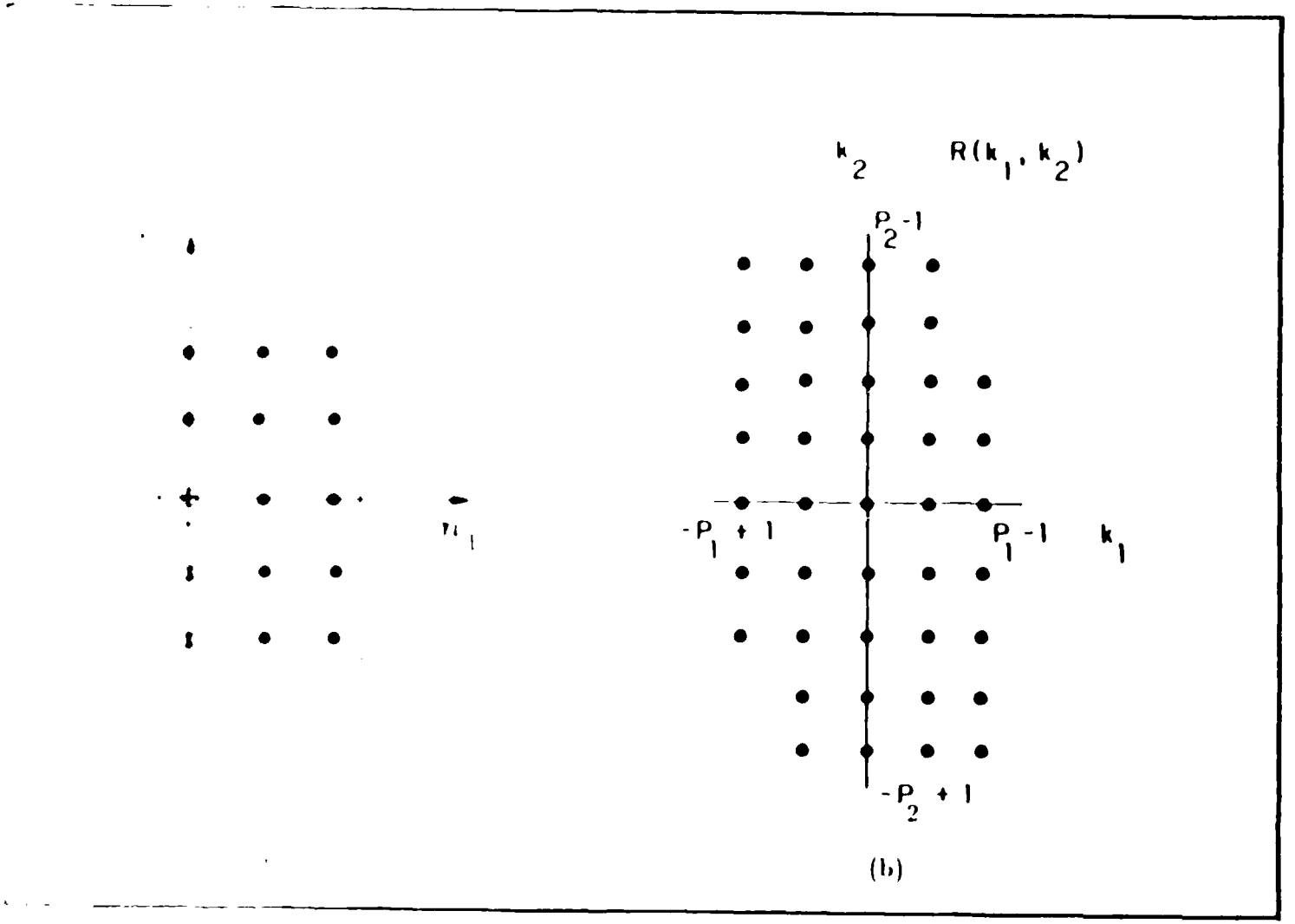

Linear prediction with NSHP support.

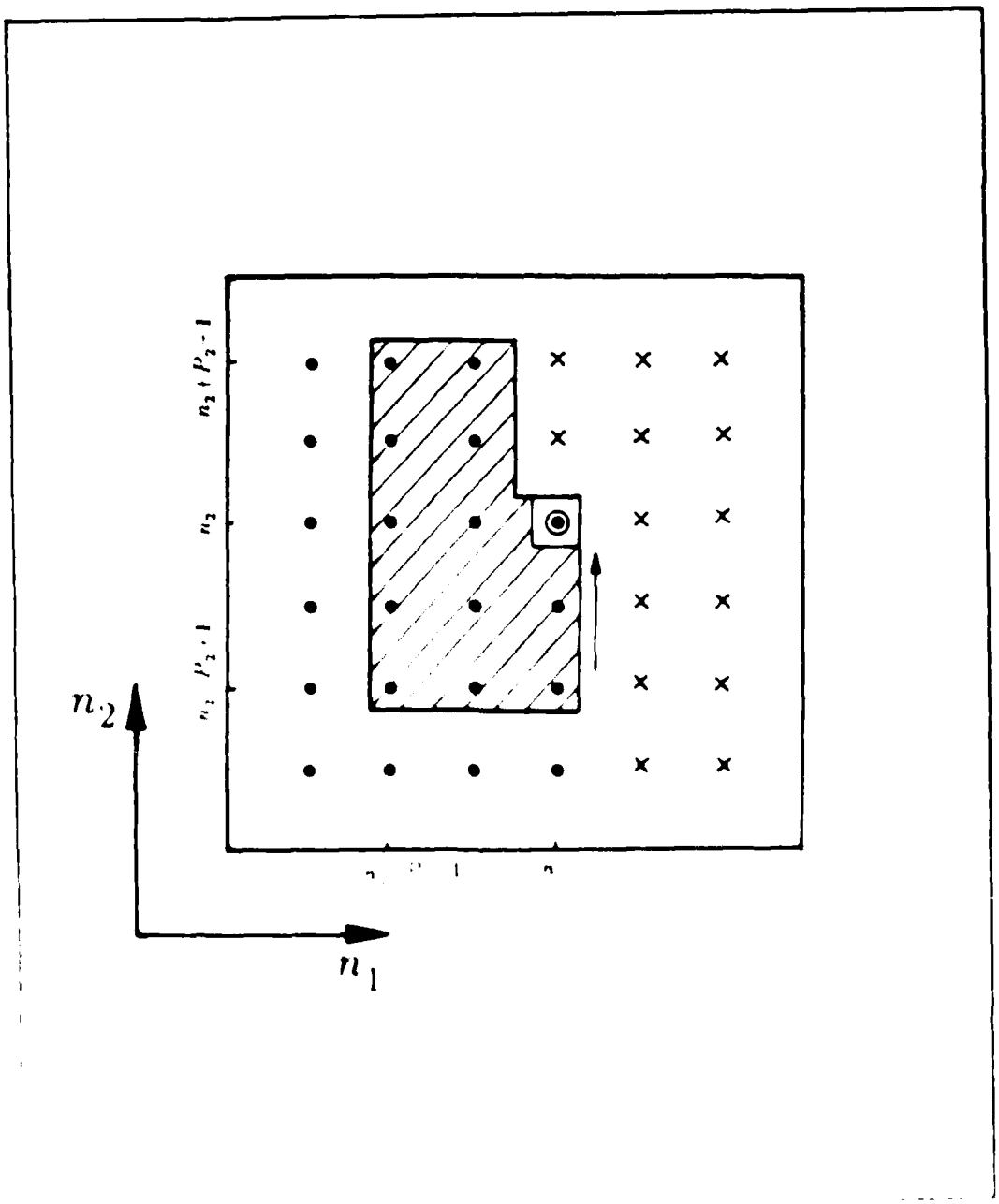
n_2
n_1

$$\mathbf{x}_{n_1 n_2} = \begin{bmatrix} \mathbf{x}_{n_1} \\ \mathbf{x}_{n_1-1} \\ \cdot \\ \cdot \\ \cdot \\ \mathbf{x}_{n_1-P_1+1} \end{bmatrix} \tag{3.39}$$

where

$$\mathbf{x}_{n_1} = \begin{bmatrix} \mathbf{x}(n_1, n_2-1) \\ \mathbf{x}(n_1, n_2-2) \\ \cdot \\ \cdot \\ \cdot \\ \mathbf{x}(n_1, n_2-P_2+1) \end{bmatrix} \tag{3.40a}$$

$$\mathbf{x}_{n_1-i} = \begin{bmatrix} \mathbf{x}(n_1-i, n_2+P_2-1) \\ \cdot \\ \cdot \\ \cdot \\ \mathbf{x}(n_1-i, n_2) \\ \\ \\ \\ \mathbf{x}(n_1-i, n_2-P_2+1) \end{bmatrix} \quad i=1,2,\ldots,P_1-1 \tag{3.40b}$$

Note that the size of the subvector $\mathbf{x}_{n_1}$ is smaller than that of $\mathbf{x}_{n_1-i}$ for $1 \le i < P_1$. If $\mathbf{x}$ is to be a minimum variance prediction estimate (i.e. one that minimizes mean square error) then the orthogonality principle must hold and leads to the following Normal equations

$$\begin{bmatrix} \mathbf{R}'(0) & \mathbf{R}'(-1) & \cdots & \mathbf{R}'(-P_1+1) \\ \mathbf{R}'(1) & \mathbf{R}(0) & \cdots & \mathbf{R}(-P_1+2) \\ \vdots & \vdots & & \vdots \\ \mathbf{R}'(P_1-1) & \mathbf{R}(P_1-2) & \cdots & \mathbf{R}(0) \end{bmatrix} \begin{bmatrix} \mathbf{A}'^{(0)} \\ \mathbf{A}^{(1)} \\ \vdots \\ \mathbf{A}^{(P_1-1)} \end{bmatrix} = \begin{bmatrix} \mathbf{S}'^{(0)} \\ \mathbf{0} \\ \vdots \\ \mathbf{0} \end{bmatrix} \tag{3.41}$$

where

$$\mathbf{R}(k) = \mathbf{R}^T(-k) = \begin{bmatrix} \mathbf{R}(k,0) & \mathbf{R}(k,-1) & \cdots & \mathbf{R}(k,-2P_2+1) \\ \mathbf{R}(k,1) & \mathbf{R}(k,0) & \cdots & \mathbf{R}(k,-P_2+2) \\ \vdots & \vdots & & \vdots \\ \mathbf{R}(k,2P_2-1) & \mathbf{R}(k,2P_2-2) & \cdots & \mathbf{R}(k,0) \end{bmatrix} \tag{3.42a}$$

$$\mathbf{A}^{(k)} = \begin{bmatrix} \mathbf{A}_{k,-P_2+1} \\ \mathbf{A}_{k,-P_2+2} \\ \vdots \\ \mathbf{A}_{k,0} \\ \vdots \\ \mathbf{A}_{k,P_2-1} \end{bmatrix} \quad k \neq 0 \tag{3.42b}$$

$$\mathbf{R}'(k) = \mathbf{R}'^T(-k) = \begin{bmatrix} \mathbf{R}(k,P_2-1) & \mathbf{R}(k,P_2-2) & \cdots & \mathbf{R}(k,-P_2+1) \\ \mathbf{R}(k,P_2) & \mathbf{R}(k,0) & & \mathbf{R}(k,-P_2+2) \\ & & & \\ \mathbf{R}(k,2P_2-1) & \mathbf{R}(k,2P_2-2) & & \mathbf{R}(k,0) \end{bmatrix} \tag{3.42c}$$

$$\mathbf{R}'(0) = \begin{bmatrix} \mathbf{R}(0,0) & \mathbf{R}(0,-1) & \cdots & \mathbf{R}(0,-P_2+1) \\ \mathbf{R}(0,1) & \mathbf{R}(0,0) & \cdots & \mathbf{R}(0,-P_2+2) \\ \cdot & \cdot & & \cdot \\ \cdot & \cdot & & \cdot \\ \cdot & \cdot & & \cdot \\ \mathbf{R}(0,P_2-1) & \mathbf{R}(0,P_2-2) & \cdots & \mathbf{R}(0,0) \end{bmatrix} \tag{3.42d}$$

$$\mathbf{A}'^{(0)} = \begin{bmatrix} \mathbf{A}_{0,0} \\ \mathbf{A}_{0,1} \\ \cdot \\ \cdot \\ \cdot \\ \mathbf{A}_{0,P_2-1} \end{bmatrix} \tag{3.42e}$$

$$\mathbf{S}'^{(0)} = \begin{bmatrix} \Sigma_\varepsilon \\ \mathbf{0} \\ \cdot \\ \cdot \\ \cdot \\ \mathbf{0} \end{bmatrix} \tag{3.42f}$$

and where

$$\Sigma_\varepsilon = E\left[(\mathbf{x}-\hat{\mathbf{x}})(\mathbf{x}-\hat{\mathbf{x}})^T \right] \tag{3.42g}$$

and $\mathbf{R}(k_1,k_2)$ is defined by Eqn. (3.33d). We refer to this as the *forward* prediction model.

For backward prediction of the process $\mathbf{x}$ we suppose that samples $\mathbf{x}(n_1-P_1+1,n_2-P_2+1), \ldots \mathbf{x}(n_1,n_2-1)$ are available as shown in Fig. 3.10, and we attempt a linear prediction of $\mathbf{x}(n_1,n_2)$ according to

$$\hat{\mathbf{x}}_b(n_1,n_2) = \sum_{k_2=1}^{P_2} \mathbf{B}'_{0,k_2}\,\mathbf{x}(n_1,n_2+k_2) + \sum_{k_1=1}^{P_1-1} \sum_{k_2=-P_2+1}^{P_2-1} \mathbf{B}'_{k_1,k_2}\,\mathbf{x}(n_1+k_1,n_2+k_2) \tag{3.43}$$

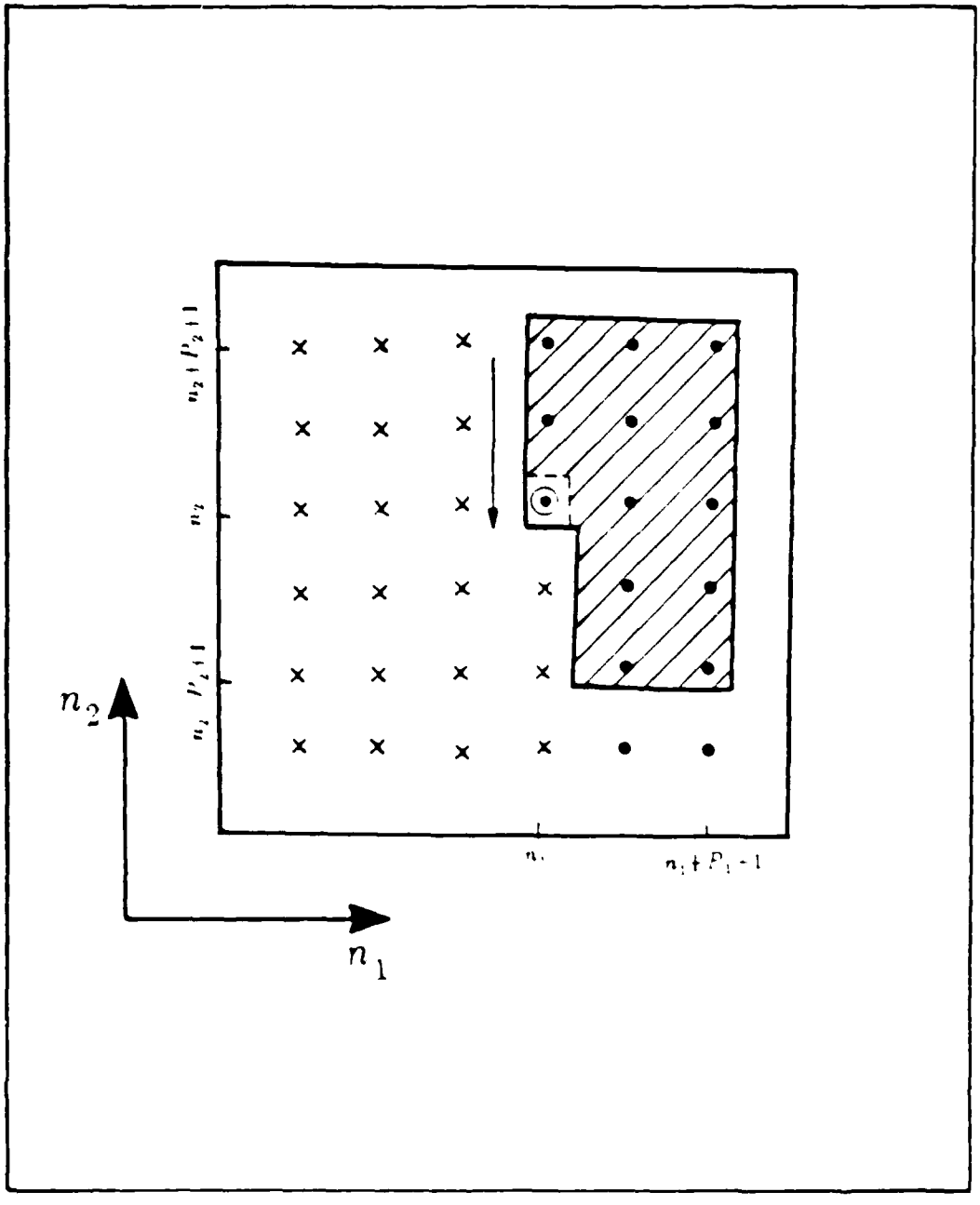

Fig. 3.1: Projection of backward DNSHP support

The backward prediction error is defined as

$$\boldsymbol{\varepsilon}_b(n_1,n_2) = \mathbf{x}(n_1,n_2) - \hat{\mathbf{x}}_b(n_1,n_2)$$

$$= \sum_{i_2=0}^{P_2-1} \mathbf{B}_{0i_2}^T \mathbf{x}(n_1,n_2+i_2) + \sum_{i_1=1}^{P_1-1} \sum_{i_2=-P_2-1}^{P_2-1} \mathbf{B}_{i_1i_2}^T \mathbf{x}(n_1+i_1,n_2+i_2) \tag{3.44}$$

If the backward prediction error filter coefficients $\mathbf{B}_{i_1i_2}$ are chosen to minimize the mean square error $\left[|\boldsymbol{\varepsilon}_b(n_1,n_2)|^2 \right]$ then the corresponding Normal equations are given by

$$\begin{bmatrix} \mathbf{R}(0) & \mathbf{R}(-1) & \cdots & \mathbf{R}'^T(-P_1+1) \\ \mathbf{R}(1) & \mathbf{R}(0) & \cdots & \mathbf{R}'^T(-P_1+2) \\ \cdot & \cdot & & \cdot \\ \cdot & \cdot & & \cdot \\ \cdot & \cdot & & \cdot \\ \mathbf{R}'^T(P_1-1) & \mathbf{R}'^T(P_1-2) & \cdots & \mathbf{R}'^T(0) \end{bmatrix} \begin{bmatrix} \mathbf{B}^{(P_1-1)} \\ \mathbf{B}^{(P_1-2)} \\ \cdot \\ \cdot \\ \cdot \\ \mathbf{B}'^{(0)} \end{bmatrix} = \begin{bmatrix} \mathbf{0} \\ \mathbf{0} \\ \cdot \\ \cdot \\ \cdot \\ \mathbf{S}_b'^{(0)} \end{bmatrix} \tag{3.45}$$

where

$$\mathbf{B}^{(k)} = \begin{bmatrix} \mathbf{B}_{k,-P_2+1} \\ \mathbf{B}_{k,-P_2+2} \\ \cdot \\ \mathbf{B}_{k,0} \\ \cdot \\ \mathbf{B}_{k,P_2-1} \end{bmatrix} \quad k \neq 0 \tag{3.46a}$$

$$\mathbf{B}'^{(0)} = \begin{bmatrix} \mathbf{B}_{0,0} \\ \mathbf{B}_{0,1} \\ \cdot \\ \cdot \\ \mathbf{B}_{0,P_2-1} \end{bmatrix} \quad \mathbf{B}_{0,0} = \mathbf{I} \tag{3.46b}$$

and

AD-A191 273 MULTICHANNEL 2-D POWER SPECTRAL ESTIMATION AND APPLICATIONS(U) NAVAL POSTGRADUATE SCHOOL MONTEREY CA H T EL-SHAER DEC 87 2/4

UNCLASSIFIED F/G 12/3 NL

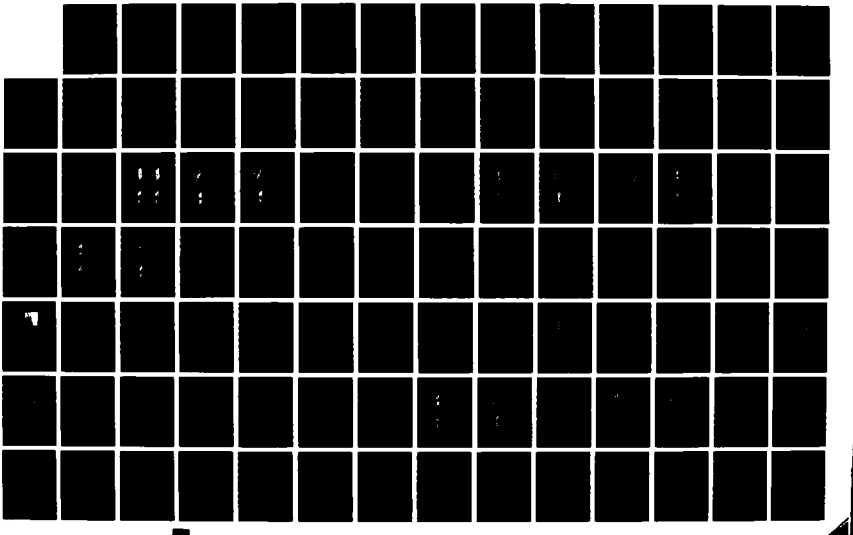

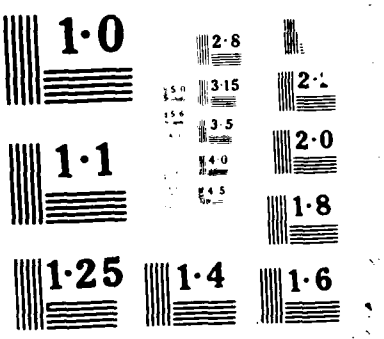
1·0
1·1
1·25
1·4
1·6
1·8
2·0
2·5
2·8
3·15
3·5
4·0
4·5

$$S'^{(0)}_b = \begin{bmatrix} \Sigma_{\varepsilon_b} \\ 0 \\ \cdot \\ \cdot \\ \cdot \\ 0 \end{bmatrix} \tag{3.46c}$$

and the other terms are as defined earlier. It is clear from the previous analysis that, the forward and backward models have distinctly different Normal equations. More specifically, if we reorder the Equations (3.45) so that they have the same partitioning as (3.41) we find that the difference between the two sets of equations is that the innermost correlation block $\mathbf{R}(k_1,k_2)$ is transposed. The solution of forward and backward Normal equations leads to different model parameters (filter coefficients and error covariances). Since the model parameters are not identical, different spectral estimates for the forward and backward models are obtained. The forward and backward models are very important and will be used in later sections.

F. AUTOREGRESSIVE MODEL FITTING

If $\mathbf{x}(n_1,n_2)$ is a zero mean stationary multichannel 2-D random process, then a causal representation of the type

$$\mathbf{x}(n_1,n_2) = - \sum_{\substack{(i_1,i_2)\varepsilon\alpha \\ (i_1,i_2)\neq(0,0)}} \mathbf{A}^T_{i_1 i_2} \mathbf{x}(n_1-i_1,n_2-i_2) + \mathbf{w}(n_1,n_2) \tag{3.47}$$

is called an autoregressive (AR) representation. The sequence $\mathbf{w}(n_1,n_2)$ is a zero mean white noise random process independent of the past outputs with covariance

$$\Sigma_w = E\left[\mathbf{w}(n_1,n_2)\, \mathbf{w}^T(n_1,n_2) \right] \tag{3.48}$$

If $\mathbf{x}(n_1,n_2)$ is an AR process defined by (3.47) then the quantity

$$\hat{\mathbf{x}}(n_1,n_2) = - \sum_{\substack{(i_1,i_2)\varepsilon\alpha \\ (i_1,i_2)\neq(0,0)}} \mathbf{A}^T_{i_1 i_2} \mathbf{x}(n_1-i_1,n_2-i_2) \tag{3.49}$$

is the best mean-square predictor of $\mathbf{x}(n_1,n_2)$ based on all of its past. Thus equation

(3.47) becomes

$$\mathbf{x}(n_1,n_2) = \hat{\mathbf{x}}(n_1,n_2) + \mathbf{w}(n_1,n_2) \tag{3.50}$$

which says the sample at (n_1,n_2) is the sum of its minimum variance causal prediction estimate plus the prediction error which is white noise. This is also called the innovations representation.

Now define the polynomial

$$\mathbf{H}(z_1,z_2) = \sum_{n_1,n_2 \varepsilon \alpha} \mathbf{A}^T_{i_1 i_2} z_1^{-n_1} z_2^{-n_2} \tag{3.51}$$

Then it can be seen from Eqn. (3.47) that the transfer function of an AR representation is $\left[\mathbf{H}(z_1,z_2)\right]^{-1}$ which is an all pole model. Figure 3.11 illustrates the relation between linear prediction and autoregressive modeling. While linear prediction uses an FIR filter, AR modeling employs a recursive or IIR filter.

In general when linear prediction is applied to arbitrary 2-D random process, a white noise error signal does not result. Nevertheless, for sufficiently large regions α the residual may be found to be close to a white noise process in practice. This is true especially when the model has NSHP support. For a model with NSHP support the AR model becomes a close approximation to any given random process if the order becomes sufficiently large. This argument follows from results in Refs. (Ekstrom and Woods,1976) and (Marzetta,1978) that show that arbitrary 2-D power spectra can be factored into forward and backward models with (generally infinite) NSHP support. Thus it is reasonable to seek to represent 2-D random processes by suitable AR models and to derive the parameters by formulating and solving Normal equations.

G. MULTICHANNEL 2-D BURG TECHNIQUE

There has been in the past decade strong interest and much activity in developing high resolution power spectrum estimation techniques, particularly for short data records. The Burg maximum entropy method (MEM) and the associated algorithms for estimating the AR model parameters directly from the data have especially received much attention in this regard.

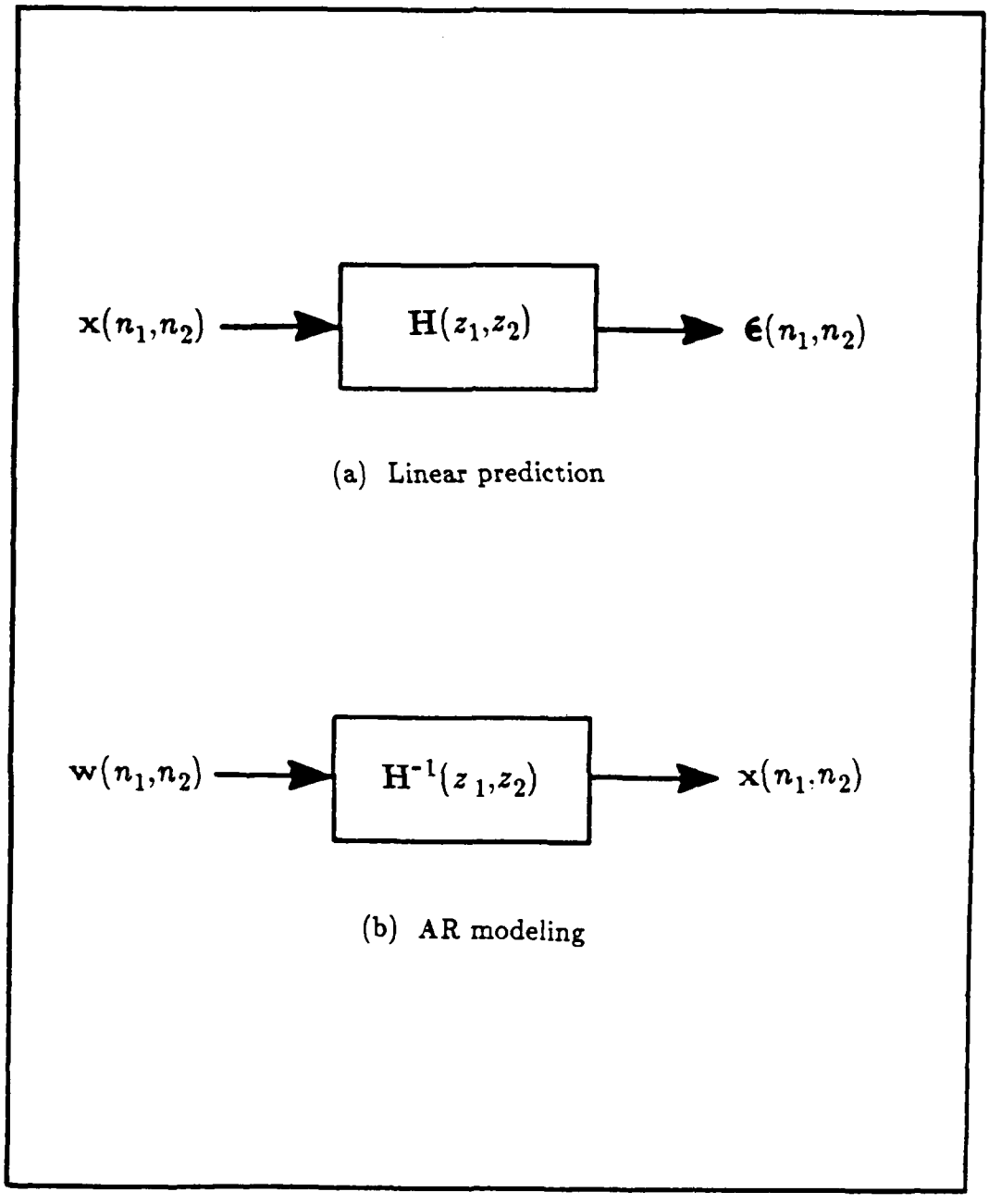

Fig. 3.11 Linear prediction and AR modeling.

A 2-D multichannel Burg algorithm can be developed as a straightforward combination of a 2-D Burg algorithm (see Chapter II), and a 1-D multichannel Burg algorithm (details are given in Appendix D).

As in the case of the single channel 2-D Burg algorithm, this method does not result in spectral estimates (perhaps because procedure does not in fact solve the Normal equations and the low order terms in the recursion do not result in reasonable approximations to whitening filters). Fortunately, it is possible to generate another procedure that estimates the filter parameters directly from the data and *does* result in good spectral estimates. This procedure is discussed in the next section.

H. DIRECT PARAMETER ESTIMATION TECHNIQUE

1. Multidimensional and Multichannel Relations

As we mentioned in Chapter II there is an exact relation between single channel 2-D linear prediction and multichannel 1-D linear prediction (Therrien,1981). These kinds of relations also exist for multidimensional linear prediction problems of higher orders.

In this thesis we will specifically take advantage of the relations between multichannel 2-D linear prediction problems and higher order 1-D multichannel linear prediction problems. The results will be used to estimate the model parameters of a multichannel 2-D random process directly from the data without prior estimation of the autocorrelation function.

A multichannel linear prediction problem with first quadrant support of order $(P_1 \times P_2)$ and with three channels is shown in Fig. 3.12a. In this case the points surrounded by the cylinder are predicted from all the other points appearing in the three planes. The Normal equations are given generally by Eqn. (3.27) and specifically for this case by Eqns. (3.32) and (3.33). The corresponding multichannel 1-D linear prediction problem is shown in Fig. (3.12b). In this figure the same data of Fig. 3.12a are used but these data are now considered to be a collection of discrete 1-D signals evolving along the n_1 direction. The total number of these signals is MP_2 and they form an MP_2–dimensional multichannel random process. In Fig. 3.12b the single value of n_1 at

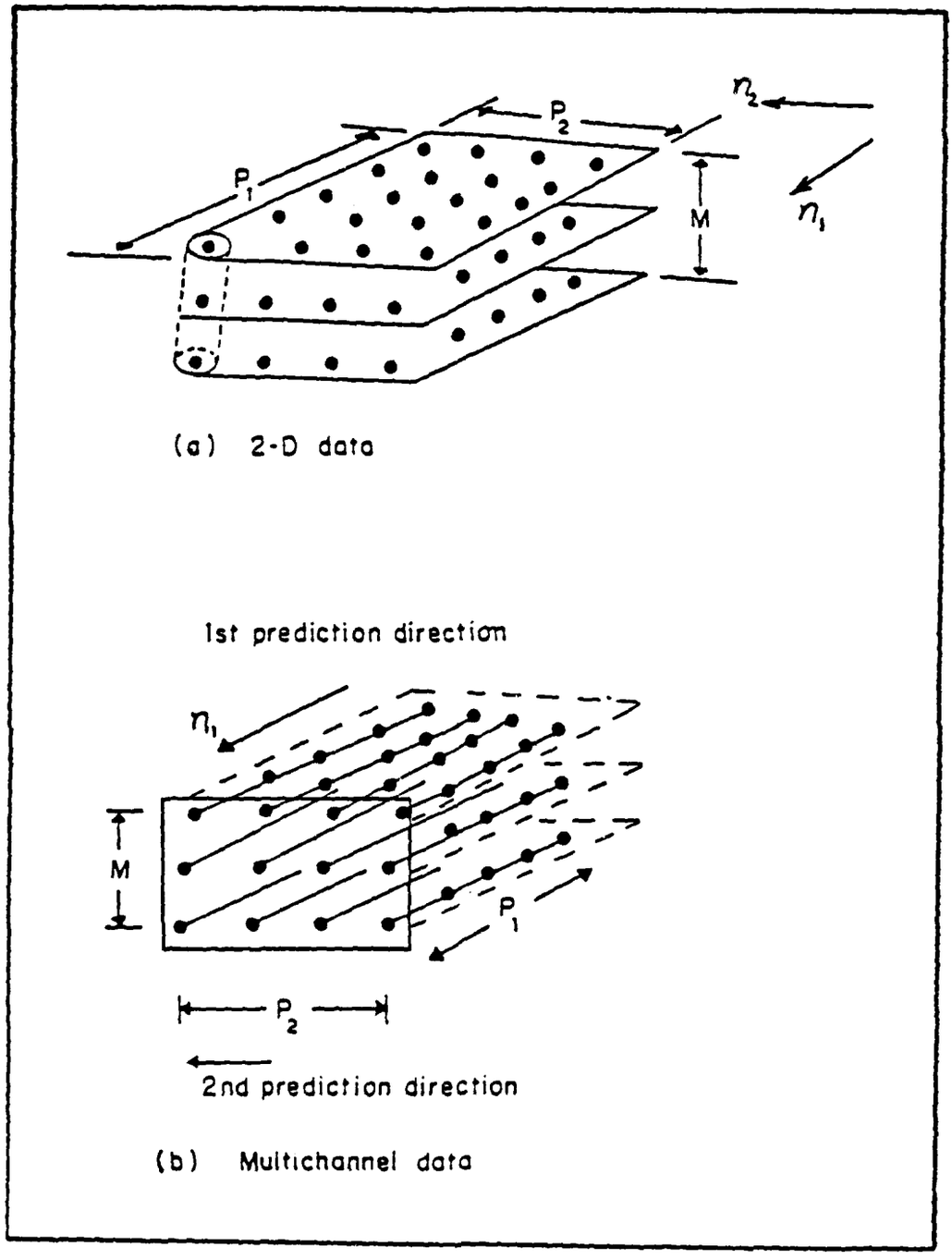

Fig. 3.12 Multichannel 2-D linear prediction and related multichannel 1-D problem (figure taken from Therrien,1986).

which the MP_2–channels of the process are to be predicted (from the signals at earlier values of n_1) is represented by all the points that appear in the solid-line box. Assume $\mathbf{x}_n$ is a vector of the data points to be predicted

$$\mathbf{x}_n = \begin{bmatrix} \mathbf{x}(n,0) \\ \mathbf{x}(n,1) \\ . \\ . \\ . \\ \mathbf{x}(n,P_2-1) \end{bmatrix} \tag{3.52}$$

In this case the P_2M-channel 1-D linear prediction problem takes the form:

$$\hat{\mathbf{x}}_n = -\sum_{i=1}^{P_1-1} \left[\alpha^{(i)}\right]^T \mathbf{x}_{n-i} \tag{3.53}$$

where $\hat{\mathbf{x}}_n$ is the estimated value of the P_2M-dimensional data vector $\mathbf{x}_n$ and $\alpha^{(i)}$ is the linear predictive filter coefficients. The corresponding Normal equations can be written as follows:

$$\begin{bmatrix} \mathbf{R}(0) & \mathbf{R}(-1) & \dots & \mathbf{R}(-P_1+1) \\ \mathbf{R}(1) & \mathbf{R}(0) & \dots & \mathbf{R}(-P_1+2) \\ . & . & & . \\ . & . & & . \\ . & . & & . \\ \mathbf{R}(P_1-1) & \mathbf{R}(P_1-2) & \dots & \mathbf{R}(0) \end{bmatrix} \begin{bmatrix} \mathbf{I} \\ \alpha^{(1)} \\ . \\ . \\ . \\ \alpha^{(P_1-1)} \end{bmatrix} = \begin{bmatrix} \mathbf{E}_{P_1} \\ \mathbf{0} \\ . \\ . \\ . \\ \mathbf{0} \end{bmatrix} \tag{3.54}$$

where

$$\alpha^{(i)} = \begin{bmatrix} \alpha_{00}^{(i)} & \alpha_{01}^{(i)} & \cdots & \alpha_{0,P_2-1}^{(i)} \\ \alpha_{10}^{(i)} & \alpha_{11}^{(i)} & \cdots & \alpha_{1,P_2-1}^{(i)} \\ \cdot & \cdot & & \cdot \\ \cdot & \cdot & & \cdot \\ \cdot & \cdot & & \cdot \\ \alpha_{P_2-1,0}^{(i)} & \alpha_{P_2-1,1}^{(i)} & \cdots & \alpha_{P_2-1,P_2-1}^{(i)} \end{bmatrix} \tag{3.55}$$

and where each block $\alpha_{kl}^{(i)}$ is of size $M \times M$ and $\mathbf{E}_{P_1}$ is the $P_2M \times P_2M$ prediction error covariance.

Now note that since the correlation matrix appearing on the left side of (3.54) is the same as that in (3.33a) we can multiply both sides of (3.54) by the term $\mathbf{A}^{(0)}$ and compare the result to (3.33a). Then (3.54) will be identical to (3.33a) if we require

$$\mathbf{E}_{P_1} \mathbf{A}^{(0)} = \mathbf{S}^{(0)} \tag{3.56}$$

and

$$\mathbf{A}^{(i)} = \alpha^{(i)} \mathbf{A}^{(0)} \qquad i=0,1, ..., P_1-1 \tag{3.57}$$

The foregoing analysis shows that the multichannel 2-D Normal equations can be solved by the following steps:

(1) Solve the P_2M-dimensional 1-D multichannel problem (3.54) using the 1-D multichannel form of the Levinson recursion. This finds the coefficient matrices $\alpha^{(n)}$ and the prediction error covariance matrix $\mathbf{E}_{P_1}$.

(2) Solve (3.56) for $\mathbf{A}^{(0)}$. Since $\mathbf{E}_{P_1}$ is not in general Block Toeplitz, no particularly fast algorithm is possible.

(3) Find the multichannel 2-D coefficients from (3.57).

This approach to solving the multichannel 2-D Normal equations has a special advantage for spectral estimation using the combined quadrant method. Specifically, the multichannel form of the Levinson recursion leads to find both the *forward and backward* 1-D filter parameters. The backward parameters relate to the second quadrant multichannel 2-D filter parameters in the same way that the forward parameters relate to the

first quadrant multichannel 2-D filter parameters. If $\beta^{(i)}$ and $\mathbf{E}'_{P_1}$ represent the backward parameters and $\mathbf{B}^{(i)}$ and $\mathbf{S}_b^{(0)}$ represent the second quadrant parameters, the relations analogous to Eqns. (3.56) and (3.57) are

$$\mathbf{E}'_{P_1}\,\mathbf{B}^{(0)} = \mathbf{S}_b^{(0)} \tag{3.58}$$

and

$$\mathbf{B}^{(i)} = \beta^{(i)}\,\mathbf{B}^{(0)}; \qquad i=0,1,\ldots,P_1-1 \tag{3.59}$$

Both the $\mathbf{A}^{(i)}$ and the $\mathbf{B}^{(i)}$ parameters are used in the CQ spectral estimation procedure and both are found in a single estimation algorithm.

2. Application to Quadrant Plane Models

The algorithm for solving the 2-D Normal equation discussed above can be further enhanced by replacing step (1) involving solution of the Normal equations by a procedure that estimates the 1-D filter parameters directly from the data. This method will be called a *direct* method since it does not require prior estimation of the correlation function.

This method capitalizes on the existence of a direct method for solving the 1-D *multichannel* linear prediction problem known as the multichannel Burg algorithm or the Nuttall-Strand algorithm. The method is based on ideas originally suggested by Burg (1975) but developed separately by Nuttall (1976) and Strand (1977).

In applying the multichannel Burg algorithm to 2-D data, the data are first partitioned into strips along the n_2 direction as shown in Fig. 3.13(a). The strips of width P_2 for an $P_1 \times P_2$ quadrant filter are catenated along the n_1 direction as shown in Fig. 3.13(b). As in the previous section this data is considered to be a 1-D process (in the n_1 direction) with P_2M channels. Discontinuities where the strips are catenated together can be ignored since they represent only a small portion of the data. The multichannel Burg algorithm is then used to estimate forward and backward linear prediction parameters $\alpha^{(1)}, \alpha^{(2)}, \ldots, \alpha^{(P_1-1)}$ and $\mathbf{E}_{P_1}$ and $\beta^{(1)}, \beta^{(2)}, \ldots, \beta^{(P_1-1)}$ and $\mathbf{E}'_{P_1}$. The error

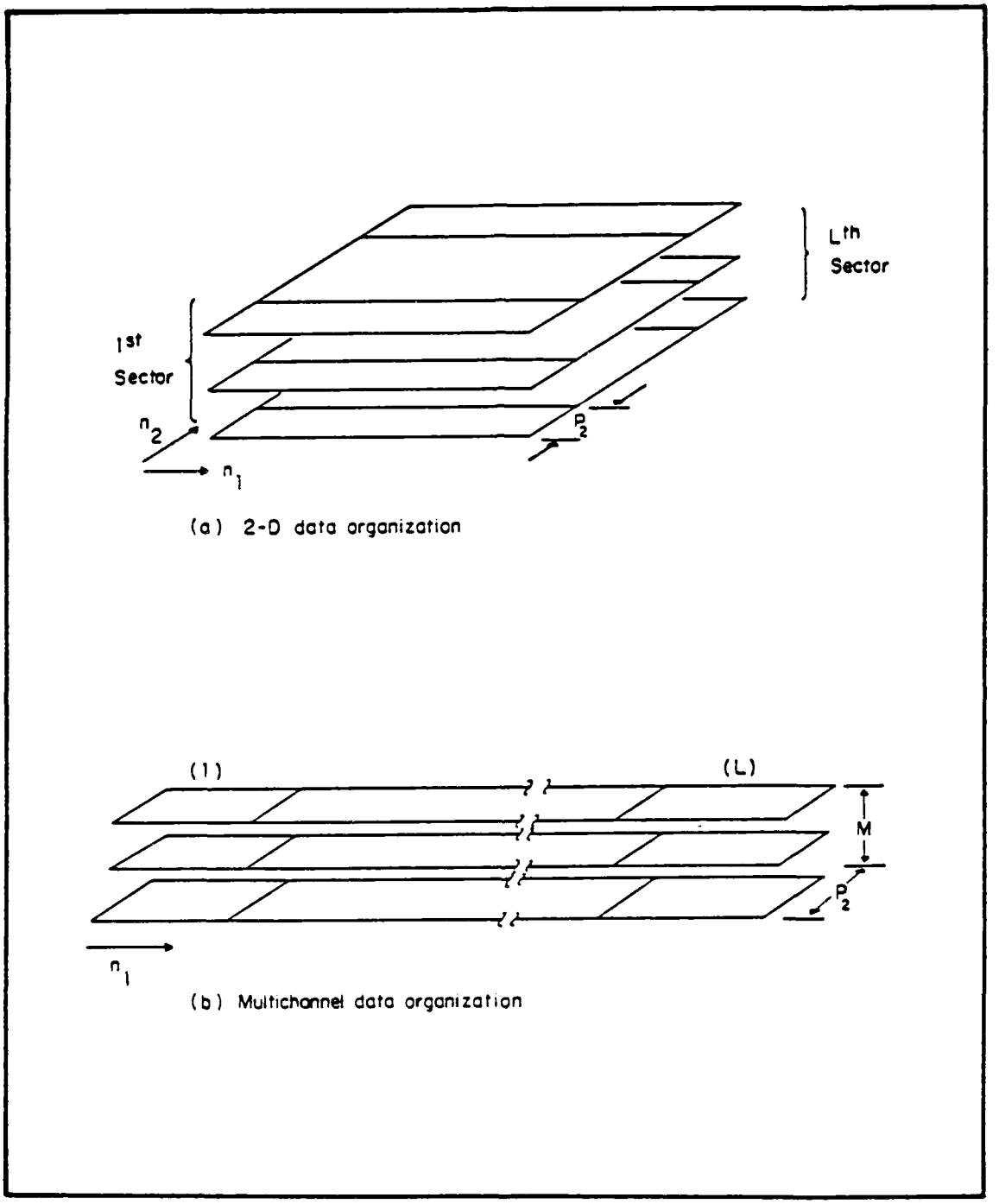

Fig. 3.13 Sectioning data for the direct method of AR parameter estimation.

covariance matrices are used to form (3.56) and (3.58). These equations are solved by conventional methods and the multichannel 2-D first and second quadrant filter coefficients are computed from (3.57) and (3.59).

I. A MEASURE FOR COMPARING RANDOM PROCESSES

In the next chapter it will be important to have a quantitative measure for comparing the *similarity* of two spectral estimates. Such a measure was cited in Chapter II and is based on the information-theoretic *divergence*. The divergence measures the closeness of the distributions for two random processes. Since we model the spectrum as that of a linear filter driven by white noise, it is reasonable to measure the closeness of two spectral estimates as the divergence between random processes produced by the models. As discussed earlier, the divergence relates to the ability to discriminate between the two random processes in a classical hypothesis test. When the white noise which drives the linear filters is Gaussian one can derive an explicit closed-form expression for the divergence. This can be expressed in terms of the model parameters or in terms of the associated spectral estimates.

The divergence is a non-decreasing function of the number of samples of the random process used in the hypothesis test. For linear white noise-driven models each new sample contributes a fixed additive amount to the divergence. This quantity has been called the *incremental divergence* and represents the information available for discrimination of two random processes with each new sample that is observed.

The representation of incremental divergence $\Delta J(1,2)$ between two multichannel 2-D random processes can be written in terms of filter parameters or in terms of spectral estimates as follows.

1. In Terms of Filter Parameters

$$\Delta J(1,2) = -M + \frac{1}{2}\left\{ tr\ \mathbf{A}_2\mathbf{R}_1\mathbf{A}_2^T\boldsymbol{\Sigma}_2^{-1} + tr\ \mathbf{A}_1\mathbf{R}_2\mathbf{A}_1^T\boldsymbol{\Sigma}_1^{-1} \right\} \tag{3.60}$$

where M represents the number of channels, $\mathbf{A}_k$ (k=1,2) represents the set of filter coefficients of the process k, $\mathbf{R}_k$ is the entire covariance matrix of the process k, and finally $\boldsymbol{\Sigma}_k$ is the error covariance matrix of process k.

2. In Terms of Spectral Estimates

$$\Delta J(1,2) = -M + \frac{1}{8\pi^2}\left[\int_{-\pi}^{\pi}\int_{-\pi}^{\pi} tr\ \mathbf{S}_1(\omega_1,\omega_2)\mathbf{S}_2^{-1}(\omega_1,\omega_2)d\omega_1 d\omega_2 \right.$$

$$\left. + \int_{-\pi}^{\pi}\int_{-\pi}^{\pi} tr\ \mathbf{S}_2(\omega_1,\omega_2)\mathbf{S}_1^{-1}(\omega_1,\omega_2)d\omega_1 d\omega_2 \right] \tag{3.61}$$

where $\mathbf{S}_1$ and $\mathbf{S}_2$ are the M×M spectral matrices of the modeled random processes. The above expressions for the incremental divergence for multichannel 2-D random processes are derived in Appendix E. The expression given in terms of spectral estimates (3.61) is our main interest in the present research.

Although the form (3.61) for the incremental divergence is based on the existence of linear models for the spectra $\mathbf{S}_1$ and $\mathbf{S}_2$ the expression (3.61) can be simply *defined* as a measure for comparing any two spectral estimates. When one of the spectra (say $\mathbf{S}_2$) is defined by the CQ method, the term in Eqn. (3.61) involving the inverse is additive. Unfortunately the other term is not, so the incremental divergence appears to defy any further interpretation.

IV. MULTICHANNEL 2-D AR SPECTRUM ANALYSIS

This chapter is concerned with multichannel 2-D spectral estimation based on AR models. Here the problem is to obtain accurate spectral estimates given a finite number of data samples. We begin by summarizing the spectral estimation models, and show that since the NSHP forward and backward models have distinctly different model parameters, in general this leads to different spectral estimates. Similarly it is shown that in general none of the four possible multichannel 2-D QP models gives the same estimate for the spectral matrix. The latter suggests a generalization of the procedure used by Jackson and Chien for combining multiple quadrant-based spectral estimates into a single combined spectral estimate. We call this procedure the combined quadrant (CQ) method, and it can be used effectively with the *direct* method of parameter estimation developed in Chapter III. A comprehensive set of experimental studies for estimating the entire spectral matrix is presented. The estimate includes the 2-D autospectrum for each channel and magnitude and phase of the cross spectra. The estimates compared correspond to NSHP, CQ, and direct CQ models.

A. SPECTRUM ESTIMATION MODELS

Parametric approaches to spectral estimation are based on an *a priori* model for the spectrum in terms of a finite and relatively small number of unknown parameters. The spectral density estimate can then be obtained by evaluating a formula in terms of the estimated parameters. When a good parametric model for the spectrum is available, estimates of the model parameters can be obtained using a number of different approaches.

Autoregressive modeling is the form of spectrum estimation that will be examined here. Filter parameters and the white noise covariance are estimated by the techniques described in Chapter III. Let the linear predictive filter transfer function be given by

$$\mathbf{H}(z_1,z_2) = \sum_{(l_1,l_2)\in\alpha} \mathbf{A}^T_{l_1 l_2} z_1^{-l_1} z_2^{-l_2} \tag{4.1}$$

Then the spectrum of the random process can be expressed as

$$\mathbf{S}(\omega_1,\omega_2) = \mathbf{H}^{-1}(\omega_1,\omega_2)\,\Sigma_w\,\left[\mathbf{H}^{H}(\omega_1,\omega_2)\right]^{-1} \tag{4.2}$$

where Σ_w represents the white noise spectral matrix. For the specific case when the number of channels (M) is equal to 2 the filter has the form

$$\mathbf{H}(\omega_1,\omega_2) = \begin{bmatrix} H_{11}(\omega_1,\omega_2) & H_{12}(\omega_1,\omega_2) \\ H_{21}(\omega_1,\omega_2) & H_{22}(\omega_1,\omega_2) \end{bmatrix} \tag{4.3}$$

and the spectral matrix has the form given by Eqn. (3.15). Thus Eqn. (4.2) produces estimates of the autospectra and the cross spectra all at once.

For purposes of developing a spectral estimate, different regions of support of the AR model can be used. We are interested here in the NSHP and QP regions of support.

1. Non-Symmetric Half Plane Models

As we mentioned in Chapter III, NSHP models of moderate size have proven to give reasonable results for spectrum estimation. The spectrum can be expressed by Equation (4.2) where $\mathbf{H}(z_1,z_2)$ is the filter transfer function for the given region of support

$$\mathbf{H}(z_1,z_2) = I + \sum_{i_2=1}^{P_2} \mathbf{A}_{0i_2}^{T} z_2^{-i_2} + \sum_{i_1=1}^{P_1} \sum_{i_2=-P_2}^{P_2} \mathbf{A}_{i_1 i_2}^{T} z_1^{-i_1} z_2^{-i_2} \tag{4.4}$$

and where $\mathbf{A}_{i_1 i_2}$ represents the filter coefficient matrices of the forward predictor. As we will see in section B, the forward and backward predictors discussed in Chapter III give *different* spectral estimates. In subsequent sections of this chapter we examine results of NSHP spectral models of various orders. Fig. 4.1 shows the definition of order used for NSHP models.

2. Quadrant Models

Quadrant support regions are also considered for the AR model. These are of interest because of their convenience of computation and estimation of the model parameters. As discussed in Chapter II there exist four different quadrant plane support models. However we will find in the multichannel 2-D case that none of the models is

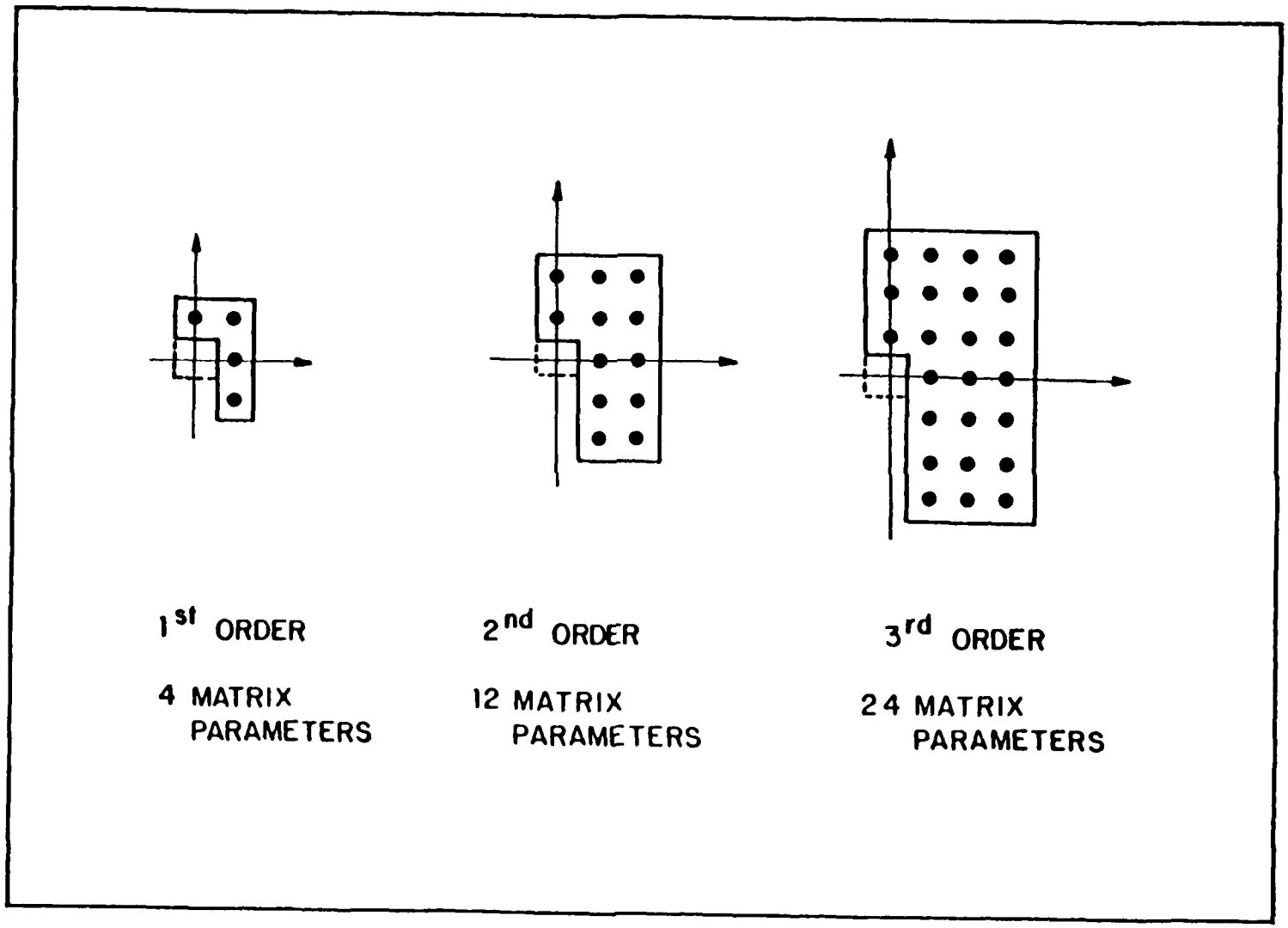

Fig. 4.1 Definition of order for NSHP models.

the same. The first quadrant filter transfer function of order (P_1,P_2) is

$$\mathbf{H}_I(\omega_1,\omega_2) = \sum_{n_1=0}^{P_1} \sum_{n_2=0}^{P_2} \mathbf{A}_{n_1n_2}^T e^{-j\omega_1 n_1} e^{-j\omega_2 n_2} \quad , \qquad \mathbf{A}_{00}=\mathbf{I} \tag{4.5}$$

where $\mathbf{A}_{n_1n_2}$ represents the first quadrant filter coefficients. The corresponding power spectral estimate evaluated from $\mathbf{H}_I(\omega_1,\omega_2)$ is:

$$\mathbf{S}_I(\omega_1,\omega_2) = \mathbf{H}_I^{-1}(\omega_1,\omega_2)\, \Sigma_{w_I} \left[\mathbf{H}_I^H(\omega_1,\omega_2)\right]^{-1} \tag{4.6}$$

where Σ_{w_I} is the error covariance matrix of the first quadrant model. Similarly the spectral estimate of the second quadrant model is given as

$$\mathbf{S}_{II}(\omega_1,\omega_2) = \mathbf{H}_{II}^{-1}(\omega_1,\omega_2)\, \Sigma_{w_{II}} \left[\mathbf{H}_{II}^H(\omega_1,\omega_2)\right]^{-1} \tag{4.7}$$

where

$$\mathbf{H}_{II}(\omega_1,\omega_2) = \sum_{n_1=0}^{P_1} \sum_{n_2=0}^{P_2} \mathbf{B}_{n_1n_2}^T e^{j\omega_1 n_1} e^{-j\omega_2 n_2} \quad , \qquad \mathbf{B}_{00}=\mathbf{I} \tag{4.8}$$

and where $\mathbf{B}_{n_1n_2}$ are the second quadrant filter coefficients and $\Sigma_{w_{II}}$ represents the error covariance matrix of the second quadrant model. The third and fourth quadrant filters are given by similar expressions and are also distinct as we will see in the next section.

It will be seen that first, second, third, and fourth quadrant AR models when used individually give poor estimates of the spectrum of many random processes. For the analysis of sinusoids in noise the use of any quadrant filter alone results in a spreading of the peak in one direction. However a certain combination of the models has proven to give good results for estimation of spectra in 2-D single channel problems (Jackson & Chien, 1979). In section B we propose a generalization of this method to 2-D multichannel spectrum estimation. The definition of order used for QP models is shown in Fig. 4.2.

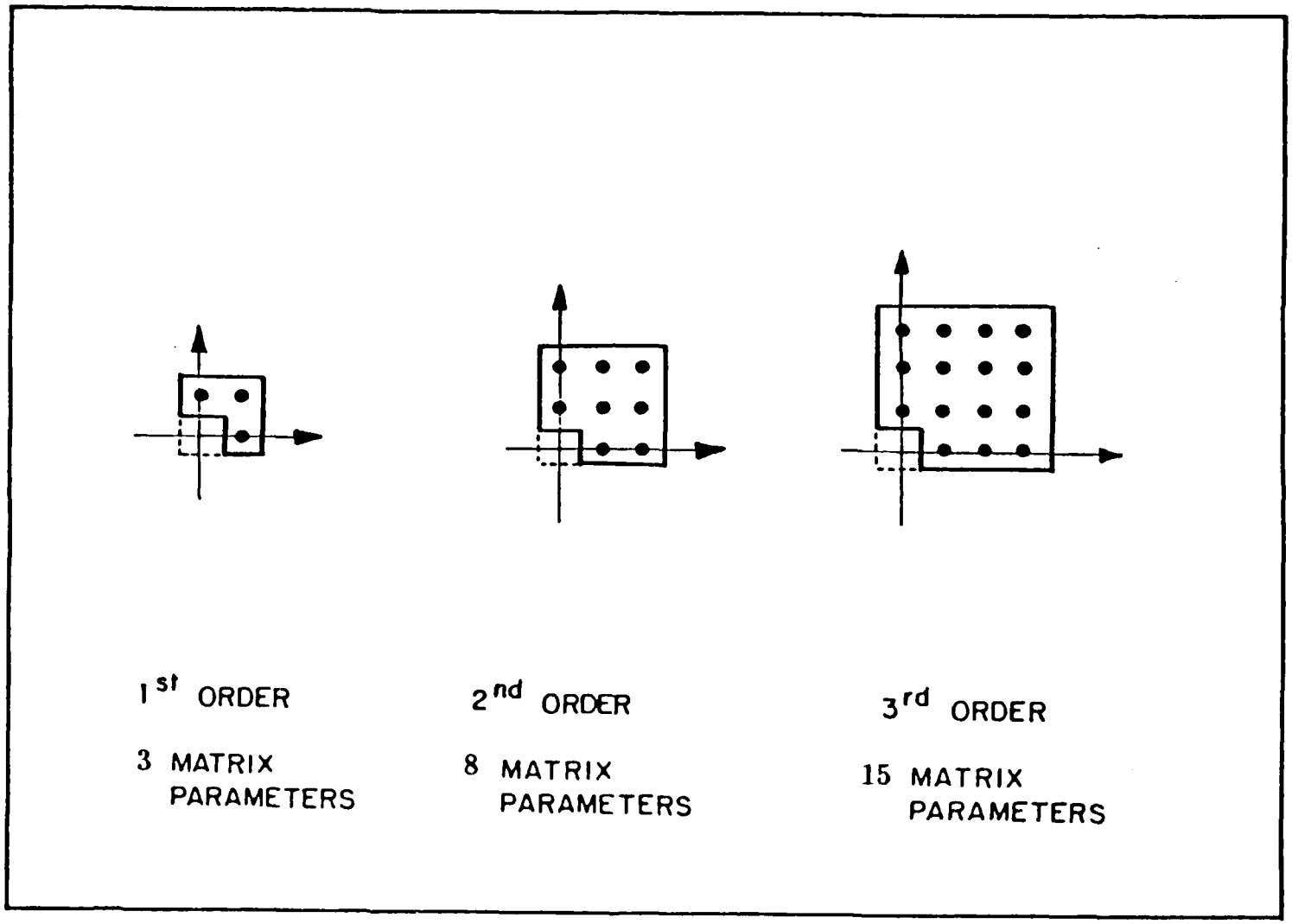

Fig. 4.2 Definition of order for quadrant plane models.

B. FORWARD AND BACKWARD SPECTRAL ESTIMATION

The forward and backward AR models for 1-D or 2-D single channel signals have the same power spectra. That is, the estimates produced by these models are always identical. The reason for this is as follows: The correlation functions in the single channel case have the symmetry properties $R(k) = R(-k)$ for 1-D and $R(k_1,k_2) = R(-k_1,-k_2)$ for 2-D. Because of this the correlation matrices appearing in the Normal equations for the forward and backward models are identical and thus lead to identical model parameters (i.e. filter coefficients and error covariance). This in turn leads to identical spectral estimates.

In the 1-D multichannel case the correlation matrices appearing in the Normal equations for the forward and backward models are not identical because the (matrix) correlation function satisfies only the symmetry condition $\mathbf{R}(k)=\mathbf{R}^T(-k)$. Specifically the matrices in the Normal equations differ in that the innermost blocks are transposed. Likewise for the 2-D multichannel case the correlation function satisfies only $\mathbf{R}(k_1,k_2) = \mathbf{R}^T(-k_1,-k_2)$ and the Normal equations have innermost blocks transposed. The solution of these Normal equations gives different forward and backward model parameters. However Nuttall (1976) shows that the forward and backward 1-D multichannel power spectral estimates are *identical*. The proof is based on the *existence* of an underlying maximum entropy random process that matches the given correlation function and extends it. The common spectral estimate computed by both the forward and the backward models is the true spectrum of the underlying maximum entropy process (see (Nuttall,1976) for details).

In the multichannel 2-D case it is not in general possible to match and extend the correlation function. Thus, except in the asymptotic case (i.e. as the support tends to infinity) there is no underlying process that the two models have in common. In general this leads to *different* spectral estimates for the forward and backward models (see Fig. 4.3) and these estimates may not even be positive definite. This is a significant difference between multichannel 2-D AR models and lower-dimensional models. Thus the difference between forward and backward 2-D multichannel spectral estimates is seen to be due to the fact that the correlation function in 2-D may not be extendible

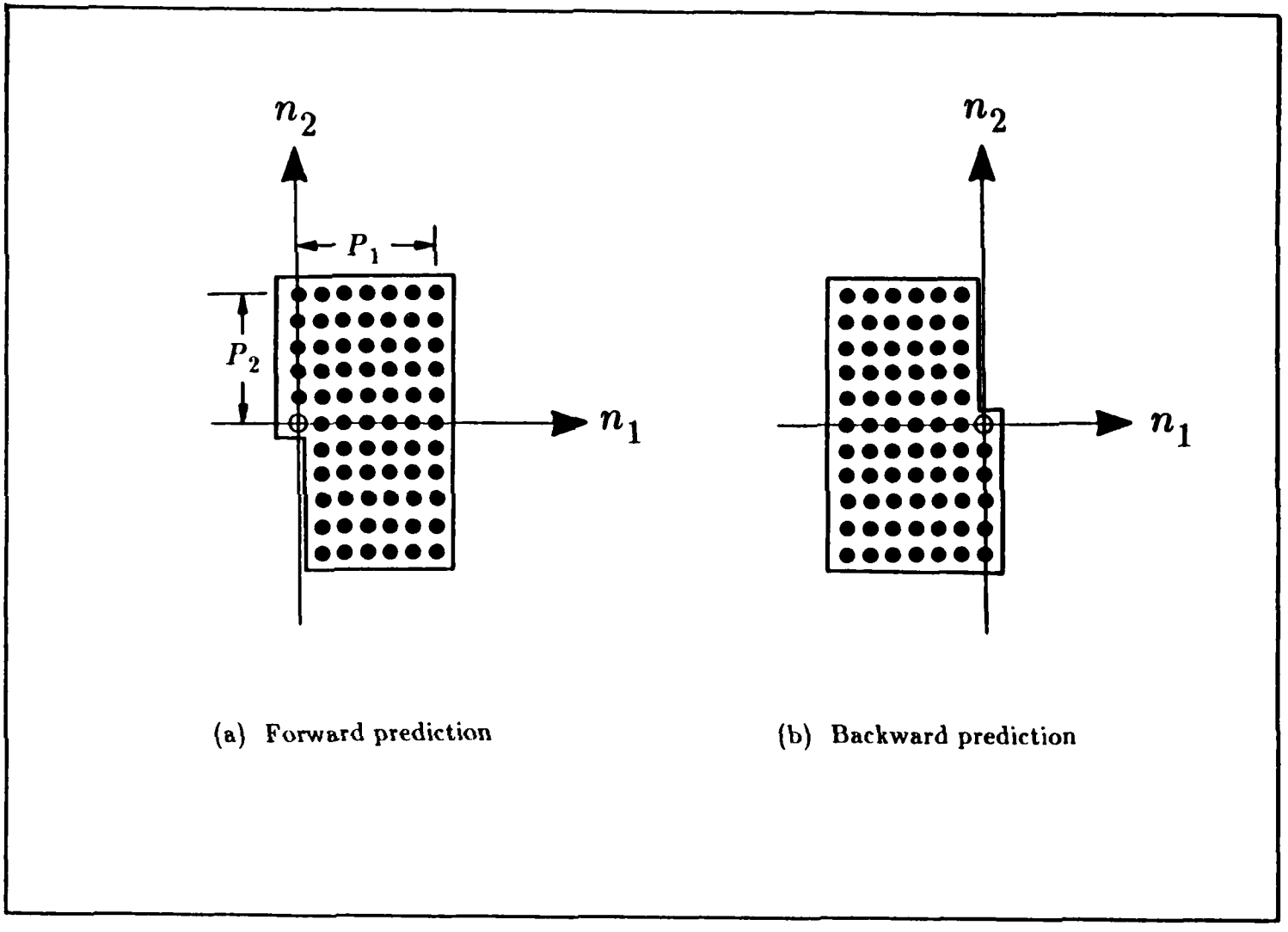

Fig. 4.3 The filter of support α for NSHP.

(Dickinson,1980). In essence there may be no underlying random process that would be whitened by the given linear predictive filter.

To see specifically where the system breaks down let us for the moment *assume* that the linear predictive filter truly whitens the random process and thus corresponds to the AR model of the form

$$\mathbf{w}(n_1,n_2) = \sum_{(i_1,i_2)\in\alpha} \mathbf{A}_{i_1 i_2}^T \mathbf{x}(n_1-i_1,n_2-i_2) \tag{4.9}$$

It follows that

$$E\left[\mathbf{w}(n_1,n_2)\mathbf{w}^T(n_1-k_1,n_2-k_2)\right] = \sum_{(i_1,i_2)\in\alpha}\sum_{(j_1,j_2)\in\alpha} \mathbf{A}_{i_1 i_2}^T \mathbf{R}(k_1+j_1-i_1,k_2+j_2-i_2)\mathbf{A}_{j_1 j_2}$$

$$= \Sigma_w \delta(k_1,k_2) \tag{4.10}$$

Taking the z transform of (4.10) and making the substitution of variables $l_n = k_n + j_n - i_n$ results in

$$\sum_{(i_1,i_2)\in\alpha} \mathbf{A}_{i_1,i_2}^T z_1^{-i_1} z_2^{-i_2} \sum_{l_1=-\infty,l_2=-\infty}^{\infty,\infty} \mathbf{R}(l_1,l_2) z_1^{-l_1} z_2^{-l_2} \sum_{(j_1,j_2)\in\alpha} \mathbf{A}_{j_1 j_2} z_1^{j_1} z_2^{j_2} = \Sigma_w \tag{4.11}$$

Finally letting $z_n = e^{j\omega_n}$ and using the definition (4.1) leads to (4.2) where $\mathbf{S}(\omega_1,\omega_2)$ is seen to be the Fourier transform of the correlation function:

$$\mathbf{S}(\omega_1,\omega_2) = \sum_{(l_1,l_2)=(-\infty,-\infty)}^{(\infty,\infty)} \mathbf{R}(l_1,l_2) e^{-j(l_1\omega_1+l_2\omega_2)} \tag{4.12}$$

It is clear from this analysis that if $\mathbf{x}(n_1,n_2)$ also satisfies a backward form of AR model then (4.9)-(4.12) is also be obtained except that the $\mathbf{A}_{i_1 i_2}$ and Σ_w are replaced by the backward model parameters and $\mathbf{R}(l_1,l_2)$ is replaced by $\mathbf{R}^T(l_1,l_2)$. Further, since

$$\mathbf{R}^T(l_1,l_2) = \mathbf{R}(-l_1,-l_2) \tag{4.13}$$

and the sum in (4.12) is over all values of l_1 and l_2, the spectral matrix defined by (4.12) for the backward problem is identical to that for the forward problem. Thus we see that when an AR model in the form of Eqn. (4.9) truly exists for the random process, then both forward and backward spectral estimates will be identical. The procedure breaks

down if we must use a colored noise to obtain a model in the form of Eqn. (4.9). In this case we cannot write Eqn. (4.11) and the spectral estimates are not identical.

The spectral matrix corresponding to the forward linear prediction $S(\omega_1,\omega_2)$ and backward linear prediction $S'(\omega_1,\omega_2)$ can be written in the following forms, respectively

$$\mathbf{S}(\omega_1,\omega_2) = \mathbf{H}^{-1}(\omega_1,\omega_2)\,\Sigma_w\,(\mathbf{H}^H(\omega_1,\omega_2))^{-1} \tag{4.14}$$

$$\mathbf{S}'(\omega_1,\omega_2) = \mathbf{H}'^{-1}(\omega_1,\omega_2)\,\Sigma'_w\,(\mathbf{H}'^H(\omega_1,\omega_2))^{-1} \tag{4.15}$$

where $\mathbf{H}$, $\mathbf{H}'$ represent the forward and backward matrix frequency response

$$\mathbf{H}(\omega_1,\omega_2) = \sum_{(n_1,n_2)\in\alpha} \mathbf{A}^T_{n_1,n_2} e^{-j(\omega_1 n_1+\omega_2 n_2)} \tag{4.16}$$

$$\mathbf{H}'(\omega_1,\omega_2) = \sum_{(n_1,n_2)\in\alpha} \mathbf{B}^T_{n_1,n_2} e^{j(\omega_1 n_1-\omega_2 n_2)} \tag{4.17}$$

and Σ_w, Σ'_w are the forward and backward covariance error matrices, respectively.

In the limit, as α approaches a NSHP with infinite support, the linear predictive model and the AR model become identical. This is implicit in the work of Ekstrom and Woods (1976), Marzetta (1978), and Jain (1981). In this case the spectrum of the process is truly given by (4.14) and the spectral matrix can be represented in terms of either the forward *or* the backward model parameters. While one cannot use infinite NSHP support in practical applications, larger orders can approximate the limiting case and the two spectral estimates have been found to give very close results.

It is of interest to consider a numerical example to study the behaviour of forward and backward spectral estimation. This example is concerned with the power spectral estimation of a two-channel 2-D single sinusoid in additive noise. The signals generated in channels 1 and 2 were

$$x_1(n_1,n_2) = \cos(n_1\omega_1+n_2\omega_2) + w_1(n_1,n_2) \tag{4.18a}$$

$$x_2(n_1,n_2) = \cos(n_1\omega_3+n_2\omega_4+\phi) + w_2(n_1,n_2) \tag{4.18b}$$

where $w_1(n_1,n_2)$ and $w_2(n_1,n_2)$ are zero-mean independent white noise signals.

Spectrum estimation results are given for a dataset size of 64×64. The forward and backward matrix parameters of the AR models are shown in Figs. 4.4 and 4.5 respectively. It is clear that they are not the same. Table 4.1 shows the values of the spectral estimates at $\omega_1=\omega_2=0$. Observe that as the model order increases the value of the individual terms in the forward and backward spectral matrices become closer. The last column in Table 4.1 gives the value of the incremental divergence for the two spectral estimates. This quantity, which is defined in Chapter III, measures the closeness of the spectral matrices over all frequencies. Since lower numbers represent closer spectra, the results indicate that the forward and backward spectral estimates tend to converge as the model order increases. A summary of forward and backward prediction model characteristics for different random processes is given in Table 4.2.

1. Combined Quadrant Models

From considerations similar to those above, it can be seen that in general none of the four possible multichannel 2-D models with quadrant support (see Fig. 4.6) give the same estimate for the spectral matrix. This again is different from the single channel case where for example the first and third quadrant models, being degenerate cases of forward and backward NSHP support, produce identical spectral estimates. This suggests a generalization of the procedure used by Jackson and Chien (1979) for single channel 2-D spectrum estimation. In particular, a combined estimate for the spectral matrix can be formed as

$$S(\omega_1,\omega_2) = (S_I^{-1}(\omega_1,\omega_2) + S_{II}^{-1}(\omega_1,\omega_2) + S_{III}^{-1}(\omega_1,\omega_2) + S_{IV}^{-1}(\omega_1,\omega_2))^{-1} \qquad (4.19)$$

where S_I, S_{II}, S_{III}, and S_{IV} are the spectral matrices computed from (4.14) using the four possible quadrant models. This procedure will be called the combined quadrant (CQ) method. Although it appears that four quadrant models would be required in general, it was found experimentally that the combination of only first and second quadrants is sufficient to obtain good results.

$$S(\omega_1,\omega_2) = (S_I^{-1}(\omega_1,\omega_2) + S_{II}^{-1}(\omega_1,\omega_2))^{-1} \qquad (4.20)$$

This form is analogous to the form proposed by Jackson and Chien for the single channel

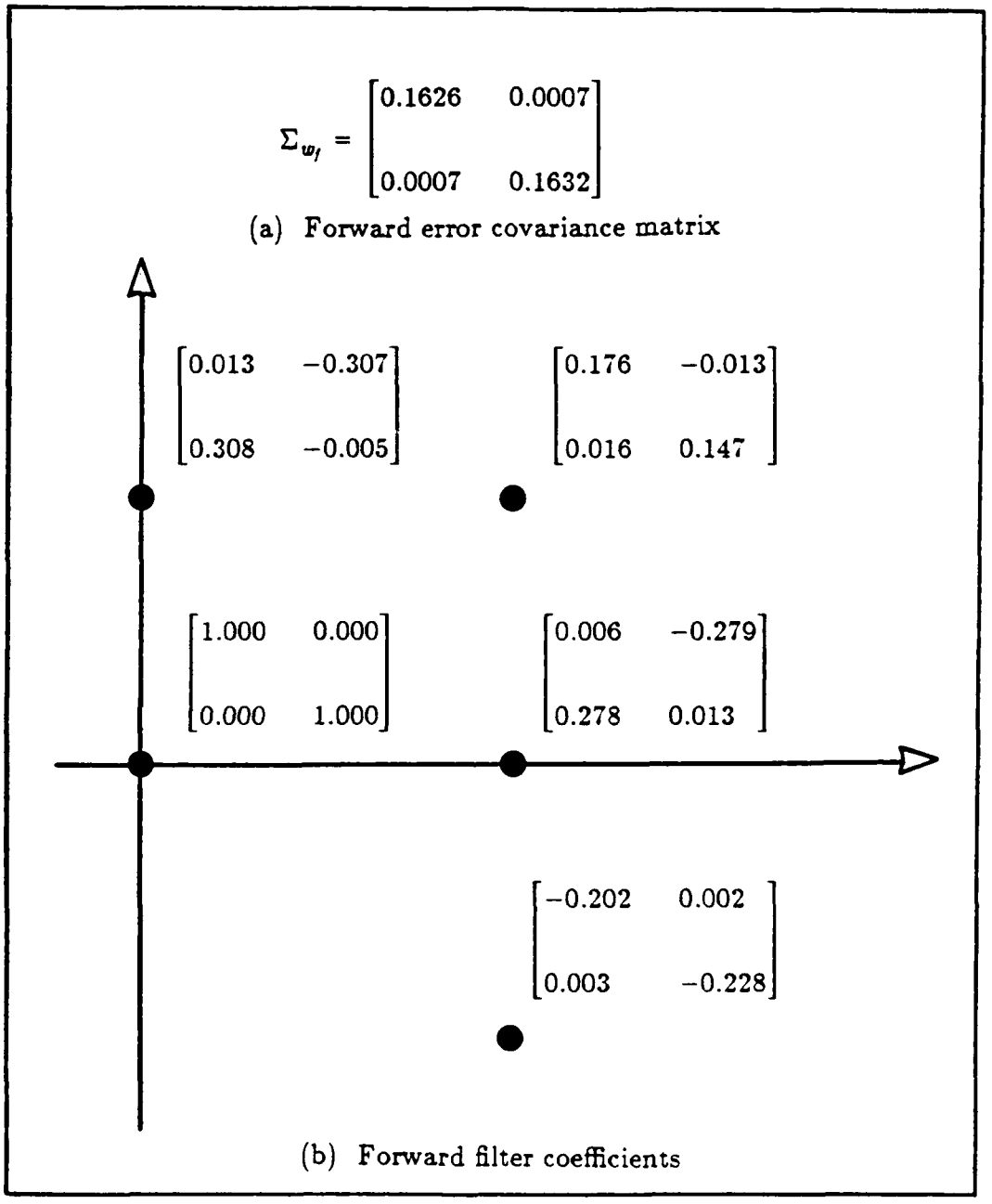

Fig. 4.4 Forward model parameters of first order NSHP model.

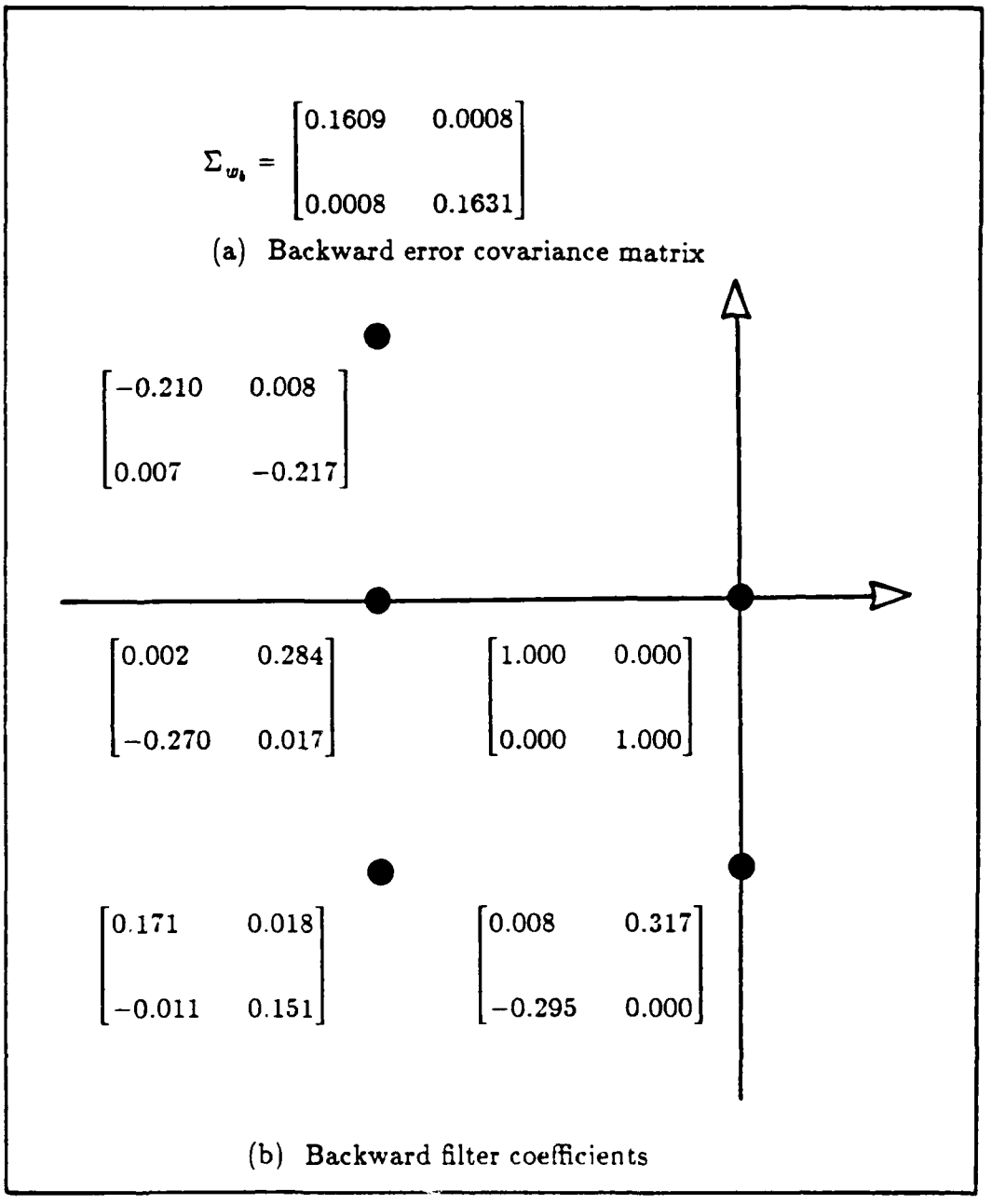

Fig. 4.5 Backward NSHP model parameters of first order.

TABLE 4.1 COMPARISON BETWEEN FORWARD AND BACKWARD SPECTRAL ESTIMATES

Order	*Forward Spectral Estimate* $S_F(0,0)$	*Backward Spectral Estimate* $S_B(0,0)$	*Incremental Divergence* ΔJ
1	$\begin{bmatrix} 0.1754 & 0.0325 \\ 0.0325 & 0.1575 \end{bmatrix}$	$\begin{bmatrix} 0.1241 & 0.0257 \\ 0.0257 & 0.4518 \end{bmatrix}$	0.3739
2	$\begin{bmatrix} 0.1400 & 0.0359 \\ 0.0359 & 0.1721 \end{bmatrix}$	$\begin{bmatrix} 0.1069 & 0.0030 \\ 0.0030 & 0.2068 \end{bmatrix}$	0.0914
3	$\begin{bmatrix} 0.0812 & 0.0192 \\ 0.0192 & 0.0836 \end{bmatrix}$	$\begin{bmatrix} 0.0893 & 0.0128 \\ 0.0128 & 0.0732 \end{bmatrix}$	0.0769
4	$\begin{bmatrix} 0.0711 & 0.0199 \\ 0.0199 & 0.0635 \end{bmatrix}$	$\begin{bmatrix} 0.0744 & 0.0203 \\ 0.0203 & 0.0618 \end{bmatrix}$	0.0703

TABLE 4.2 FORWARD AND BACKWARD PREDICTION MODEL CHARACTERISTICS.

	Forward and Backward Model Parameters	Forward and Backward Spectral Estimate
1-D single channel	same	same
2-D single channel	same	same
1-D multichannel	different	same
2-D multichannel	different	different

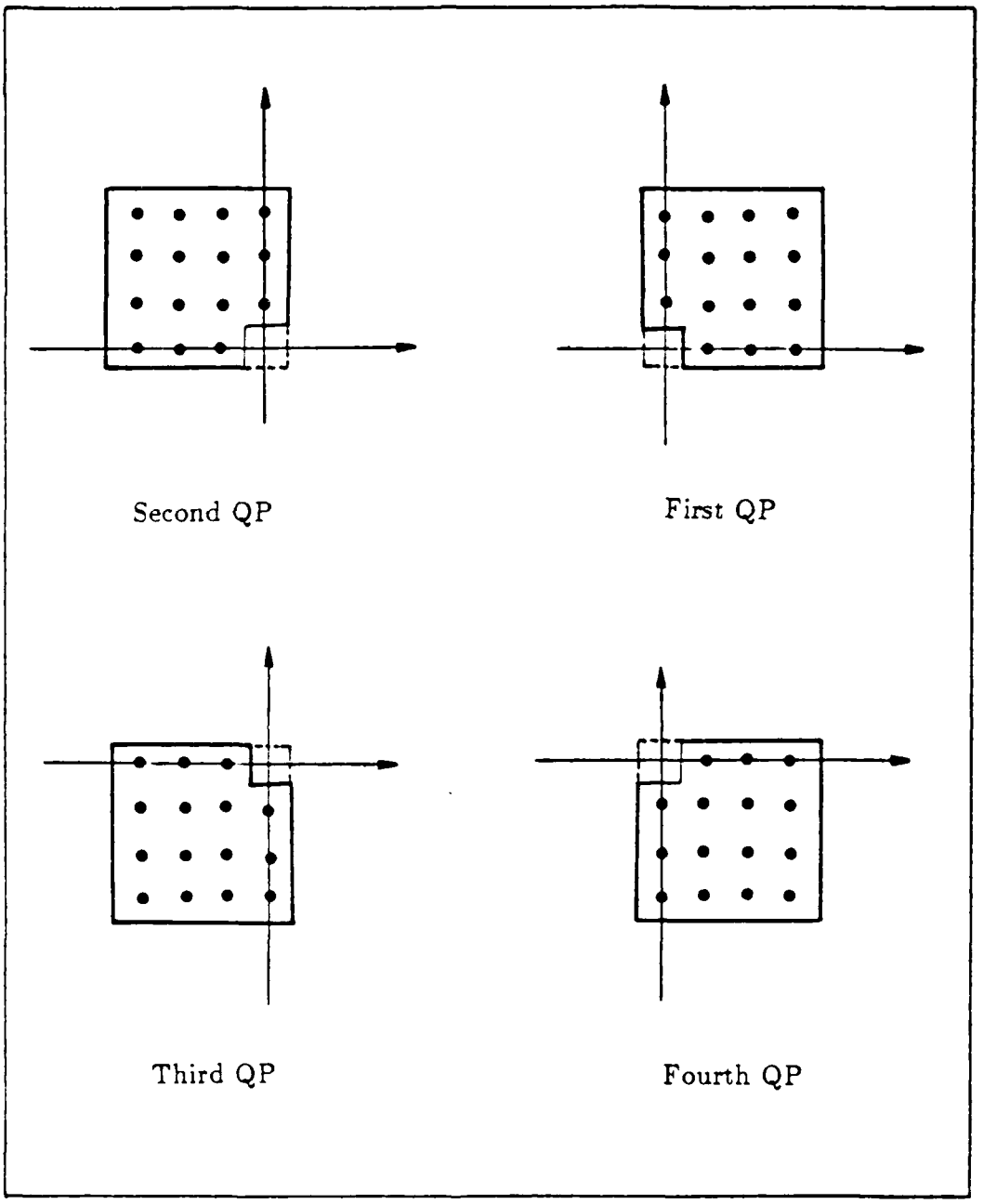

Fig. 4.6 Filter support α for quadrant plane models.

case. From Eqns. (4.20) and (4.2) one can therefore write

$$\mathbf{S}(\omega_1,\omega_2) = \left[\mathbf{H}_I^H(\omega_1,\omega_2)\, \Sigma_{w_I}^{-1}\, \mathbf{H}_I(\omega_1,\omega_2) + \mathbf{H}_{II}^H(\omega_1,\omega_2)\Sigma_{w_{II}}^{-1}\mathbf{H}_{II}(\omega_1,\omega_2) \right]^{-1} \quad (4.21)$$

When we are interested only in the detection of sharp peaks in the spectrum and not in the true power level the following simpler form can be used

$$\mathbf{S}(\omega_1,\omega_2) = \left[\mathbf{H}_I^H(\omega_1,\omega_2)\mathbf{H}_I(\omega_1,\omega_2) + \mathbf{H}_{II}^H(\omega_1,\omega_2)\mathbf{H}_{II}(\omega_1,\omega_2) \right]^{-1} \quad (4.22)$$

(where we have set $\Sigma_{w_I} = \Sigma_{w_{II}} = \mathbf{I}$) and appears to produce satisfactory results.

In order to check the performance of the four quadrant plane power spectral estimate, a numerical example is considered. This example is concerned with the analysis of spectra for two-channel 2-D sinusoidal signals in additive noise. The signals generated in channels 1 and 2 were:

$$x_1(n_1,n_2)=\sum_{i=1}^{L}\cos(n_1\omega_{i1}+n_2\omega_{i2})+w_1(n_1,n_2) \quad (4.23a)$$

$$x_2(n_1,n_2)=\sum_{i=1}^{L}\cos(n_1\omega_{i3}+n_2\omega_{i4}+\phi_i)+w_2(n_1,n_2) \quad (4.23b)$$

where $w_1(n_1,n_2)$ and $w_2(n_1,n_2)$ are zero mean independent white noise signals, and L represents the number of sinusoids. We assume L=2, with $\omega_{11}=\omega_{12}=\frac{\pi}{2}$, $\omega_{21}=\omega_{22}=\frac{\pi}{3}$, $\omega_{13}=\omega_{14}=\frac{\pi}{2}$, $\omega_{23}=\omega_{24}=\frac{\pi}{3}$, ϕ_1=1.5 radian, and ϕ_2=0.5 radian. Spectrum estimates are given for a dataset size of (64×64) and second order filter. The cross spectrum amplitude for first, second, third, and fourth quadrants is shown in Fig. 4.7, while the amplitude and phase of the cross spectrum of the combined quadrant estimate (Eqn. (4.20)) is shown in Fig. 4.8. The cross spectrum amplitude and phase of the total 4-combined quadrant estimate (Eqn. (4.19)) is shown in Figure 4.9. Table 4.3 shows values of the incremental divergence between the different quadrant plane spectral estimates. Here CQ_4 represents the four-quadrant CQ estimate (Eqn. (4.19)), and CQ_2 represents the simple two-quadrant CQ estimate (Eqn. (4.20)). The results indicate a closeness between the first and third quadrant estimates, second and fourth quadrant estimates, and the

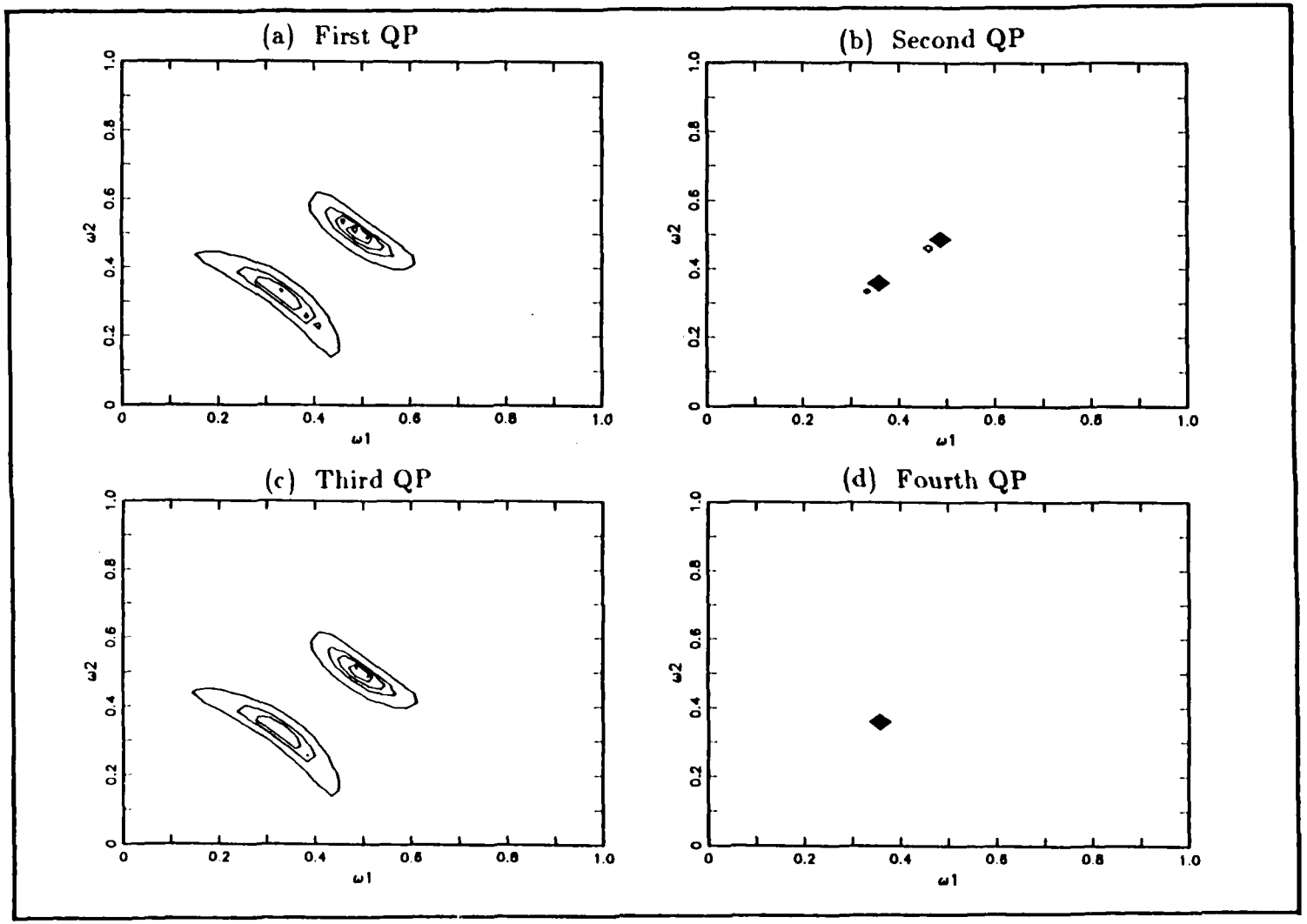

Fig. 4.7 Amplitude of cross spectral estimation of two sinusoids in noise (contour plot).

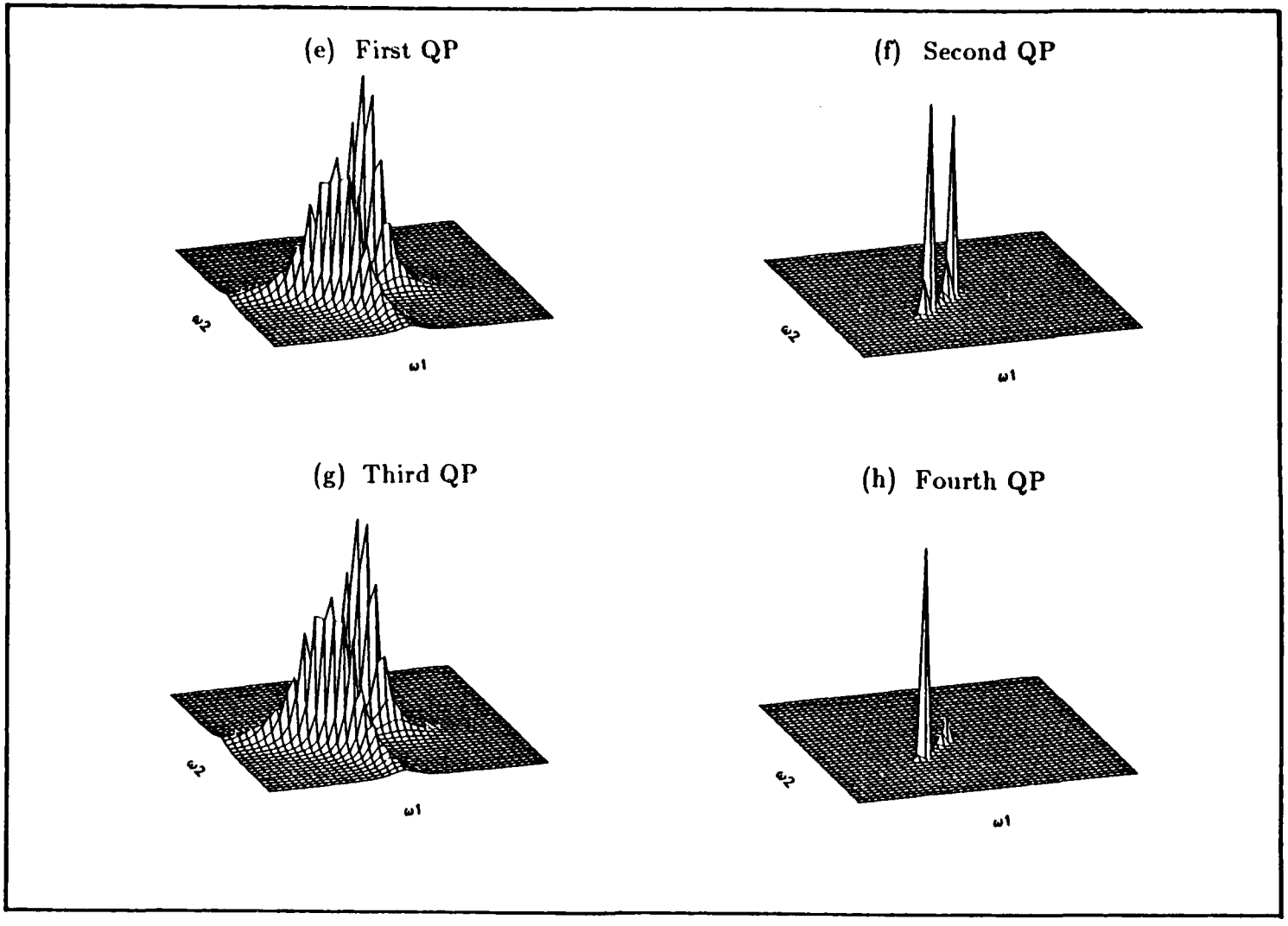

Fig. 4.7 Amplitude of cross spectral estimation of two sinusoids in noise (surface plot). (cont'd)

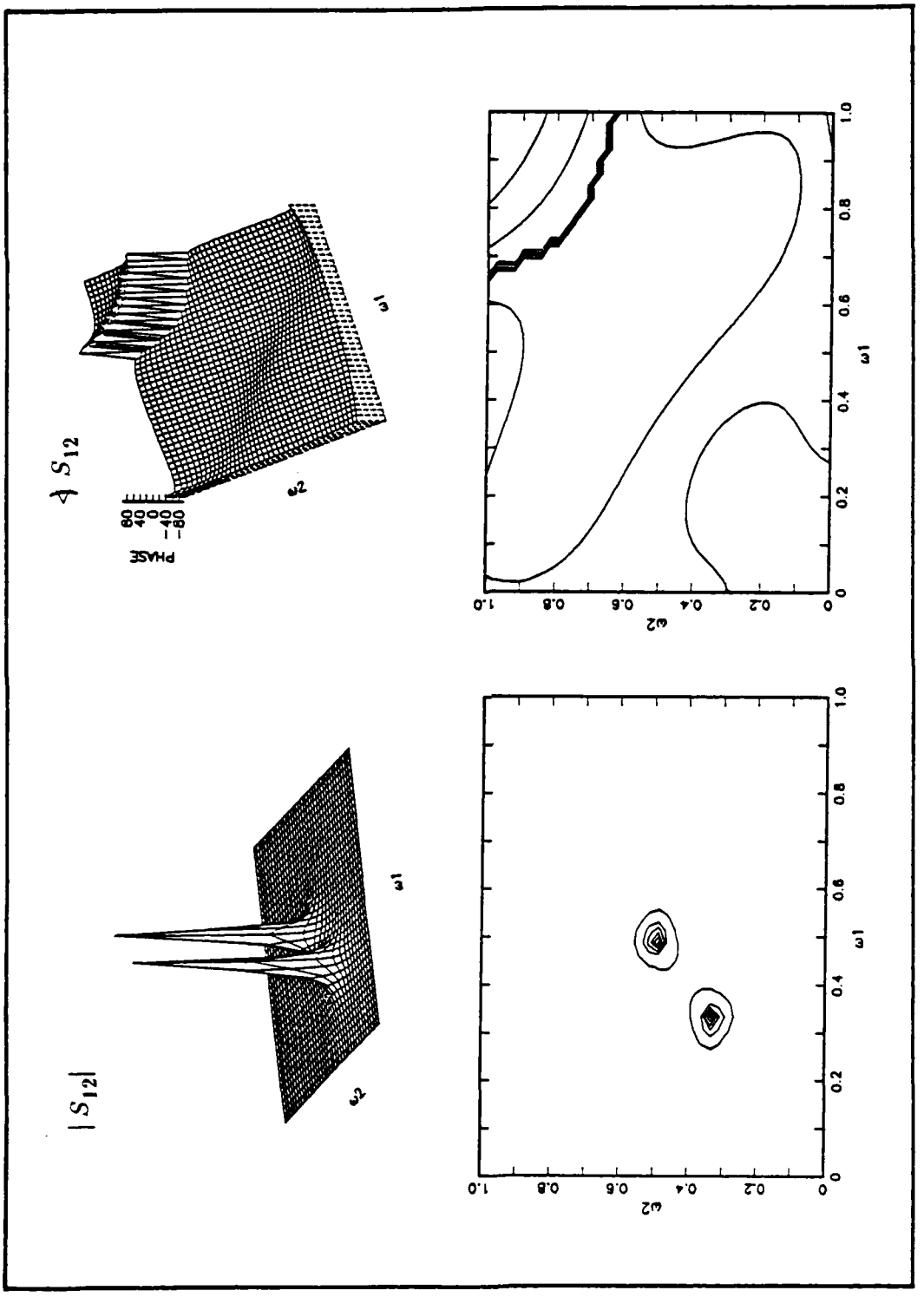

Fig. 4.8 Cross spectrum estimation of two sinusoids (CQ_2).

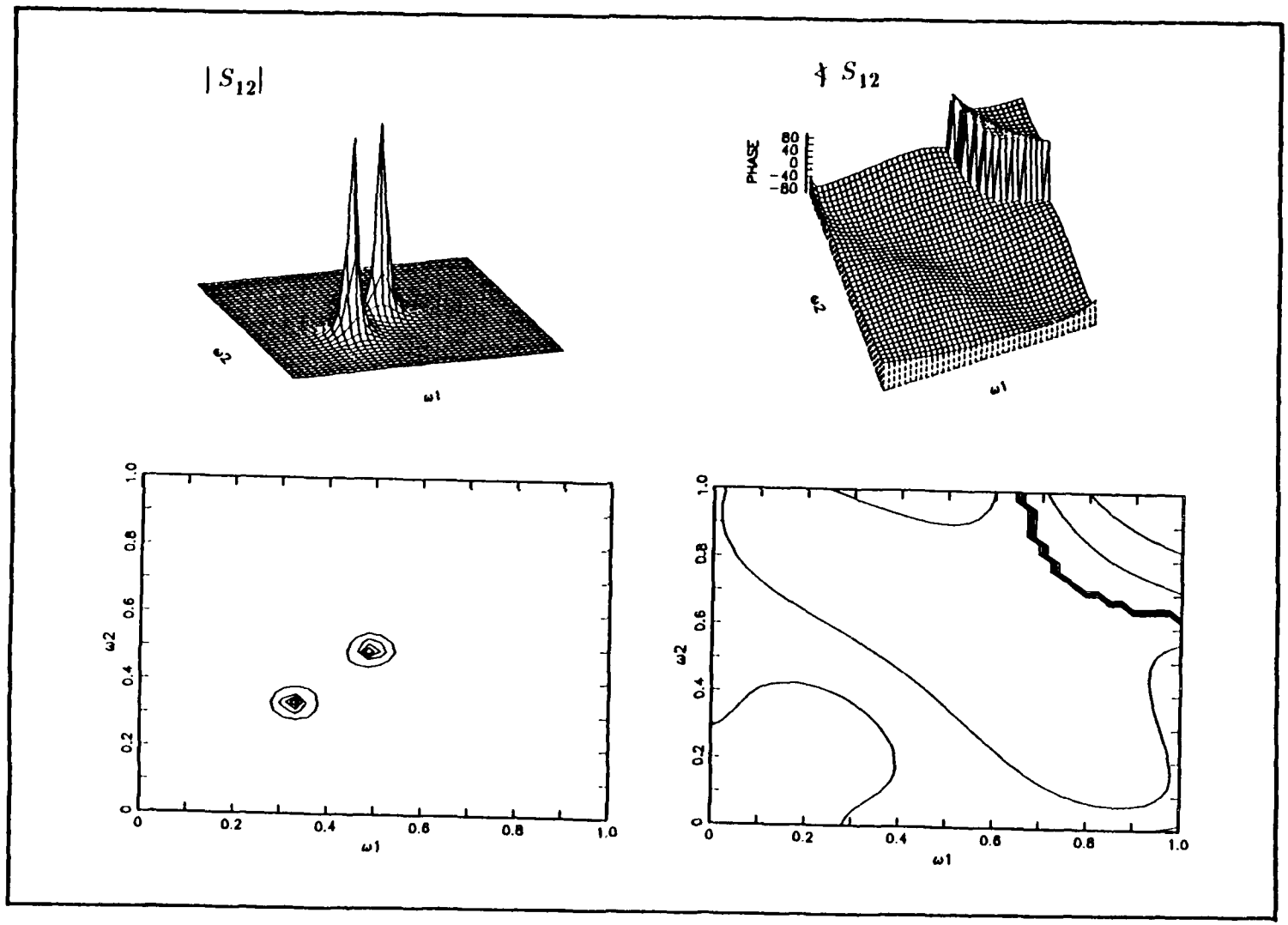

Fig. 4.9 Cross spectrum estimation of two sinusoids (CQ_4).

TABLE 4.3 INCREMENTAL DIVERGENCE OF QUADRANT-BASED MODELS

(a) Comparison between CQ_4 (Eqn. 4.19) and quadrant-based models.

Comparison between CQ_4 &	Incremental divergence (ΔJ)
CQ_2	0.02
1st QP	0.2
2nd QP	0.2
3rd QP	0.2
4th QP	0.26

(b) Comparison between CQ_2 (Eqn. 4.20) and quadrant-based models.

Comparison between CQ_2 &	Incremental divergence (ΔJ)
1st QP	0.07
2nd QP	0.07
3rd QP	0.07
4th QP	0.1

(c) Comarison between quadrant-based models.

Comparison between	Incremental divergence (ΔJ)
1st and 2nd QP	0.09
1st and 3rd QP	0.01
1st and 4th QP	0.12
2nd and 3rd QP	0.09
2nd and 4th QP	0.004
3rd and 4th QP	0.12

CQ_2 and CQ_4 estimates. Although S_{III} is not identical to S_I and S_{IV} is not identical to S_{II} it has been found experimentally in several cases that the simpler CQ_2 estimate (Eqn. (4.20)) gives results very close to the total CQ_4 estimate (Eqn. (4.19)). It will be seen also that the CQ_2 estimate produces results that are very similar to the NSHP results and usually requires less computation. Further when the model parameters are computed directly from the data as described in section III H the estimate was found to have improved resolution.

C. EXPERIMENTAL RESULTS USING NSHP MODELS

A comprehensive set of experimental studies for simulating the entire spectral matrix is presented. The estimate includes the 2-D autospectrum for each channel and magnitude and phase of the cross spectra. Estimates using NSHP models are first computed for sinusoids in white noise backgrounds. A set of experiments were performed to determine the performance of the spectrum estimation procedures as a function of model order, dataset size, and signal-to-noise ratio. Shift estimation experiments are then carried out to test for linearity and accuracy of the phase estimate of the cross spectra. Finally an example of system identification is given to further test the cross spectral estimate when used to identify an unknown 2-D system on the basis of input/output measurements.

1. Sinusoids in Noise Background Experiments

In this section the NSHP model is used to obtain the estimated spectra of sinusoidal signals buried in white noise. The estimated spectra are computed and plotted.

a. Tone Estimation

Here we discuss the estimation of a sinusoid in a white noise background. Three numerical examples are presented which illustrate the results.

(1) Example 1

This example is concerned with the analysis of spectra for a two-channel 2-D single sinusoid signal with different phase in additive noise. The signals generated in channels 1 and 2 are given by Eqn. (4.18). Spectrum estimation results are given for a third order NSHP filter. Two cases are considered in this example. In the first

case we suppose that the two channels have the same frequency but different phase

$$\left\{\omega_1 = \omega_2 = \pi/3,\ \omega_3 = \omega_4 = \pi/3, \text{ and } \phi = 1 \textit{ radian}\right\}$$

while in the second case, we assume the two channels have different frequencies *and* different phase:

$$\left\{\omega_1 = \omega_2 = \pi/2,\ \omega_3 = \omega_4 = \pi/3, \text{ and } \phi = 1 \textit{ radian}\right\}$$

Fig. 4.10 shows the results for the components of the spectral matrix in the first case. Only the cross term $S_{12}(\omega_1,\omega_2)$ is shown (magnitude and phase) since the term $S_{21}(\omega_1,\omega_2)$ is theoretically and numerically identical. The results show a distinct peak in each of the three components S_{11}, S_{12}, and S_{22} corresponding to the location of the sinusoid. The center of the peak is accurately located near $(\pi/3,\pi/3)$. Although the phase of the cross spectrum shows various artifacts around the edge of the region (where the magnitude is small and the phase is that of the noise) the phase at the location of the sinusoid is accurately estimated to be 1.01 radians.

Fig. 4.11 shows $S(\omega_1,\omega_2)$ for the second case (different frequencies). The power spectrum estimates of the first and second channels S_{11} and S_{22} have a single-peak at the location of the sinusoid. Although the cross spectra should theoretically show no presense of sinusoids some small amount of energy is detectable at those frequencies in the cross spectrum. Similar effects have been observed in 1-D multichannel spectrum estimation and have been attributed to non-exact pole-zero cancellations in the estimate for the cross spectrum (Marple and Nuttall,1986).

(2) Example 2

Two-channel 2-D signals with two sinusoids in additive noise are considered in this example. The signals in the channels are defined by Eqn. (4.23) with the parameters given above.

The power spectrum estimation results for a second order NSHP model are given in Fig. 4.12. The results are close to the theoretical results. $S_{11}(\omega_1,\omega_2)$ and $S_{22}(\omega_1,\omega_2)$ show that the two sinusoids are easily resolved. The estimated amplitudes are unequal, but this characteristic has been observed in even 1-D AR spectrum

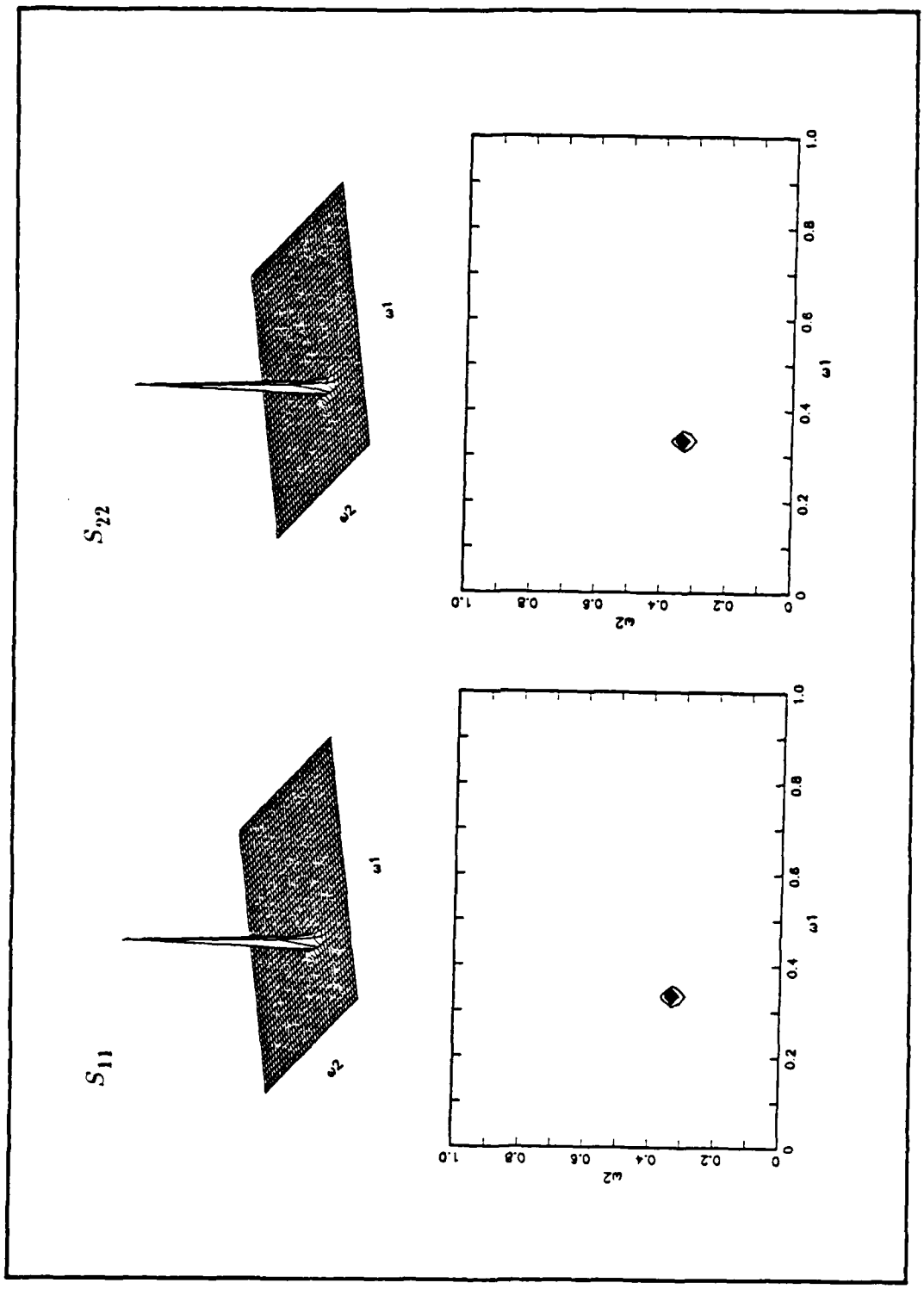

Fig. 4.10 Estimate of spectra for sinusoids at same frequecy.

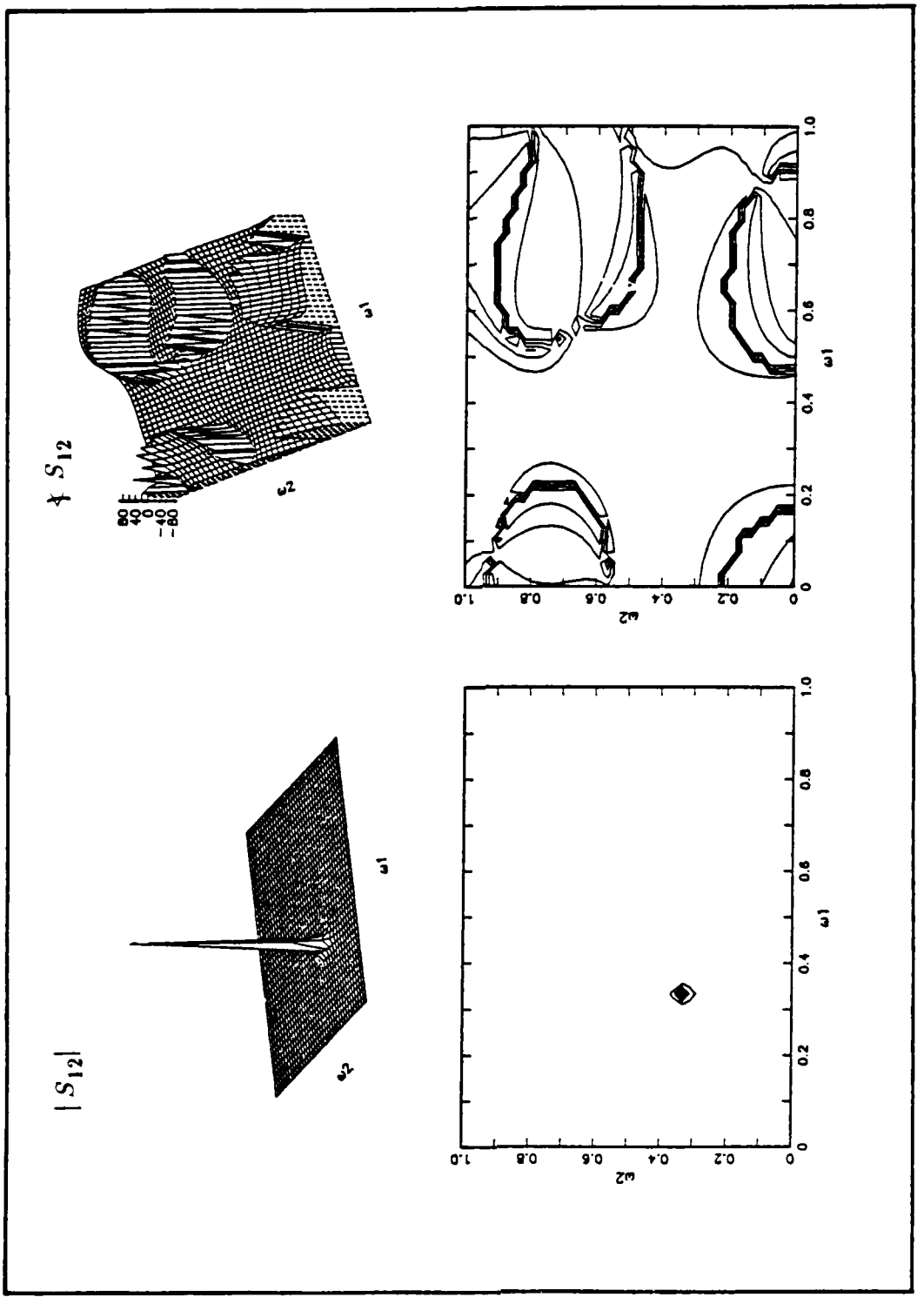

Fig. 4.10 Estimate of spectra for sinusoids at same frequency. (cont'd)

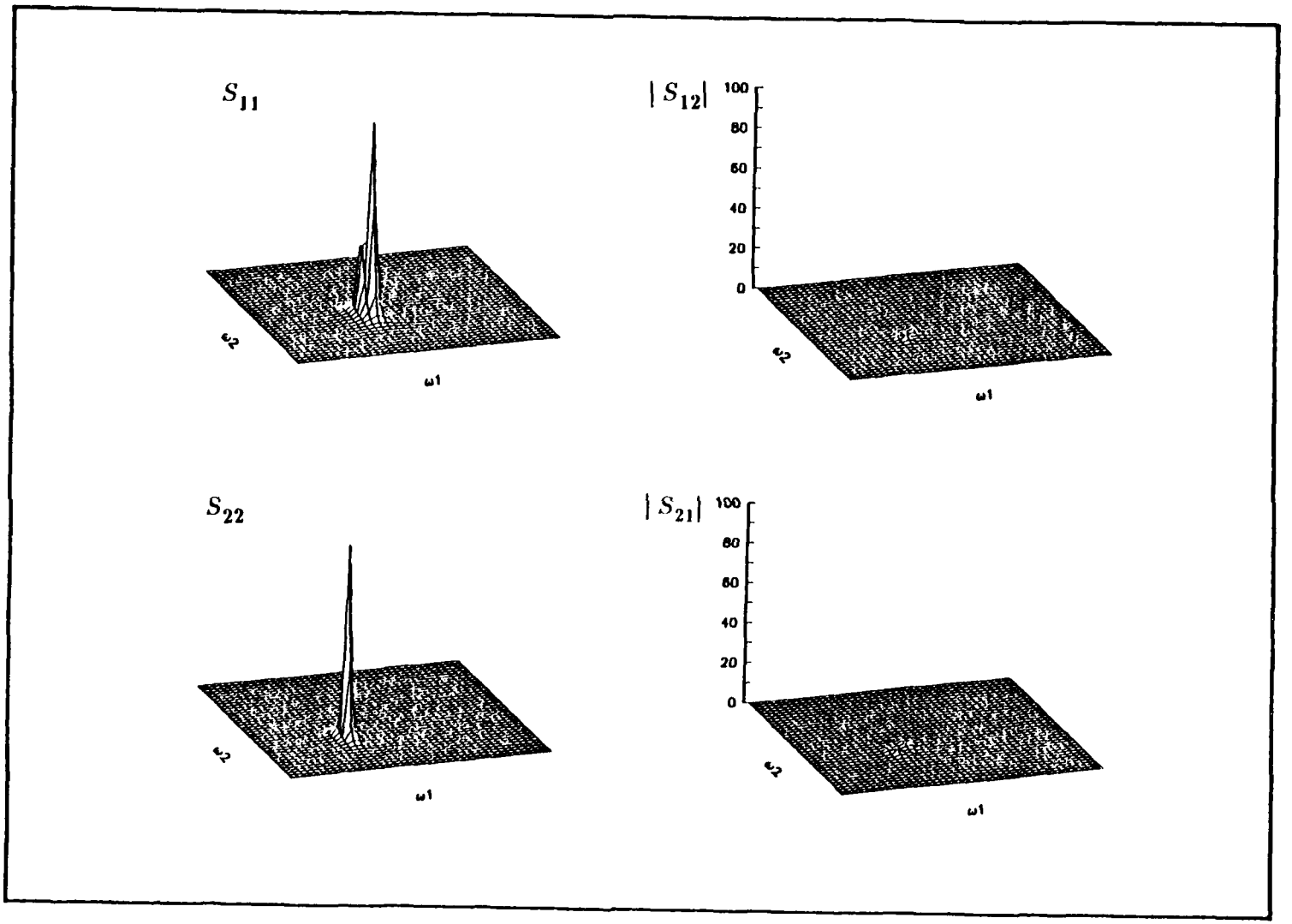

Fig. 4 11 Estimate of spectra for sinusoids at different frequency.

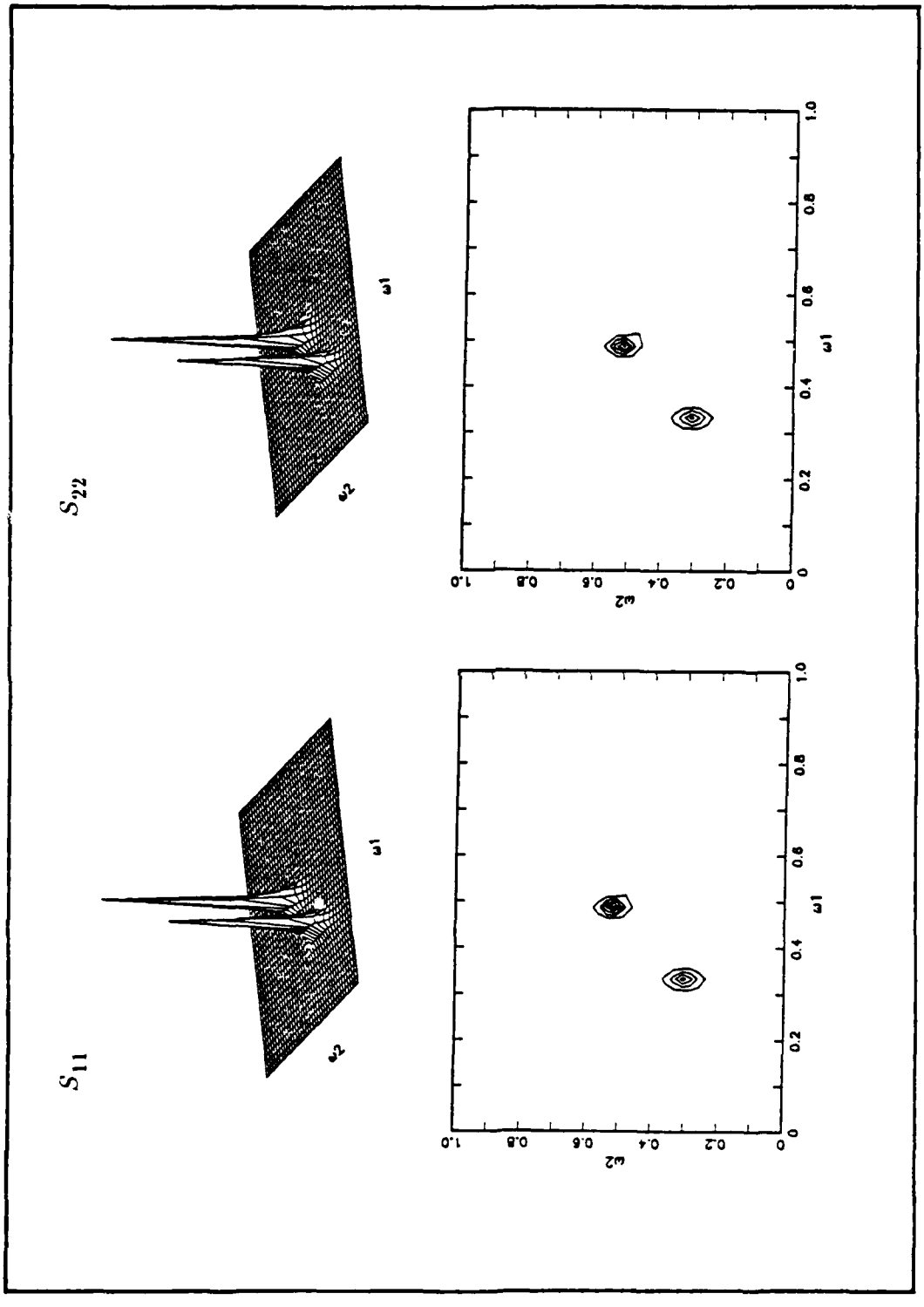

Fig. 4.12 Estimate of two sinusoids in white noise.

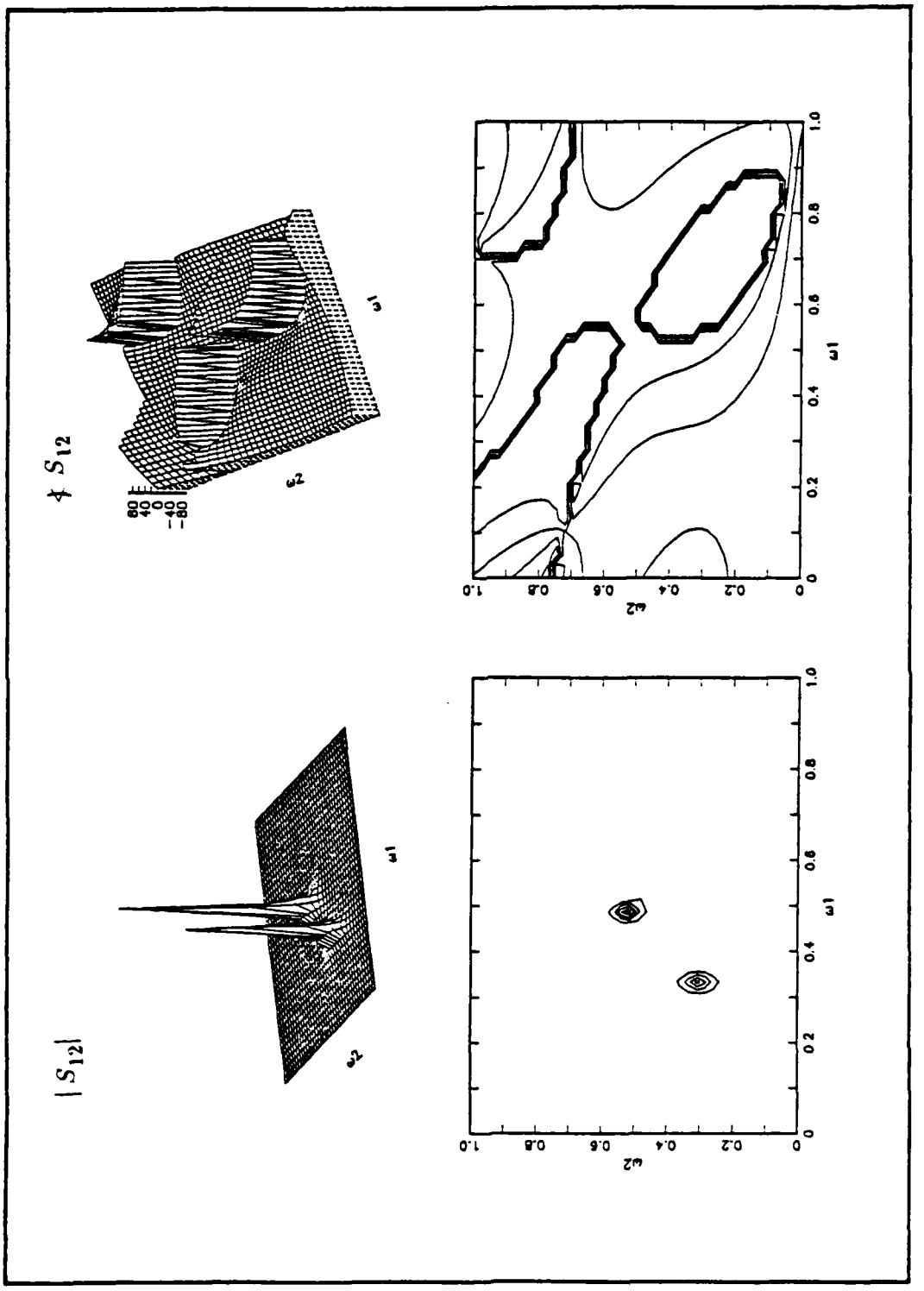

Fig. 4.12 Estimate of two sinusoids in white noise (cont'd)

estimates. The cross-spectrum $S_{12}(\omega_1,\omega_2)$ shows the sinusoids resolved and the phase estimate is $\phi_1 = 1.495$ radians and $\phi_2 = 0.511$ radians which is close to the true phase of $\phi_1 = 1.5$ radians and $\phi_2 = 0.5$ radians.

(3) Example 3

In this example we considered three sinuosids in each channel. The location of the sinusoids is shown in Fig. 4.13. The sinusoids are impeded in white noise as in the previous examples. Again a dataset of size 64×64 was used. The phase of the sinusoids in channel 2 differ from those in channel 1 by 1 radian.

Figure 4.14 shows 3-D and contour plots for the components of the spectral matrix estimated using a fourth order NSHP model. The cross-lines (+) in the contour plots show the true location of the sinusoids. The results show a very slight bias in estimation of the position of the sinusoids in the autospectra and the cross spectra and good resolution. There is almost no evidence of energy from sinusoids ω_B and ω_D appearing in the spectrum of the opposite channel or in the cross spectrum. The phase of the cross spectrum shows various artifacts but since these correspond to the noise background, they are of no particular interest. However in the region where the peaks are located, the phase is slowly varying and estimated with values of $\phi_1 = 0.92$ radians, and $\phi_2 = 0.95$ radians (at the peaks). The slow variation of the phase in the region near the sinusoids makes its estimation relatively insensitive to any inaccuracies in location of the spectral peaks.

b. Effects of Model order and Dataset size

A comprehensive set of experiments was carried out to determine performance of the spectrum estimation procedures as a function of model order and dataset size.

The results showed that to some extent the lack of resolution resulting from a small dataset size could be compensated for by choosing a larger model order. There is a limit to this trade-off however since a larger model has more parameters and thus should require more data to estimate parameters that are statistically reliable. The experimental observation may be restated in the following way. When the dataset is large a lower order model can produce results that are comparable to a higher order model.

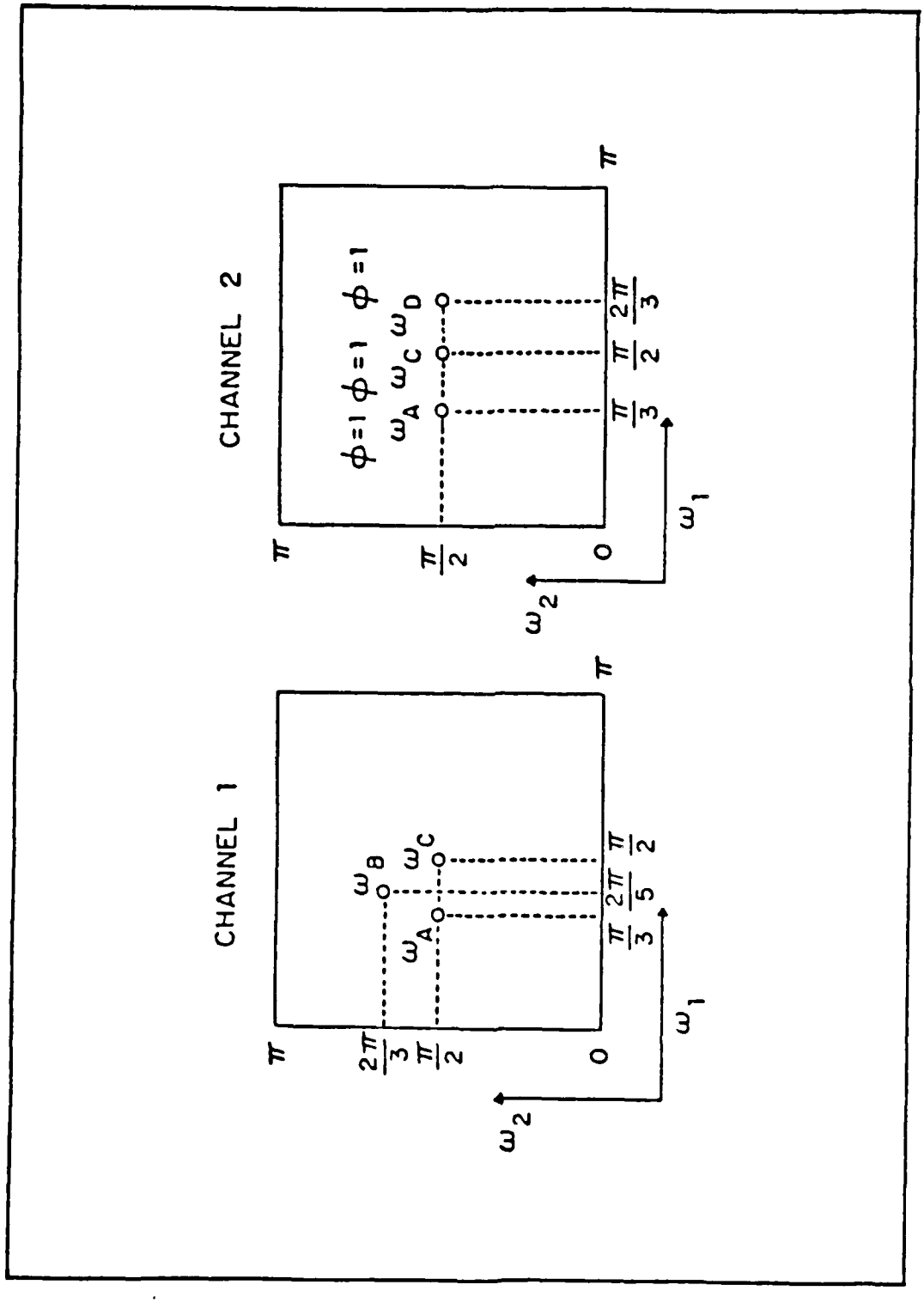

Fig. 4.13 Location of sinusoids.

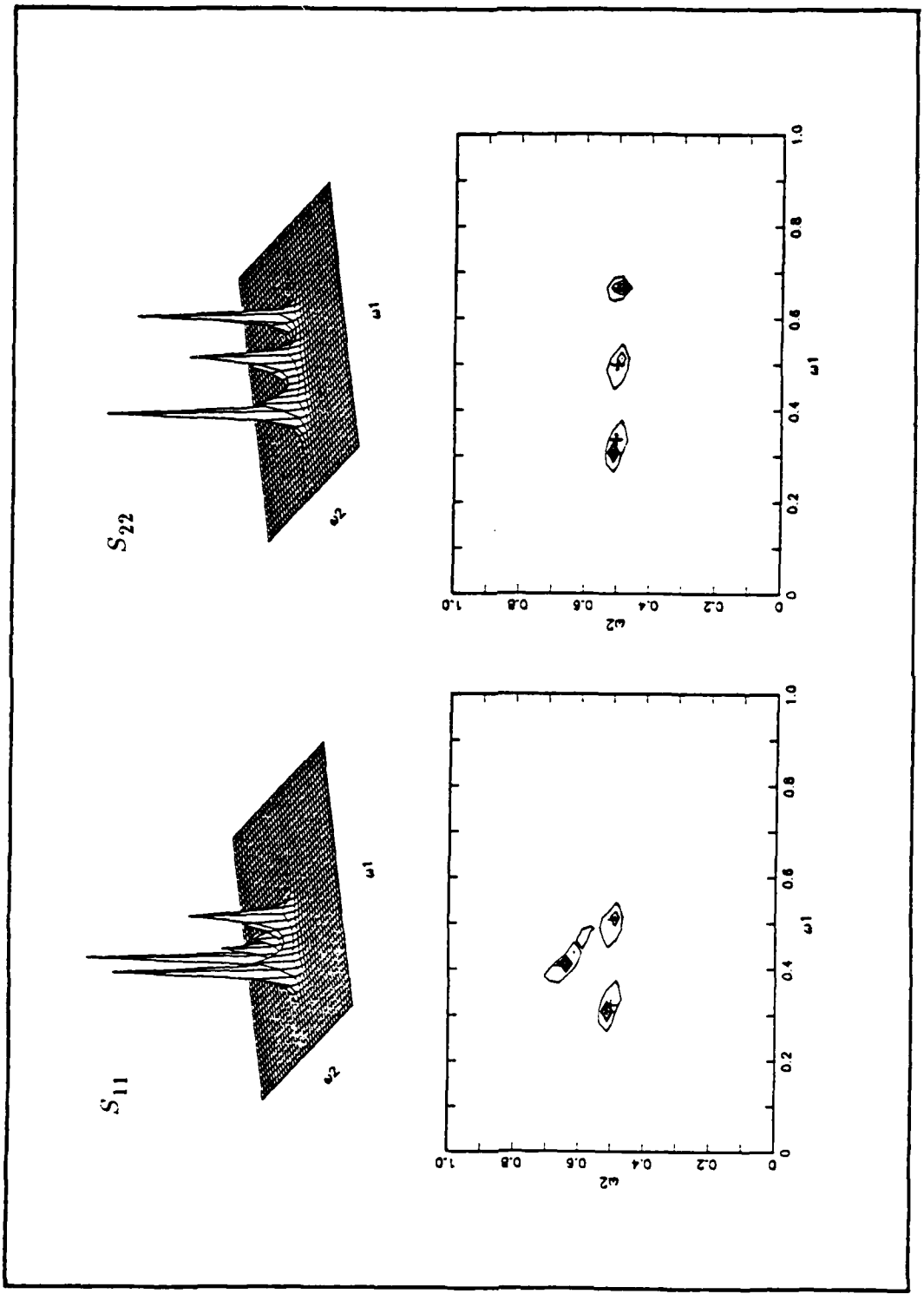

Fig. 4.14 Estimate of three sinusoids in white noise (NSHP).

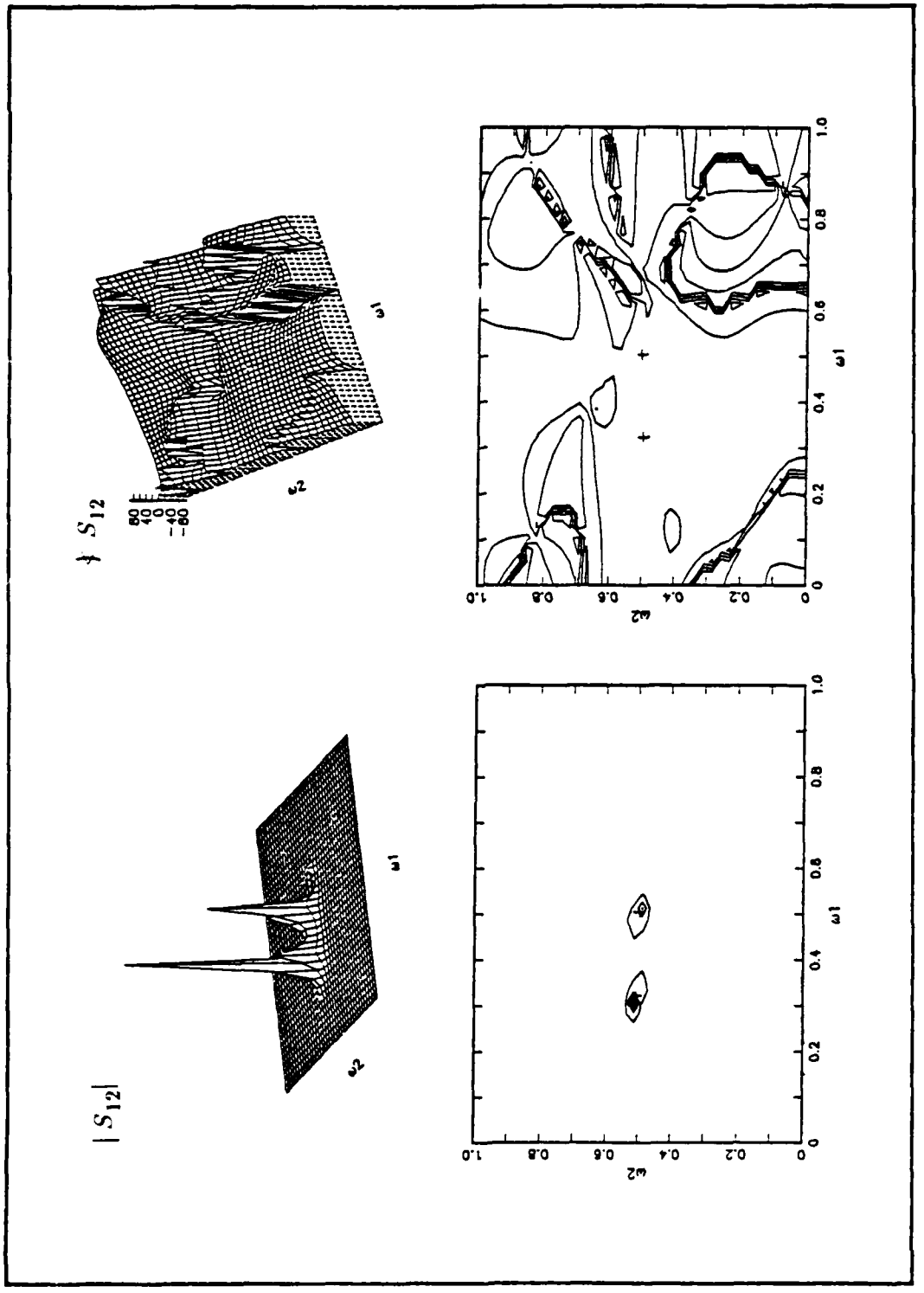

Fig. 4.14 Estimate of three sinusoids in white noise (NSHP). (cont'd)

As a specific example, two-channel 2-D sinusoidal signals in additive noise were again considered. The signals used are defined by (4.23) with the number of sinusoids L=2, and other parameters $\omega_{11}=\omega_{12}=\frac{\pi}{2}$, $\omega_{21}=\omega_{22}=\frac{2\pi}{5}$, $\omega_{13}=\omega_{14}=\frac{\pi}{2}$, $\omega_{23}=\omega_{24}=\frac{2\pi}{5}$, ϕ_1=1 radian, and ϕ_2=1 radian. The simulation was performed for different values of the model order and also for different values of the dataset size. Figure 4.15 shows the effect of model order on the cross spectral estimation $S_{12}(\omega_1,\omega_2)$ amplitude and phase when the dataset size is 64×64. For a first order model we have poor resolution and the two peaks appear as only one peak. The resolution increases with increasing order and the phase gets very close to the actual value.

For a dataset size of 32×32 (not shown) we get approximately the same power spectral estimation results as for a dataset size of 64×64, although in the 64×64 dataset we get more sharpness in the peaks.

The cross spectral estimate for a dataset size of 16×16 is shown in Fig. 4.16 using three different model orders. Autospectra are not shown. The second peak starts to be seen for the second order and the two peaks are found in their correct location for the third order. Figure 4.17 shows the cross spectrum estimate for a dataset size of 8×8. Only one peak appears for first and second order estimates. Two peaks appear when the order of the model is increased to third order, but the peaks are not sharp at all.

The results of these experiments can be summarized as follows. For a second order filter the results of spectrum estimation using a 32×32 point dataset were essentially the same as those using the 64×64 point dataset. For smaller datasets the results degraded considerably. However the resolution obtained using a second order NSHP filter on a 16×16 point dataset was similar to that obtained with a third order filter on a 8×8 point dataset. For the 8×8 point dataset the resolution is greatly improved by going from a second to a third order filter. However there is a noticeable bias along the ω_1 direction in the location of the peaks. Phase estimates remain quite stable. Table 4.4 shows some selected values of the peak locations and the corresponding estimated phase values at those peaks.

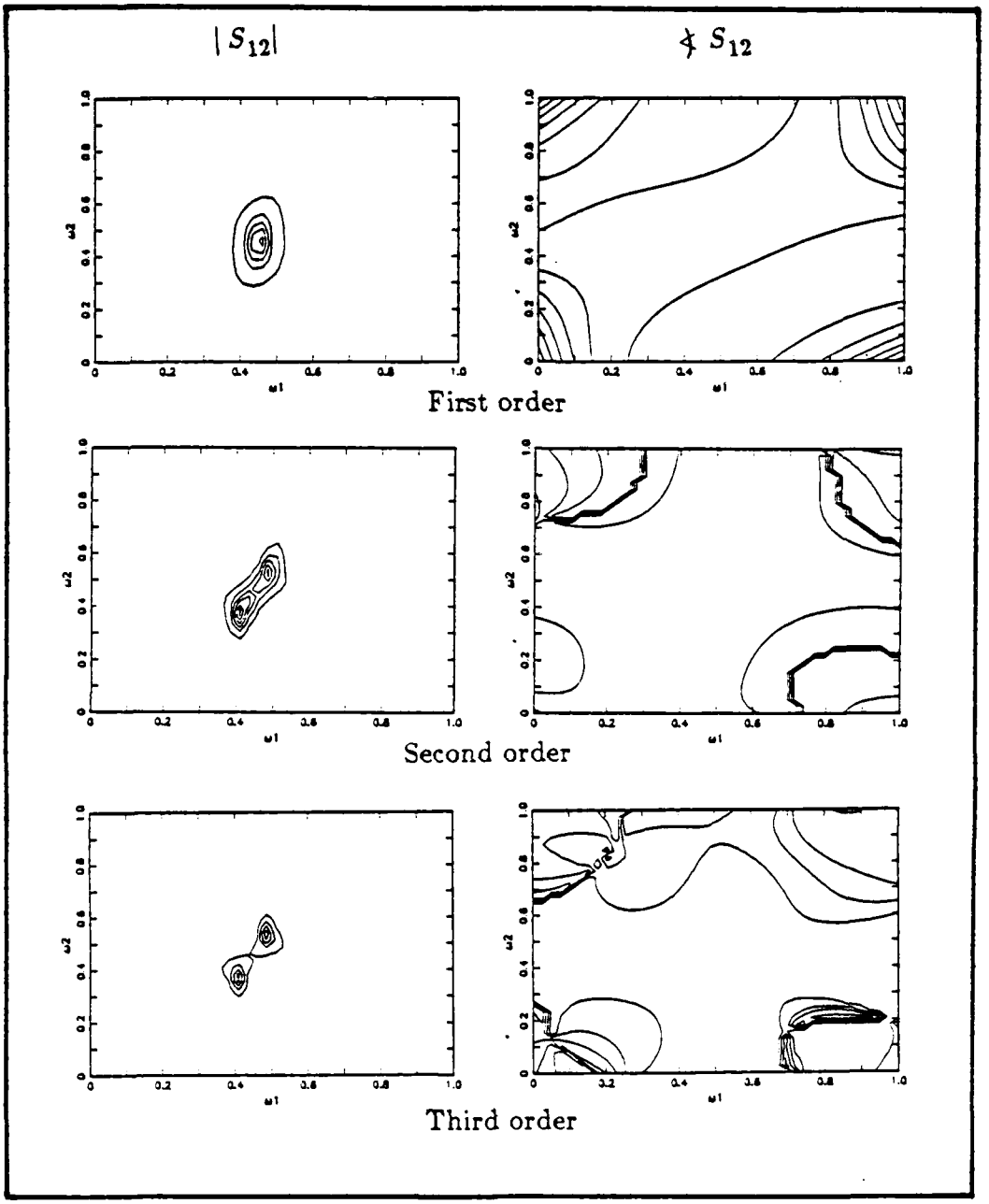

Fig. 4.15 Effect of model order and dataset size (64x64).

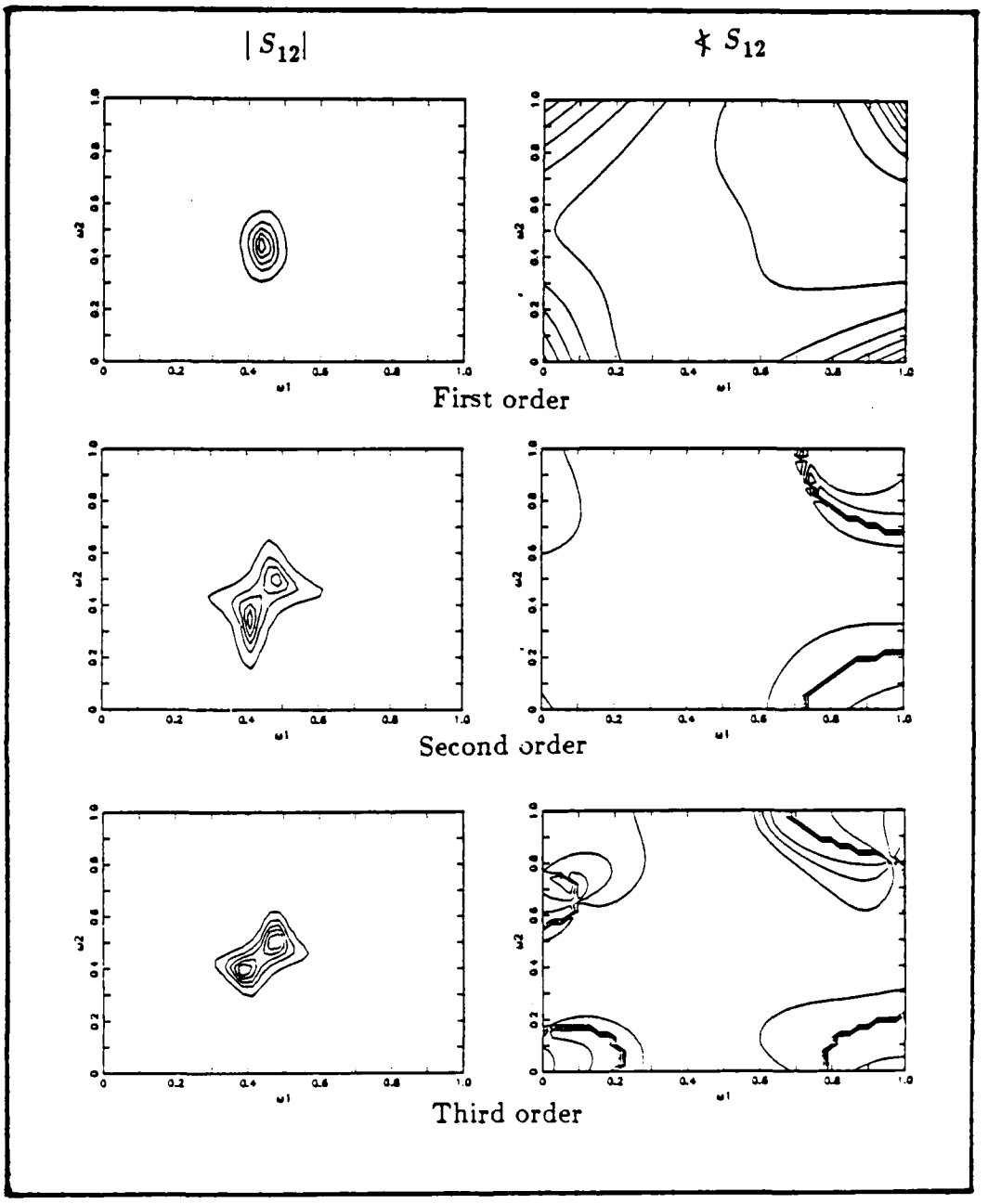

Fig. 4.16 Effect of model order and dataset size (16x16).

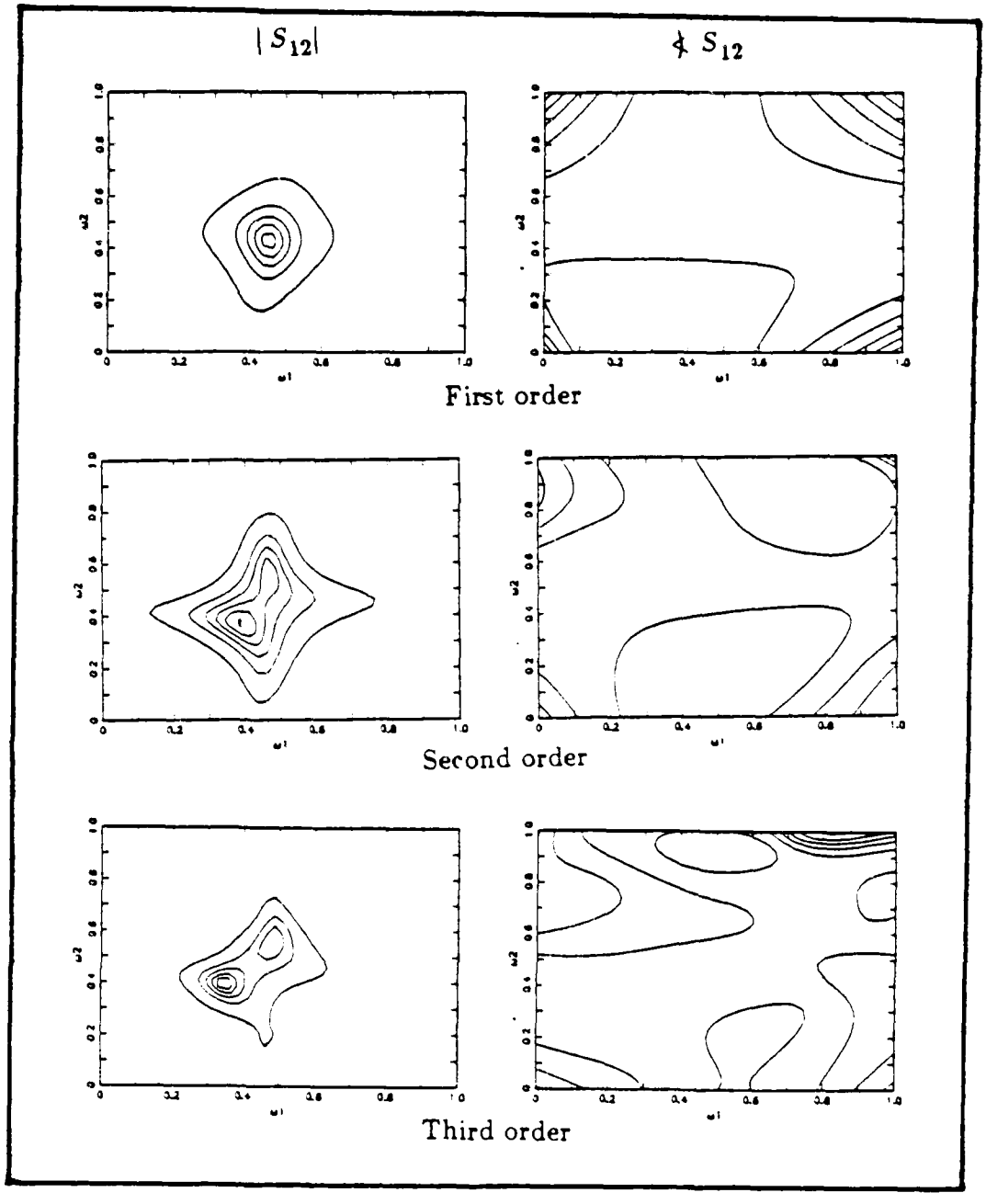

Fig. 4.17 Effect of model order and dataset size (8x8).

c. Signal to Noise Ratio Experiment

The signal/noise ratio for two sinusoids in noise was defined by : $SNR = 10 \log_{10}\left[\frac{C^2}{\sigma^2}\right]$, where C is the amplitude of each sinusoidal component and σ^2 is the white noise variance. The results of the cross spectrum estimation for a 64×64 point data set for each channel with sinusoids of frequencies $\omega_{11}=\omega_{21}=\frac{\pi}{2}$, and $\omega_{12}=\omega_{22}=\frac{\pi}{3}$ are shown here. The model used for these experiments was second order. Estimated values for the frequencies and phase are listed in Table 4.5. At a SNR value of 12 dB the sinusoids are completely resolved with sharp peaks as shown in Fig. 4.18. At a SNR value of 3.5 dB the peaks begin to merge (see Fig. 4.19) and at 0 dB (Fig. 4.20) the peaks become a single ridge making it difficult to predict that there are two sinusoids present. The phase obtained by this method however remains nearly constant over a wide region near the true peaks for all of the signal-to-noise values. The phase plots show a rather slowly varying character in the region around the two sinusoids.

2. Shift Estimation

This section contains examples of multichannel 2-D spectrum analysis involving narrowband and broadband data. These cases were designed to test the accuracy of estimating a linear phase term in the cross spectrum and the ability to estimate

TABLE 4.4 EFFECT OF DATA SET SIZE ON THE ESTIMATED PARAMETERS

	Estimated Parameters [rad.]			*True Parameters [rad]*
	16×16 2^{nd} *order*	8×8 2^{nd} *order*	8×8 3^{rd} *order*	
ϕ_1	1.02	undefined	0.96	1
ϕ_2	0.97	1.06	1.04	1
ω_{11}	1.51	undefined	1.52	1.57
ω_{12}	1.57	undefined	1.64	1.57
ω_{21}	1.25	1.24	1.16	1.05
ω_{22}	1.20	1.28	1.25	1.05

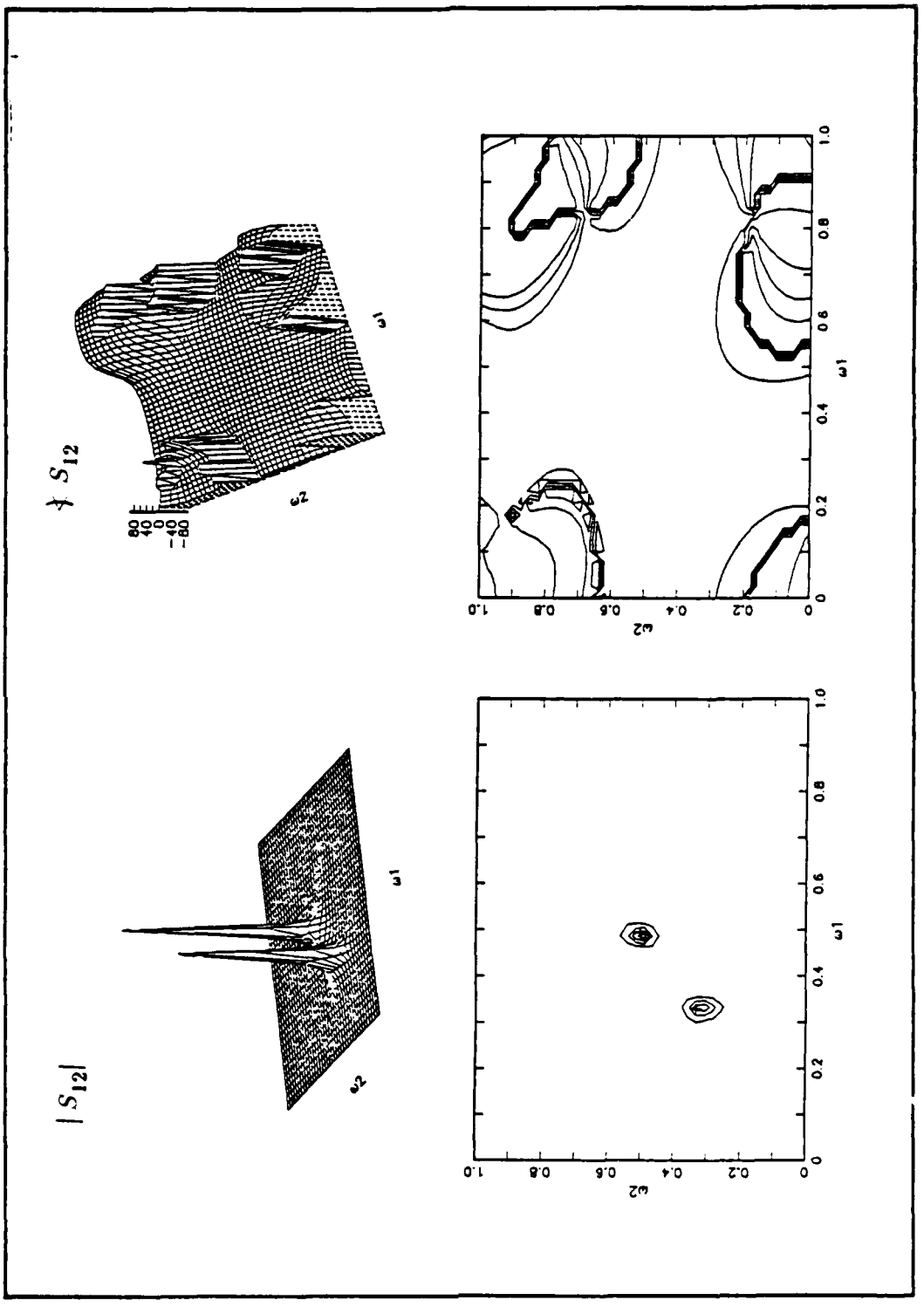

Fig. 4.18 Cross spectrum estimation at SNR=12 dB.

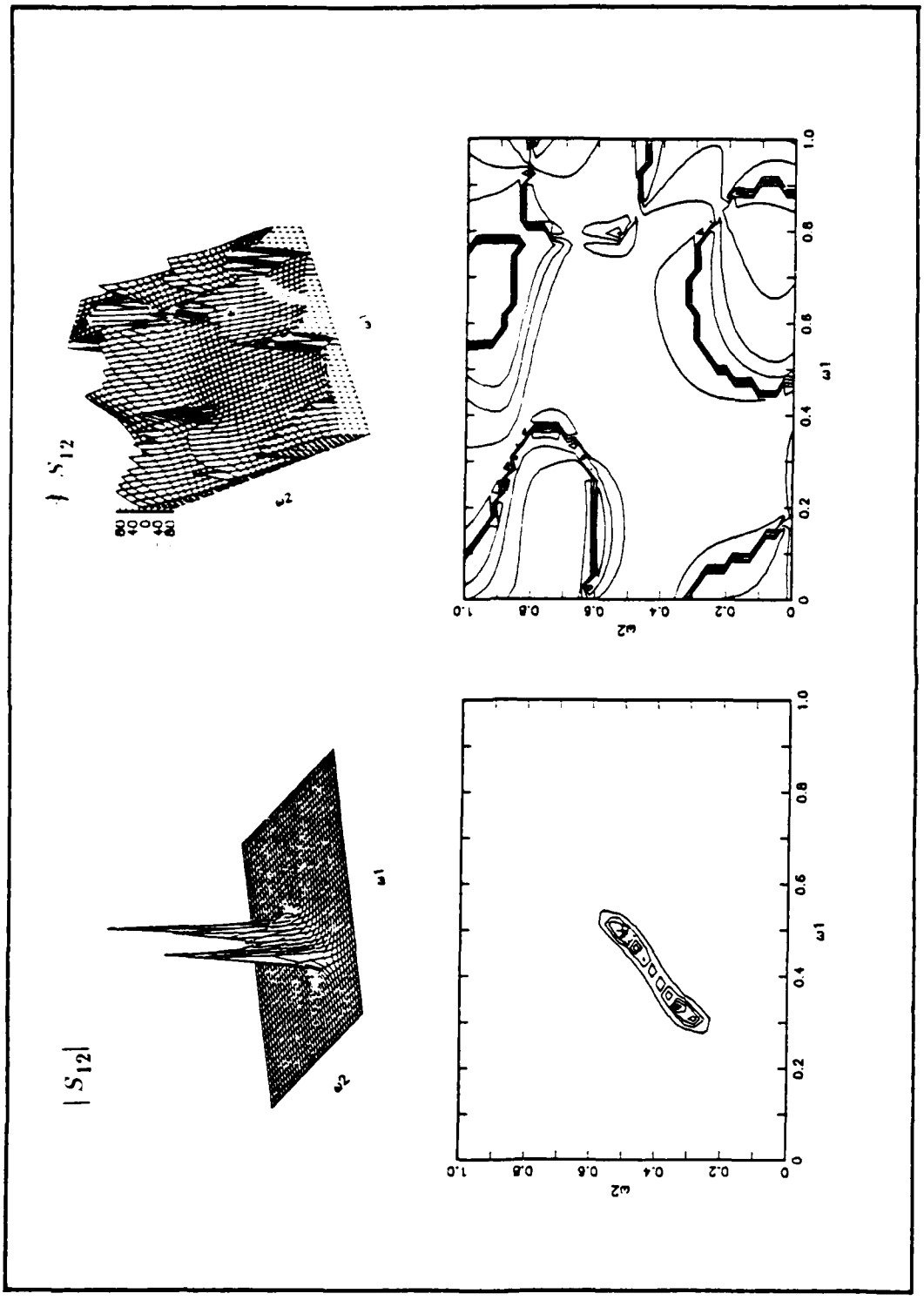

Fig. 4.19 Cross spectrum estimation at SNR=3.5 dB.

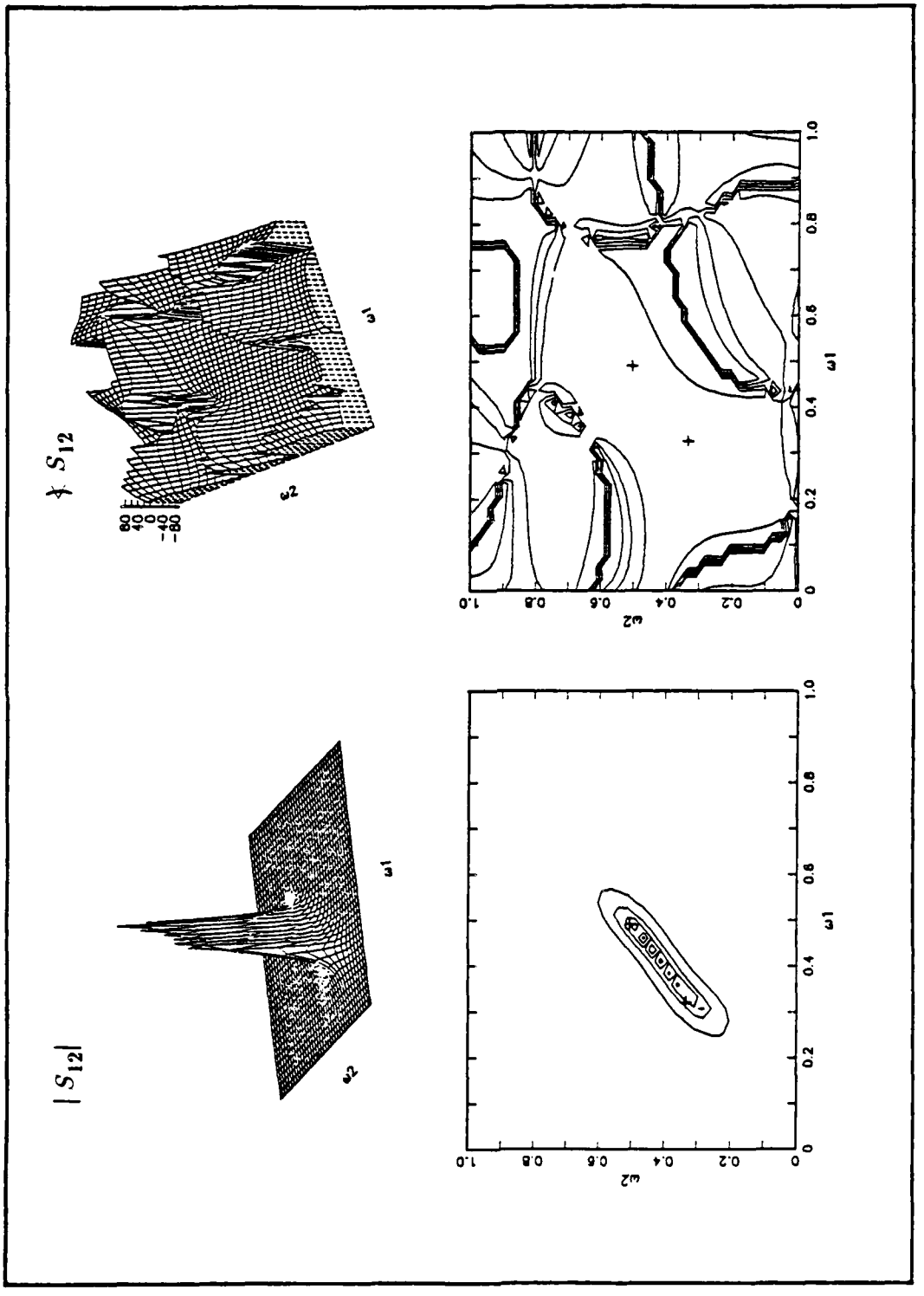

Fig. 4.20 Cross spectrum estimation at SNR=0 dB.

parameters of a known 2-D random process from data. Three different numerical experiments are considered.

a. Experiment (1)

For this experiment two channels of data were defined by:

$$x_1(n_1,n_2) = w_1(n_1,n_2) \tag{4.24a}$$

$$x_2(n_1,n_2) = C\ x_1(n_1-d_1,n_2-d_2)+w_2(n_1,n_2) \tag{4.24b}$$

where $w_1(n_1,n_2)$ and $w_2(n_1,n_2)$ are white noise terms with unit variance and the other parameters are C=0.5, $d_1 = d_2 = 1$. Spectral estimates were generated and the slope of the phase of the cross spectrum was measured to estimate the delays d_1 and d_2. Fig. 4.21-a,b shows the autospectra and Fig. 4.21-c,d shows the cross spectrum estimate that was obtained using a second order filter. The magnitude of the cross spectrum is constant and the phase shows a linear dependence with slope corresponding to $d_1 = d_2 = 1$.

b. Experiment (2)

For this experiment two-channels of real data were defined by:

$$x_1(n_1,n_2) = f\,(n_1,n_2) \tag{4.25a}$$

TABLE 4.5 EFFECT OF SNR ON THE ESTIMATED PARAMETERS

	Estimated Parameters [rad.]			*True Parameters [rad]*
	12 *dB*	3.5 *dB*	0 *dB*	
ϕ_1	1.01	1.03	1.04	1.00
ϕ_2	0.99	0.98	0.98	1.00
ω_{11}	1.53	1.50	*undefined*	$\pi/2$
ω_{12}	1.57	1.50	*undefined*	$\pi/2$
$2\omega_{21}$	1.00	1.04	*undefined*	$\pi/3$
ω_{22}	1.00	1.00	*undefined*	$\pi/3$

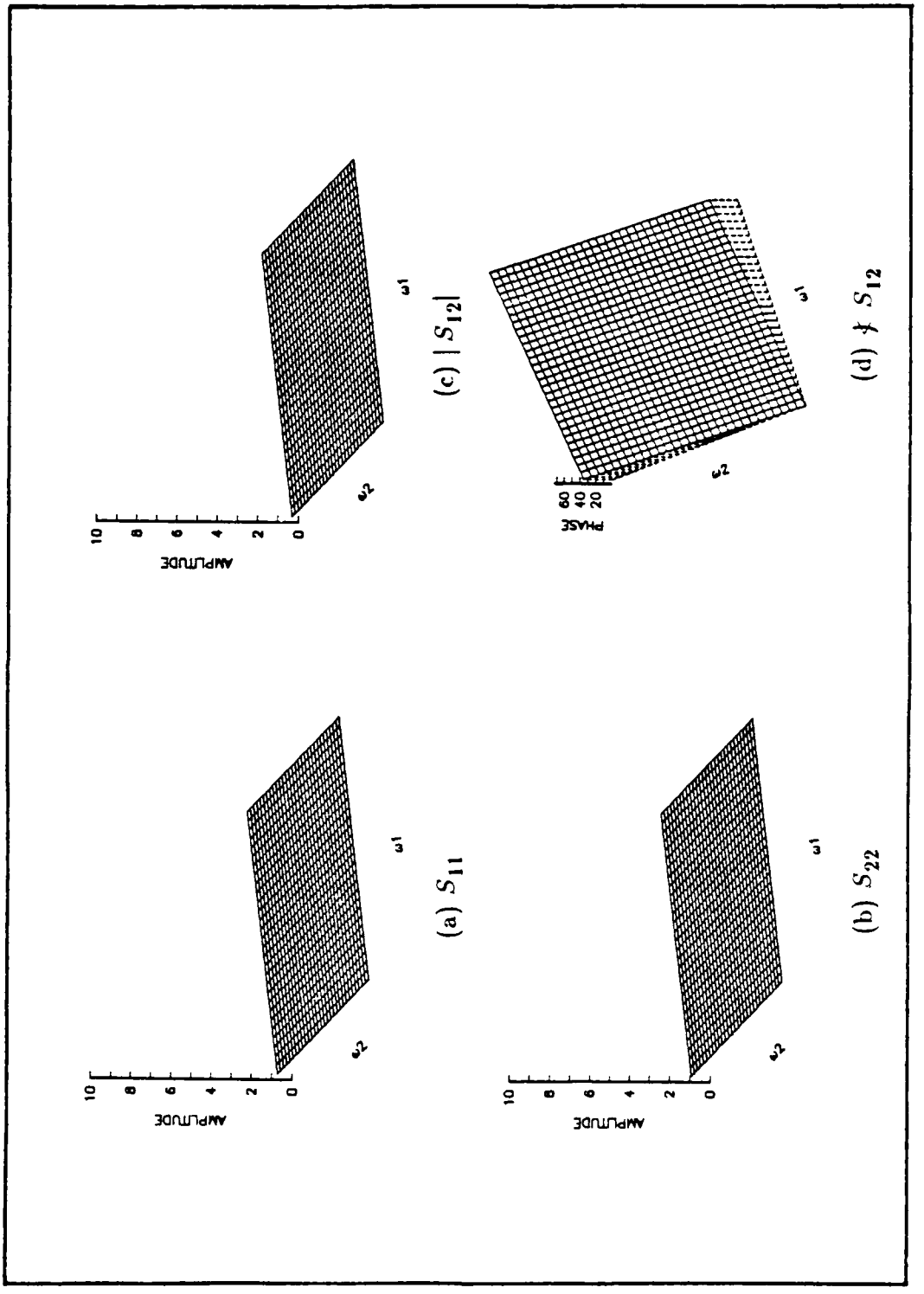

Fig. 4.21 Linear phase estimation.

$$x_2(n_1,n_2) = C\ f\ (n_1-d_1,n_2-d_2) + w\,(n_1,n_2) \tag{4.25b}$$

where $f\,(n_1,n_2)$ is a 64×64 portion of the image shown in Fig. 4.22 (an aerial photograph of fields) and $w(n_1,n_2)$ is a zero mean white noise process. Spectral estimates were generated and the slope of the phase of the cross spectrum was measured to estimate the shifts d_1 and d_2. Figure 4.23 shows the phase and magnitude of the spectral estimate that was obtained using a third order NSHP model for signal data that had parameter values of C = 0.5, d_1=3, d_2=5 and white noise with unit variance. The estimated phase shows a linear dependence with slope corresponding to d_1=3.0, d_2=4.5 which rounds to integer values of d_1=3, d_2=5.

c. Experiment (3)

For this experiment two channels of sinusoidal signals are considered

$$x_1(n_1,n_2) = \sum_{i=1}^{L} \cos(n_1\omega_{i1}+n_2\omega_{i2}) + w_1(n_1,n_2) \tag{4.26a}$$

$$x_2(n_1,n_2) = C\ x_1(n_1-d_1,n_2-d_2) + w_2(n_1,n_2) \tag{4.26b}$$

where $w_1(n_1,n_2)$ and $w_2(n_1,n_2)$ are zero mean independent white noise signals, and L represents the number of sinusoids. The parameters of the first channel are given in section 1a Example (3) and the peak locations are as shown in Fig. 4.13b. Spectrum estimation results are given for with C = 1 and $d_1 = d_2 = 1$. Fig. 4.24 shows the autospectrum of the two channels, while Fig. 4.25 shows the magnitude and phase of the cross spectrum. The peaks are shown in the correct location and the phase is approximately linear but not so linear as in the other previous two cases. This is probably because the magnitude of the spectrum is small except around the peaks and the phase in this case is more influenced by the noise except at the peaks location. Nevertheless the phase at the location of the sinusoid peaks is quite accurately estimated.

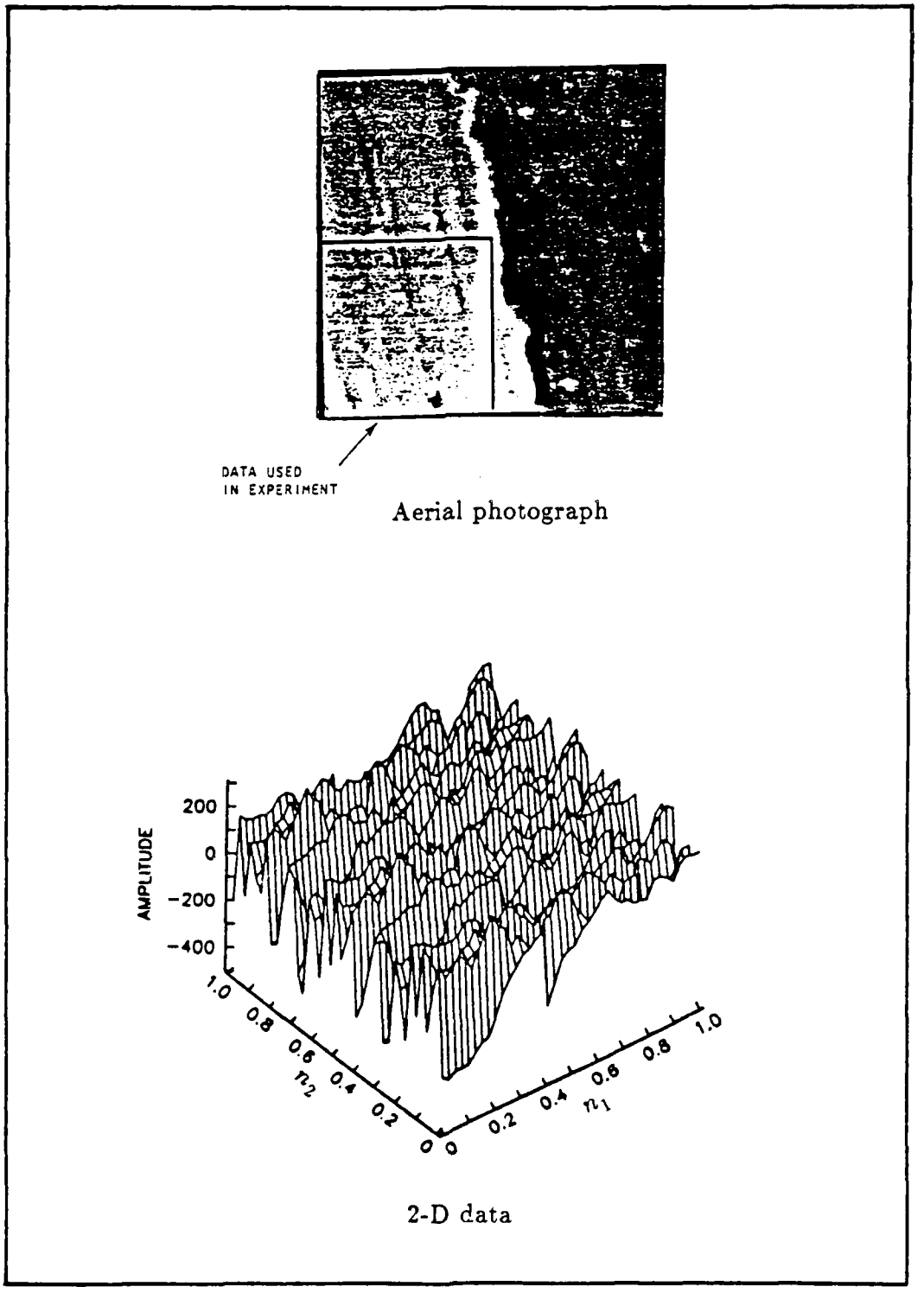

Fig. 4.22 Image used for shift estimation experiment.

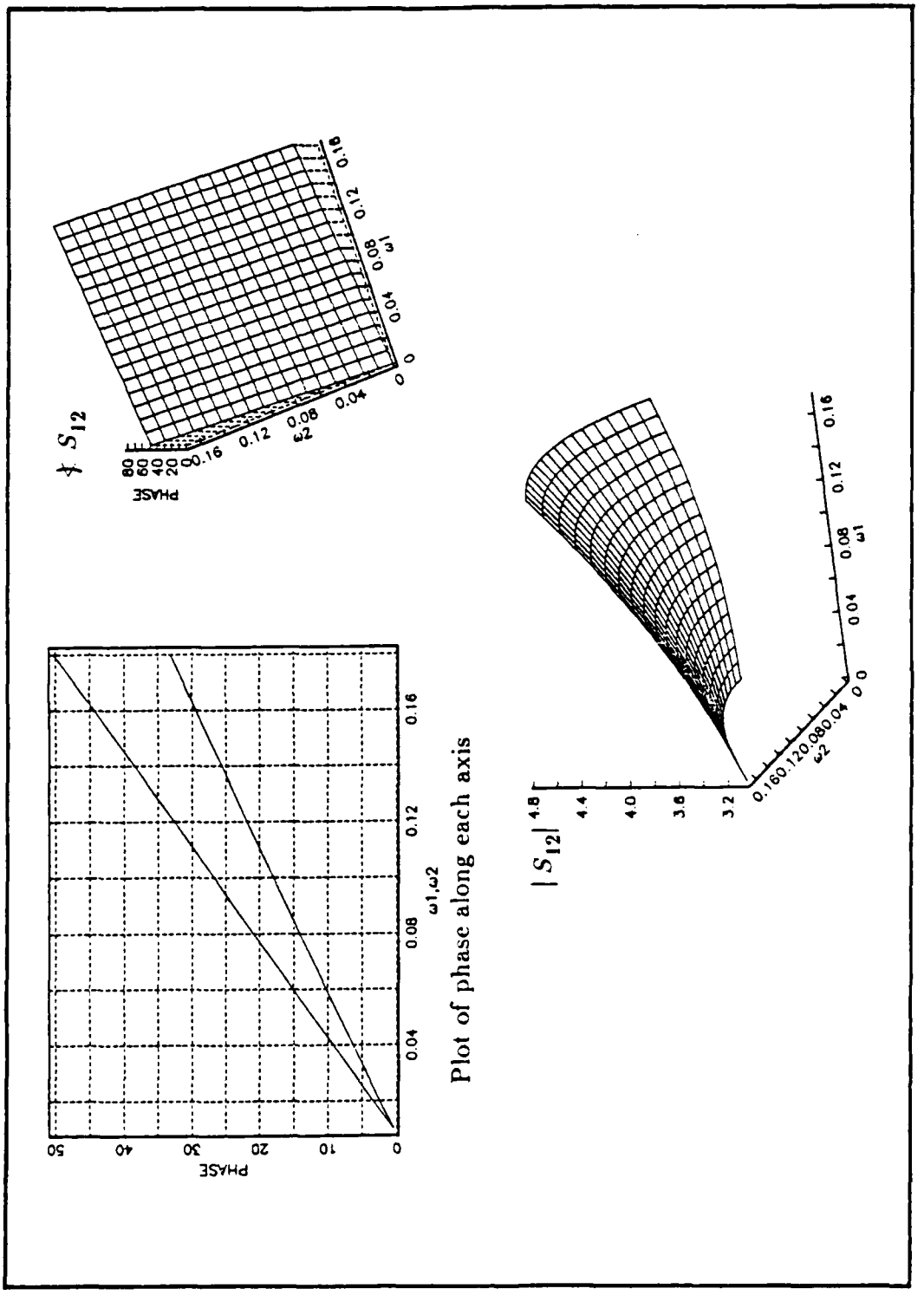

Fig. 4.23 Estimated cross spectrum for shift estimation.

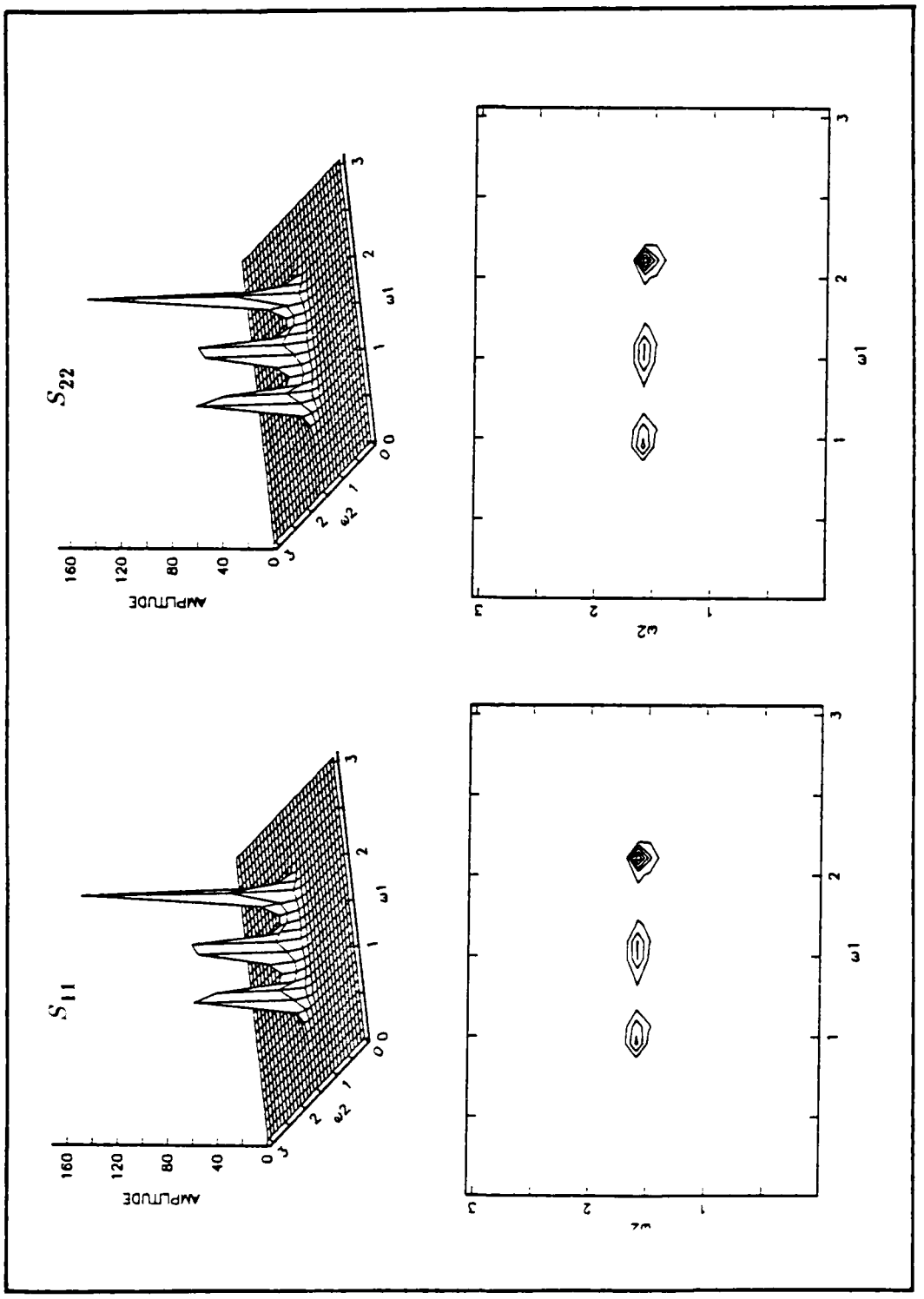

Fig. 4.24 Linear phase estimation of sinusoids in noise (autospectra).

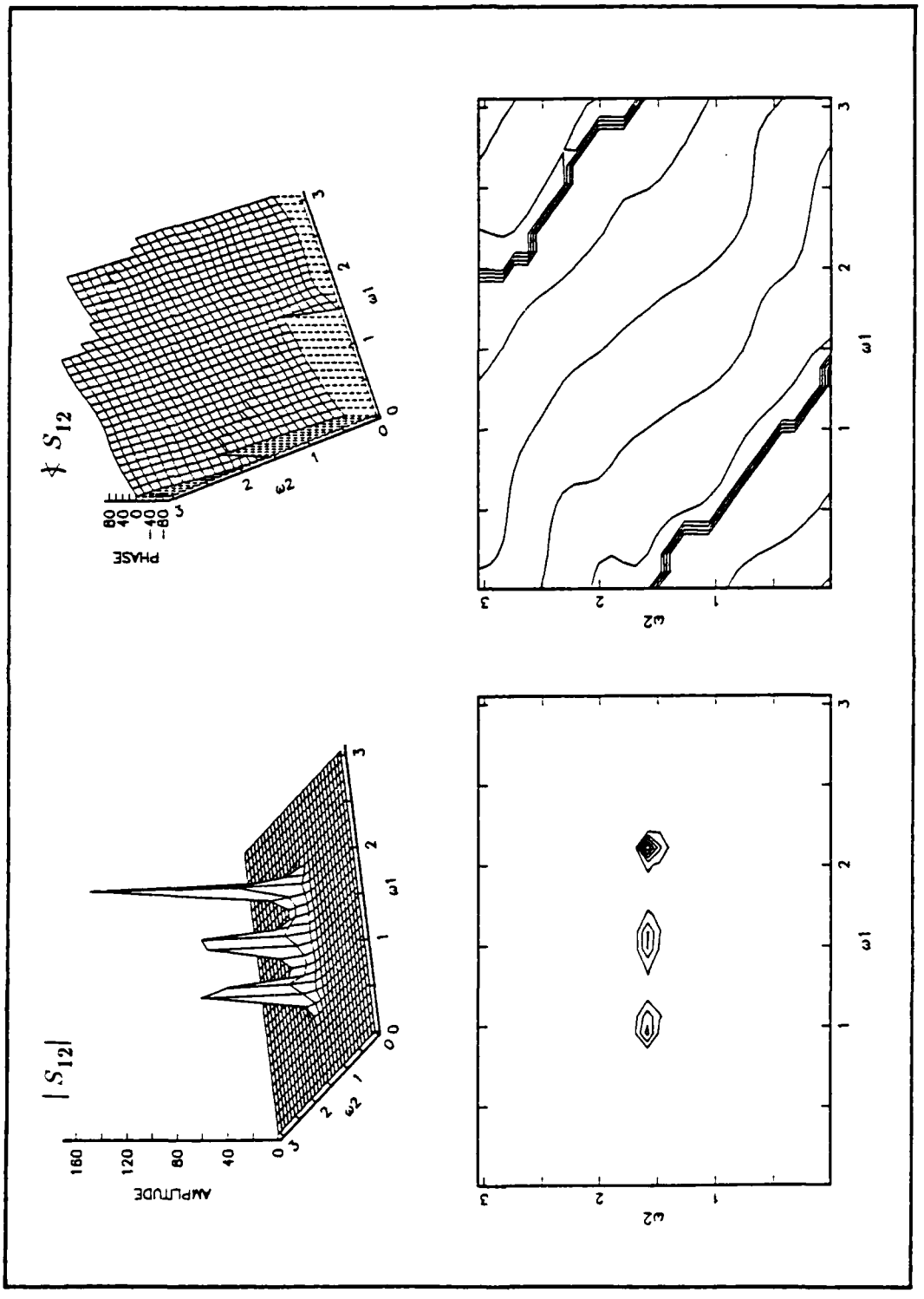

Fig. 4.25 Linear phase estimation of sinusoids in noise (cross spectra).

3. System Identification

a. Experiment (1)

The purpose of this experiment is to generate data from a given two-channel 2-D difference equation, and estimate the difference equation parameter from these data by using linear prediction with a NSHP model. The estimated parameter coefficients are then compared with the true parameters. Our investigated process is the first order two-channel 2-D difference equation given by:

$$\mathbf{x}(n_1,n_2) = \mathbf{A}_{01}\mathbf{x}(n_1,n_2-1)+\mathbf{A}_{-1,-1}\mathbf{x}(n_1+1,n_2+1)+\mathbf{A}_{10}\mathbf{x}(n_1-1,n_2) + \mathbf{A}_{11}\mathbf{x}(n_1-1,n_2-1) + \mathbf{W}(n_1,n_2) \tag{4.27a}$$

A data array 2×(64×64) is generated from the following numerical values:

$$\begin{bmatrix} x_1(n_1,n_2) \\ x_2(n_1,n_2) \end{bmatrix} = \begin{bmatrix} 0.6 & 0 \\ 0.5 & 0 \end{bmatrix} \begin{bmatrix} x_1(n_1,n_2-1) \\ x_2(n_1,n_2-1) \end{bmatrix} + \begin{bmatrix} 0 & -0.7 \\ 0 & 0.4 \end{bmatrix} \begin{bmatrix} x_1(n_1-1,n_2) \\ x_2(n_1-1,n_2) \end{bmatrix} + \begin{bmatrix} w_1(n_1,n_2) \\ w_2(n_1,n_2) \end{bmatrix} \tag{4.27b}$$

where: $w_i(n_1,n_2)$, $(i=1,2)$ are two independent white noise signals. This process actually has support only in the first quadrant but a first order NSHP model was used to test the estimation procedure.

Table 4.6 shows the result of estimating the parameters with a (64×64) point data set. The estimates for the non-zero parameters of the model are close to the given values, and all of the remaining parameters but one are at least one order of magnitude smaller. The estimated spectral components for this process are shown in Fig. 4.26. Energy is spread over a wide range of frequencies with concentration near higher values of ω_1 and lower values of ω_2. This is consistent with the signs of the terms in the defining equations for the process.

TABLE 4.6 MODEL PARAMETERS ESTIMATION OF
A FIRST ORDER NSHP MODEL

	Estimated Parameters	*True Parameters*
$\mathbf{A}_{0,0}$	$\begin{bmatrix} 1.00 & 0.00 \\ 0.00 & 1.00 \end{bmatrix}$	$\begin{bmatrix} 1.00 & 0.00 \\ 0.00 & 1.00 \end{bmatrix}$
$\mathbf{A}_{0,1}$	$\begin{bmatrix} 0.564 & -0.027 \\ 0.604 & -0.036 \end{bmatrix}$	$\begin{bmatrix} 0.60 & 0.00 \\ 0.50 & 0.00 \end{bmatrix}$
$\mathbf{A}_{1,-1}$	$\begin{bmatrix} 0.014 & 0.143 \\ 0.000 & 0.022 \end{bmatrix}$	$\begin{bmatrix} 0.00 & 0.00 \\ 0.00 & 0.00 \end{bmatrix}$
$\mathbf{A}_{1,0}$	$\begin{bmatrix} -0.051 & -0.585 \\ 0.012 & 0.352 \end{bmatrix}$	$\begin{bmatrix} 0.00 & -0.70 \\ 0.00 & 0.40 \end{bmatrix}$
$\mathbf{A}_{1,1}$	$\begin{bmatrix} -0.017 & -0.014 \\ 0.034 & -0.005 \end{bmatrix}$	$\begin{bmatrix} 0.00 & 0.00 \\ 0.00 & 0.00 \end{bmatrix}$

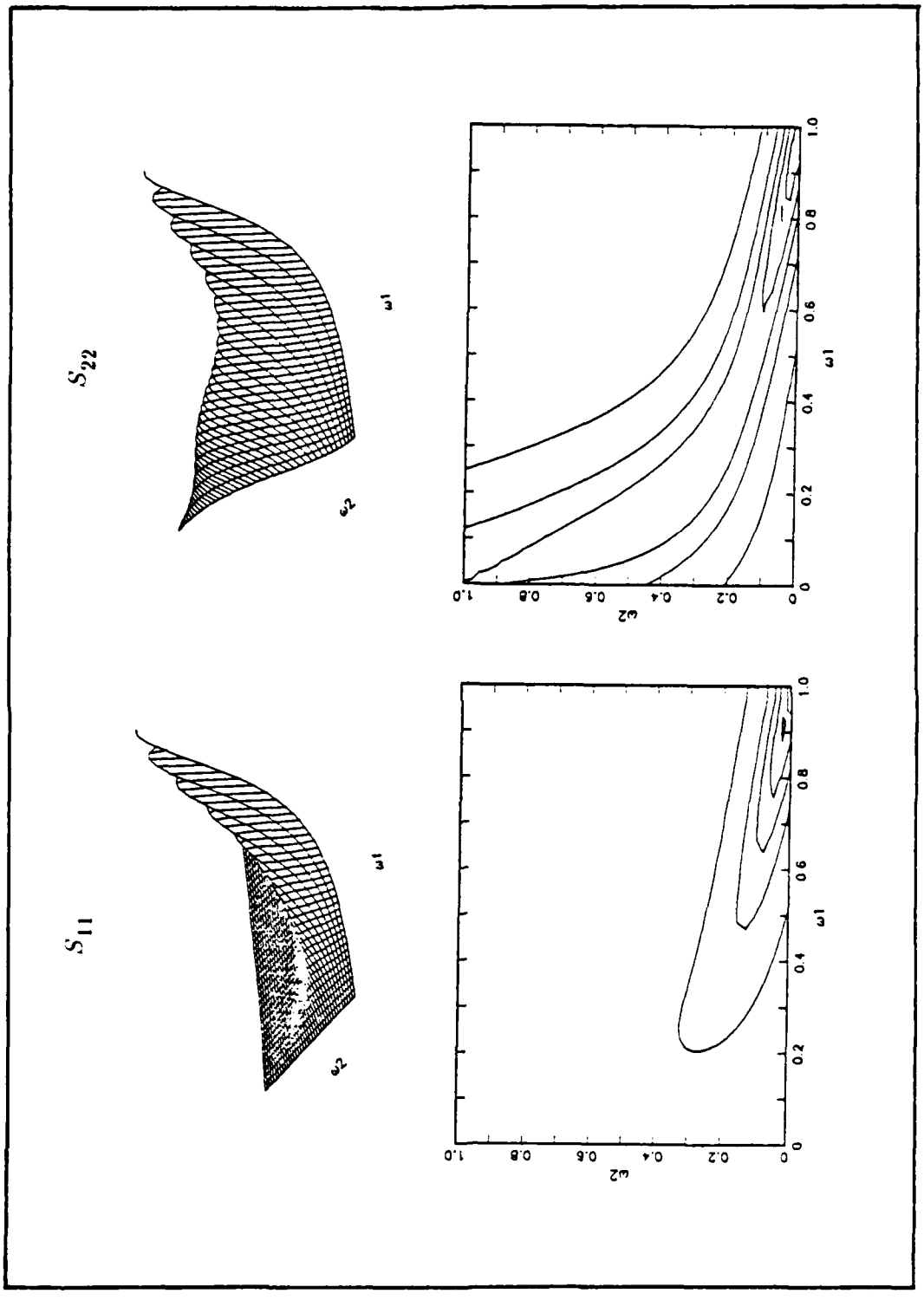

Fig 4.26 Estimated power spectra for a multichannel 2-D linear process.

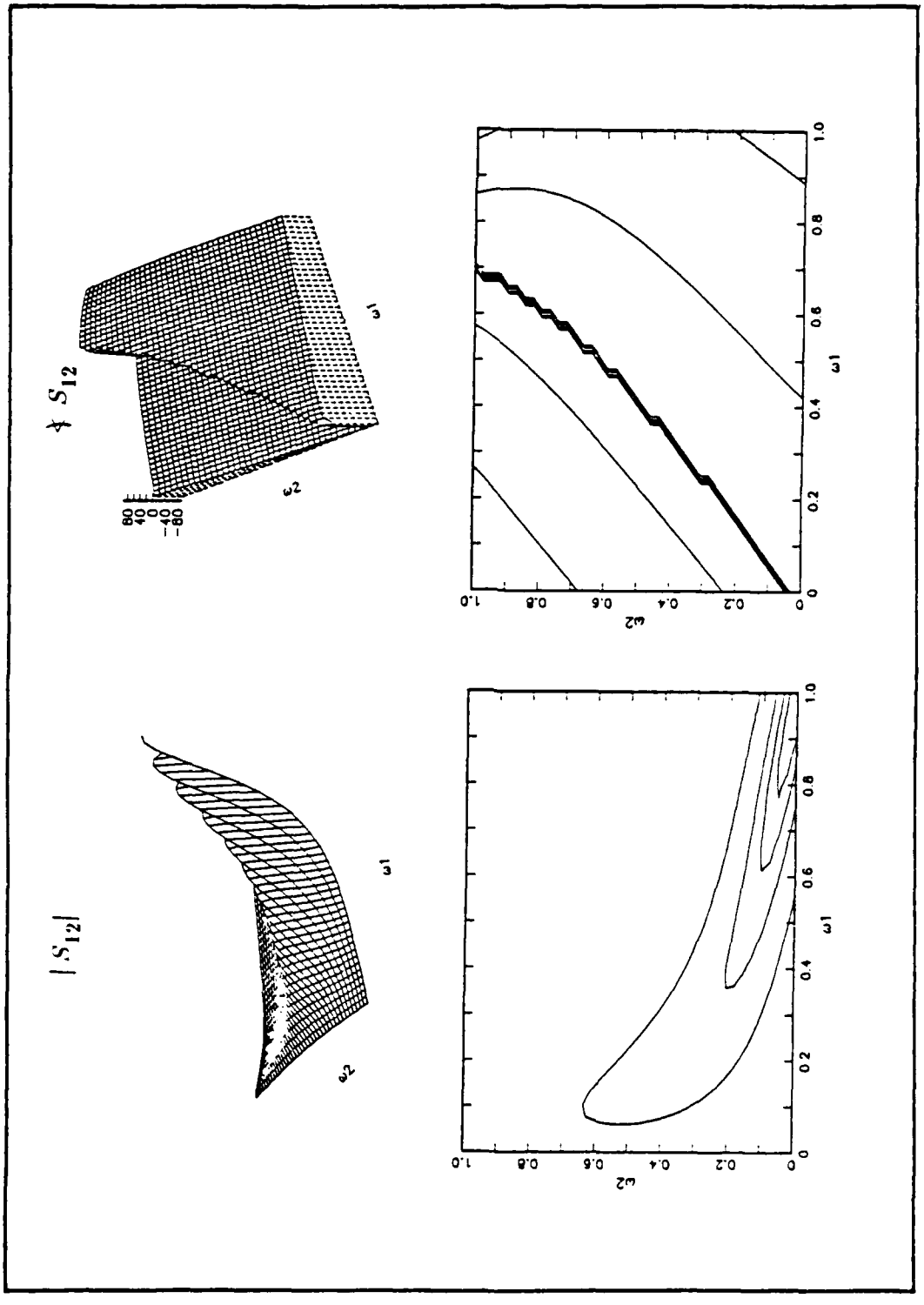

Fig. 4.26 Estimated power spectra for a multichannel 2-D linear process. (cont'd)

b. Experiment (2)

The goal of this experiment was to identify an unknown system $H(\omega_1,\omega_2)$ on the basis of input/output measurements. Two-dimensional white noise $w(n_1,n_2)$ which is considered as a first channel $x_1(n_1,n_2)$ is sent through the unknown system whose output $x_2(n_1,n_2)$ is considered to be the second channel. The cross spectrum between the channels is proportional to the frequency response of the unknown system. The example considered here corresponds to the system:

$$x_2(n_1,n_2)=x_1(n_1,n_2)-0.38x_1(n_1,n_2-1)-0.38x_1(n_1-1,n_2)-0.24x_1(n_1-1,n_2-1) \tag{4.28}$$

Fig. 4.27(a) shows the actual frequency response of the system, while Fig. 4.27(b) shows the estimated frequency response (amplitude and phase of the cross spectrum). The estimated system parameters are given in Table 4.7. Since NSHP support was assumed in the spectral estimate the parameter $a_{1,-1}$ comes out to be very near zero. The other parameters in Table 4.7 are close to the system parameters in (4.28).

D. ESTIMATES USING CQ MODELS

This section discusses the results of the CQ method on the examples used for the NSHP experiments above. The results are found to be quite comparable. Spectrum estimates for Examples 1, 2, and 3 were also computed using quadrant plane models. The estimates for Examples 1 and 2 were based on 2×2 regions of support (first order model)

TABLE 4.7 COMPARISON BETWEEN THE ACTUAL AND ESTIMATED PARAMETERS OF THE SYSTEM IDENTIFICATION PROBLEM

	Estimated Parameters	True Parameters
$a_{0,0}$	1.00	1.00
$a_{0,1}$	-0.4002	-0.38
$a_{1,-1}$	-0.00001	0.00
$a_{1,0}$	-0.3844	-0.38
$a_{1,1}$	-0.1928	-0.24

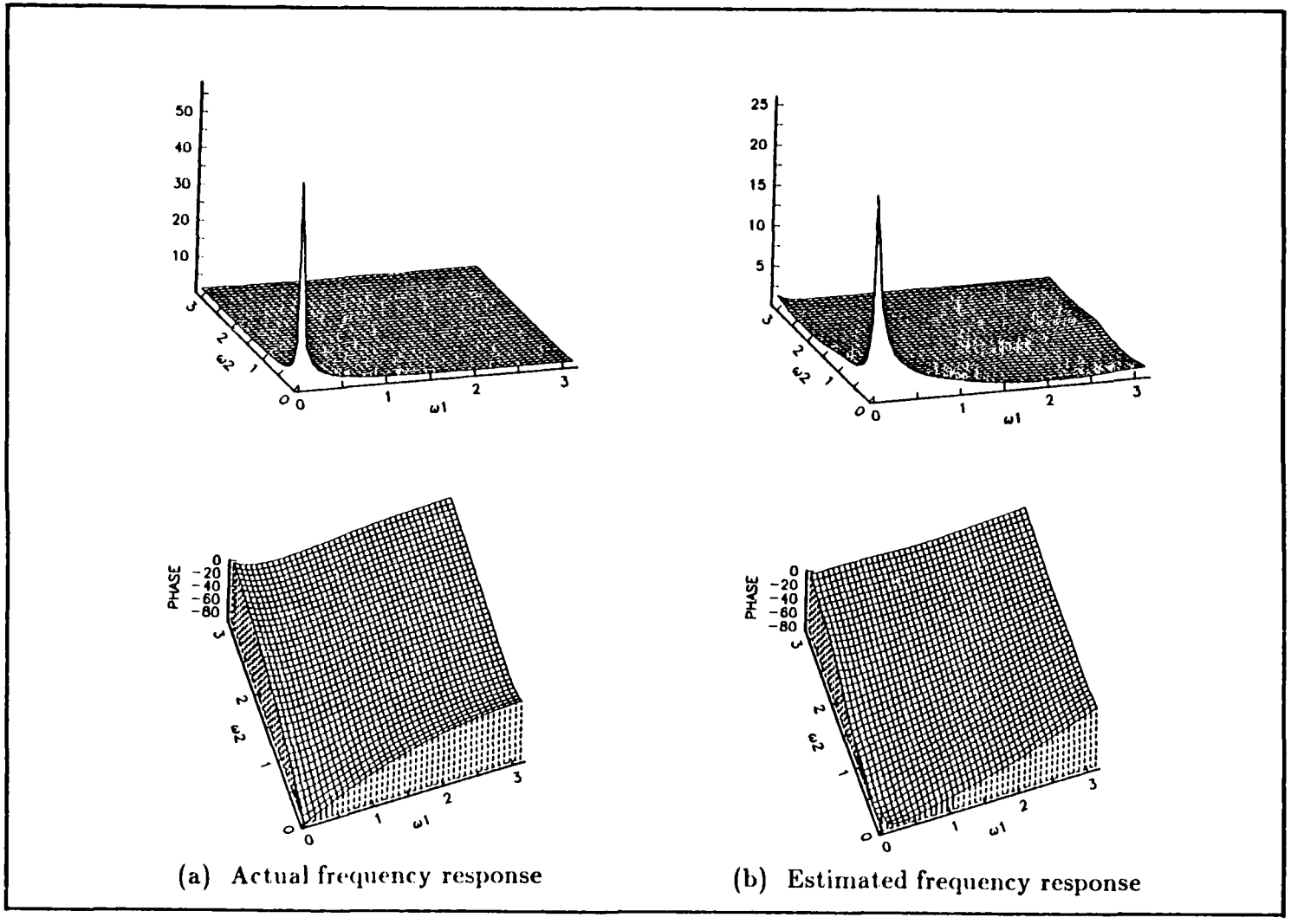

(a) Actual frequency response

(b) Estimated frequency response

Fig. 4.27 Comparison of results for system identification experiment.

for the first and second quadrant filters. Figure 4.28(a) shows the component S_{11} of the spectral matrix. Results for S_{22} are similar. The use of either the first or second quadrant filter alone results in a spreading of the peak in one direction. The combined estimate (Eqn. (4.20)) gives a more accurate result similar to that of the NSHP model. Figure 4.28(b) shows the magnitude and phase estimates for the cross spectrum S_{12}. A similar spreading phenomenon is observed in the magnitude estimate but the estimation of phase is correct for both the individual and the combined spectrum estimates. Figure 4.29 shows the spectrum estimate for two sinusoids in white noise corresponding to Example 2. The results of this quadrant based model can be qualitatively compared to the results for the NSHP model of Figure 4.12. The placement of the sinusoid along a diagonal shows some characteristics of the quadrant models. The first quadrant results show a very significant spreading of the peaks along a direction orthogonal to the line connecting their centers. This is observed in both the autospectral components and the cross spectra. The second quadrant estimates show good resolution with little spreading of the peak. However the combined estimate gives the best results with sharp peaks and with magnitudes more nearly equal than those observed with the NSHP model. The phase in Fig. 4.29(b) is slowly varying in the region of the sinusoids for all of the estimates with a correct values of approximately 1.5 and 0.5 radians at the locations of the sinusoids. (Exact values produced by the combined estimate are 1.42 and 0.57 radians respectively.)

Fig. 4.30 shows the results for estimation of the three sinusoids given in Fig. 4.13 using combined sixth order first and second quadrant filters. These results can be compared to those of Figure 4.14. Although the sinusoids are resolved and estimated in approximately the correct position, the peaks are less sharp than for the NSHP estimate. Computational requirements for the sixth order CQ estimate and the fourth order NSHP estimate are approximately the same.

Figure 4.31 shows the amplitude of S_{12} estimated by using the first and second quadrant filters, separately. We have seen that use of the individual quadrant filters can result in a significant bias and spreading of the peaks. In the particular case of Fig. 4.31, we notice that in addition to the bias the first quadrant estimate for the cross spectrum has a false peak near the frequency ω_B of Figure 4.13. The second quadrant estimate almost misses the frequency ω_A.

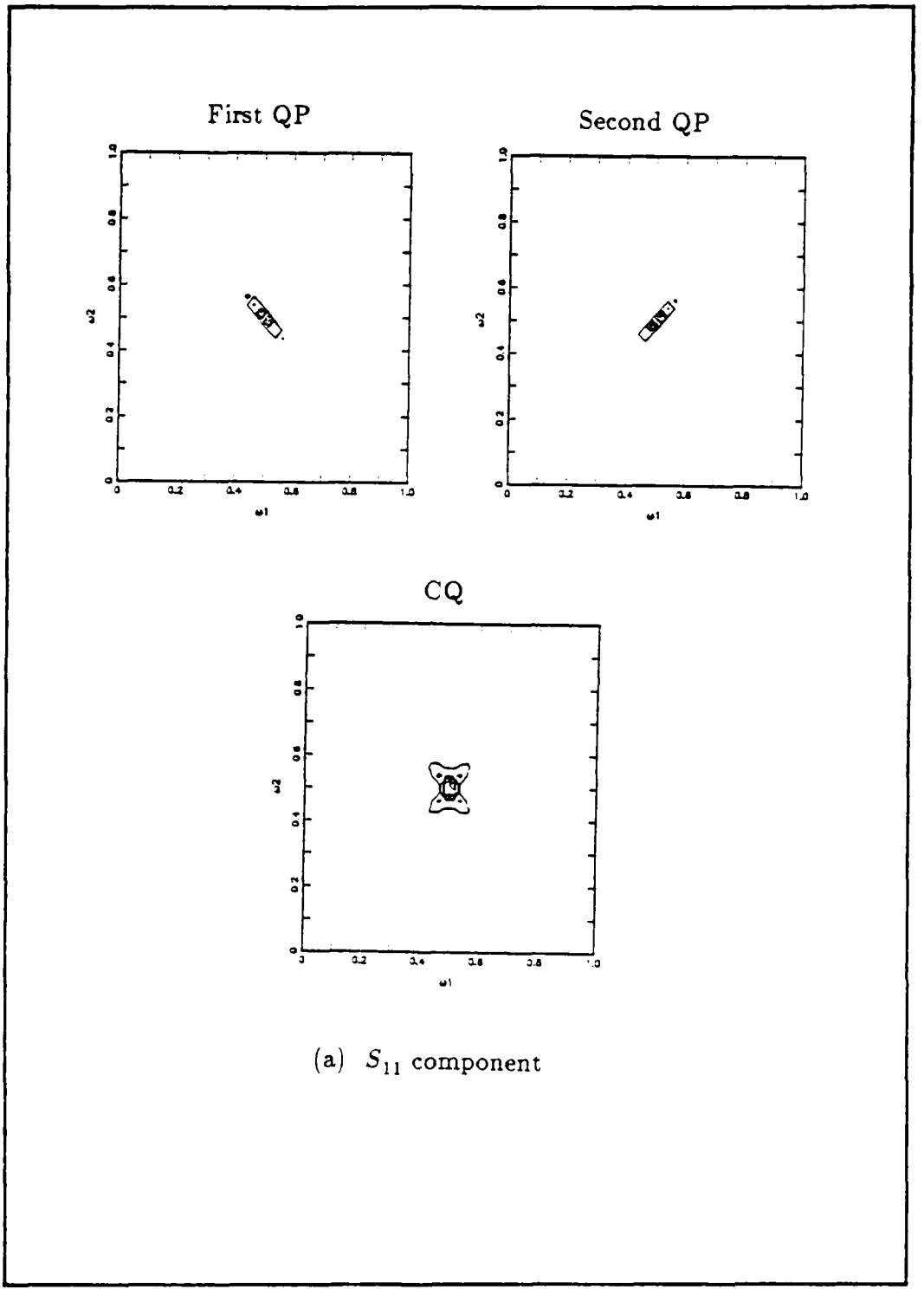

(a) S_{11} component

Fig. 4.28 Estimation of single sinusoid using quadrant models.

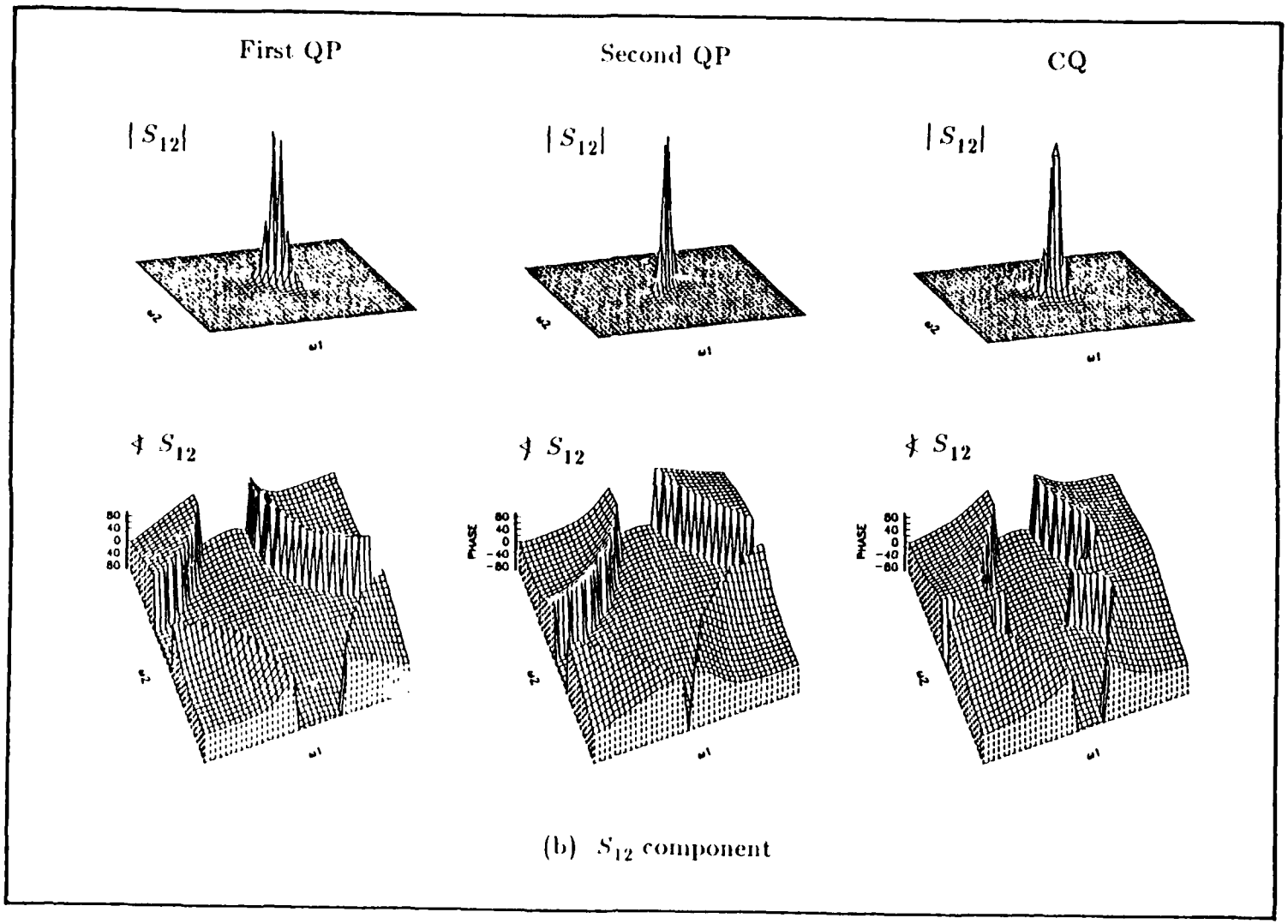

(b) S_{12} component

Fig. 4.28 Estimation of single sinusoid using quadrant models. (cont'd)

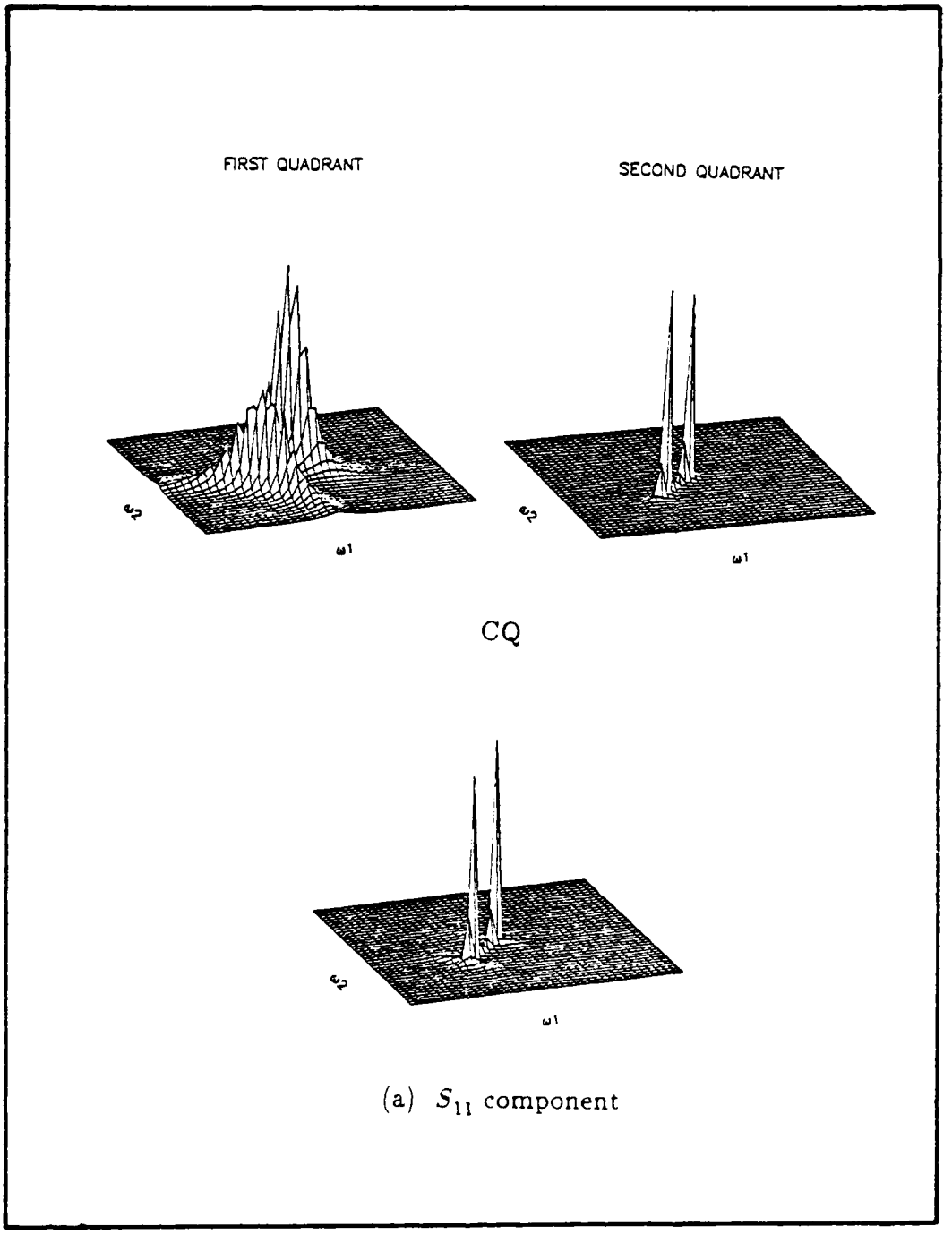

(a) S_{11} component

Fig. 4.29 Estimation of two sinusoids using quadrant models.

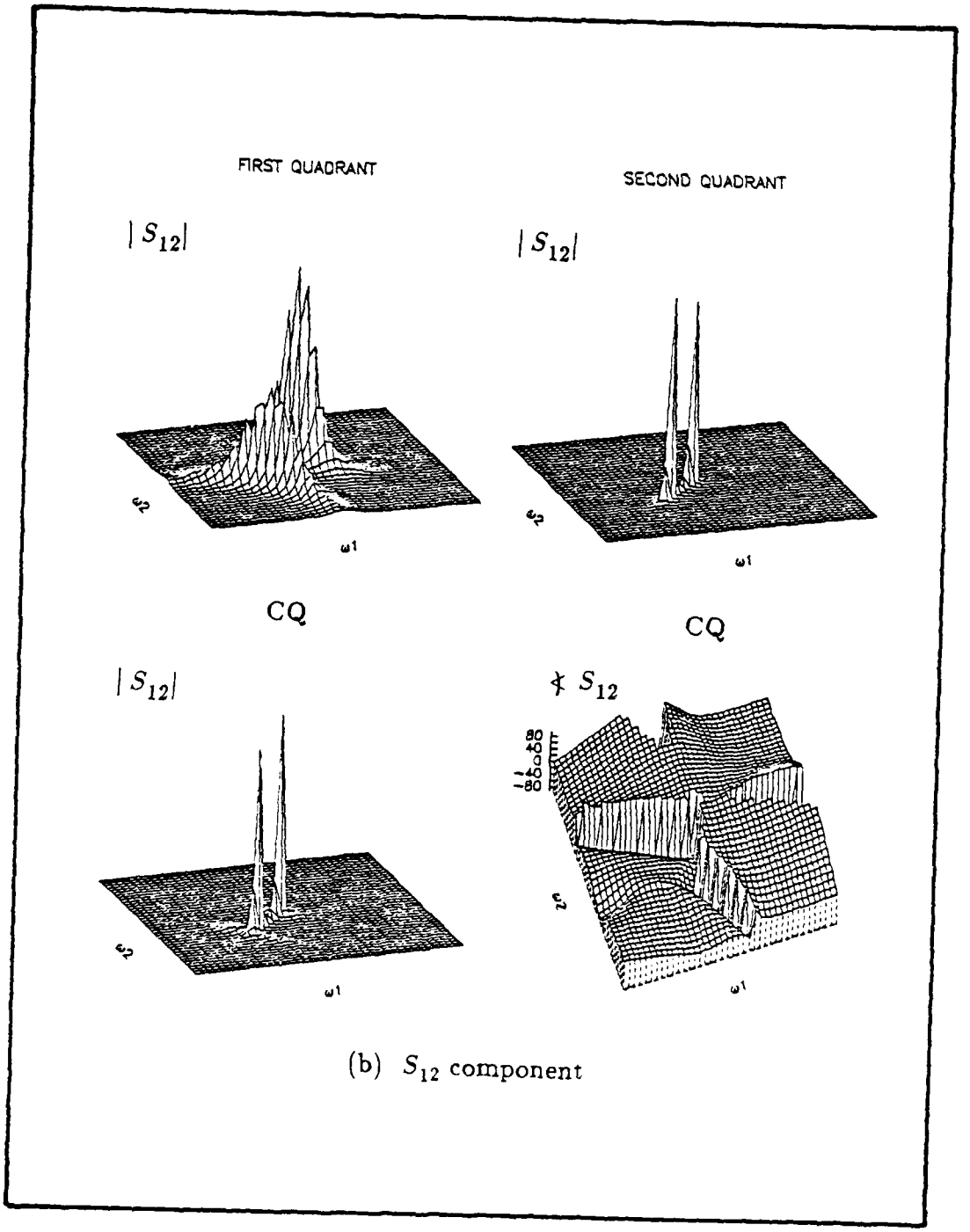

(b) S_{12} component

Fig. 4.29 Estimation of two sinusoids using quadrant models. (cont'd)

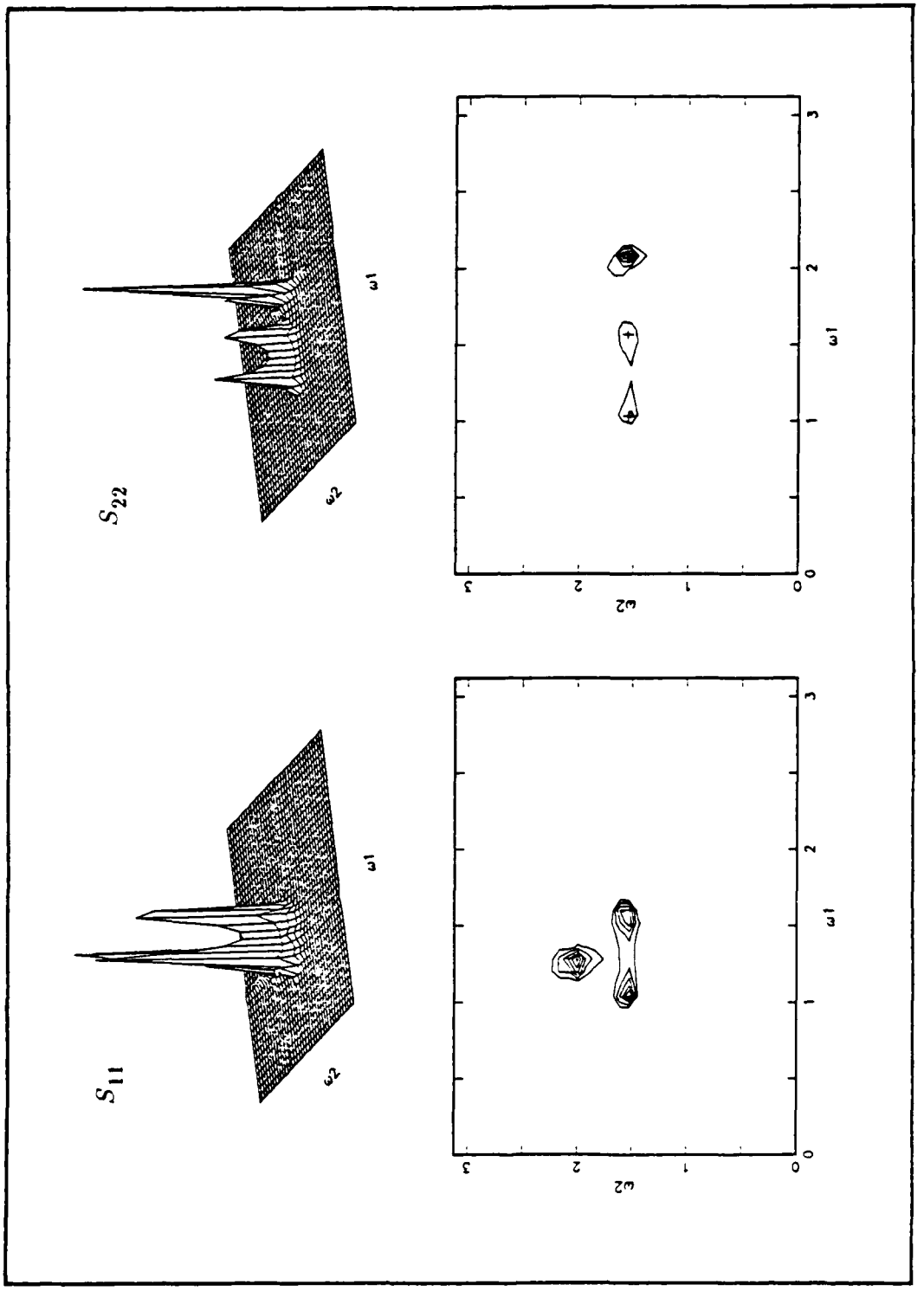

Fig. 4.30 Estimation of three sinusoids in white noise (CQ).

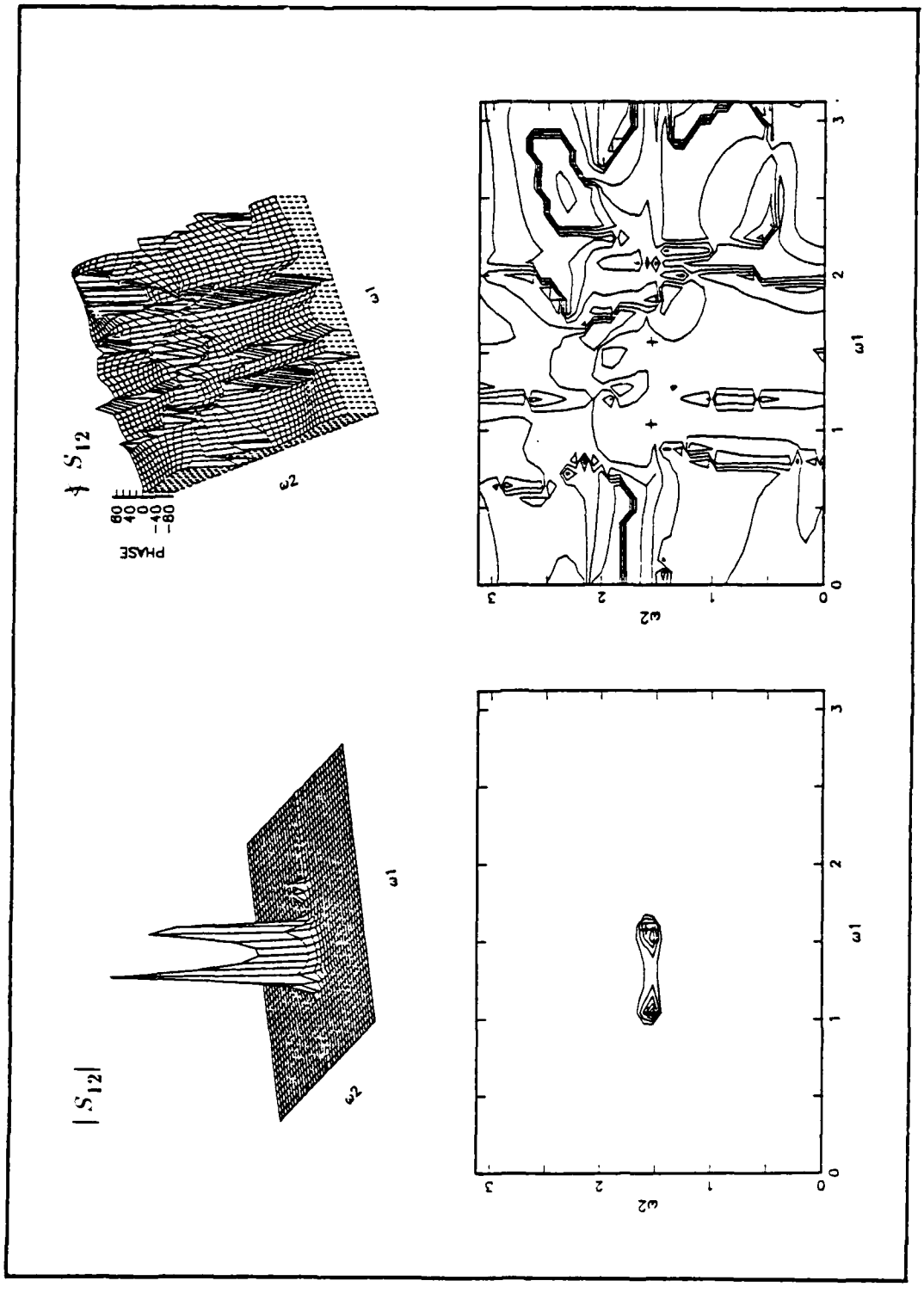

Fig. 4.30 Estimation of three sinusoids in white noise (CQ). (cont'd)

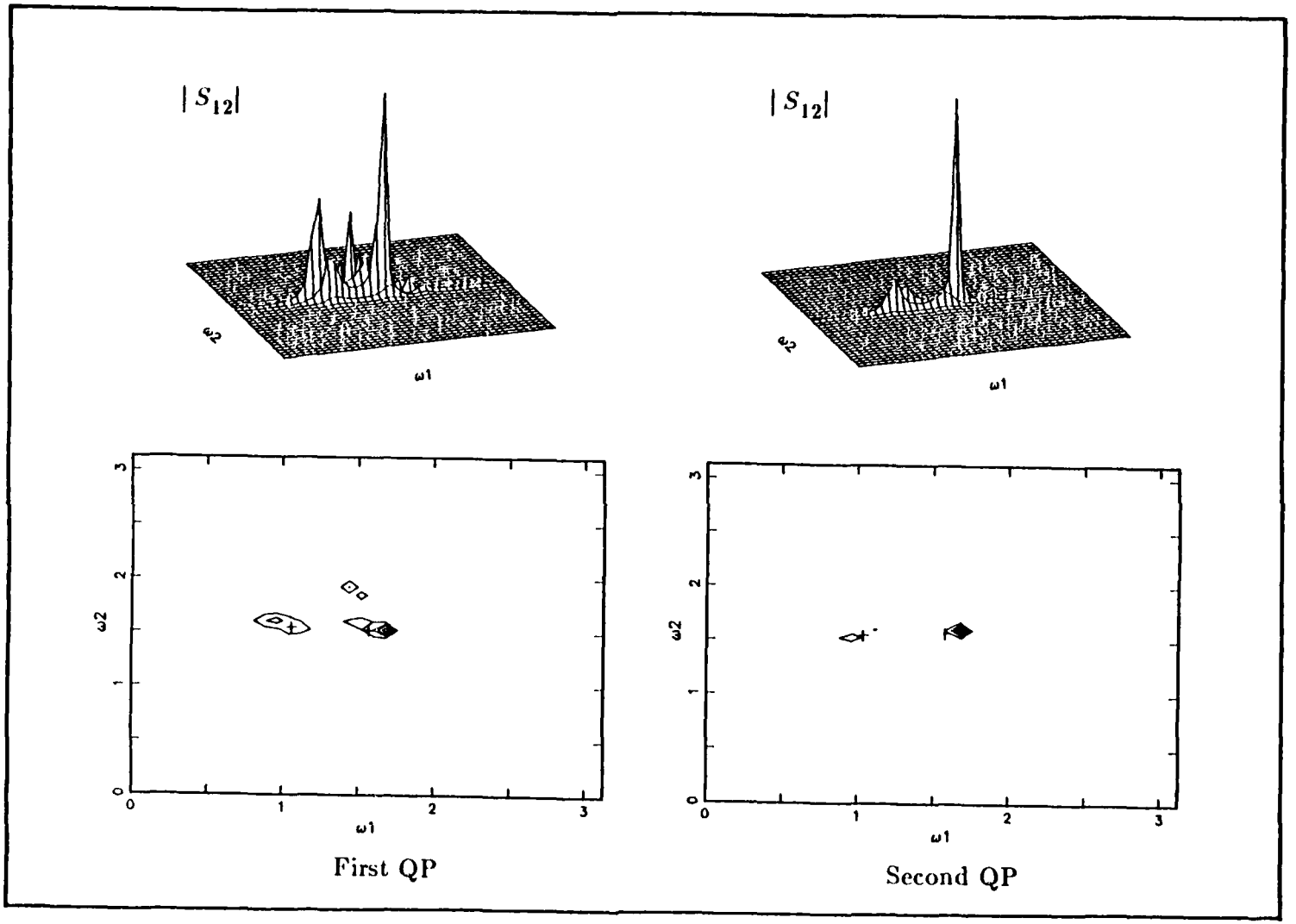

Fig. 4.31 Cross spectrum estimation of first and second quadrant models.

These experiments indicate that the result of spectrum estimation using a single quadrant model is not generally reliable but the estimate resulting from combining the two models according to Eqn. (4.20) is quite accurate.

E. ESTIMATES USING THE 2-D BURG TECHNIQUE

The results described in the previous sections were based on algorithms that first estimate the 2-D matrix correlation function and then solve Normal equations to determine the AR model parameters. These methods will be called *indirect* since they require estimation of the correlation function as a prerequisite to determining the model parameters. Here the 2-D multichannel Burg algorithm cited in Chapter III is used to form the spectral estimate.

Two test cases are presented; both involve sinusoids buried in white noise. In the first test case, we use the data of section C, Example (1). Fig. 4.32 shows the autospectra (S_{11}, S_{22}) and the amplitude and phase of cross spectrum (S_{12}). In the second case, we use the data of section C, Example (2). Fig. 4.33 shows the autospectra and the amplitude and phase of the cross spectrum. It is clear that we have a good estimate for single sinusoid while we get a poor estimate when the number of sinusoids increases. This is similar to what happens in the single channel 2-D Burg algorithm.

F. ESTIMATES USING THE DIRECT CQ METHOD

A direct method for estimating the model parameters, i.e., a method that estimates the parameters directly from the data was described in Chapter III. This method is very well suited to spectrum estimation using combined first and second quadrant models since it estimates both sets of filter parameters simultaneously.

The results of the direct CQ method on the examples used for NSHP and CQ experiments above are found to be quite comparable. Figure 4.34 shows the results of estimating a single sinusoid in white noise using the same data considered in section C (compare this to Fig. 4.28). The direct method yields a sharper peak with somewhat lower sidelobes. Estimates of the one radian phase shift between the channels are 1.05 rad. for the indirect method and 1.03 rad. for the direct method.

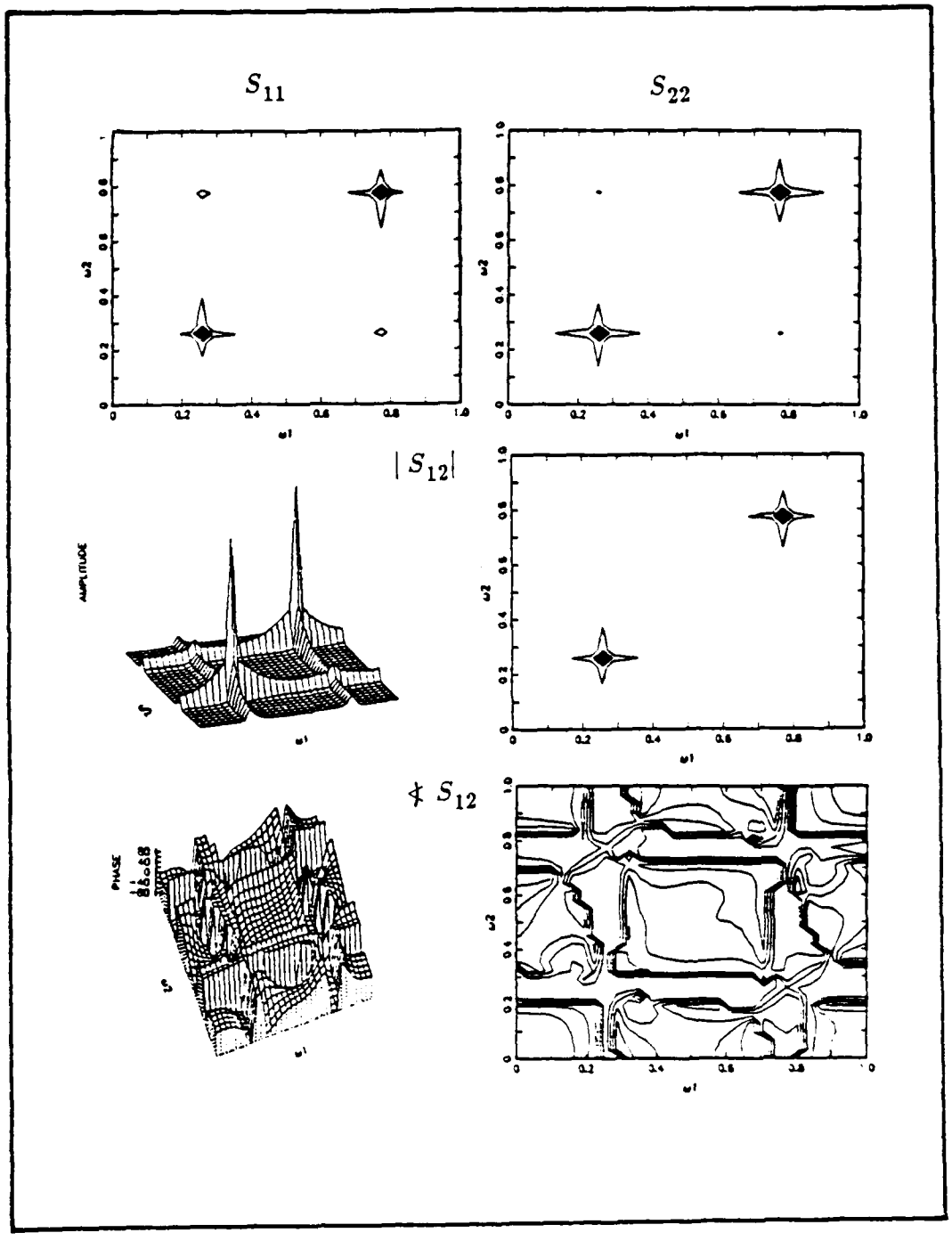

Fig. 4.32 Estimate of spectra for one sinusoid in white noise (Burg).

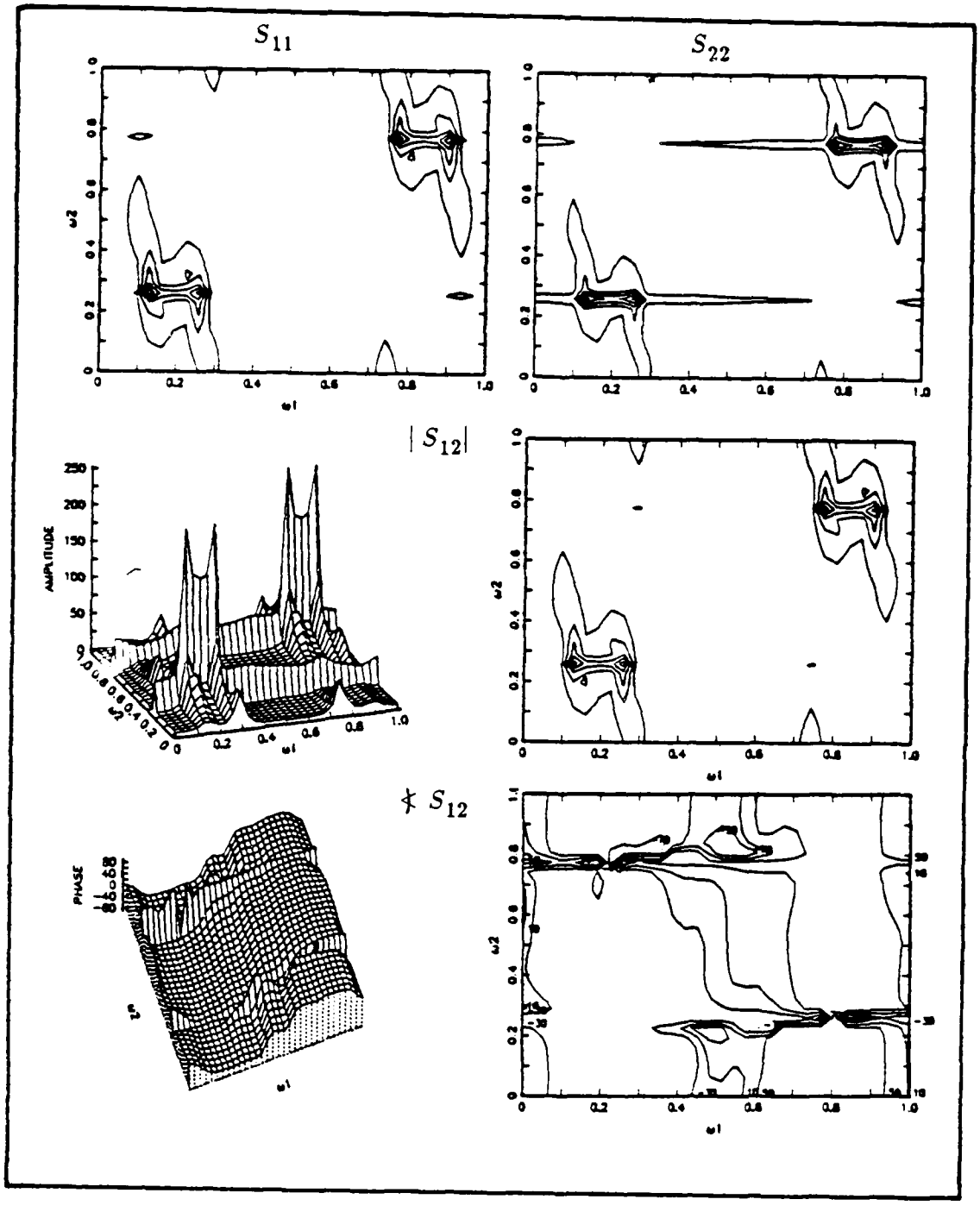

Fig. 4.33 Estimate of spectra for two sinusoids in white noise (Burg).

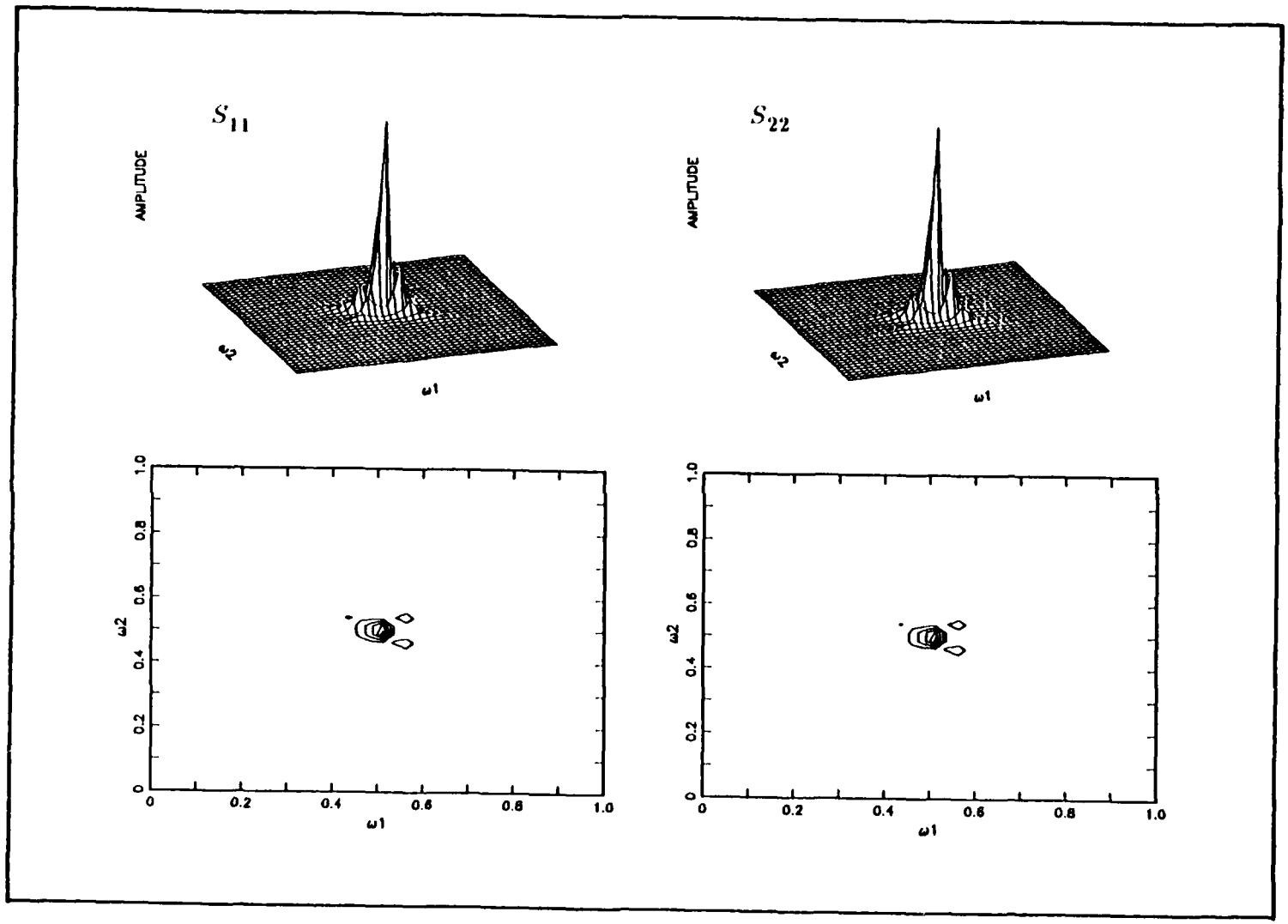

Fig. 4.34 Estimation of single sinusoid in white noise (direct CQ).

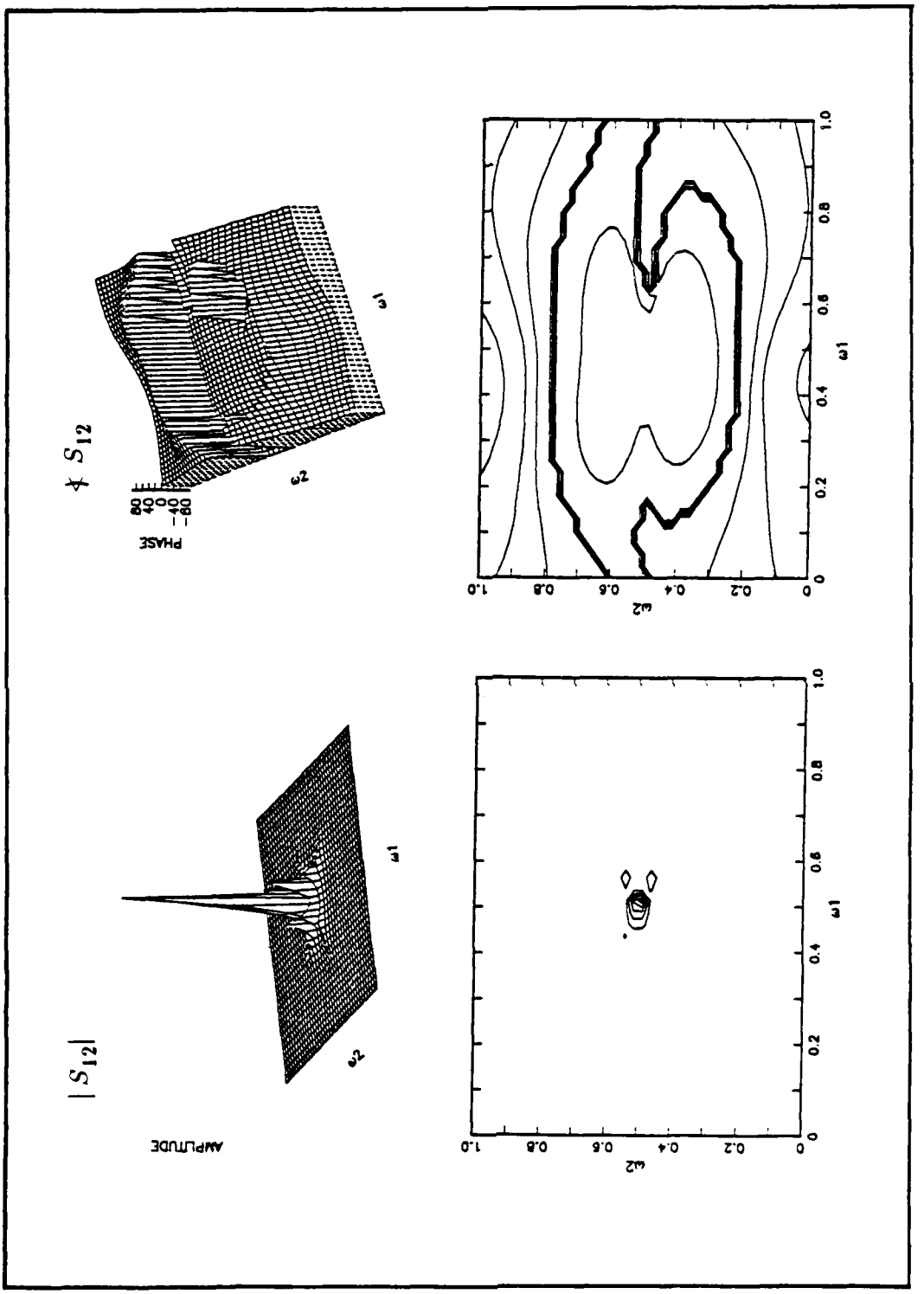

Fig. 4.34 Estimation of single sinusoid in white noise (direct CQ). (cont'd)

Figure 4.35 shows the results for estimating two sinusoids in white noise using combined second order quadrant filters with parameters estimated by the indirect method. These results are nearly equivalent to those shown earlier in Figure 4.29. A few minor peaks appear in both cases. For the indirect method these peaks appear closer to the main peak while for the direct method they appear further out. Phase estimates at the peak locations are 1.48 and 0.50 radians for the direct CQ method while they are 1.47 and 0.55 radians for the indirect method. The values produced by the direct method are slightly closer to the true values of 1.5 and 0.5 radians.

Figure 4.36 shows the results for estimating three sinusoids in white noise using two combined sixth order quadrant filters with parameters estimated by the direct method. The results are typical of those obtained in other examples. The sinusoids are resolved more sharply than in Fig. 4.30 and are quite similar to the NSHP results of Fig. 4.14.

The results for the shift estimation and the linear model examples are not shown here but were found to be comparable to the NSHP and CQ results.

An important advantage of the CQ method over the NSHP is its reduced computation. This is discussed further in the next section where a quantitative comparison of the estimates is given.

G. COMPARISON RESULTS

1. Effect of Model Order on Resolution

In order to compare the resolution characteristics of the NSHP and the CQ method quantitatively, the signal-to-noise ratio was kept constant at 12 *dB* and the model order was changed. The results are given for two-channel 2-D signals, each channel having two sinusoids buried in white noise with the data of section C, Example (2). The criterion of resolution was defined as the minimum frequency separation, below which two sinusoids are not resolved. Figure 4.37 summarizes the cross spectrum resolution performance of the methods as a function of the order of the model. As shown in the figure, as the model order increases, the resolution increases. Table 4.8a shows the phase of the NSHP estimate as a function of the model order while Table 4.8b shows the same results for the CQ method. As shown in the table, the phase estimate is good even when the resolution is poor. The results shows an estimate which is consistently close to the actual

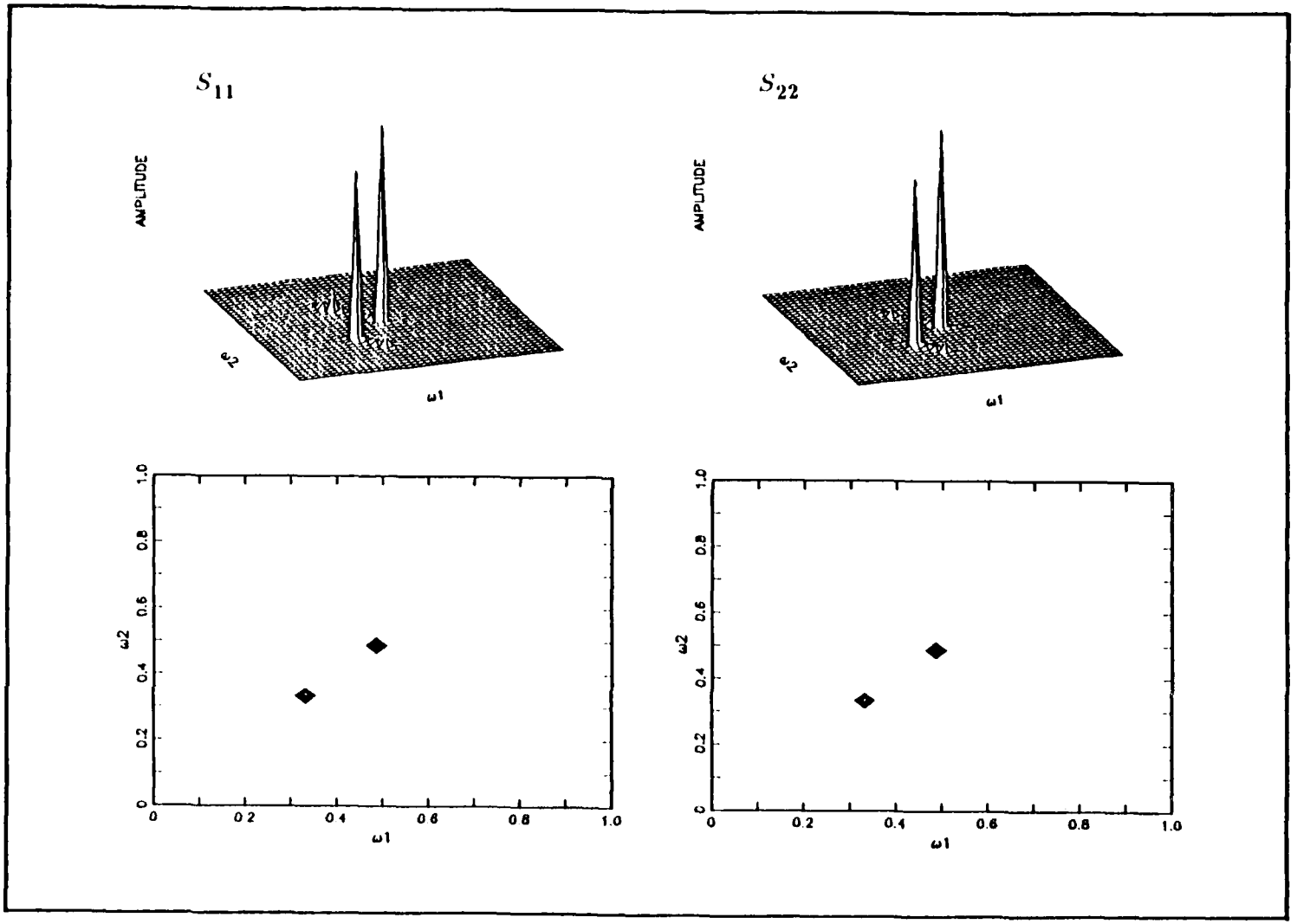

Fig. 4.35 Estimation of two sinusoids in white noise (direct CQ)

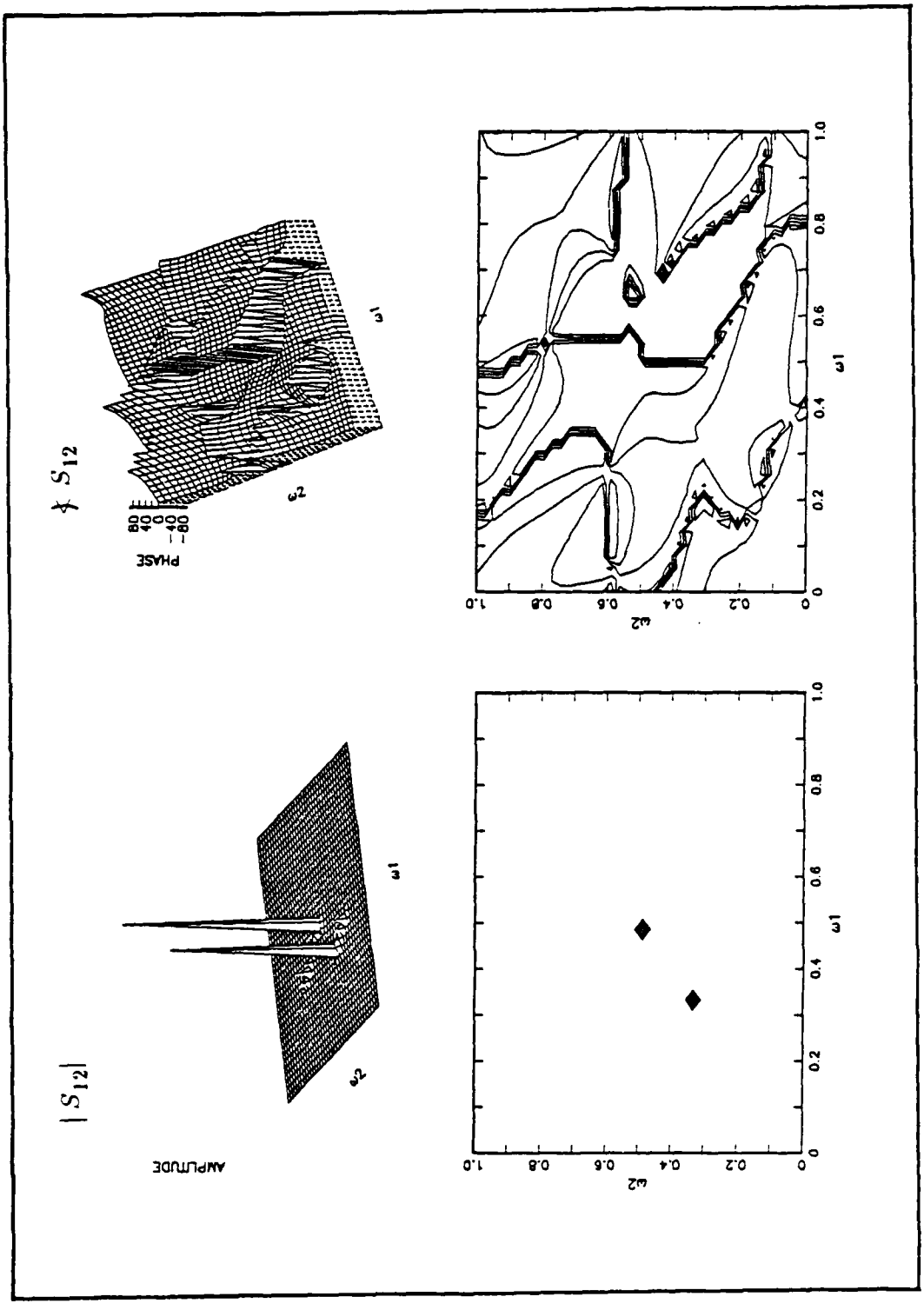

Fig. 4.35 Estimation of two sinusoids in white noise (direct CQ). (cont'd)

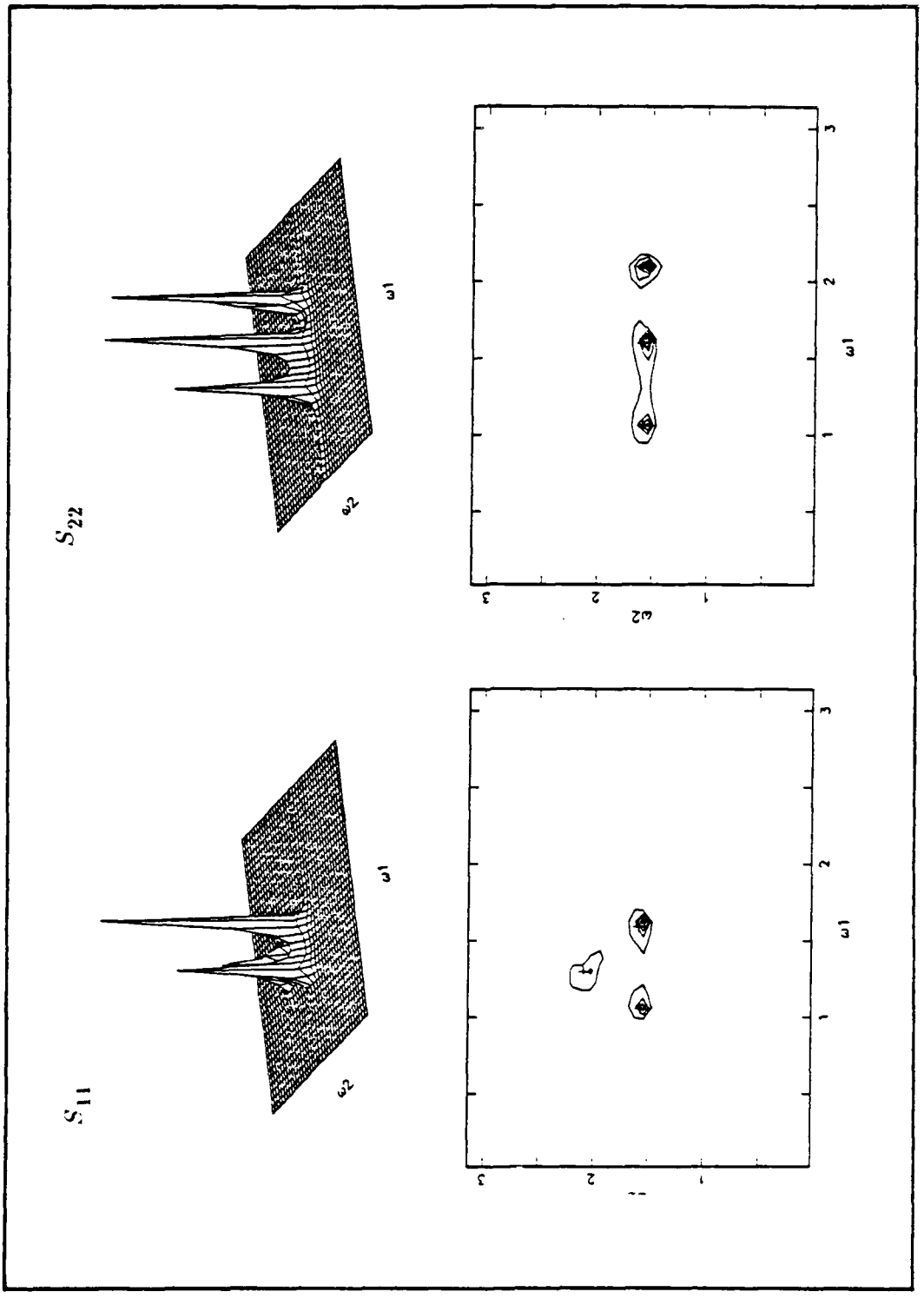

Fig. 4.36 Estimation of three sinusoids in white noise (direct CQ).

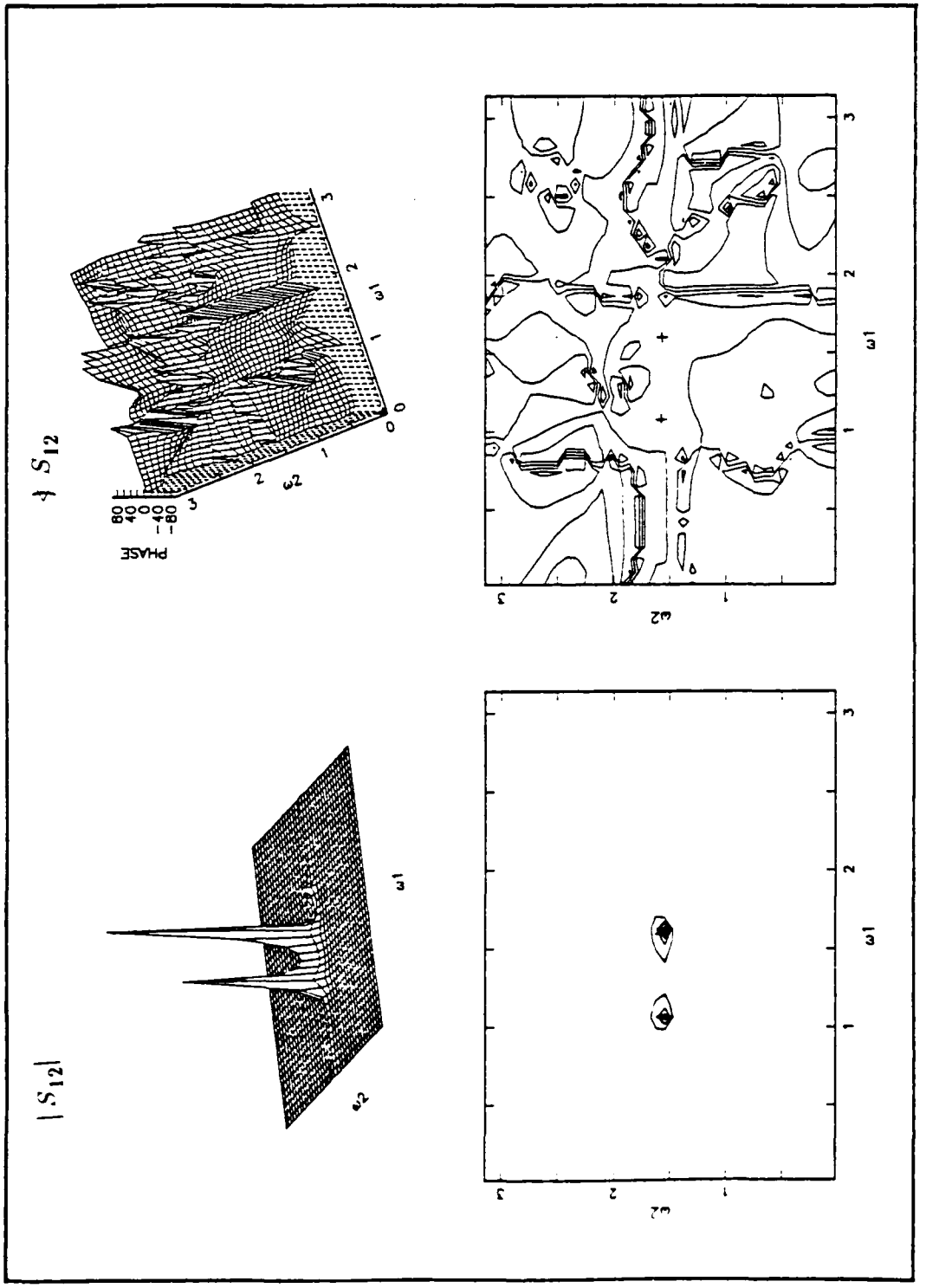

Fig. 4.36 Estimation of three sinusoids in white noise (direct CQ). (cont'd)

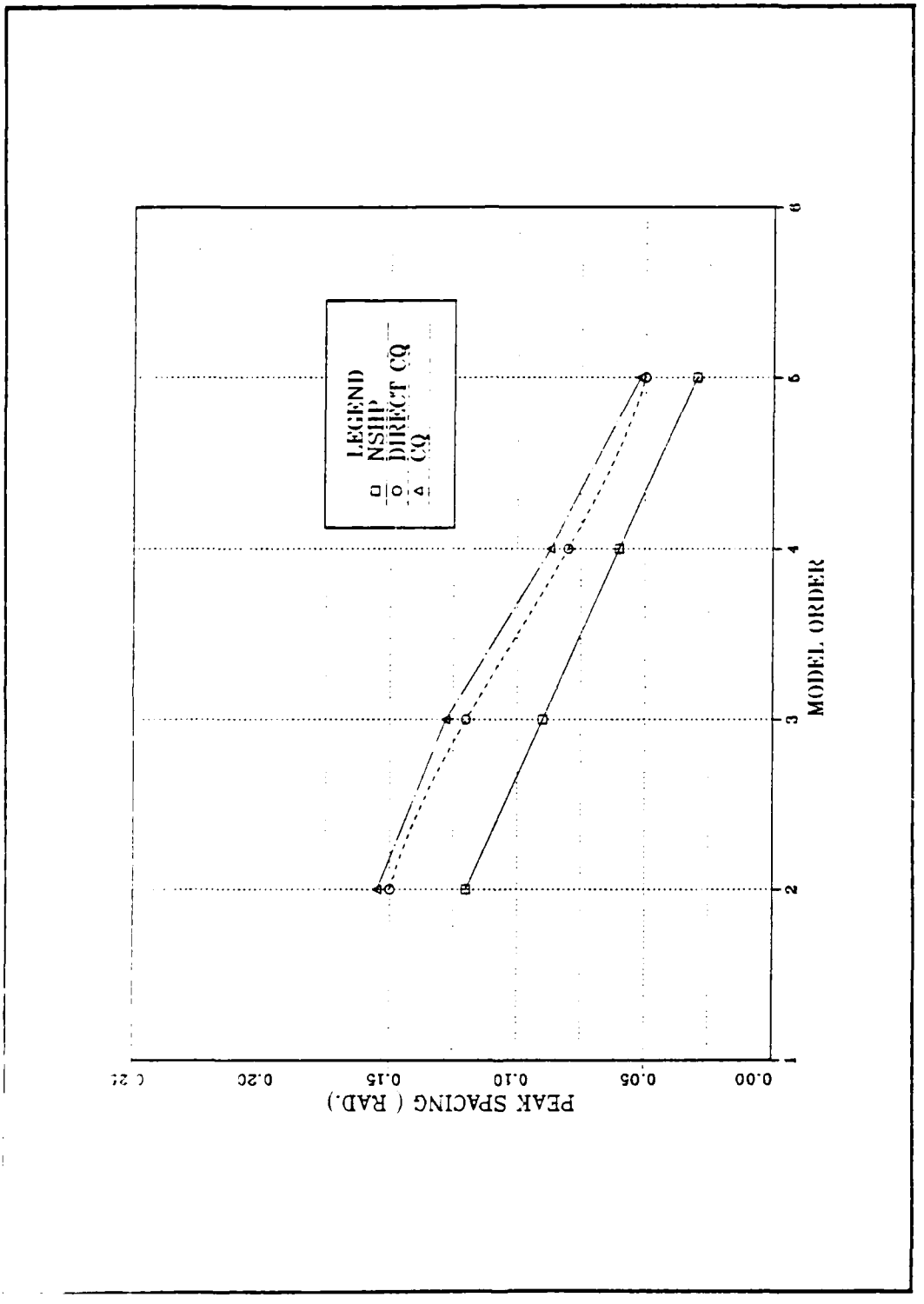

Fig. 4.37 Effect of model order on resolution.

TABLE 4.8 PHASE ESTIMATION COMPARISON OF DIFFERENT AR MODELS

(a) The estimated phase of NSHP method as a function of the model order.

Model Order	ϕ_1	ϕ_2
2nd	1.48	0.509
3rd	1.489	0.514
4th	1.487	0.506
5th	1.493	0.540

(b) Phase estimation of CQ method as a function of model order.

Model order	ϕ_1	ϕ_2
2nd	1.481	0.550
3rd	1.488	0.498
4th	1.502	0.489
5th	1.510	0.493

values (ϕ_1=1.5 radians, ϕ_2=0.5 radians) and varies only slowly with changes in the order of the model.

The NSHP estimate has a somewhat higher resolution than the CQ estimate for a fixed order N but the number of computations required is considerably higher. In particular if we assume that the solution of the Normal equations requires a number of computations related to the size of the matrix cubed then the ratio of the computations (NSHP/CQ) is approximately

$$\left[\left[2N\ (N+1)+1\right] / (N+1)^2\right]^3$$

which has a minimum value of about 2 and a maximum value of 8 for large N. If the computations required for solution of the Normal equations is proportional only to the square of the size of the matrix, then the ratio varies between 1.5:1 and 4:1. If we consider an order where both methods have approximately the same resolution we can compare the computation. For example if we compare the 3^{rd} order NSHP to a 4^{th} order CQ estimate, we find that the number of computations is about the same. However for higher values of N the CQ method has a definite computational advantage.

The CQ method exhibits a slightly but consistently better resolution when the parameters are estimated by the direct method. In addition since the computational requirements are proportional to the *square* of the order of the matrix in Eqn. (3.54), the method has a computational advantage as well.

2. Divergence Measurement

In this final section we apply the incremental divergence measure (3.61) to the comparison of the NSHP and CQ spectral estimates for three examples. The results are similar to those in Chapter II for a single channel 2-D estimate. The data show quantitatively that the CQ method gives a spectral estimate that compares closely to the NSHP estimate but that use of a single quadrant model alone produces an estimate that compares poorly with the NSHP estimate.

In the first example, two-channel 2-D signals consisting of two sinusoids in each channel in additive noise (tone estimation) are considered. In the second example, we assume a two-channel 2-D signal with linear phase difference. Finally in the third

example, we consider a more general discrete two-channel 2-D AR random process with NSHP support. The parameters of this more general process are given in Table 4.6. In all cases, equal orders were used for the NSHP and quadrant models.

Table 4.9a shows the results of incremental divergence of NSHP and quadrant models while Table 4.9b shows the results of incremental divergence of the NSHP and quadrant models with parameters estimated by the direct method. The tables show that the incremental divergence between the NSHP model and the individual (first or second) quadrant models is relatively high and that the incremental divergence for the NSHP and CQ models is considerably lower indicating a closeness of the spectral estimates.

TABLE 4.9 INCREMENTAL DIVERGENCE MEASUREMENT FOR DIFFERENT AR MODELS

(a) Comparison between NSHP and CQ models.

Incremental Divergence			
Comparison between	Ex.(1)	Ex.(2)	Ex.(3)
NSHP & 1st quadrant	0.1735	0.0628	0.3857
NSHP & 2nd quadrant	0.2576	0.0943	0.2762
NSHP & CQ	0.0657	0.0262	0.0869

(b) Comparison between NSHP and direct CQ models.

Incremental Divergence			
Comparison between	Ex.(1)	Ex.(2)	Ex.(3)
NSHP & 1st quadrant	0.1922	0.0361	0.4147
NSHP & 2nd quadrant	0.2584	0.0965	0.2728
NSH & direct CQ	0.1046	0.0157	0.1229

V. MULTICHANNEL 2-D MLM SPECTRAL ANALYSIS

A. INTRODUCTION

The maximum likelihood method (MLM) of spectrum estimation was originally proposed by Capon (1969) in a multidimensional case as an array processing technique and designed to accommodate non-uniformly spaced data. One estimates the power spectral density by effectively measuring the power output of a narrowband filter as this filter is swept across the frequency band of interest (Lacoss,1971).

It was seen that MLM has the ability to resolve closely spaced features in the spectrum using only a relatively small data set. Further, although the MLM has resolution not as good as the AR spectral estimation method, it is widely used in practice, especially in array processing. In addition the method is quite simple to apply.

In this chapter we review the 2-D single channel Maximum Likelihood Method (MLM) of spectral estimation and describe extensions by Baggeroer and Lagunas *et al* to cross spectrum estimation for 1-D random processes. We then develop the MLM method specifically for the 2-D multichannel case and compare our results to a 2-D version of the earlier results where the components of the spectral matrix are computed individually. We discuss the differences in the methods and compare results experimentally.

Since MLM estimates generally have significantly poorer resolution than AR model-based estimates, we also consider the so-called Improved MLM (IMLM) of Lim and Dowla and develop it for the multichannel case. This method retains the simplicity of the MLM, but gives better resolution. We carry out an experiment to compare the amplitude and phase of cross spectra of AR, MLM and IMLM techniques. Finally, in this chapter we measure and compare the resolution properties of the estimate experimentally as a function of SNR and as a function of model order.

B. SURVEY OF SINGLE CHANNEL 2-D MLM

In the 1-D case, the MLM spectral estimate at frequency ω_0 is determined by designing an FIR filter which passes the power in a very narrow band around ω_0 and rejects the

power due to other frequency components. The same interpretation can be applied to 2-D spectral analysis.

Suppose the output of a linear 2-D FIR filter is:

$$y(n_1,n_2) = \sum_{i_1,i_2 \in \alpha} \sum a_{i_1 i_2} x(n_1 - i_1, n_2 - i_2) \tag{5.1}$$

where α is the region of support, x is the sampled input, and $a_{i_1 i_2}$ are the filter coefficients. Suppose further that we wish to estimate the power spectrum $S_{ML}(\omega_1,\omega_2;\alpha)$ at the specific frequency $(\omega_1^{(0)},\omega_2^{(0)})$. The filter weights $a_{i_1 i_2}$ are determined by minimizing $E\left[|y(n_1,n_2)|^2 \right]$ subject to the constraint that the filter passes the frequency component of $x(n_1,n_2)$ at $(\omega_1^{(0)},\omega_2^{(0)})$ with unit gain and zero phase shift. The formulation is as follows

$$\underset{a_{i_1 i_2}}{\textit{minimize}} \quad E\left[|y(n_1,n_2)|^2 \right] \tag{5.2}$$

subject to the constraint

$$\sum_{(l_1,l_2) \in \alpha} \sum a_{l_1 l_2} e^{-j\omega_1 l_1} e^{-j\omega_2 l_2} = 1 \tag{5.3}$$

The spectral estimate $S_{ML}(\omega_1^{(0)},\omega_2^{(0)};\alpha)$ in this case is taken to be the average power $E\left[|y(n_1,n_2)|^2 \right]$ of the output of the filter with the calculated filter coefficients $a_{l_1 l_2}$. Then we can say that the MLM estimates the power spectrum $S_{ML}(\omega_1,\omega_2;\alpha)$ by designing at each frequency $(\omega_1^{(0)},\omega_2^{(0)})$ a different FIR filter such that the filter passes the frequency component $(\omega_1^{(0)},\omega_2^{(0)})$ without modification and minimizes the power due to other interfering spectral components. When the optimal filter is determined and substituted into the expression for the output power (Lacoss,1971), the resulting estimate takes the simple form

$$S_{ML}(\omega_1,\omega_2;\alpha) = \frac{1}{\mathbf{e}_\alpha^{*T} \mathbf{R}_\alpha^{-1} \mathbf{e}_\alpha} \tag{5.4}$$

where $\mathbf{R}_\alpha$ is the correlation matrix corresponding to the data $x(n_1,n_2)$ in α in Eqn. (5.1)

and $\mathbf{e}_\alpha$ is the correspondingly ordered vector of complex sinusoids.

$$\mathbf{e}_\alpha = Col\left[e^{j(\omega_1 n_1 + \omega_2 n_2)}\right]_{(n_1,n_2)\varepsilon\alpha} \tag{5.5}$$

The resolution performance of the MLM spectral estimate actually lies somewhere between that of the Fourier transform technique and that of the AR method. The reason is clear from a relation that exists between the MLM and AR methods which is cited below.

1. Relationship Between MLM and AR Spectral Estimation

Burg (1972) showed that there exists a simple, exact relationship between maximum entropy spectra and maximum likelihood spectra in the 1-D case, when the correlation function is known at uniform intervals of lag for $-K \le k \le K$. The relationship is given by:

$$S_{ML}(\omega;K) = \frac{1}{\frac{1}{K}\sum_{n=1}^{K}\frac{1}{S_{ME}(\omega;n)}} \tag{5.6}$$

where $S_{ML}(\omega;K)$ represents the MLM spectral estimate of order K,[1] and $S_{ME}(\omega;n)$ represents the MEM spectral estimate of order n. Eqn. (5.6) shows that the reciprocal of the MLM spectrum is equal to the average of the reciprocals of the maximum entropy spectra obtained using from one point up to K-point prediction error filters.

For the 2-D case Dowla and Lim (1984) have shown that there is an exact relationship between the MLM spectra and the spectra obtained by AR signal modeling using a known autocorrelation sequence $R(i_1,i_2)$ of a 2-D random signal in the region α. This relation is

$$S_{ML}(\omega_1,\omega_2;\alpha) = \frac{1}{\sum_{\gamma\varepsilon\alpha}\frac{1}{S_{AR}(\omega_1,\omega_2;\gamma)}} \tag{5.7}$$

where if all samples in the region are ordered in some arbitrary fashion then

---

[1] That is, the support of the 1-D filter is a set of K adjacent points.

$S_{AR}(\omega_1,\omega_2;\gamma)$ represents the spectrum of the linear predictive filter that estimates sample number γ from "previous" samples in the ordering. The sum is over all such spectra.

2. Improved MLM

Recently the improved MLM (IMLM) was proposed by Lim and Dowla (1983,1985) for multidimensional spectral analysis as an alternative to the MLM. The method is based on the relation that exists between MLM and AR spectral estimates (Eqn. (5.7)). The IMLM algorithm to compute the spectral estimate S_{IML} is a combination of two MLM estimates and has the form (Lim and Dowla,1985):

$$S_{IML}(\omega_1,\omega_2;\alpha,\beta) = \frac{1}{\frac{1}{S_{ML}(\omega_1,\omega_2;\alpha)} - \frac{1}{S_{ML}(\omega_1,\omega_2;\beta)}} \tag{5.8}$$

where at frequency (ω_1,ω_2), $S_{ML}(\omega_1,\omega_2;\alpha)$ represents the MLM spectral estimate based on all the known correlation points for the region α (Eqn. (5.4)). And $S_{ML}(\omega_1,\omega_2;\beta)$ represents the MLM spectral estimate given on the region β where β is a subset of α.

$$S_{ML}(\omega_1,\omega_2;\beta) = \frac{1}{\mathbf{e}_\beta^{*T}\,\mathbf{R}_\beta^{-1}\,\mathbf{e}_\beta} \tag{5.9}$$

Lim and Dowla proved that the resulting $S_{IML}(\omega_1,\omega_2;\alpha,\beta)$ is always non-negative whenever β is a subset of α.

To illustrate the performance of the IMLM discussed above, we present one example. Consider a single channel 2-D random process $x(n_1,n_2)$ consisting of two-sinusoids in white noise $w(n_1,n_2)$ as given in Eqn. (2.56) with the same parameters. The correlation matrix is developed from these real data. Region α is taken to be the rectangular region $(-P_1,-P_2) \le (i_1,i_2) \le (P_1,P_2)$ where P_1 and P_2 are chosen to be $P_1 = P_2 = 3$. Region β is a subset of α and formed from region α by removing the point (P_1,P_2) from the filter support. Figure 5.1a shows the result of MLM and Fig. 5.1b shows the result of IMLM. It is clear, and in fact not surprising, that the IMLM has significantly better resolution properties than the MLM.

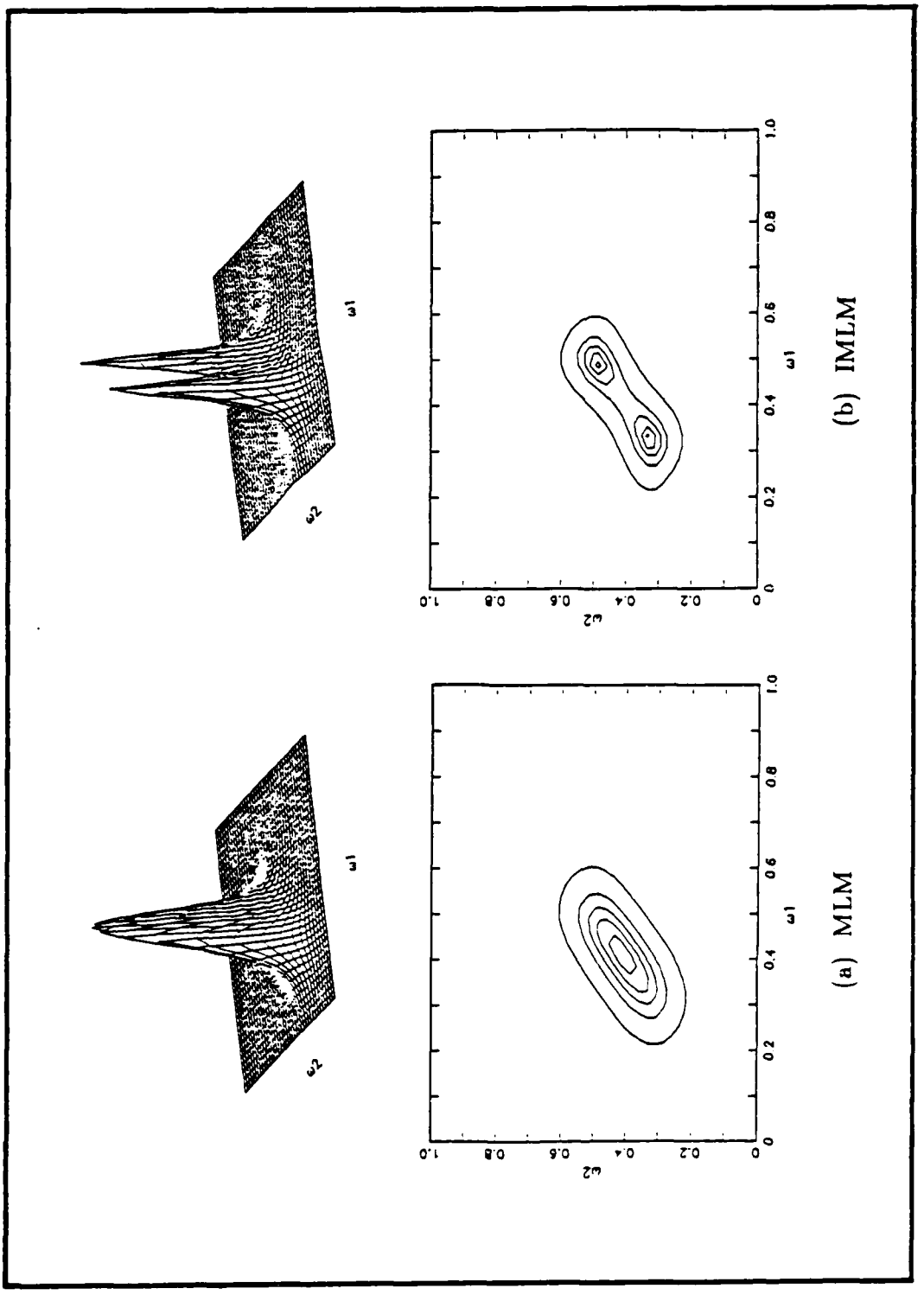

Fig. 5.1 Single channel 2-D spectral estimation of two sinusoids.

C. CROSS SPECTRUM ML ESTIMATION TECHNIQUE

The MLM as originally developed applies to multidimensional signals but computes only the autospectrum of a single m-D data set. Subsequent efforts were made by Baggeroer (1975), and Lagunas *et al* (1985) separately, to estimate the cross spectrum between two data sets. In their methods each channel is treated separately. We refer to this method as the cross spectrum procedure. Our goal is to apply these methods to the 2-D case and compare the experimental results with the general solution given in the next section.

In this section, we review the cross spectrum procedure as it would apply to two 2-D random processes before describing our more general extension of the ML spectrum estimation technique to the multichannel case.

The problem of obtaining a cross spectral estimate for two stationary random processes $x_1(n_1,n_2)$ and $x_2(n_1,n_2)$ with zero means as developed in Baggeroer (1975) and Lagunas et al (1985) is based on the design of two narrow-band FIR filters $H_1(\omega_1,\omega_2)$ and $H_2(\omega_1,\omega_2)$ centered at the same frequency $(\omega_1^{(0)},\omega_2^{(0)})$.

If the input to $H_1(\omega_1,\omega_2)$ and $H_2(\omega_1,\omega_2)$ are $x_1(n_1,n_2)$ and $x_2(n_1,n_2)$ respectively, then the outputs $y_1(n_1,n_2)$ and $y_2(n_1,n_2)$ should contain the spectral components at $(\omega_1^{(0)},\omega_2^{(0)})$ and minimize the effects of spectral components at other frequencies. Let the filter outputs be given by

$$y_1(n_1,n_2) = \left[\mathbf{a}_\alpha^{(1)}\right]^T \mathbf{x}_1 \tag{5 10}$$

And

$$y_2(n_1,n_2) = \left[\mathbf{a}_\alpha^{(2)}\right]^T \mathbf{x}_2 \tag{5.11}$$

where $\mathbf{x}_1$ and $\mathbf{x}_2$ are vectors of the signal values $\mathbf{x}_1(n_1-i_1,n_2-i_2)$ and $\mathbf{x}_2(n_1-i_1,n_2-i_2)$ for $(i_1,i_2)\varepsilon\alpha$ and $\mathbf{a}_\alpha^{(1)}$ and $\mathbf{a}_\alpha^{(2)}$ represent the filter coefficient vectors in the region of support α for the filters H_1 and H_2.

Capon (1969) has shown that the resulting filter coefficients for the $\mathbf{x}_1$ and $\mathbf{x}_2$ random processes can be written in the following form:

$$\mathbf{a}_\alpha^{(1)} = \frac{\left[\mathbf{R}_{11}^{-1}\,\mathbf{e}_\alpha\right]}{\left[\mathbf{e}_\alpha^{*T}\,\mathbf{R}_{11}^{-1}\,\mathbf{e}_\alpha\right]} \tag{5.12}$$

and

$$\mathbf{a}_\alpha^{(2)} = \frac{\left[\mathbf{R}_{22}^{-1}\,\mathbf{e}_\alpha\right]}{\left[\mathbf{e}_\alpha^{*T}\,\mathbf{R}_{22}^{-1}\,\mathbf{e}_\alpha\right]} \tag{5.13}$$

where $\mathbf{R}_{11}$ and $\mathbf{R}_{22}$ represent the correlation matrices of the two random processes $\mathbf{x}_1$ and $\mathbf{x}_2$, respectively, and $\mathbf{e}_\alpha$ is defined by Eqn. (5.5). Then the cross power estimate is taken to be

$$\begin{aligned} S_{12}(\omega_1,\omega_2;\alpha) &= E\left[y_1(n_1,n_2)\,y_2(n_1,n_2)\right] \\ &= \left[\mathbf{a}_\alpha^{(1)}\right]^T \mathbf{R}_{12}\,\mathbf{a}_\alpha^{(2)} \end{aligned} \tag{5.14}$$

where

$$\mathbf{R}_{12} = E\left[\mathbf{x}_1\,\mathbf{x}_2^T\right] \tag{5.15}$$

If Eqns. (5.12) and (5.13) are substituted in Eqn. (5.14), the cross spectrum power estimate can finally be written in the form

$$S_{12}(\omega_1,\omega_2;\alpha) = \frac{\mathbf{e}_\alpha^{*T}\,\mathbf{R}_{11}^{-1}\,\mathbf{R}_{12}\,\mathbf{R}_{22}^{-1}\,\mathbf{e}_\alpha}{\left[\mathbf{e}_\alpha^{*T}\,\mathbf{R}_{11}^{-1}\,\mathbf{e}_\alpha\right]\left[\mathbf{e}_\alpha^{*T}\,\mathbf{R}_{22}^{-1}\,\mathbf{e}_\alpha\right]} \tag{5.16}$$

This is the cross spectrum procedure.

D. DEVELOPMENT OF MULTICHANNEL 2-D MLM

In this section we describe a more general extension of the MLM spectral estimation procedure to the M-channel case. In this case the all components of the spectral matrix

$$\mathbf{S}_{ML}(\omega_1,\omega_2;\alpha) = \begin{bmatrix} S_{11}(\omega_1,\omega_2;\alpha) & S_{12}(\omega_1,\omega_2;\alpha) & \cdots & S_{1M}(\omega_1,\omega_2;\alpha) \\ S_{21}(\omega_1,\omega_2;\alpha) & S_{22}(\omega_1,\omega_2;\alpha) & \cdots & S_{2M}(\omega_1,\omega_2;\alpha) \\ \vdots & \vdots & & \vdots \\ S_{M1}(\omega_1,\omega_2;\alpha) & S_{M2}(\omega_1,\omega_2;\alpha) & \cdots & S_{MM}(\omega_1,\omega_2;\alpha) \end{bmatrix} \tag{5.17}$$

are computed at once.

Suppose we are given samples of a 2-D multichannel random process $\mathbf{x}(n_1,n_2)$ over some region of the plane. This signal is to be processed by a multichannel FIR narrowband filter to obtain an estimate of the power matrix at frequency $(\omega_1^{(0)},\omega_2^{(0)})$. The output $\mathbf{y}(n_1,n_2)$ of this filter is given by :

$$\mathbf{y}(n_1,n_2) = \sum_{(k_1,k_2)\in\alpha} \sum \mathbf{A}_{k_1,k_2}^T \mathbf{x}(n_1-k_1,n_2-k_2) \tag{5.18}$$

where α represents the region of support and $\mathbf{A}_{k_1,k_2}$ are $M\times M$ matrix coefficients. Assume that the input to the filter is a complex sinusoid given by

$$\mathbf{x}(n_1,n_2) = \mathbf{c}\, e^{j(\omega_1^{(0)}n_1 + \omega_2^{(0)}n_2)} \tag{5.19}$$

where $\mathbf{c}$ is constant. We want to choose the filter weights, $\mathbf{A}_{k_1,k_2}$, such that the filter passes the signal in each channel with zero phase and unit gain and there is no cross coupling. That is, we require

$$\mathbf{y}(n_1,n_2) = \mathbf{c}\, e^{j(\omega_1^{(0)}n_1 + \omega_2^{(0)}n_2)} \tag{5.20}$$

or equivalently that the frequency response $\mathbf{H}(\omega_1^{(0)},\omega_2^{(0)})$ satisfies

$$\mathbf{H}(\omega_1^{(0)},\omega_2^{(0)}) = \sum_{k_1,k_2\in\alpha} \sum \mathbf{A}_{k_1,k_2}\, e^{-j(\omega_1^{(0)}k_1 + \omega_2^{(0)}k_2)} = \mathbf{I} \tag{5.21}$$

where $\mathbf{I}$ is the $(M\times M)$ identity matrix. This constraint (Eqn. 5.21) can be expressed as

$$\mathbf{I} = \mathbf{E}_{\alpha}^{*T} \mathbf{A}_{\alpha} \tag{5.22}$$

where $\mathbf{E}_{\alpha}$ is the block matrix of complex sinusoids defined by the direct product

$$\mathbf{E}_{\alpha} = \mathbf{e}_{\alpha} \otimes \mathbf{I} \tag{5.23}$$

where

$$\mathbf{e}_{\alpha} = Col \left[e^{j(\omega_1 n_1 + \omega_2 n_2)} \right]_{(n_1, n_2) \in \alpha} \tag{5.24}$$

and $\mathbf{A}_{\alpha}$ represents the correspondingly-ordered block matrix of filter coefficients. The filter output power matrix is given by

$$\mathbf{P} = E\left[\mathbf{y}(n_1, n_2) \mathbf{y}^T(n_1, n_2) \right] = \mathbf{A}_{\alpha}^{*T} \mathbf{R}_{\alpha} \mathbf{A}_{\alpha} \tag{5.25}$$

where

$$\mathbf{R}_{\alpha} = E\left[\mathbf{x}_{\alpha} \mathbf{x}_{\alpha}^T \right] \tag{5.26}$$

and $\mathbf{x}_{\alpha}$ is the ordered vector of the given samples. The MLM spectral estimate is defined as the power matrix of the filter that minimizes (5.25) subject to the constraint (5.22).

The general solution to this problem which yields the optimal set of filter coefficients is

$$\mathbf{A}_{\alpha} = \left[\mathbf{R}_{\alpha}^{-1} \mathbf{E}_{\alpha} \right] \left[\mathbf{E}_{\alpha}^{*T} \mathbf{R}_{\alpha}^{-1} \mathbf{E}_{\alpha} \right]^{-1} \tag{5.27}$$

If this is substituted in Eqn. (5.25) the spectral estimate can be written as

$$\mathbf{S}_{ML}(\omega_1, \omega_2; \alpha) = \left[\mathbf{E}_{\alpha}^{*T} \mathbf{R}_{\alpha}^{-1} \mathbf{E}_{\alpha} \right]^{-1} \tag{5.28}$$

To show the specific form of this result for a particular case, suppose the filter has rectangular support of order (P_1, P_2). Then the matrix $\mathbf{A}_{\alpha}$ is defined by:

AD-A191 273 MULTICHANNEL 2-D POWER SPECTRAL ESTIMATION AND APPLICATIONS(U) NAVAL POSTGRADUATE SCHOOL MONTEREY CA H T EL-SHAER DEC 87 3/4

UNCLASSIFIED F/G 12/3 NL

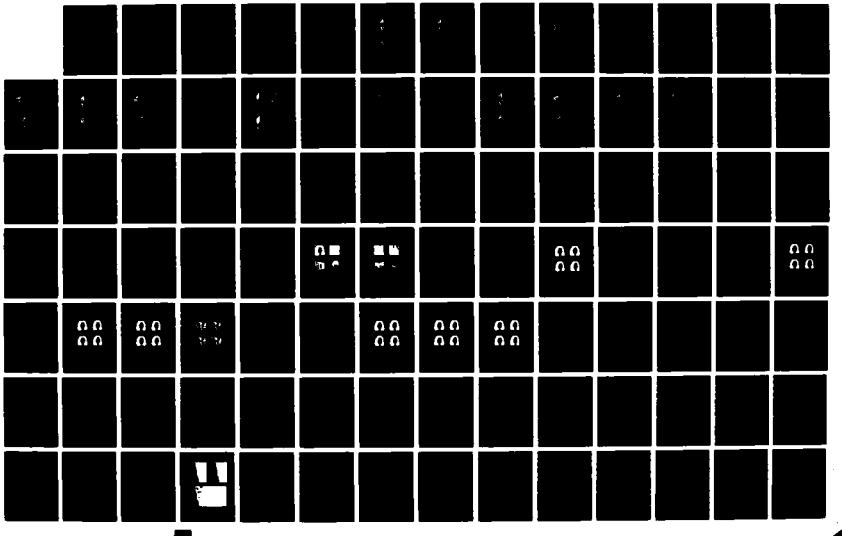

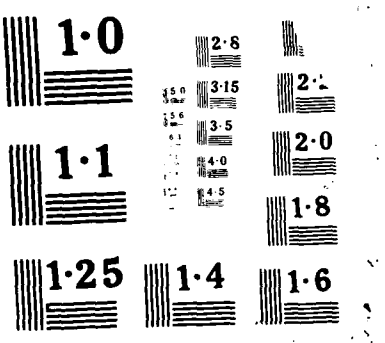
1·0
1·1
1·25
1·4
1·6
1·8
2·0
2·8
3·15
3·5
4·0
4·5

$$\mathbf{A}_\alpha = \begin{bmatrix} \mathbf{A}_0 \\ \mathbf{A}_1 \\ \cdot \\ \cdot \\ \cdot \\ \mathbf{A}_{P_1} \end{bmatrix} \tag{5.29}$$

where

$$\mathbf{A}_i = \begin{bmatrix} \mathbf{A}_{(i,0)} \\ \mathbf{A}_{(i,1)} \\ \cdot \\ \cdot \\ \cdot \\ \mathbf{A}_{(i,P_2)} \end{bmatrix} \tag{5.30}$$

and each submatrix $\mathbf{A}_{(i,j)}$ is given by

$$\mathbf{A}_{(i,j)} = \begin{bmatrix} a_{00}(i,j) & a_{01}(i,j) & \cdots & a_{0M}(i,j) \\ a_{10}(i,j) & a_{11}(i,j) & \cdots & a_{1M}(i,j) \\ \cdot & \cdot & & \cdot \\ \cdot & \cdot & & \cdot \\ \cdot & \cdot & & \cdot \\ a_{M0}(i,j) & a_{M1}(i,j) & \cdots & a_{MM}(i,j) \end{bmatrix} \tag{5.31}$$

The matrix of complex exponentials $\mathbf{E}_\alpha$ is now defined by the Kronecker product

$$\mathbf{E}_\alpha = (\mathbf{e}_2 \otimes \mathbf{e}_1) \otimes \mathbf{I} \tag{5.32}$$

where $\mathbf{e}_1$ and $\mathbf{e}_2$ are given by

$$\mathbf{e}_1 = \begin{bmatrix} e^{j0} \\ e^{j\omega_1} \\ e^{j2\omega_1} \\ . \\ . \\ . \\ e^{jP_1\omega_1} \end{bmatrix} \tag{5.33}$$

and

$$\mathbf{e}_2 = \begin{bmatrix} e^{j0} \\ e^{j\omega_2} \\ e^{j2\omega_2} \\ . \\ . \\ . \\ e^{jP_2\omega_2} \end{bmatrix} \tag{5.34}$$

Also the ordered vector $\mathbf{x}_\alpha$ given by Eqn. (5.26) can be written as

$$\mathbf{x}_\alpha = \begin{bmatrix} \mathbf{x}^1 \\ \mathbf{x}^2 \\ . \\ . \\ . \\ \mathbf{x}^{P_1} \end{bmatrix} \tag{5.35}$$

with

$$\mathbf{x}^p = \begin{bmatrix} \mathbf{x}(n_1-p, n_2) \\ \mathbf{x}(n_1-p, n_2-1) \\ . \\ . \\ . \\ \mathbf{x}(n_1-p, n_2-P_2) \end{bmatrix} \tag{5.36}$$

The matrix $\mathbf{R}_\alpha$ in this case has the specific form

$$\mathbf{R}_{\alpha} = \begin{bmatrix} \mathbf{R}(0) & \mathbf{R}(-1) & \cdots & \mathbf{R}(-P_1) \\ \mathbf{R}(1) & \mathbf{R}(0) & \cdots & \mathbf{R}(-P_1+1) \\ \cdot & \cdot & & \cdot \\ \cdot & \cdot & & \cdot \\ \cdot & \cdot & & \cdot \\ \mathbf{R}(P_1) & \mathbf{R}(P_1-1) & \cdots & \mathbf{R}(0) \end{bmatrix} \tag{5.37}$$

where

$$\mathbf{R}(k) = \begin{bmatrix} R(k,0) & R(k,-1) & \cdots & R(k,-P_2) \\ R(k,1) & R(k,0) & \cdots & R(k,-P_2+1) \\ \cdot & \cdot & & \cdot \\ \cdot & \cdot & & \cdot \\ \cdot & \cdot & & \cdot \\ R(k,P_2) & R(k,P_2-1) & \cdots & R(k,0) \end{bmatrix} \tag{5.38}$$

and each submatrix $\mathbf{R}(k,l)$ is the 2-D $(M \times M)$ matrix correlation function.

In order to check the performance of this technique, two different examples are considered here and the results are compared with the cross spectrum ML estimate given in the previous section.

In the first example, we compare the results of autospectrum estimation using the single channel MLM and the results of cross spectrum estimation between two 2-D data sets obtained by applying the cross spectrum procedure to the results of the multichannel MLM developed here. Two data records representing the two channels are given by

Channel (1):

$$x_1(n_1,n_2) = \sum_{i=1}^{L} \cos(n_1\omega_{i1} + n_2\omega_{i2}) + w_1(n_1,n_2) \tag{5.39a}$$

Channel (2) :

$$x_2(n_1,n_2) = \sum_{i=1}^{L} \cos(n_1\omega_{i3} + n_2\omega_{i4} + \phi_i) + w_2(n_1,n_2) \tag{5.39b}$$

where $w_1(n_1,n_2)$ and $w_2(n_1,n_2)$ are zero mean independent white noise signals and L represents the number of sinusoids. Spectrum estimation results are given for a dataset size of 64×64 and rectangular support with $P_1 = P_2 = 5$. We assume L=2, with

$\omega_{11}=\omega_{12}=\frac{\pi}{2}$, $\omega_{21}=\omega_{22}=\frac{\pi}{3}$, $\omega_{13}=\omega_{14}=\frac{\pi}{2}$, $\omega_{23}=\omega_{24}=\frac{\pi}{3}$, ϕ_1=1.5 radians, and ϕ_2=0.5 radians. Fig. 5.2 shows the autospectrum estimate of the first and second channels using the single channel MLM and Fig. 5.3 shows the autospectrum (S_{11},S_{22}) components of the spectral matrix from the multichannel MLM. Fig. 5.4 shows the cross spectrum estimation results, amplitude and phase, using the cross spectrum procedure while Fig. 5.5 shows the results of the cross spectrum component for the multichannel MLM. The estimated phase at the corresponding peaks for the cross spectrum method are $\phi_1 = 1.480$ radians, and $\phi_2 = 0.530$ radians while they are 1.481 and 0.529 radians in case of multichannel MLM respectively. The actual values are $\phi_1 = 1.5$ radians and $\phi_2 = 0.5$ radians. The results for this example as in others where the noise in the two channels is uncorrelated, were found to be very close.

In the second example we make two changes to the data. First the location of the sinusoids are move closer to each other ($\omega_{11}=\omega_{12}=\frac{\pi}{2}$, $\omega_{21}=\omega_{22}=\frac{2\pi}{5}$, $\omega_{13}=\omega_{14}=\frac{\pi}{2}$, and $\omega_{23}=\omega_{24}=\frac{2\pi}{5}$). Secondly the noise in the two channels was made highly correlated with covariance

$$\Sigma_w = \begin{bmatrix} 1 & 0.9 \\ 0.9 & 1 \end{bmatrix}$$

and zero mean.[2] Fig. 5.6 shows the cross spectrum estimation results using the cross spectrum procedure while Fig. 5.7 shows the S_{12} component using multichannel MLM. The peaks are resolved more sharply in Fig. 5.7 than in Fig. 5.6.

E. IMPROVED MLM POWER SPECTRAL ESTIMATION

The MLM has significantly poorer resolution than the AR method, but it is widely used in practice due to its relative simplicity. As stated earlier Lim and Dowla (1983) have proposed an improvement to the MLM method based on the relation that exists between the MLM and AR spectrum estimation methods (Dowla and Lim,1984). Their

---

Observe that the noise is still "white" noise since it is spatially uncorrelated.

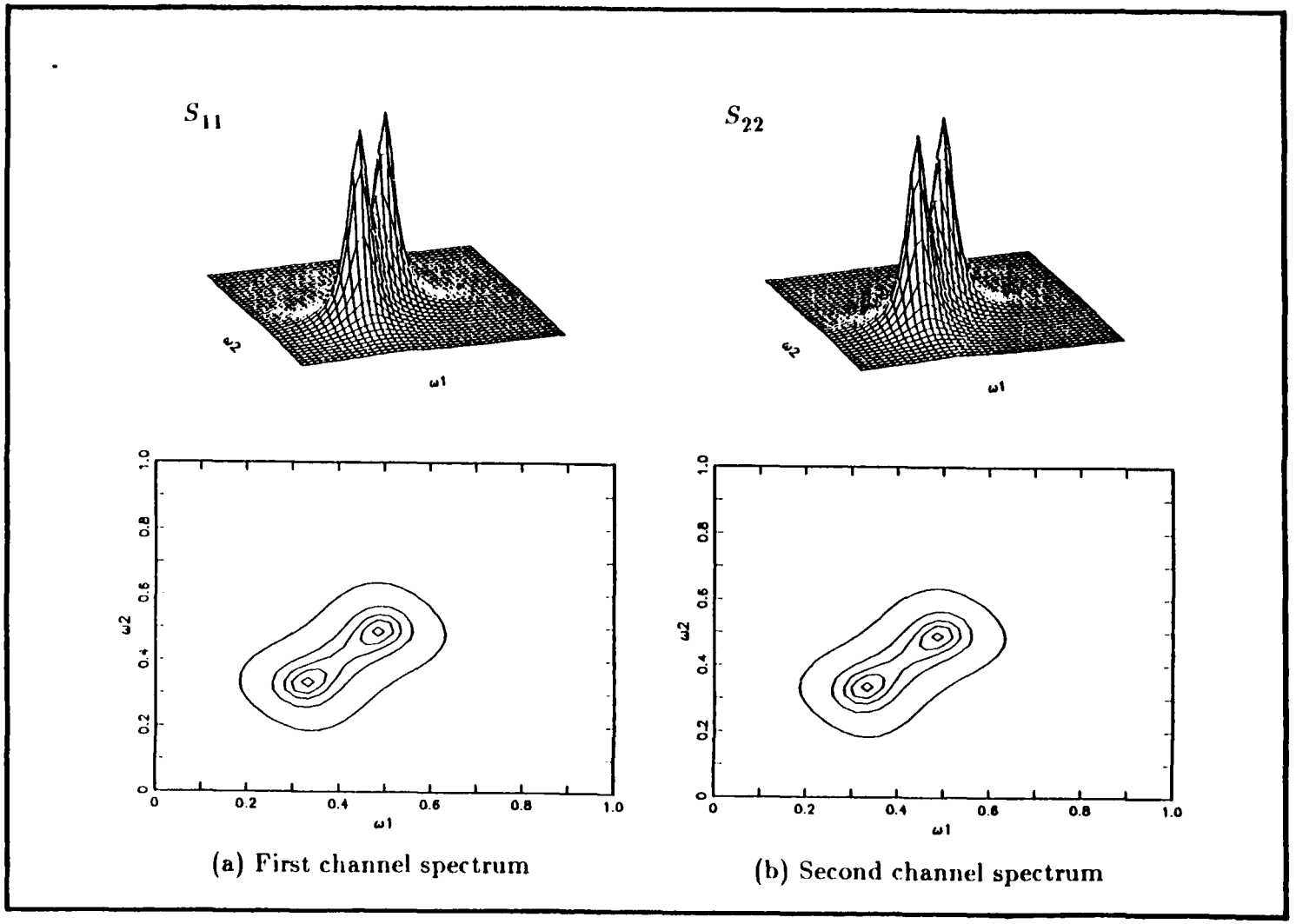

(a) First channel spectrum

(b) Second channel spectrum

Fig. 5.2 Autospectrum estimation (cross spectrum procedure).

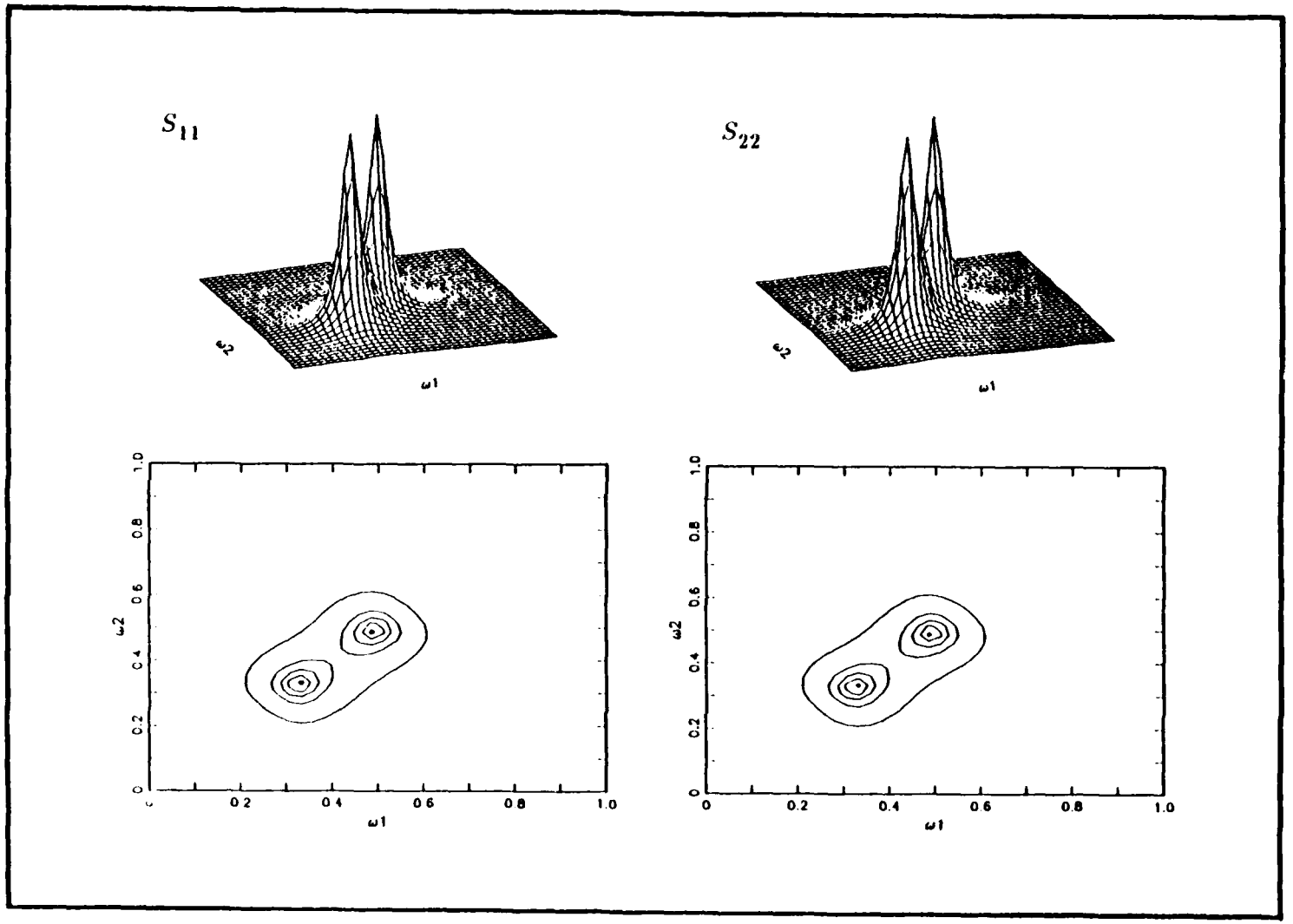

Fig. 5.3 Autospectrum components of the spectral matrix (multichannel MLM).

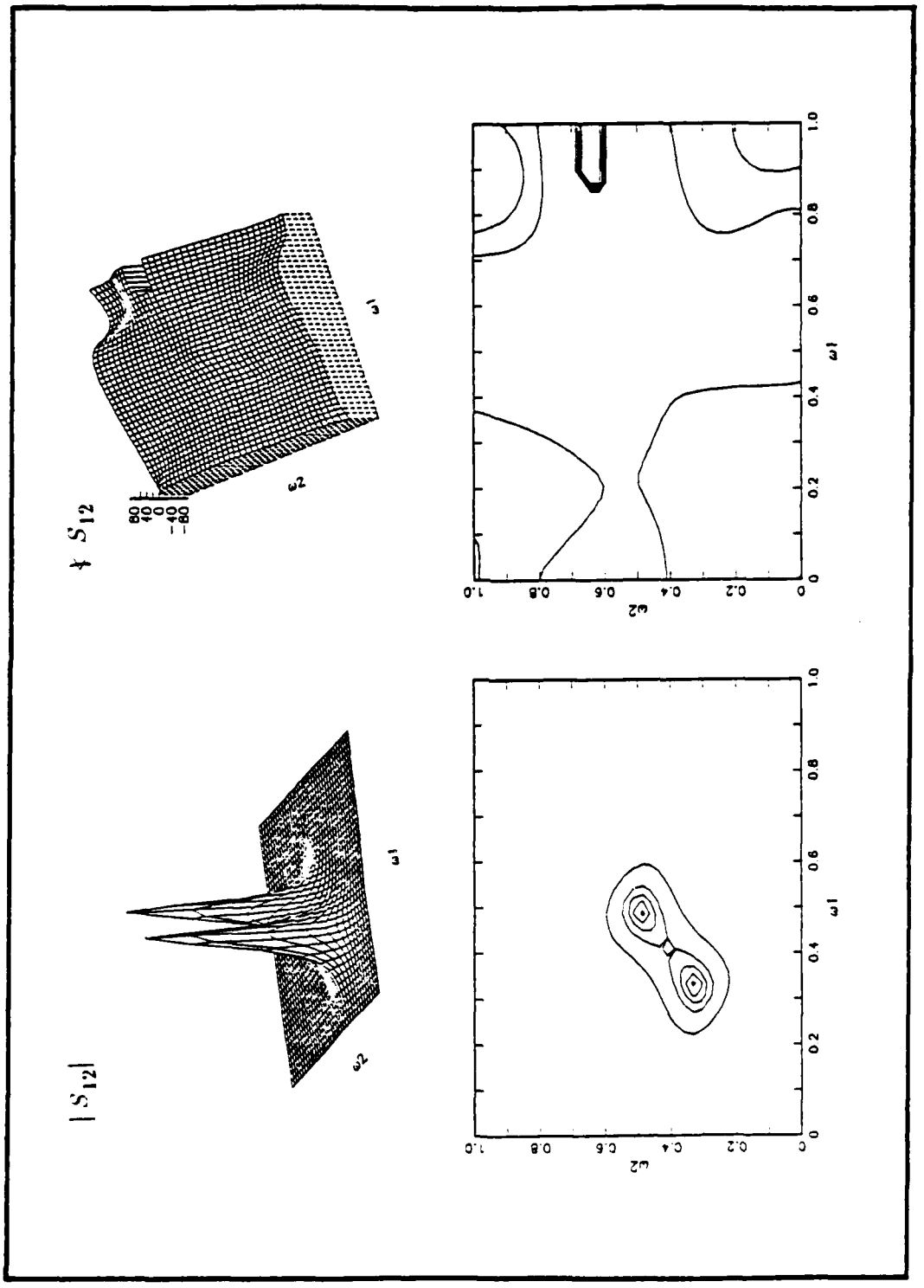

Fig. 5.4 Cross spectrum estimation (cross spectrum procedure).

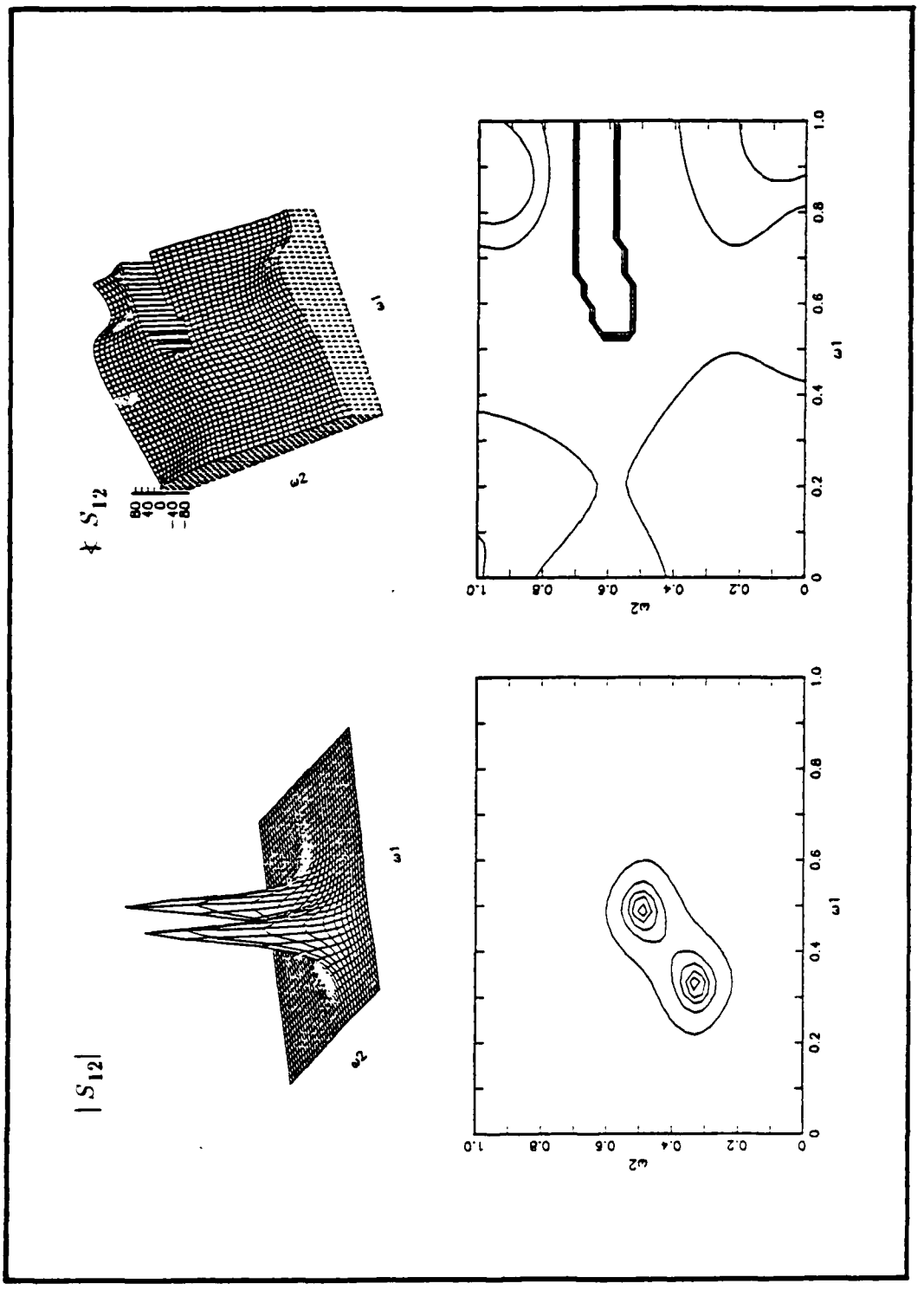

Fig. 5.5 Cross spectrum estimation (multichannel MLM).

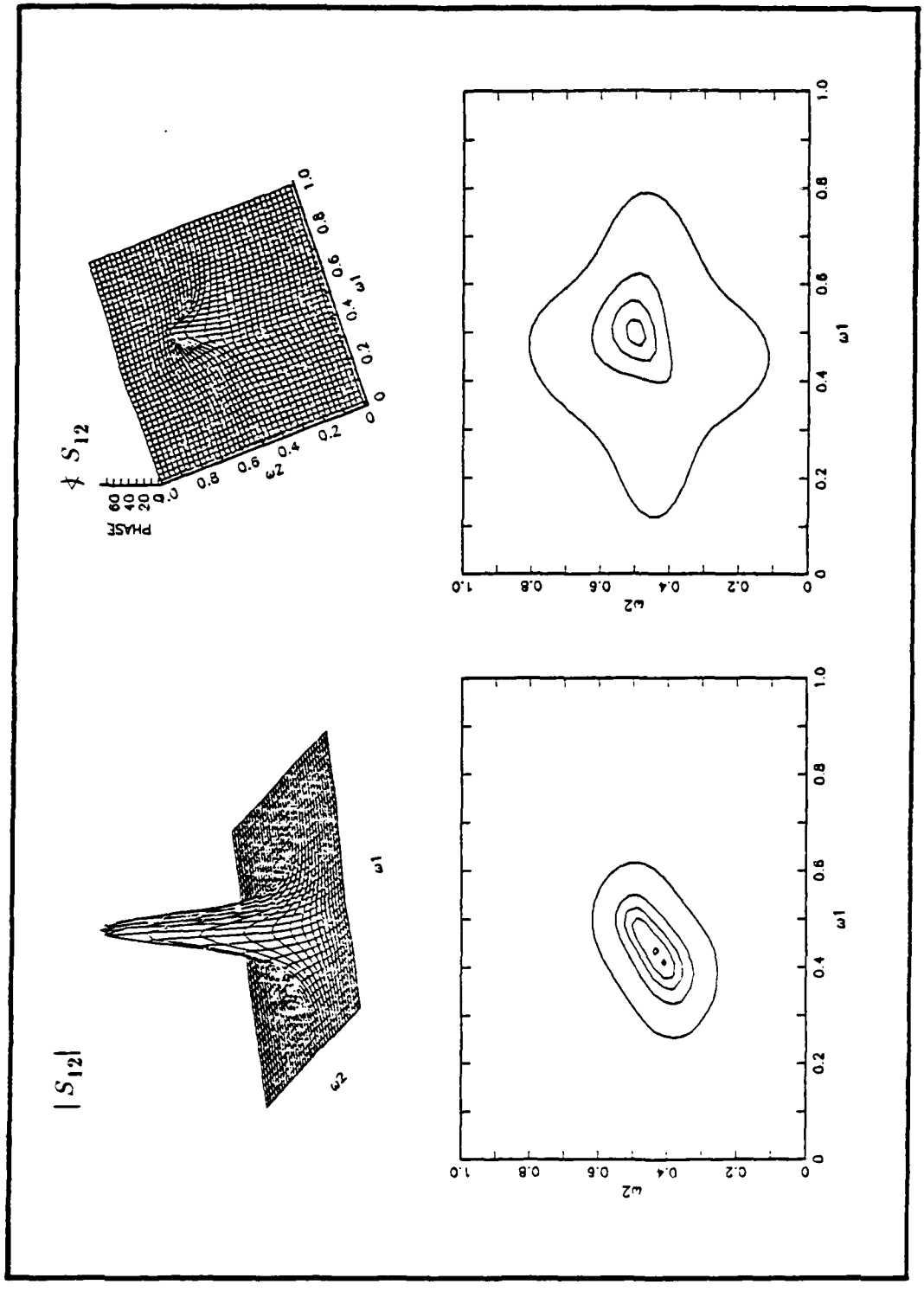

Fig. 5.6 Cross spectrum estimation of two sinusoids (cross spectrum procedure).

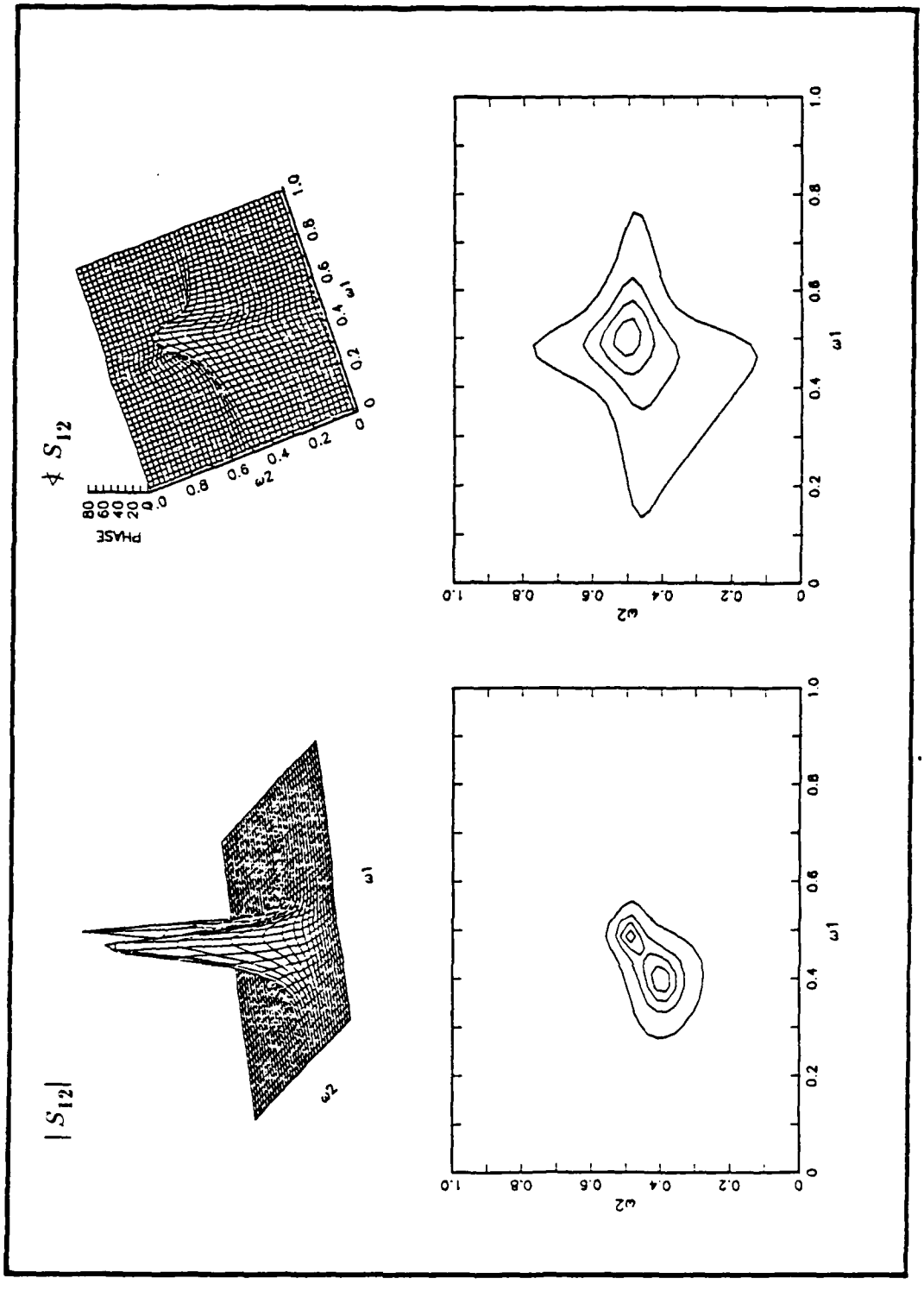

Fig. 5.7 Cross spectrum estimation of two sinusoids (multichannel MLM).

idea can be applied to our procedure for estimation of the multichannel 2-D spectral matrix.

Let the points in the region α be divided into two subsets β and $\alpha-\beta$. Then the "improved" maximum likelihood method (IMLM) for spectral matrix estimation is defined by

$$\mathbf{S}_{IML}(\omega_1,\omega_2;\alpha,\beta) = \left[\mathbf{S}_{ML}^{-1}(\omega_1,\omega_2;\alpha) - \mathbf{S}_{ML}^{-1}(\omega_1,\omega_2;\beta)\right]^{-1} \tag{5.40}$$

where $\mathbf{S}_{ML}(\omega_1,\omega_2;\alpha)$ represents the 2-D multichannel MLM spectral estimate based on all the known correlation points in the region α (see Eqn. (5.28)), and $\mathbf{S}_{ML}(\omega_1,\omega_2;\beta)$ is the ML spectral matrix estimates using support region β

$$\mathbf{S}_{ML}(\omega_1,\omega_2;\beta) = \left[\mathbf{E}_\beta^{*T}.\mathbf{R}_\beta^{-1}.\mathbf{E}_\beta\right]^{-1} \tag{5.41}$$

The IMLM of Lim and Dowla has demonstrated higher resolution properties than the MLM for single channel 2-D data. This property will be seen to carry over to the estimation of the entire spectral matrix using (5.40). Three different examples are considered here.

1. **Example 1**

In this example we carried out an experiment to compare the autospectra and the amplitude and phase of cross spectra of the MLM and IMLM techniques. In the two methods we considered a 2-D two-channel real process $\mathbf{x}(n_1,n_2)$ consisting of sinusoids buried in white noise. The two data records which represent the two channels are given by Eqn. (5.39) with the same parameters cited following that equation. The results are given for $P_1=P_2=4$. Fig. 5.8 shows the auto- and cross spectra results of the MLM method. Fig. 5.9 shows the results of IMLM. This example shows the higher resolution properties of the IMLM relative to the MLM. The values of the phase of the cross spectra, at the peak locations for each of the two techniques, are close to each other and very close to the actual values.

We have considered many similar examples with different choices of the model order and the peak positions. In all cases, we observed that IMLM provides significantly better resolution than MLM.

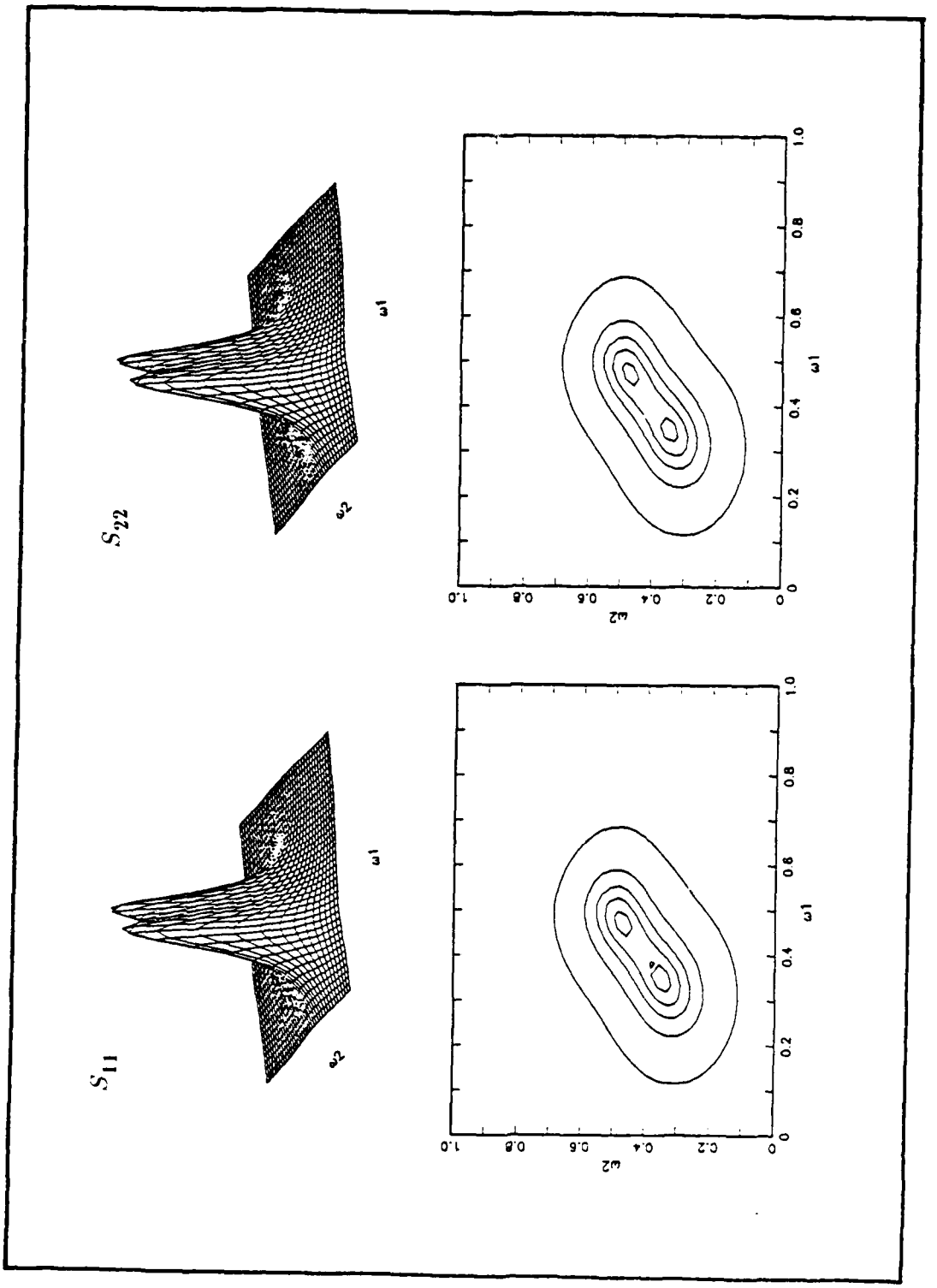

Fig. 5.8 Estimation of two sinusoids (MLM).

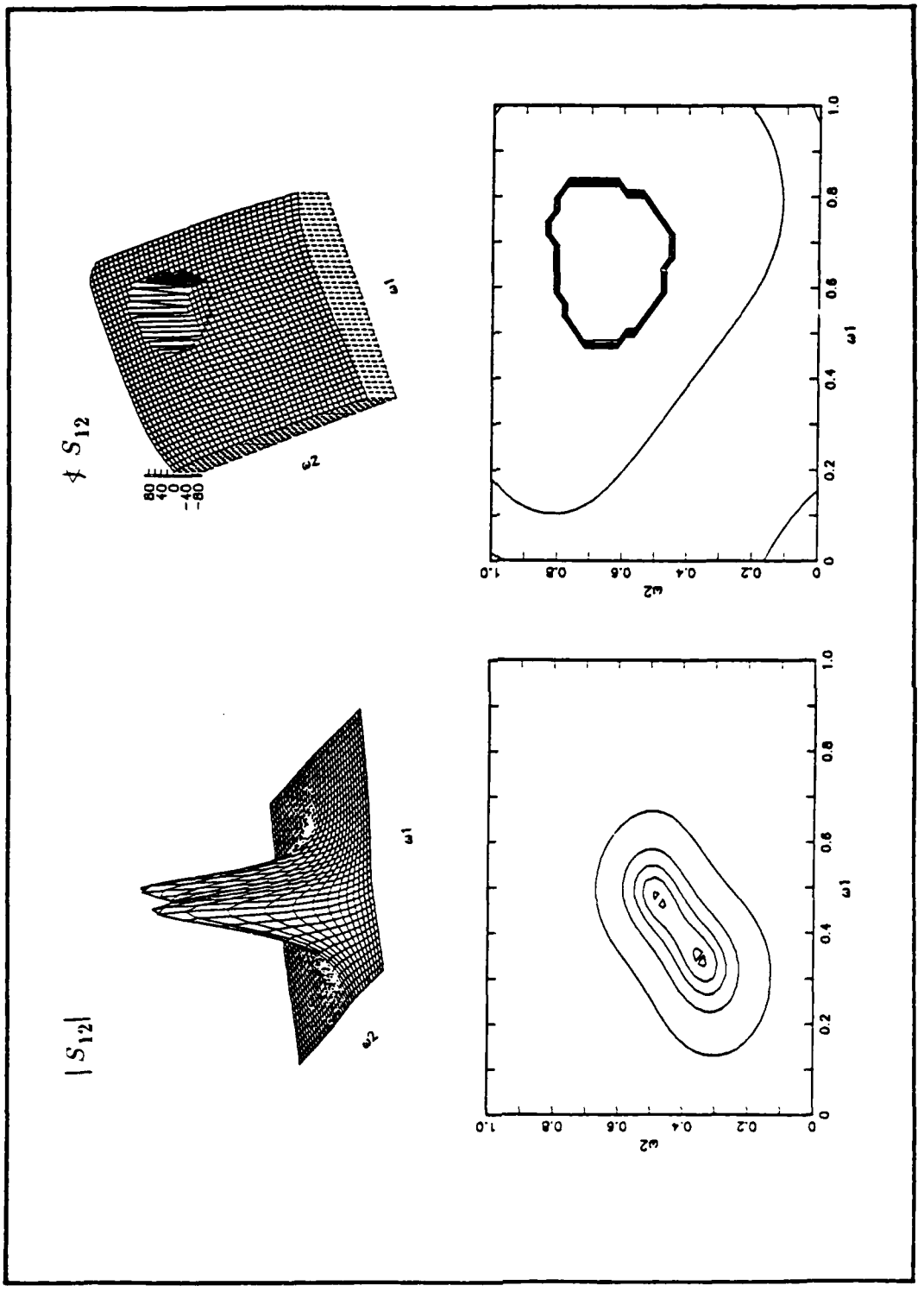

Fig. 5.8 Estimation of two sinusoids (MLM). (cont'd)

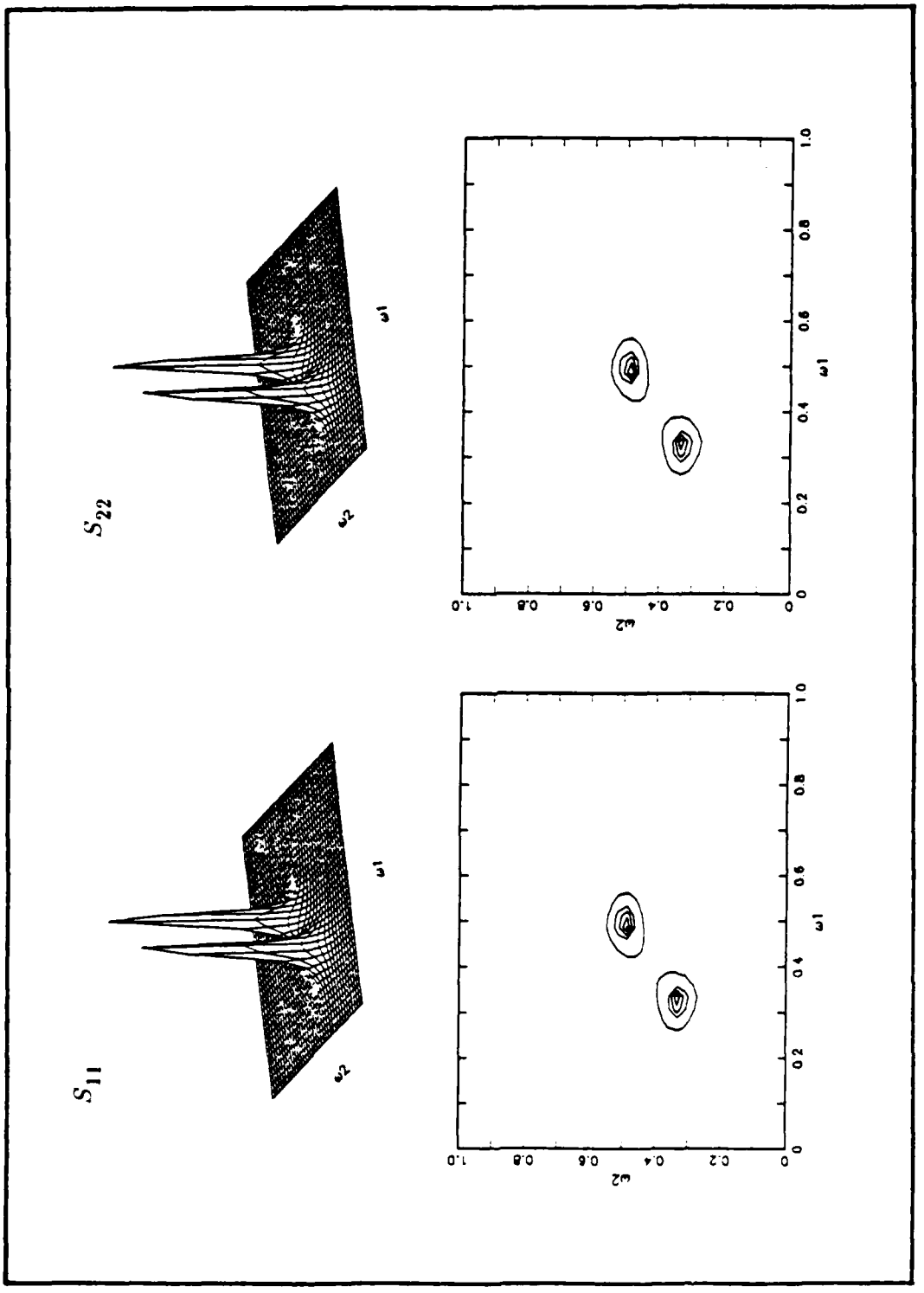

Fig. 5.9 Estimation of two sinusoids (IMLM).

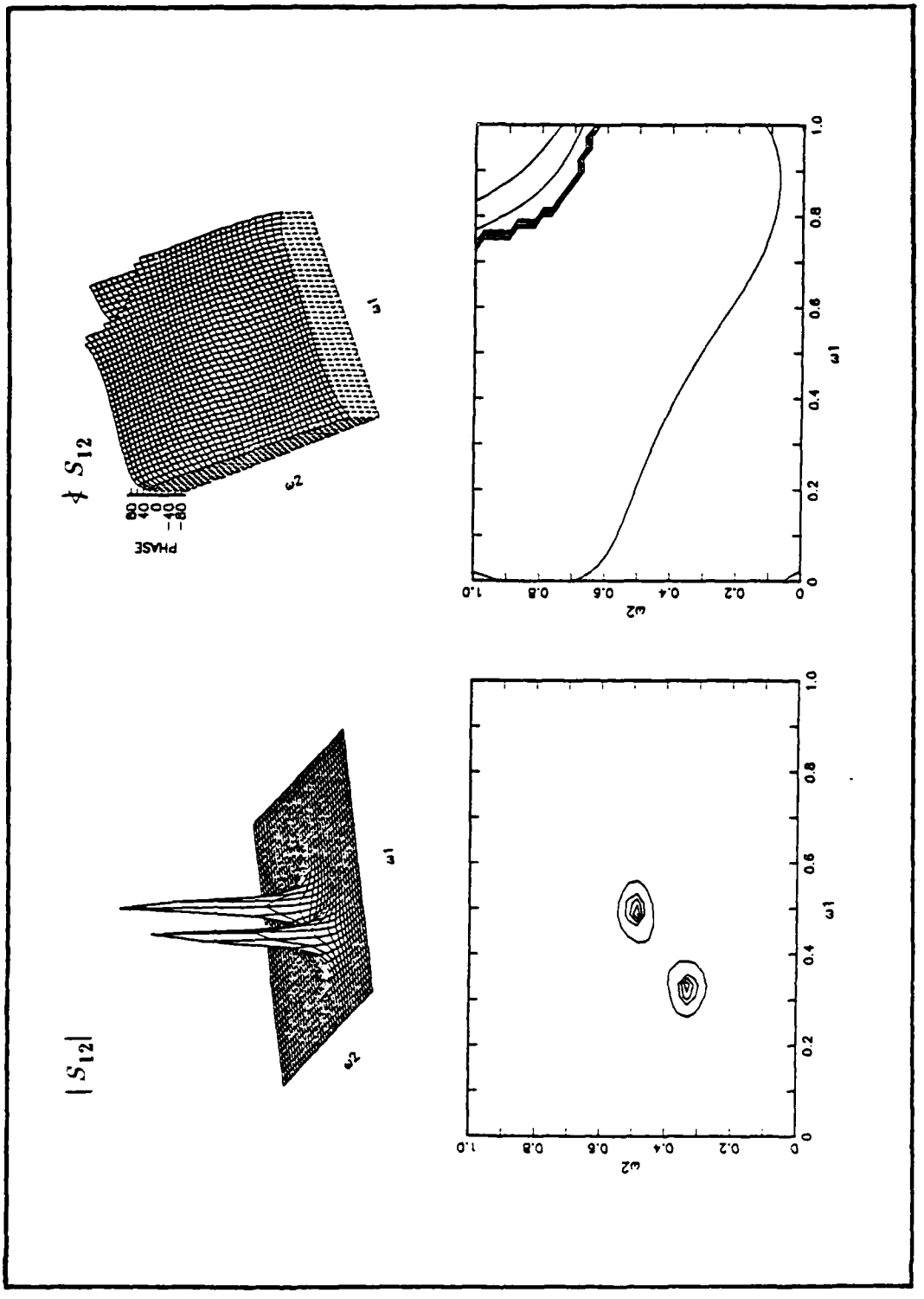

Fig. 5.9 Estimation of two sinusoids (IMLM). (cont'd)

2. Example 2

The main purpose of this experiment is to identify an unknown system $H(\omega_1,\omega_2)$ by applying multichannel 2-D MLM and IMLM techniques. In this example the first channel is a zero mean white noise, while the second channel is the output of the unknown 2-D system which is driven by the noise in the first channel. We consider here the specific example given by Eqn. (4.28) with the same parameters.

Fig. 5.10a shows the amplitude and phase of the estimated frequency response applying the IMLM technique while Fig. 5.10b shows the results using the MLM technique. The two results are similar to each other in this specific example. However comparing these results with the true frequency response given in Fig. 4.27a we find that the IMLM results are closer to the true results than the MLM.

3. Example 3

The third test example is concerned with estimation of a 2-D linear phase. The signal in the first channel consists of white noise, and the signal in the second channel is a delayed version of the first channel. The specific example shown here is given by Eqn. (4.24) with the same parameters.

In this experiment the delay between the two channels was measured by estimating the phase of the cross spectrum. The results of the spectral matrix components of the MLM and the IMLM are shown in Figs. 5.11 and 5.12 respectively. The results were found to be very close to each other. The autospectra and magnitude of cross spectra are constants. The phase of the cross spectrum is linear with slope corresponding to $d_1=d_2=1$ as we expect.

F. NUMERICAL EXAMPLE AND COMPARISON RESULTS

In order to compare the resolution and phase estimation characteristics of the AR, MLM and IMLM, we carried out additional experiments to compare the autospectra and the amplitude and phase of cross spectra of the three techniques. In all three methods, we assumed a 2-D two channel random process with the data for each channel consisting of sinusoids buried in white noise. We assumed three sinusoids with the position of the peaks as shown in Fig. 4.13 and with the same parameters.

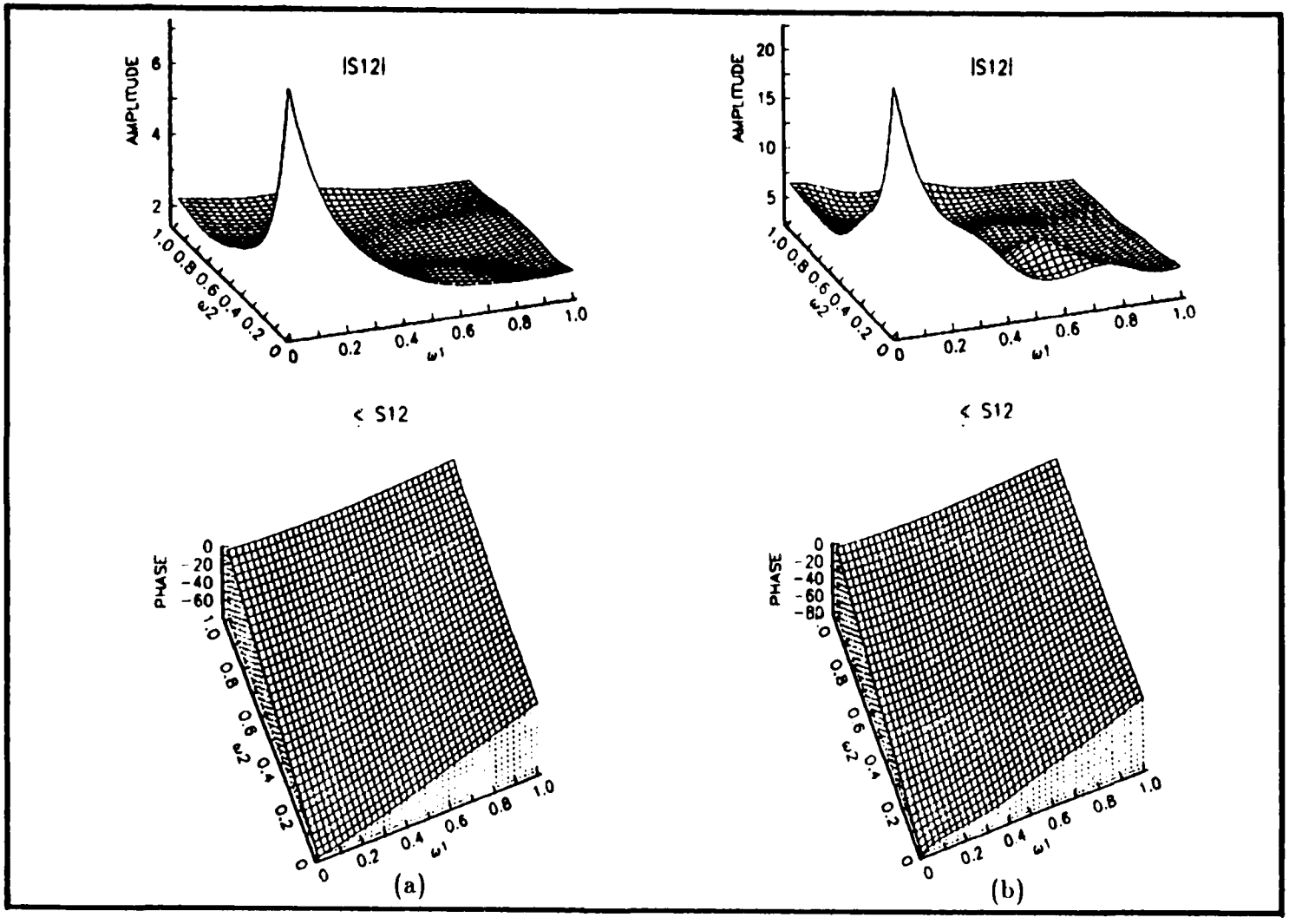

Fig. 5.10 System identification experiment results (MLM & IMLM).
(a) Estimated frequency response using IMLM technique.
(b) Estimated frequency response using MLM technique.

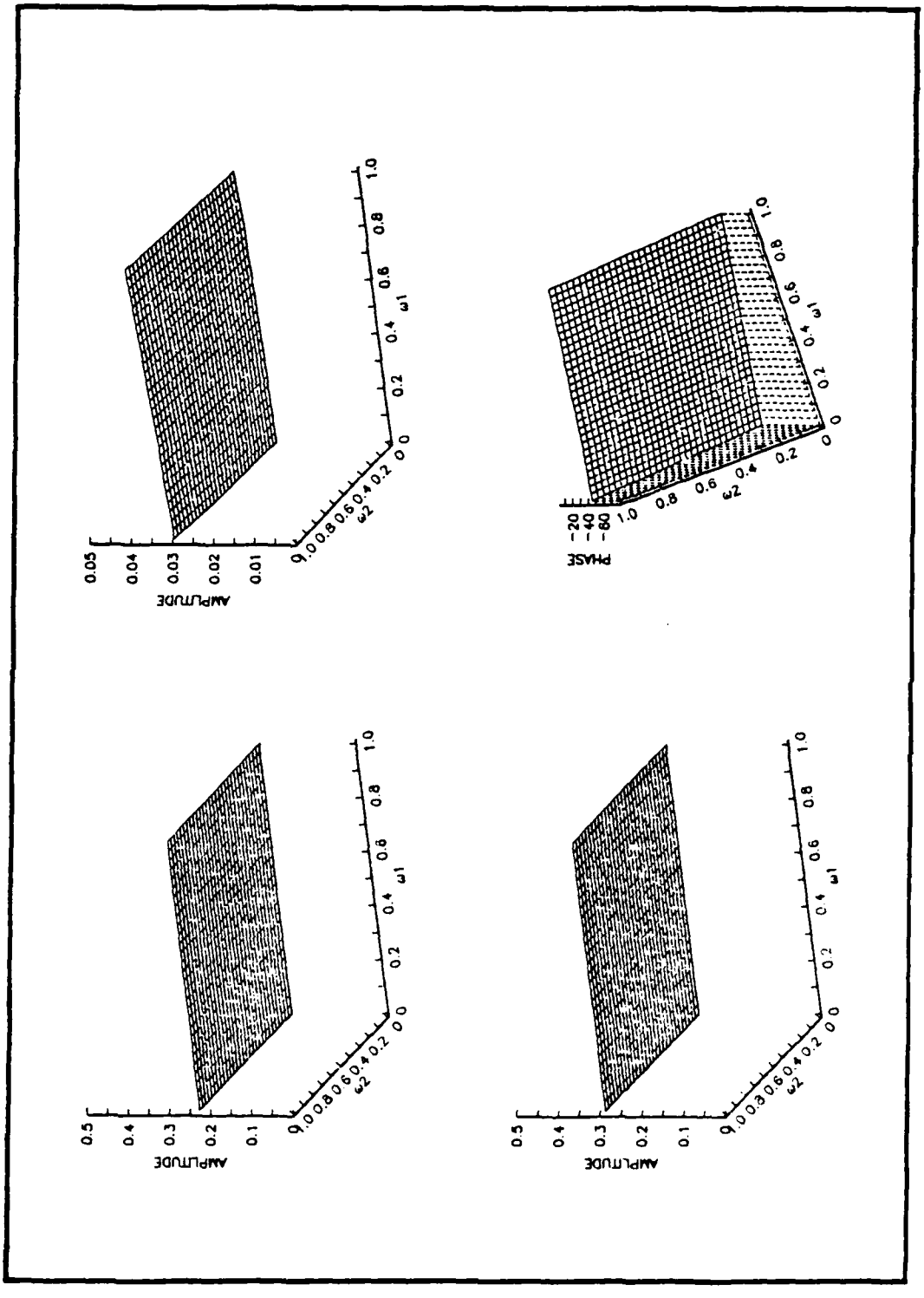

Fig. 5.11 Linear phase estimation using MLM.

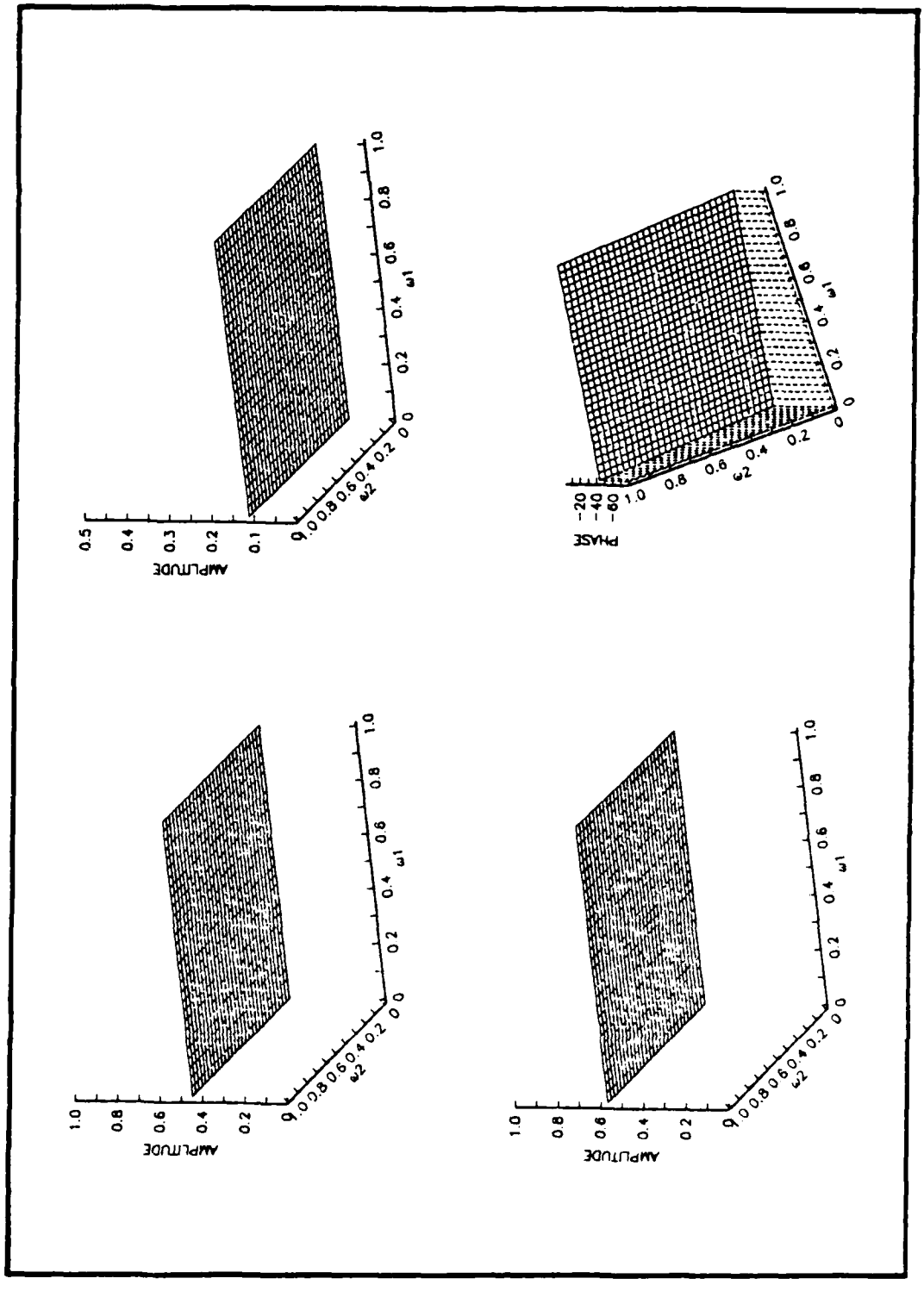

Fig. 5.12 Linear phase estimation using IMLM.

Fig. 5.13 shows the auto and cross spectra results of the MLM method. Fig. 5.14 shows the results of IMLM. The dataset size is (64×64) for each channel and the order of the model is four. The results can be compared to those obtained in Chapter IV, (see Fig. 4.14). Such a comparison results shows the high resolution properties of the AR relative to the MLM. It also shows that IMLM has resolution superior to the MLM, and that it is very close to that of the AR. The values of the phase estimate of the cross spectra, for each of the three techniques, are close to each other and very close to the actual values.

We have considered many different variations of this example with different choices of the model order, number of sinusoids and peak positions. The results show a consistently higher resolution for AR and IMLM than for MLM.

In the remaining part of this section we measure and compare the resolution properties of the three methods quantitatively. The resolution properties are studied both as a function of the signal to noise ratio (SNR) and as a function of the order of the model.

For the following studies, a two channel 2-D random process is again used. Each channel has two sinusoids buried in white noise in the form of Eqn. (5.39). The criterion for resolution, as defined before in Chapter IV, is the minimum frequency separation above which two sinusoids are not resolved. Sinusoids are considered to be resolved if there are two peaks in the spectrum with a valley between them. The smaller the value of the separation, the better the resolution.

The experimental procedure is as follows. The location of one sinusoid is kept constant, then the position of the peak of second sinusoid is changed slightly. Starting with the frequency of the second sinusoid very close to the first, we find the spectrum of the two sinusoids. If the two peaks appear as one peak we move the second sinusoid slightly away from the first one and recomput the spectrum. We repeat this procedure until we obtain a valley between the two peaks.

1. Effect of Model Order on Resolution

In order to compare the resolution characteristics of the NSHP, MLM, and IMLM quantitatively, the SNR is kept constant, SNR = 0 dB, and the model order is changed. Fig. 5.15 summarizes the cross spectrum resolution performance of the three methods as a function of the order of the model. As shown in the figure, the resolution increases with increasing model order. The NSHP AR model method has the highest

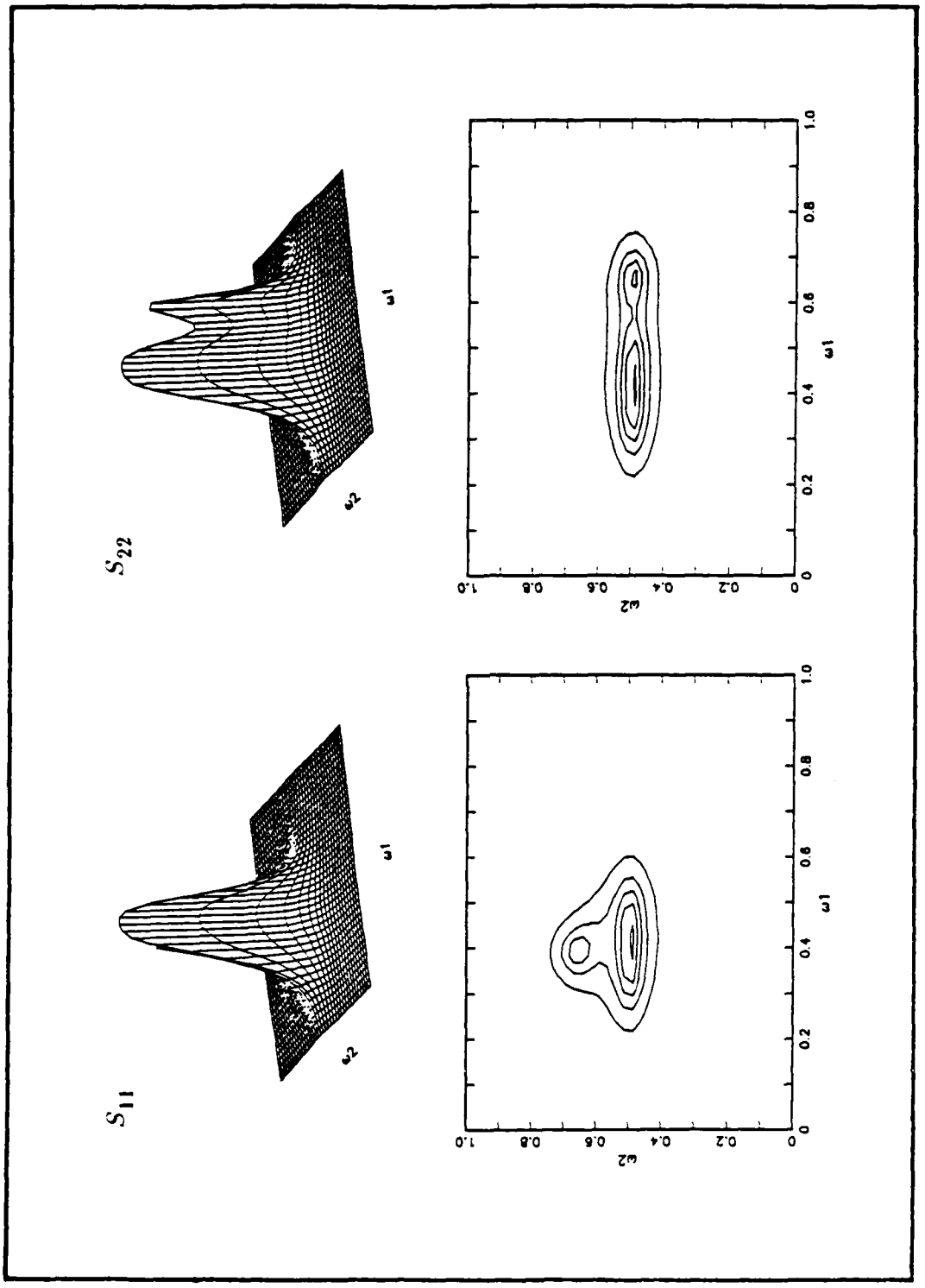

Fig. 5.13 Estimation of three sinusoids (MLM).

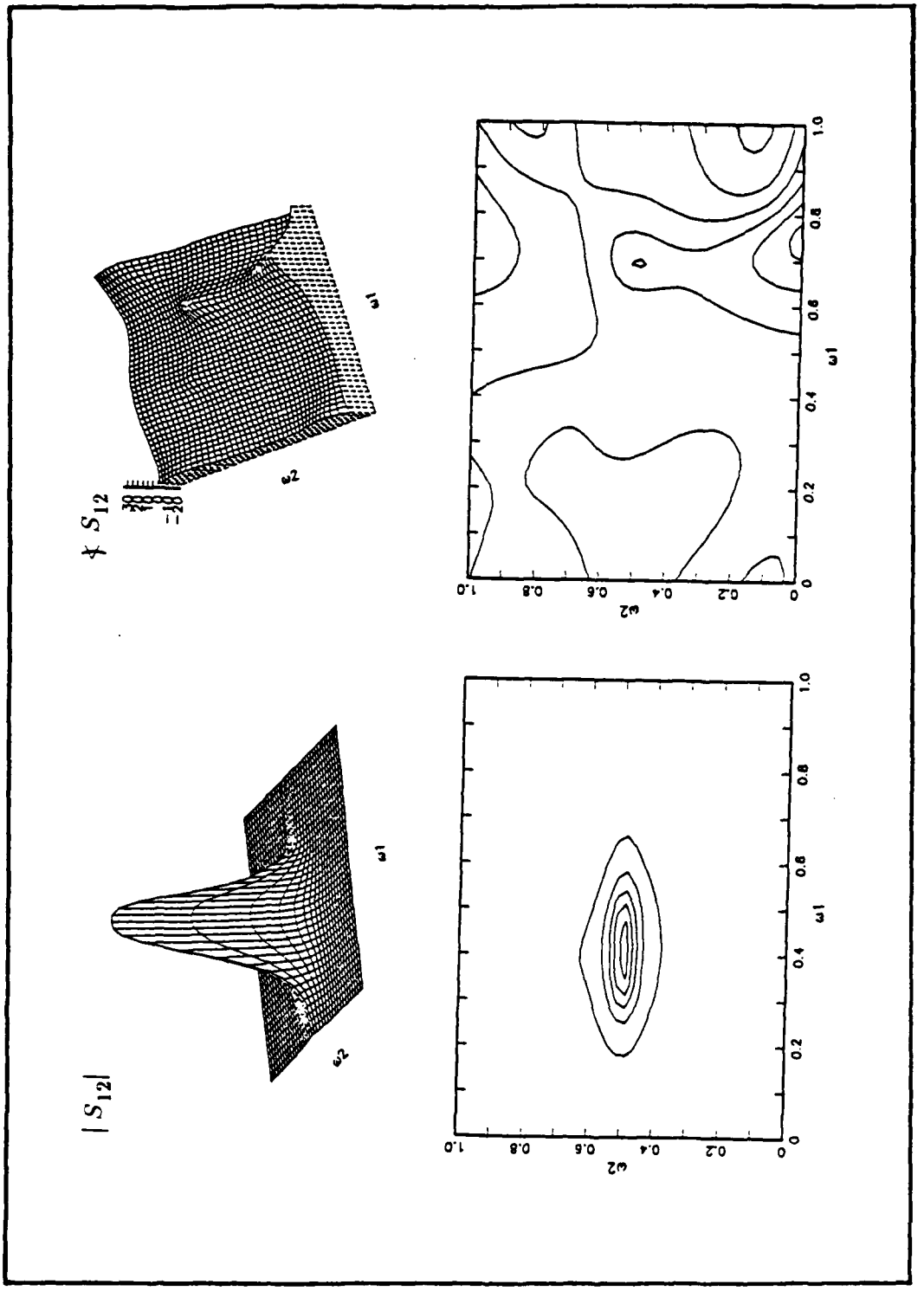

Fig. 5.13 Estimation of three sinusoids (MLM). (cont'd)

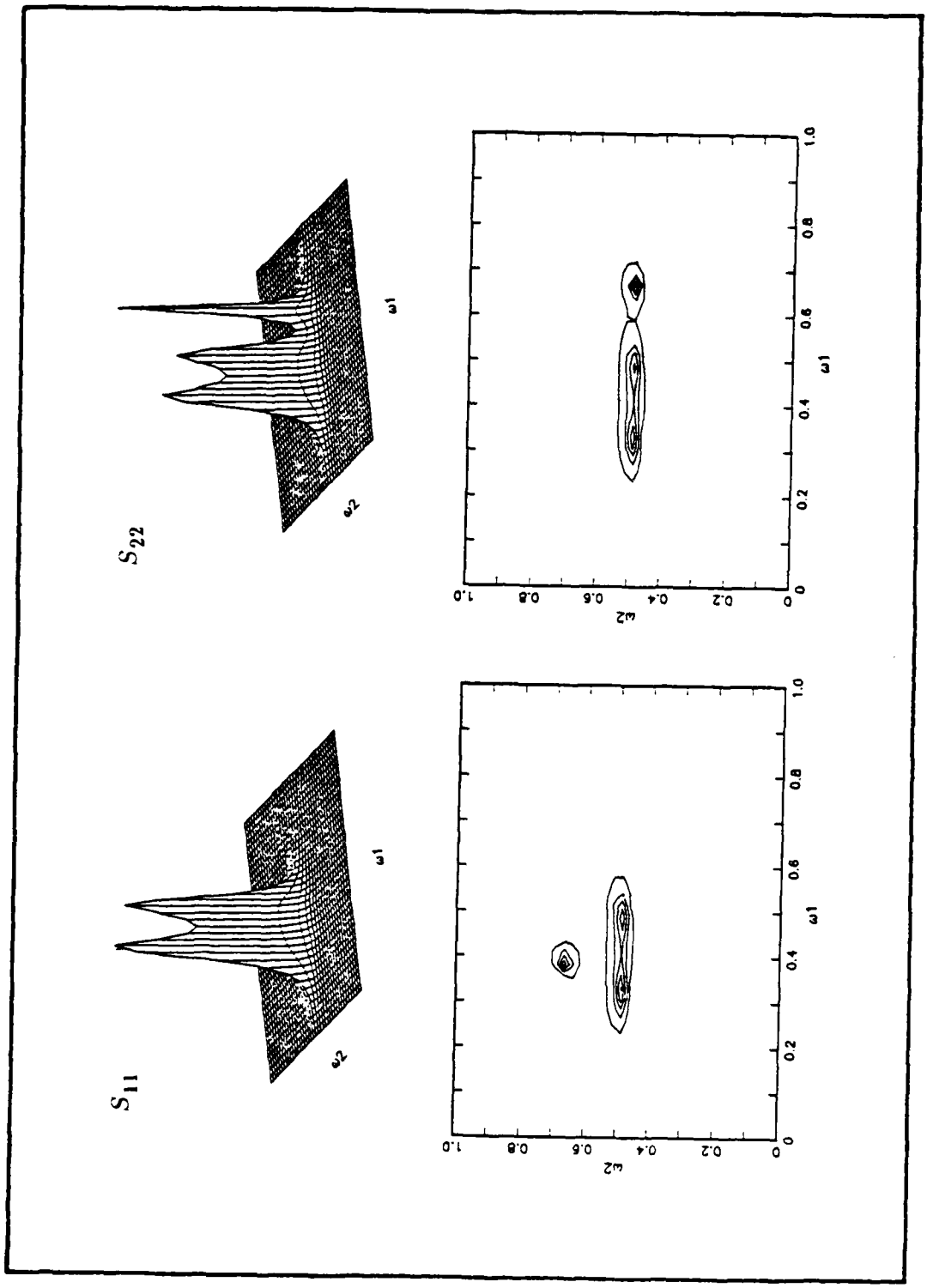

Fig. 5.14 Estimation of three sinusoids (IMLM).

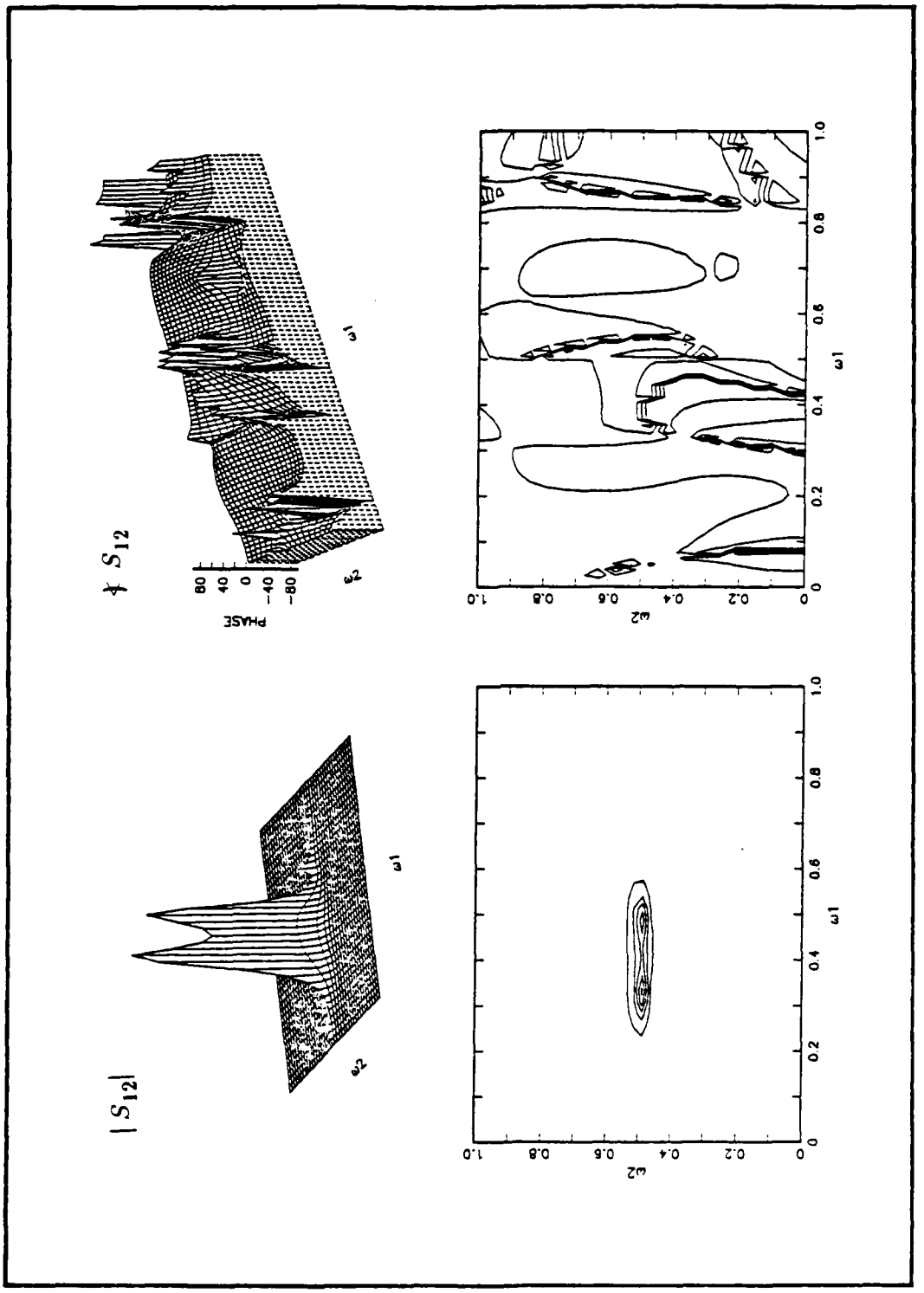

Fig. 5.14 Estimation of three sinusoids (IMLM). (cont'd)

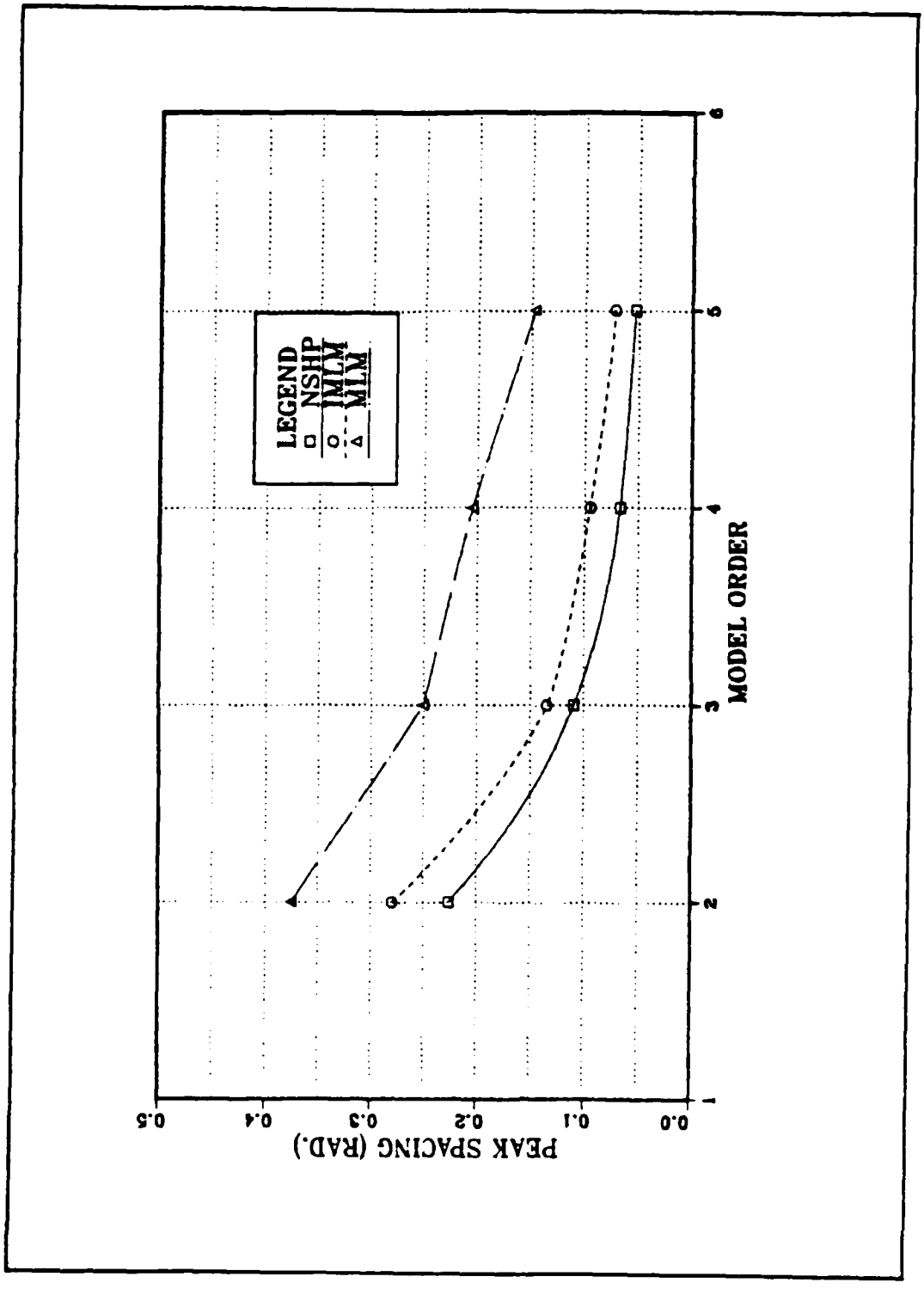

Fig. 5.15 Effect of model order on resolution.

resolution, while the MLM has the poorest resolution. The resolution of the IMLM is close to that of the NSHP.

Table 5.1 shows the phase estimate of the cross spectrum. It is clear from the table that, all three methods produce good phase estimates that are close to the true values.

2. Effect of SNR on Resolution

The experiment just described was carried out again except that this time the model order was kept constant (equal to 3) and the SNR was changed. Fig. 5.16 summarizes the cross spectrum resolution performance of the NSHP, IMLM, and MLM estimates as a function of the SNR. The results show clearly that IMLM has a resolution which is much better than the MLM and quite close to but not as good as the NSHP AR method.

The phase estimation results for the cross spectrum are shown in Table 5.2 . We have a good phase estimate for SNRs greater than -6 dB, and a poor estimate for SNRs less than -6 dB.

TABLE 5.1 CROSS SPECTRUM PHASE ESTIMATION AS A FUNCTION OF MODEL ORDER

(a) The estimated values of ϕ_1

Phase Estimation (ϕ_1)				
Method	Model Order			
	2	3	4	5
NSHP	1.464	1.478	1.476	1.520
MLM	1.450	1.452	1.456	1.467
IMLM	1.543	1.456	1.433	1.426

(b) The estimated values of ϕ_2

Phase Estimation (ϕ_2)				
Method	Model Order			
	2	3	4	5
NSHP	0.554	0.554	0.518	0.524
MLM	0.513	0.558	0.508	0.477
IMLM	0.550	0.521	0.490	0.533

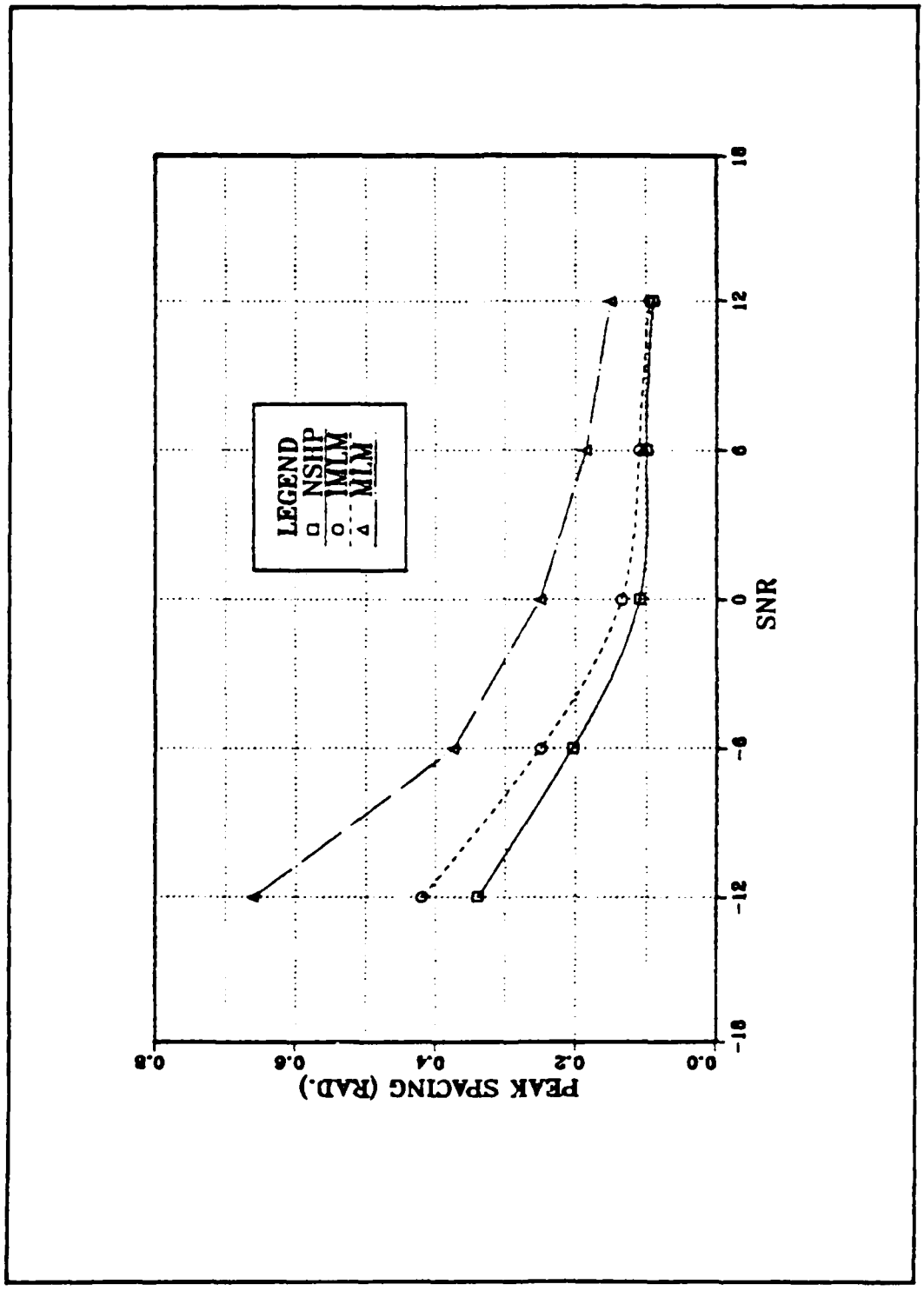

Fig. 5.16 Effect of SNR on resolution.

TABLE 5.2 SNR EFFECT ON THE ESTIMATED PHASE

(a) ϕ_1 Estimation

Phase Estimation (ϕ_1)					
Method	SNR (dB)				
	-12	-6	0	6	12
NSHP	1.250	1.409	1.478	1.480	1.489
MLM	1.412	1.435	1.452	1.472	1.436
IMLM	1.332	1.455	1.456	1.452	1.498

(b) ϕ_2 Estimation

Phase Estimation (ϕ_2)					
Method	SNR (dB)				
	-12	-6	0	6	12
NSHP	0.493	0.462	0.518	0.510	0.514
MLM	0.496	0.478	0.557	0.510	0.530
IMLM	0.402	0.510	0.521	0.491	0.485

VI. APPLICATIONS OF SPECTRAL ANALYSIS MODELS TO IMAGE CODING

A. INTRODUCTION

Image coding is a fairly new subject which has been practiced over the last 15 years. Many efforts have been made towards the implementation of digital image coding. Image coding applications can be found in television and facsimile transmission of printed materials and in the continuous source of weather photographs and earth resource pictures sent to earth by satellites. In addition applications can be found in the military field in areas such as the control of remotely piloted vehicles.

Efficient coding for these application can provide a substantial decrease in the transmission costs. As an example, broadcast digitized television signals need about 100 Mb/s which is a very high data rate. Efficient coding can bring this requirement down to a few hundred kb/s. The main purpose of coding therefore, is to decrease the transmitted bit rate, but to maintain a certain acceptable level of fidelity (Pratt,1978; Gibson,1980; Goodman and Gersho,1974; Jain,1981; Maragos et al,1984; Netravali and Limb,1980; Jayant,1974,1976; Jayant and Noll,1984; Zetterberg,1982; Makhoul,1975; Linde et al,1980; Gray,1982; Gray and Linde,1984; Cuperman,1985; Hang and Woods,1985; Goldberg,1986). The required image quality and intelligibility vary widely depending on the application. For example, in remotely piloted vehicle applications, the image intelligibility is more important than the quality, while in applications such as digital television, high quality is essential.

An overall image coding and transmission scheme is shown in Fig. 6.1. The digital image is encoded by an image coder. The output of the image coder is a sequence of bits which represents the source image. The channel coder transforms this sequence of bits to a form suitable for transmission over a communication channel by using the modulator which maps the code outputs 1 and 0 into analog signals. The demodulator at the receiving side uses an appropriate decision threshold to interpret received signals as corresponding to either 1 or 0. The image decoder reconstructs the image from this sequence of bits.

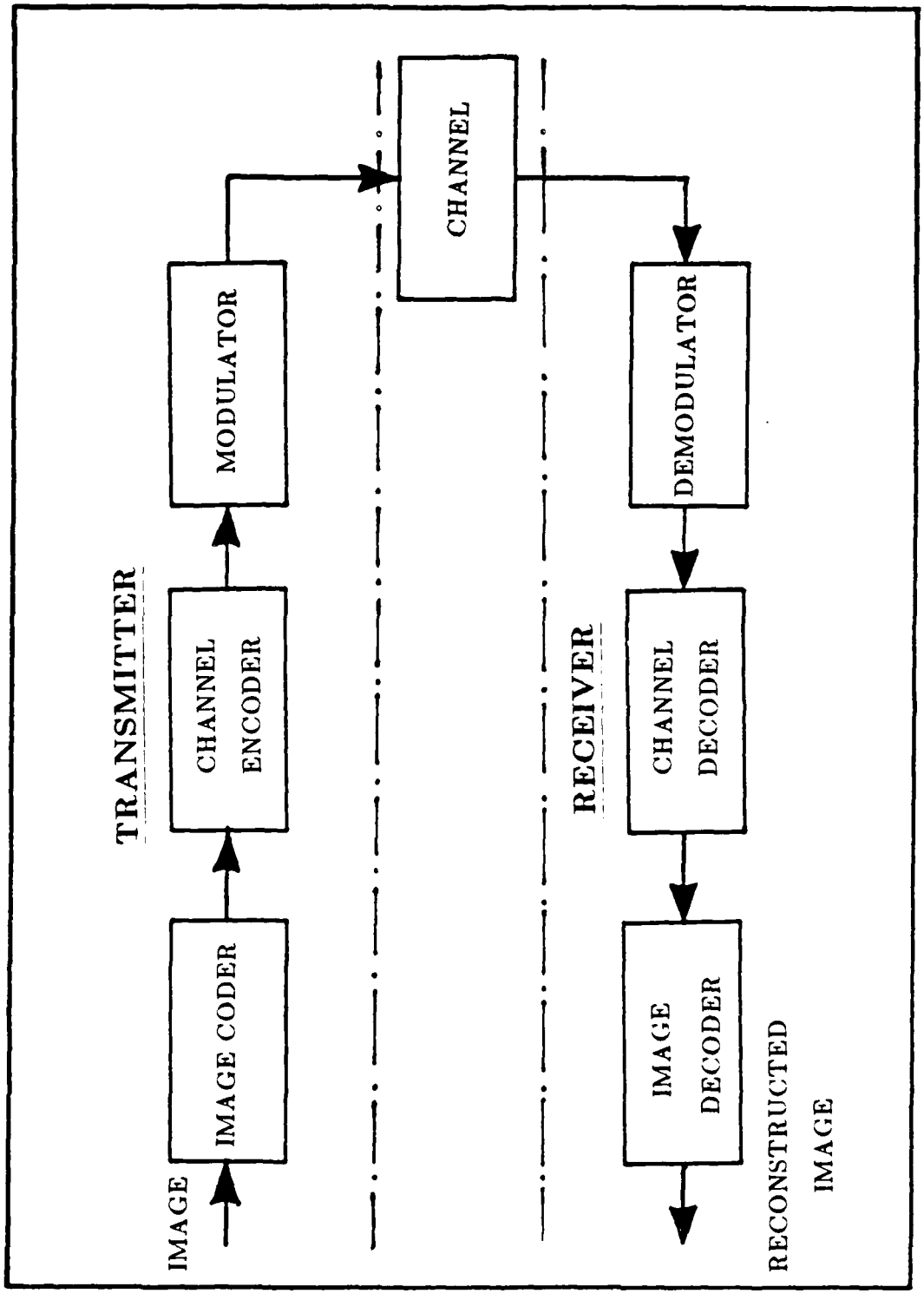

Fig. 6.1 Image coding scheme.

The image coder can be thought of as having three stages. The initial stage of image coding provides a good representation of the signal. This operation is generally reversible. The type of coding used in this stage can be classified into three categories, namely, *waveform* coders, *transform* coders, and *image model* coders. In the second stage the accuracy of representation is reduced, but, in a way that maintains the required image quality. This stage is called quantization. The quantization levels and the corresponding receiver decision levels are system parameters that must be determined. Two types of quantizers are used, namely scalar and vector quantizers. Both types of quantization are irreversible. The last stage in which any redundancy in the signal is removed is called codeword assignment. Two types of codewords can be used, namely equal-length codewords and variable-length codewords. In the case of equal-length codewords, the bit rate of individual signal values and the average bit rate are the same, while, in the case of variable-length codewords they are not. In the latter case, different bit rates result for different signal values. As an example, the shortest codeword may correspond to the most probable signal value, i.e. that which occurs most frequently. The longest codeword may correspond to the least probable signal value. The average bit rate may increase in this case. The codeword assignment operation is reversible.

In this chapter the 2-D spectral analysis models developed earlier are applied to the coding of color images. We are concerned here with predictive coding, i.e. linear prediction followed by quantization of the prediction error. Two algorithms are compared initially. In the first, the whole frame of the image is divided into subframes and the predictor coefficients are computed separately for each. In the second, predictor coefficients are obtained for the whole frame of the image. Both of these methods have the disadvantage that the linear prediction coefficient matrices must be computed in real time and transmitted to the receiver as side information. This significantly increases complexity of the coding system. As an alternative we consider using a fixed set of prediction matrices, i.e. ones that do not depend on the specific image being coded. In this way both receiver and transmitter have the linear prediction matrices and no side information has to be transmitted. Such prediction matrices can be generated by various averaging methods discussed in the chapter. We compare the results of this coding to that resulting from the previous two methods.

B. PREDICTIVE CODING

Predictive coding, (also known as differential pulse code modulation (DPCM)) involves 2-D linear prediction applied to the image and transmission of the quantized error residuals. The prediction of the sample to be encoded in predictive coding is generated from the previously coded samples (Jayant,1974; Netravali et al,1980). For our case we will be dealing with the three (red, green, and blue) components of a color image so the prediction process is multichannel 2-D linear prediction. The vector-valued error $\mathbf{e}(n_1,n_2)$ that is the difference between the predicted value and the actual value of the color element $\mathbf{x}(n_1,n_2)$ is quantized into one of a number of given discrete levels. These levels are assigned to codewords which may be fixed or variable depending on the type of coding used. The encoded information is then transmitted through the channel to the receiver.

The signal-to-noise ratio (SNR) for a given bit rate is actually increased by representing the coded input signal in terms of the prediction error samples. In this case the predictive gain can be written as:

$$\mathbf{G} = E\left[\mathbf{x}(n_1,n_2)\,\mathbf{x}^T(n_1,n_2)\right]\left\{E\left[\mathbf{e}(n_1,n_2)\,\mathbf{e}^T(n_1,n_2)\right]\right\}^{-1} \tag{6.1}$$

Note that G is an M×M matrix where M represents the number of 2-D channels (M=3 for the color images).

Fig. 6.2 shows the general predictive coding system. Fig. 6.2(a) shows the transmitter part of the system while Fig. 6.2(b) shows the receiver part. Since our concern here is with the image encoding and decoding problem, we have omitted the modulator and the demodulator from Fig. 6.2. It is clear from the figure that the predictive coder has three main components, namely the linear predictor, the quantizer, and the channel encoder. In fact the linear predictor is the main part of predictive coding system and the complexity of this system depends on the type of prediction algorithm used.

The basic predictive coding equations can be written as follows

$$\mathbf{e}(n_1,n_2) = \mathbf{x}(n_1,n_2) - \tilde{\mathbf{x}}(n_1,n_2) \tag{6 2a}$$

$$\mathbf{e}_q(n_1,n_2) = \mathbf{e}(n_1,n_2) - \mathbf{q}(n_1,n_2) \tag{6.2b}$$

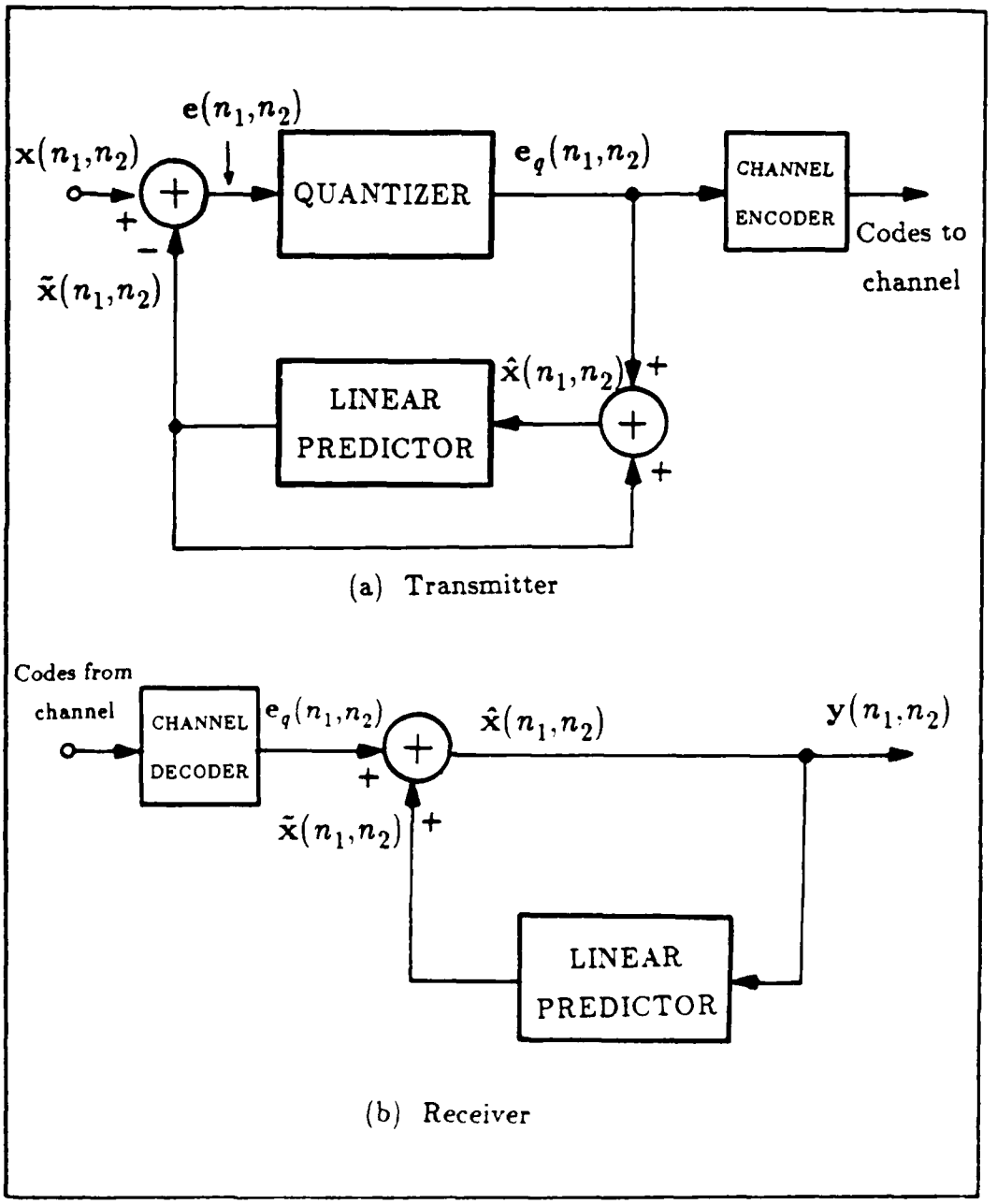

Fig. 6.2 Block diagram of predictive coding.

$$\hat{\mathbf{x}}(n_1,n_2) = \tilde{\mathbf{x}}(n_1,n_2) + \mathbf{e}_q(n_1,n_2) \tag{6.2c}$$

where $\mathbf{e}_q(n_1,n_2)$ represents the quantized prediction error of the color image, $\mathbf{q}(n_1,n_2)$ represents the quantization error, $\hat{\mathbf{x}}(n_1,n_2)$ is the predictive coding approximation of the original color input signal, and $\tilde{\mathbf{x}}(n_1,n_2)$ is the predicted value of $\hat{\mathbf{x}}(n_1,n_2)$. This notation is different from that used in Chapters II to IV where $\hat{\mathbf{x}}$ *not* $\tilde{\mathbf{x}}$ represented the predicted value. We use the present notation to be more consistent with what is conventional in the literature for image coding. Note that here $\hat{\mathbf{x}}$ is an approximation to $\mathbf{x}$ and $\tilde{\mathbf{x}}$ is the linear predicted value based on $\hat{\mathbf{x}}$.

A predictive coding system, which is easier to construct than the predictive coding system just described, is shown in Fig. 6.3. Gibson (1980) called it the prediction error coder to differentiate it from the previous system. The disadvantage of the prediction error coder is the accumulation of quantization noise at the receiver. The reason for that can be explained as follows. The same linear predictor is used in the transmitter and receiver but the input signal to each linear predictor is not the same. In the transmitter the input signal is the actual signal to be transmitted while in the receiver the input signal to the linear predictor is the quantized version. Because of this difference and the positive feedback in the receiver (as shown in Fig. 6.3), quantization noise tends to accumulate. In the usual DPCM system shown in Fig. 6.2, both transmitter and receiver use the same quantized values as input to the linear predictor. Thus quantization noise does not accumulate.

1. Linear Prediction of Color Images

The most important part of the prediction coding system is the linear predictor. Linear prediction for multichannel 2-D random processes was developed and studied in Chapter III. Color images, as we mentioned before, can be considered as 3-channel 2-D random processes. If $\mathbf{x}(n_1,n_2)$ are a set of color picture elements, a linear prediction for the $(n_1,n_2)^{th}$ color element using previous elements can be written as

$$\tilde{\mathbf{x}}'(n_1,n_2) = -\sum_{\substack{(i_1,i_2)\in\alpha \\ (i_1,i_2)\neq(0,0)}} \mathbf{A}^T_{i_1,i_2}\mathbf{x}(n_1-i_1,n_2-i_2) \tag{6.3}$$

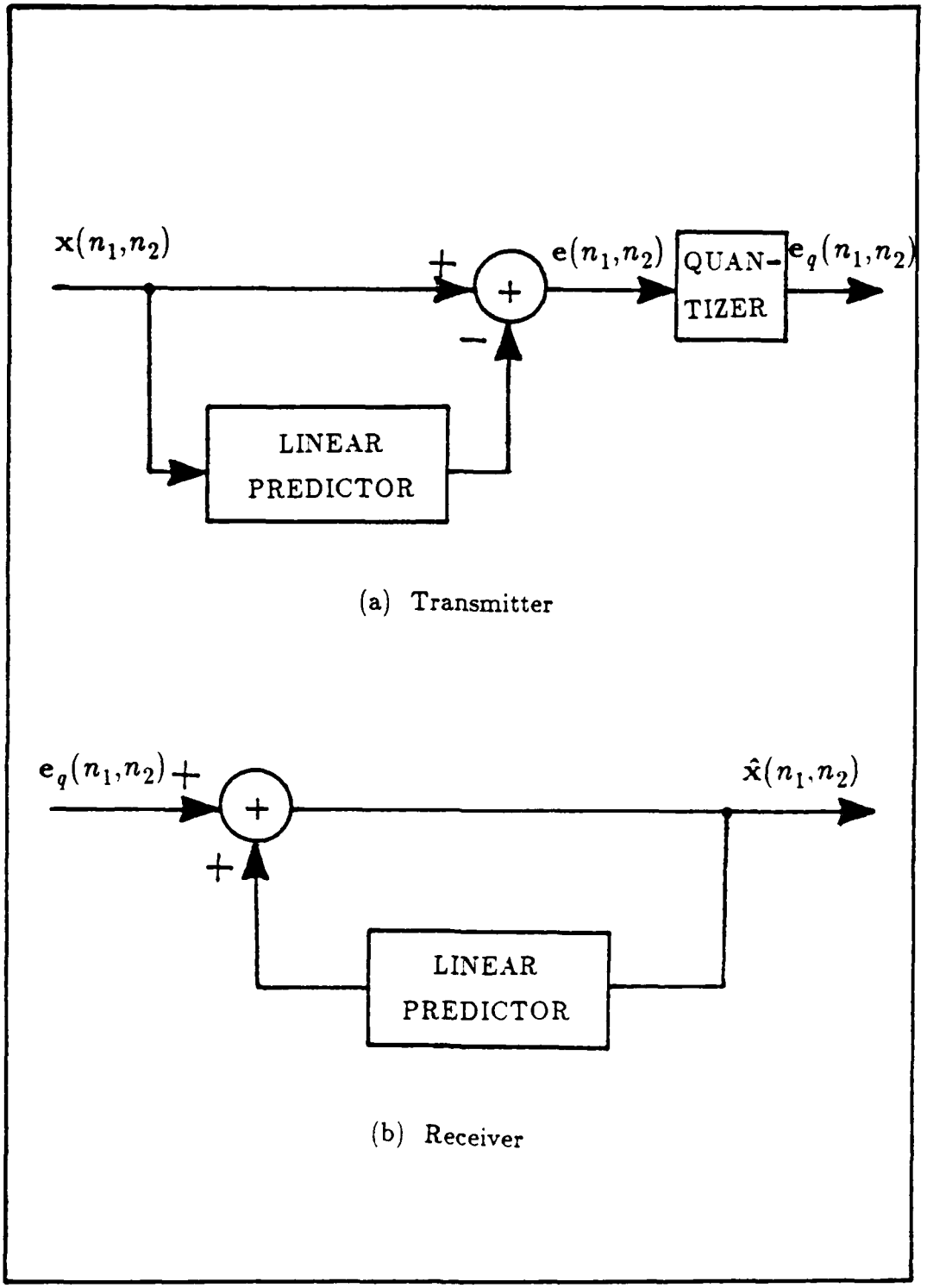

Fig. 6.3 Prediction error coder.

where α is the region of support for the prediction filter and $\tilde{\mathbf{x}}'$ represents the prediction based on the true image values. The filter coefficients $\mathbf{A}_{i_1 i_2}$ can be obtained by minimizing the mean-square prediction error and solving a set of Normal equations in the form of

$$\mathbf{R}\,\mathbf{A} = \mathbf{S} \tag{6.4}$$

as described in detail in Chapter III. In the above analysis we neglect the effect of quantization in the predictive coding system at the transmitter. Since the quantization error is small, so that

$$\mathbf{x}(n_1,n_2) \approx \hat{\mathbf{x}}(n_1,n_2) \tag{6.5}$$

the resulting filter coefficients are still approximately optimal. In the usual DPCM encoder of Fig. 6.2 the linear prediction of the present sample $\mathbf{x}(n_1,n_2)$ is done by using the past encoded estimated sample values.

$$\tilde{\mathbf{x}}(n_1,n_2) = -\sum_{\substack{(i_1,i_2)\in\alpha \\ (i_1,i_2)\neq(0,0)}} \mathbf{A}^T_{i_1 i_2}\hat{\mathbf{x}}(n_1-i_1,n_2-i_2) \tag{6.6}$$

Then the prediction error of the color image

$$\mathbf{e}(n_1,n_2) = \mathbf{x}(n_1,n_2) - \tilde{\mathbf{x}}(n_1,n_2) \tag{6.7}$$

is quantized and transmitted.

In a practical situation the intensity image possesses a nonzero mean value which is referred to as a bias. Maragos *et al* (1984) state three different ways to handle this bias. The first way is by estimating the bias and representing it in the difference equation. This method is called true bias linear prediction. A second method is to estimate the local mean of the signal, subtract it from the original signal, then use the ordinary Normal equations to get the filter coefficients. This approach is called local mean linear prediction. Finally one can decide not to subtract any estimate of the bias and simply solve the Normal equations. We refer to this technique as straight linear prediction. We use the second method in our experiments.

2. Image Quantization

The signal values to be transmitted, (i.e. the prediction error values), are originally developed as continuous-amplitude analog quantities. To deal with these analog quantities through a digital system we have to represent each signal value by an integer number proportional to the amplitude of the analog signal. Hence the analog signal is sampled and a discrete representation of the samples is produced. This conversion process is called quantization. As mentioned earlier, there are two types of quantization, namely scalar quantization and vector quantization. Our concern here with scalar quantization. Vector quantization is addressed briefly in Appendix G.

For the development of the scalar quantization technique, let x represent the amplitude of the scalar signal sample which may represent a value for the prediction error (pixel intensity). Then scalar quantization can be interpreted as a method of representing x with a finite number of bits corresponding to one of the J given levels of the signal. The quantized value $\hat{x}$ can be expressed as

$$\hat{x} = Q(x) \tag{6.8}$$

where Q represents the quantization operation. The quantization problem is to specify a set of decision levels d_j and a set of reconstruction levels r_j such that if x falls between d_{j-1} and d_j, it is mapped to the reconstruction level r_j. If the reconstruction levels and decision levels are uniformly spaced we refer to this method as *uniform* quantization.

In general the decision and reconstruction levels are chosen to minimize the average distortion D defined by

$$D = E\left[d(x, \hat{x}) \right] \tag{6.9}$$

where d is a measure of the local distortion at each pixel. For example in the case of a mean-square error quantization criteria, the error e_Q can be expressed as

$$e_Q = \hat{x} - x \tag{6.10}$$

and d is defined as

$$d = e_Q^2 = \left[\hat{x} - x \right]^2 \tag{6.11}$$

The average distortion can then be written in the form (Pratt,1978)

$$D = \sum_{j=0}^{J-1} \int_{d_j}^{d_{j+1}} \left[x - r_j\right]^2 p(x)\, dx \tag{6.12}$$

where J represents the number of quantization levels and $p(x)$ is the probability density function of the signal x. The optimum values of the reconstruction levels and the decision levels can be determined by minimizing D with respect to r_k and d_k. If in the case of Eqn. (6.12) we require

$$\frac{\partial D}{\partial r_k} = 0 \tag{6.13a}$$

and

$$\frac{\partial D}{\partial d_k} = 0 \tag{6.13b}$$

for all values of k. Then we can obtain the following results

$$r_k = \frac{\int_{d_k}^{d_{k+1}} x\, p(x)\, dx}{\int_{d_k}^{d_{k+1}} p(x)\, dx} \tag{6.14}$$

$$d_k = \frac{r_k + r_{k+1}}{2} \tag{6.15}$$

We see from the above two equations that the reconstruction level r_k is the centroid of $p(x)$ over the range $d_k \leq x \leq d_{k+1}$ and the decision level d_k is the mid-point between two adjacent reconstruction levels.

Solving the two equations (6.14) and (6.15) is a non-linear problem. Max (1960) solved the problem for the cases of uniform, Gaussian, Laplacian, and Rayleigh densities. The results are put in tables (Pratt,1978; Jayant and Noll,1984) and we refer to this quantizer as the Max quantizer.

Fig. 6.4 represents a specific example of the uniform quantizer for two and three levels. Fig. 6.4(a) represents a two-level quantizer with step size Δ while Fig. 6.4(b) represents the three-level quantizer with threshold levels $d = d(1), d(2)$ and reconstruction levels $r = r(1), r(2), r(3)$.

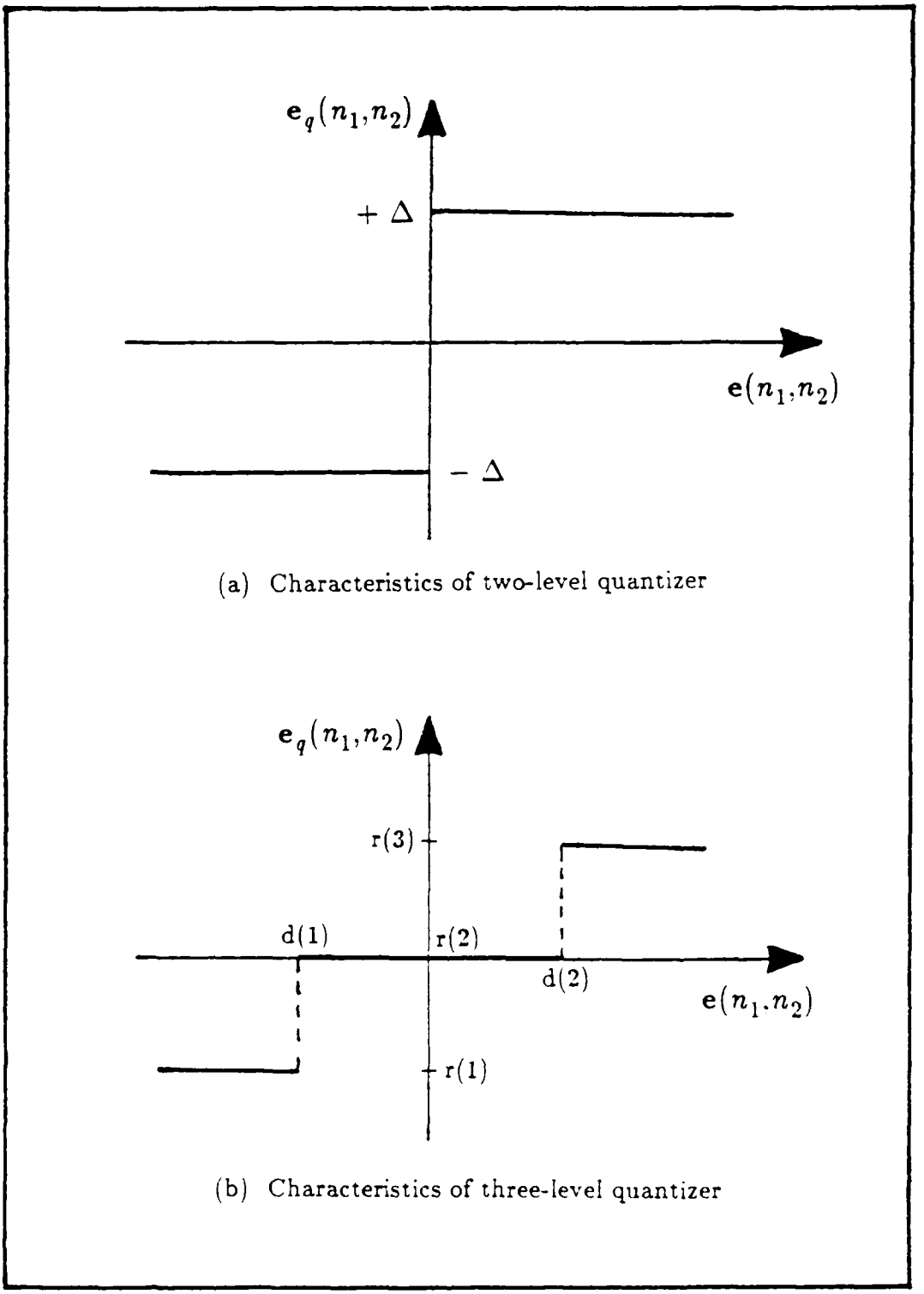

(a) Characteristics of two-level quantizer

(b) Characteristics of three-level quantizer

Fig. 6.4 Characteristics of uniform quantizer.

Nonuniform quantization has been considered as another type of quantization, (Jayant,1974). In this case, as we go further from the center of the quantizer, the step size increases. The advantage of this quantizer is that a reduction in bit rate for a given quality of encoding can usually be obtained.

A more recent type of scalar quantizer is the adaptive quantizer. Here the step size is modified according to the status of the quantizer memory. In particular the present step size is multiplied by a factor depending on previous knowledge about the step size used for the past samples. (Jayant,1974)

Poor design of the quantizer used in predictive coding can cause different types of degradation, such as granular noise, edge busyness, and slope overload. These effects are illustrated in Fig. 6.5 (Netravali et al,1980). Granular noise is caused by the coarseness of the minimum quantizer step in the coding of a signal which has a very slow change in the shape of its waveform. Slope overload distortion appears when the maximum value of the quantizer step is not enough to follow a suddenly and rapidly changing input. Edge busyness is a distortion specific to image coding that occurs when there is a gradual change in the contrast of the edges. In this case the output of the quantizer oscillates between two levels around the actual value of the signal. This oscillation may cause a change from one line to the other which gives the appearance of a "busy edge". (Netravali and Limb,1980)

The characteristics and the requirements on a given quantizer depend on the type of application. As an example, the requirements on the quantizer in a moving area of an image is completely different from the requirements for the background areas. In case of background a low granular noise effect is required and this can be achieved by designing a fine quantizer (small step size). In the case of moving areas, slope overload distortion must be avoided. To satisfy this we have to choose a coarse quantizer with high dynamic range.

In general a tradeoff between coarse and fine quantizers must be determined. A fine quantizer will generate the slope overload distortion which can be seen as an unclear sharp edge; while a coarse quantizer may produce the granular noise and edge busyness discussed above.

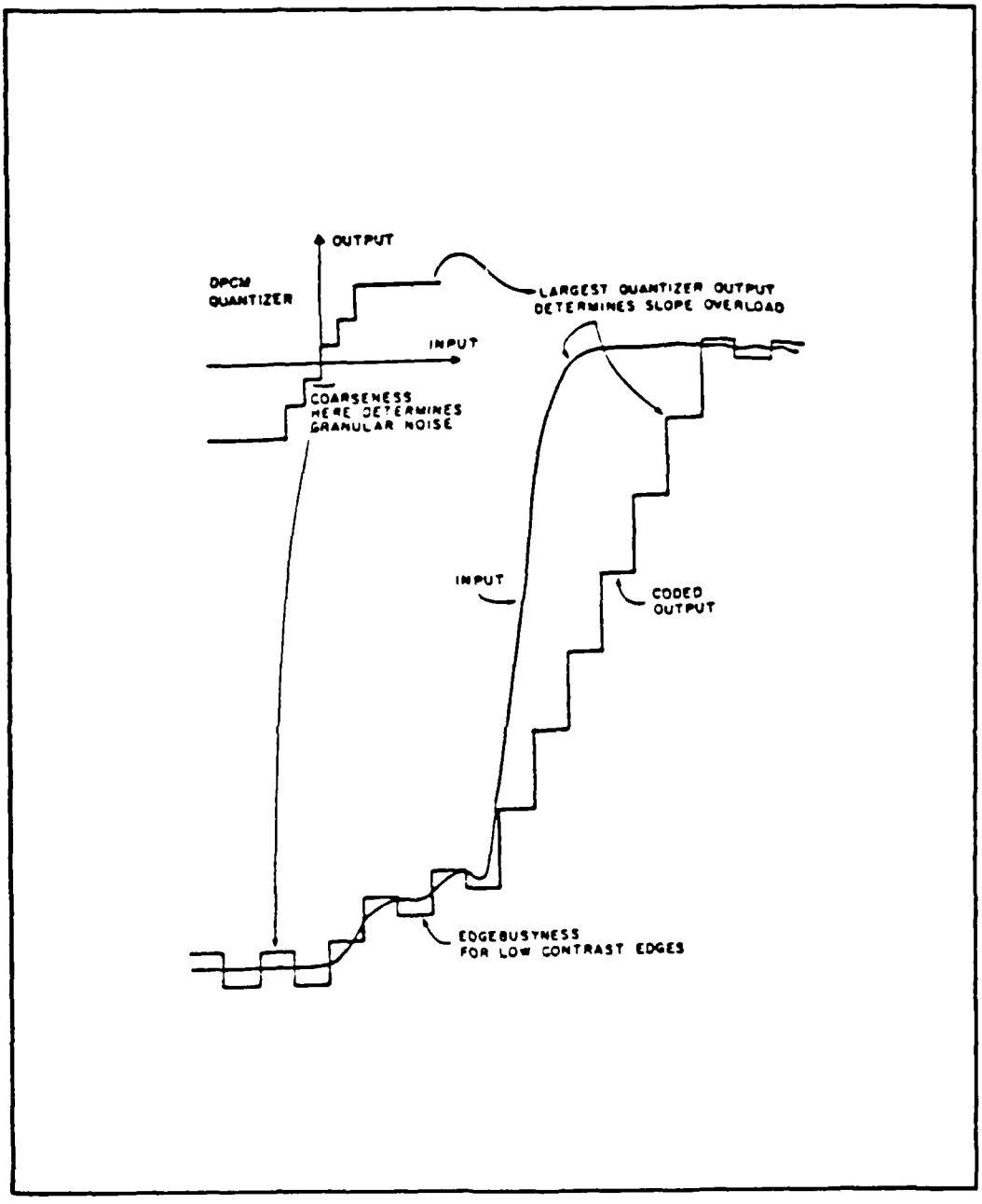

Fig. 6.5 Illustration of waveform coding by predictive coding and a different types of reconstruction error (Netravali and Limb.1980).

Various measures have been developed to measure the overall performance of a predictive coder. The most widely used measures are the normalized mean square error (NMSE) and the signal-to-noise ratio (SNR). These can be defined in case of multichannel 2-D random processes as follows:

$$NMSE = Covar\left[\mathbf{x}(n_1,n_2) - \hat{\mathbf{x}}(n_1,n_2)\right]\left\{Covar\left[\mathbf{x}(n_1,n_2)\right]\right\}^{-1} \tag{6.16}$$

$$SNR\ (dB) = 10\log\left[NMSE\right]^{-1} \tag{6.17}$$

where *Covar* [.] represents the covariance matrix for the quantity. Note that the NMSE and the SNR are in the form of matrices with dimension M×M. It is known that the SNR is not a perfect measurement of image quality. There are cases, as we will see in the next section, where the coder that has the highest value of the SNR generates a reconstructed signal which is subjectively lower in quality than one generated by a lower SNR coder (Gibson,1980). The reason for that lies in the dependence of the quality on the amplitude of the quantization noise and not on its power (see Eqn. (6.16)). However the SNR defined by Eqn. (6.17) is still the measure most widely used because of its computational simplicity and ease of interpretation.

3. Side Information

In addition to quantizing and transmitting the residual of the color image, we have to also quantize and transmit the predictor filter coefficients. We refer to this as *side information*. The size of the predictor coefficient matrix of the color image depends on the model order used. As an example a first order NSHP model has 12 (matrix) parameters, while an eighth order NSHP model has 381 such parameters. These numbers of parameters are very large compared to the corresponding number of parameters for the single channel 2-D case.

The size of the predictive filter is of concern not only because of the amount of side information that needs to be transmitted but also because of the real time computation requirement. For predictive coding systems a set of Normal equations needs to be solved to get the predictor parameters. This operation uses the image data itself and is done in real time. This significantly slows the predictive coding process and increases the complexity of the coding system.

In this research we considered a possible way to overcome the disadvantage of the real time computation and transmission of side information. The idea is to select a fixed set of predictor parameters and apply it directly to the data. In this case no real time computations are required, and there is no need to transmit the side information. The criteria for selecting the fixed predictor parameters will be explained in detail in the next section.

C. CODING EXPERIMENTS WITH COLOR IMAGES

In this work a color image is represented by its red, green, and blue (RGB) components. An alternative representation that may have some advantages is in terms of luminance-chrominance (YIQ) components. However this is not explored here.

The original pictures used in this thesis are 256×256 pixels in size but in order to stay within our computational budget we selected portions of the original pictures with sizes of 128×128 pixels as shown in Fig. 6.6. A variety of pictures used in the experiments are shown in the figure.

The linear predictive models developed in this thesis were applied to the coding of these color images. Two different procedures were used initially. In the first procedure the total frame of the image is divided into four subframes with 64×64 pixels each. The predictor coefficients and the error covariance matrix are obtained separately for each subframe by solving a set of Normal equations. The different linear predictive filters derived are then applied to the different subframes. The residual error covariance matrix and the set of filter coefficients for each subframe are coded and transmitted. Since there is a specific filter for each subframe, a discontinuity appears at the subframe edges. To overcome this effect we overlap the subframes by four pixels and average the results in the overlapped regions.

In the second procedure, the whole frame of the image is taken, and the Normal equations are solved to get only one set of predictor matrices. This single error covariance matrix and the set of filter coefficients for the whole frame are coded and transmitted along with the residuals as in the first procedure.

Note that in both of these procedures the predictor matrices must be calculated in real time. In the first case the real time calculation is done for each subframe and in the

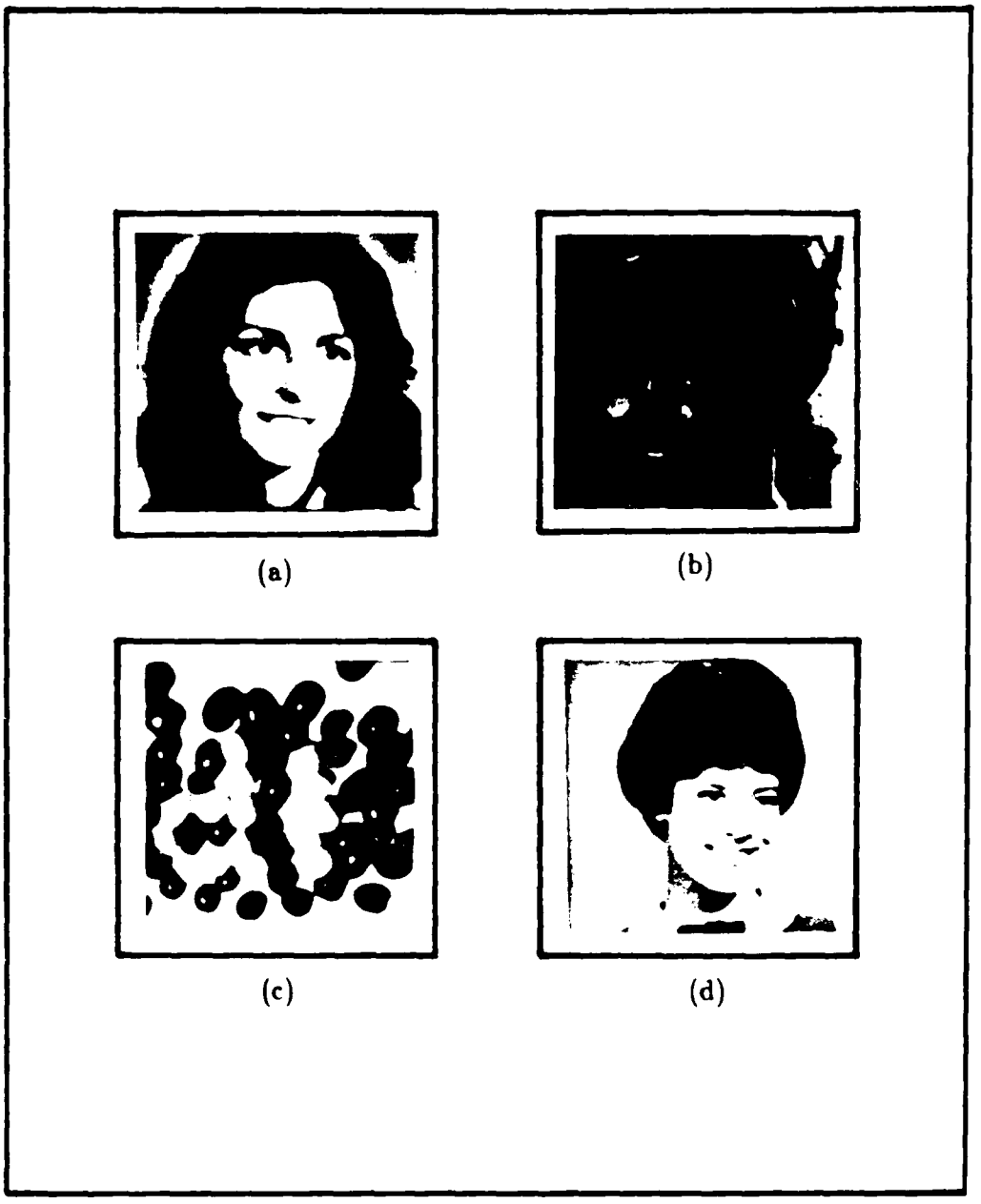

Fig. 6.6 Original pictures.

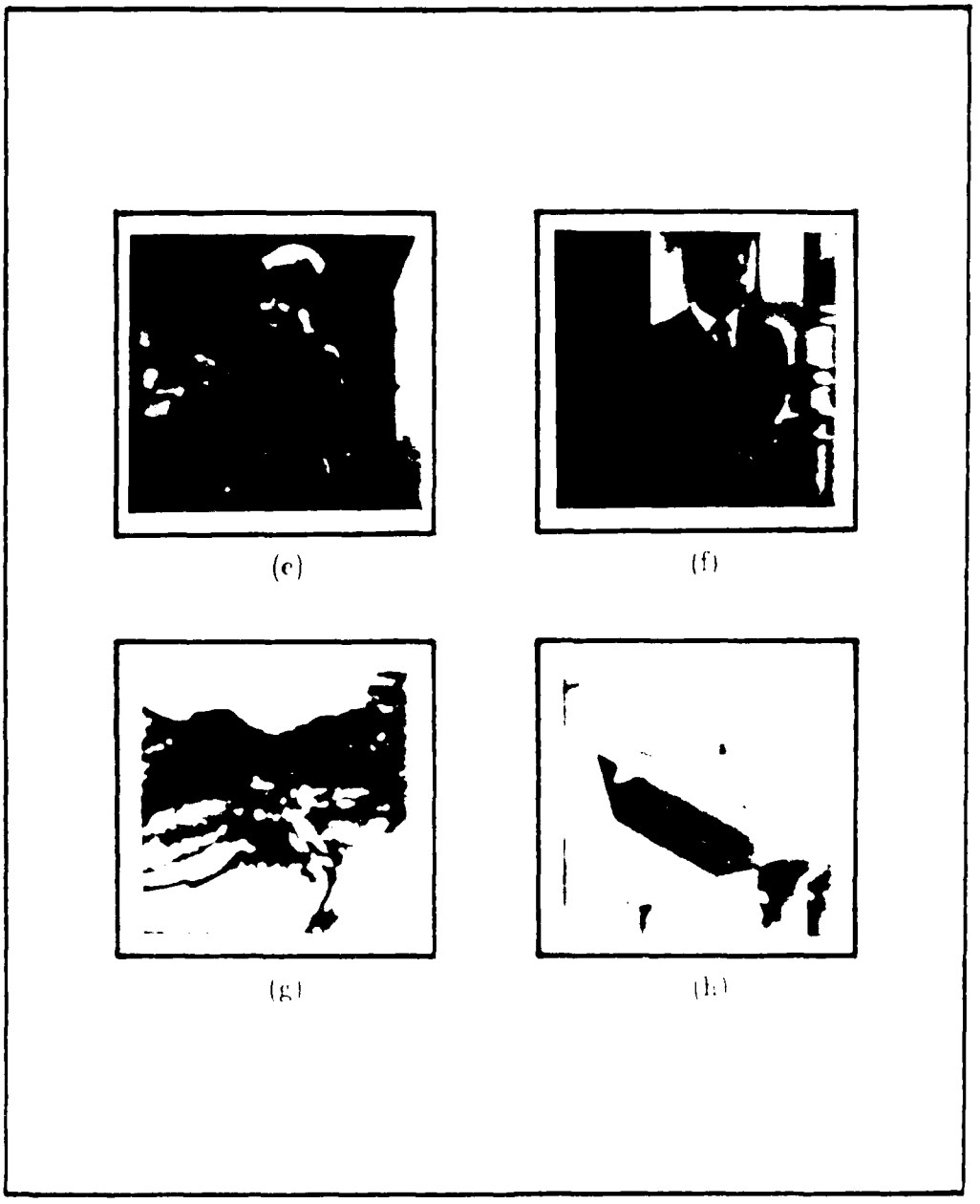

Fig. 6.6 Original pictures (cont'd)

second case it is done for the whole frame. These real time computations and the need to send results as side information, greatly increase the complexity of the coding system.

As an alternative we considered two new procedures which overcome the disadvantages of the previous ones. In the first of these new procedures a fixed set of predictor matrices is used. We refer to this in the experiments as the *third* procedure. The fixed set of predictor matrices is chosen on the basis of the following criteria. The filter parameters for multichannel 2-D linear prediction are determined for each of the different images separately. We use all the original pictures shown in Fig. 6.6 except the jelly bean picture of Fig. 6.6c. A new fixed set of parameters is obtained by averaging the parameters corresponding to the different images. Then this new set is applied in our process.

In the second new procedure a fixed autocorrelation matrix is generated by averaging a group of autocorrelation matrices estimated from the same data, i.e. all images except the jelly beans. The predictor parameters are developed by solving a set of Normal equations involving the fixed average autocorrelation matrix. As in the previous case the residual is quantized and sent to the receiver and there is no need to send any side information. We refer to this in the experiments as the *fourth* procedure.

For purposes of the coding experiments two images are used. The first is the lady's face of Fig. 6.6(a) which is one of the images used to derive the fixed set of prediction parameters. The second is the jelly bean picture of Fig. 6.6(c) which was *not* included in the set of images used to derive the fixed parameters. For each of these images the residual is quantized and transmitted. No side information needs to be transmitted and this procedure requires no real time computation.

Different experiments are given to show the performance of the third and fourth (new) procedures by comparing their results with the results of the first and second (original) procedures. Although our experiments here used scalar quantization, the ideas can also be applied to the case of vector quantization (see Appendix G). For the scalar quantizer two and three levels of quantization are used. Linear prediction is performed using second and third order models. The SNR measurement defined by Eqn. (6.17) is used as a measure of the performance of the different predictive coders used in this section.

1. Predictive Coding With Two-Level Quantizer

In this experiment we used a uniform two-level quantizer with step size Δ defined by

$$\Delta = \gamma \sigma^2 \tag{6.18}$$

where γ is a factor controlling the dynamic range of the quantizer (this also has an effect on the granular noise and the sharpness of the edges) and σ^2 represents the prediction error variance. The input output characteristic of this uniform 2-level quantizer is given in Fig. 6.4a. The behaviour of the quantizer is varied by varying the step size Δ. A second order linear predictive filter and a 2-level quantizer with different values of step sizes is used in this experiment.

Four different step size quantization levels are considered here ($\gamma = 1.5, 0.7979, 0.7071$, and 0.5) starting with a 2-level quantizer with large step size ($\gamma = 1.5$). Fig. 6.7 shows the results of the four procedures where (a) is the result of using the first procedure (dividing total frame into four subframes i.e. L=4), (b) is the result of using the second procedure (using the whole frame i.e. L=1), (c) shows the simulation results using the third procedure (applying the averaged set of filter coefficients), and (d) is the result of the fourth procedure (averaging the autocorrelation function).

When the reconstructed coded pictures are compared with the original picture shown in Fig. 6.6a it seems that sharp edges are very clear for all the procedures but granular noise is apparent in the reconstructed pictures. Note that the alternative procedures (three and four) produce good coded results which are quite similar to the results of the first and second procedures.

Error pictures of the four procedures are shown in Fig. 6.8. These are generated by taking the difference between the original picture and the reconstructed one. Fig. 6.9 shows the error picture for the same procedures but after quantization. Most of the essential information is retained in the quantized error picture.

Table 6.1 shows the SNR values obtained by applying the four different procedures, for the red, green, and blue components of the color picture. The SNR of the second procedure is given as the average of the values obtained for the four different subframes. It is clear from the table that the SNR values for the various procedures are close

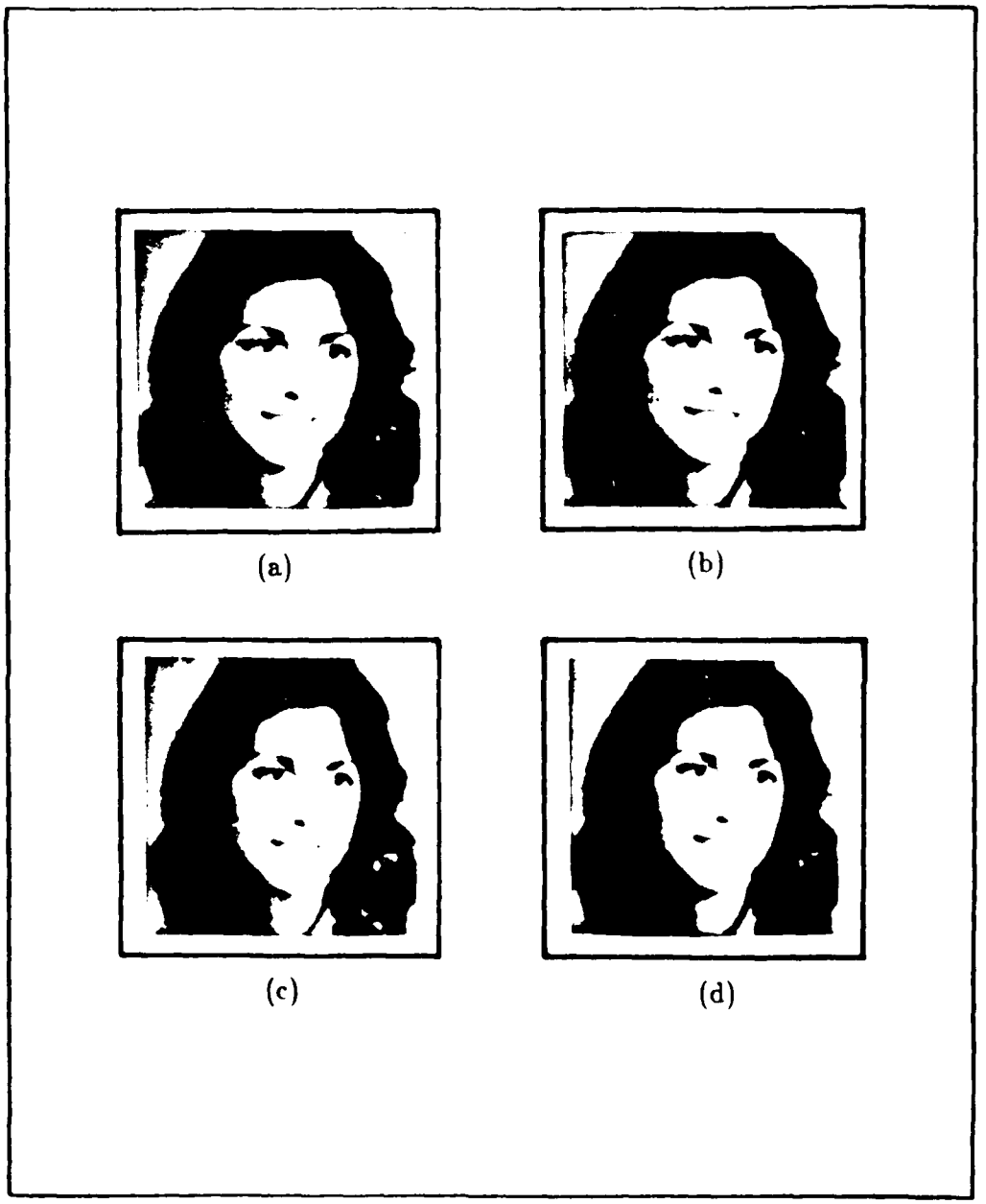

Fig. 6.7 Coded images $(\gamma=1.5)$.
(a) First procedure (b) Second procedure
(c) Third procedure (d) Fourth procedure

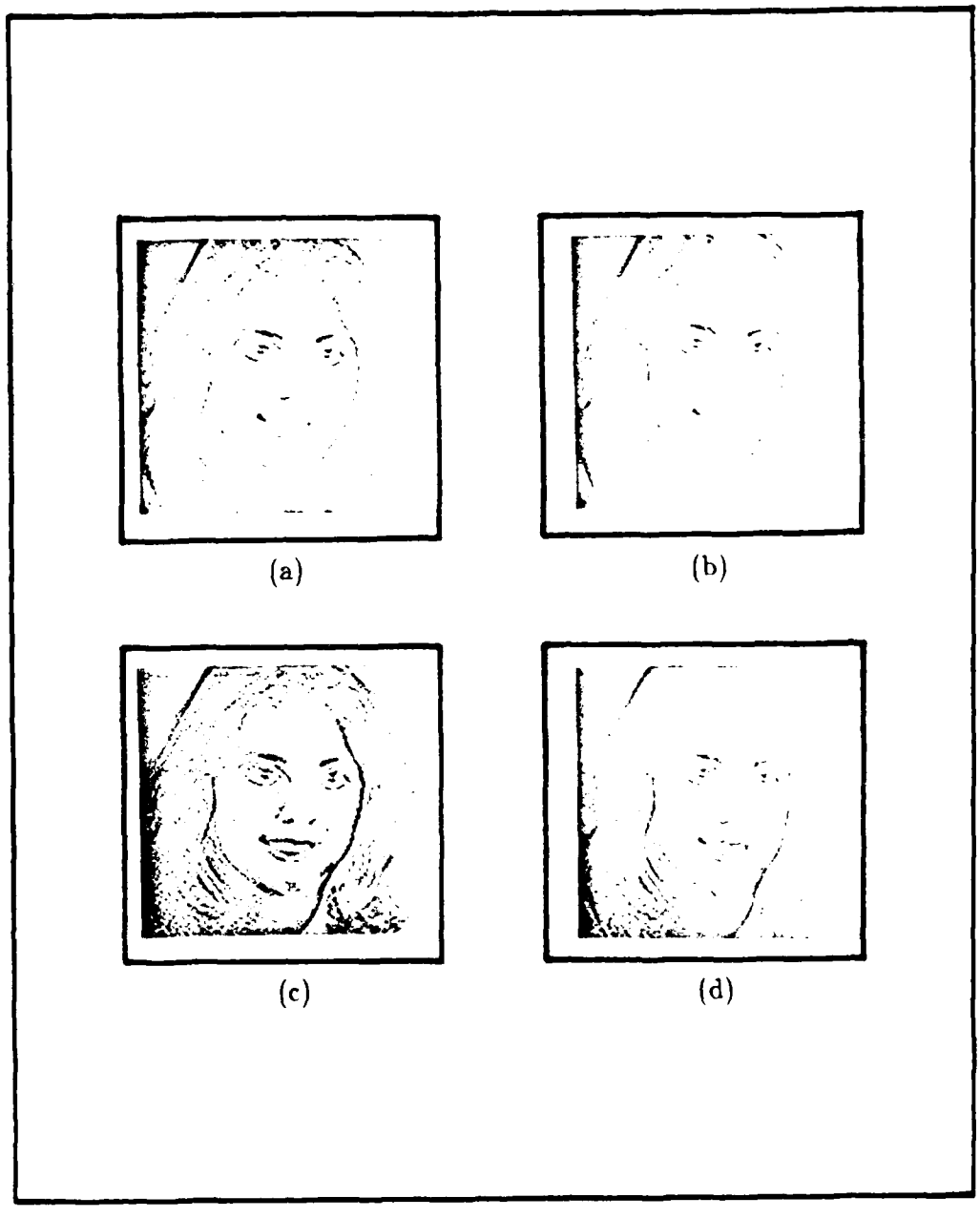

Fig. 6.8 Error images ($\gamma = 1.5$).
(a) First procedure (b) Second procedure
(c) Third procedure (d) Fourth procedure

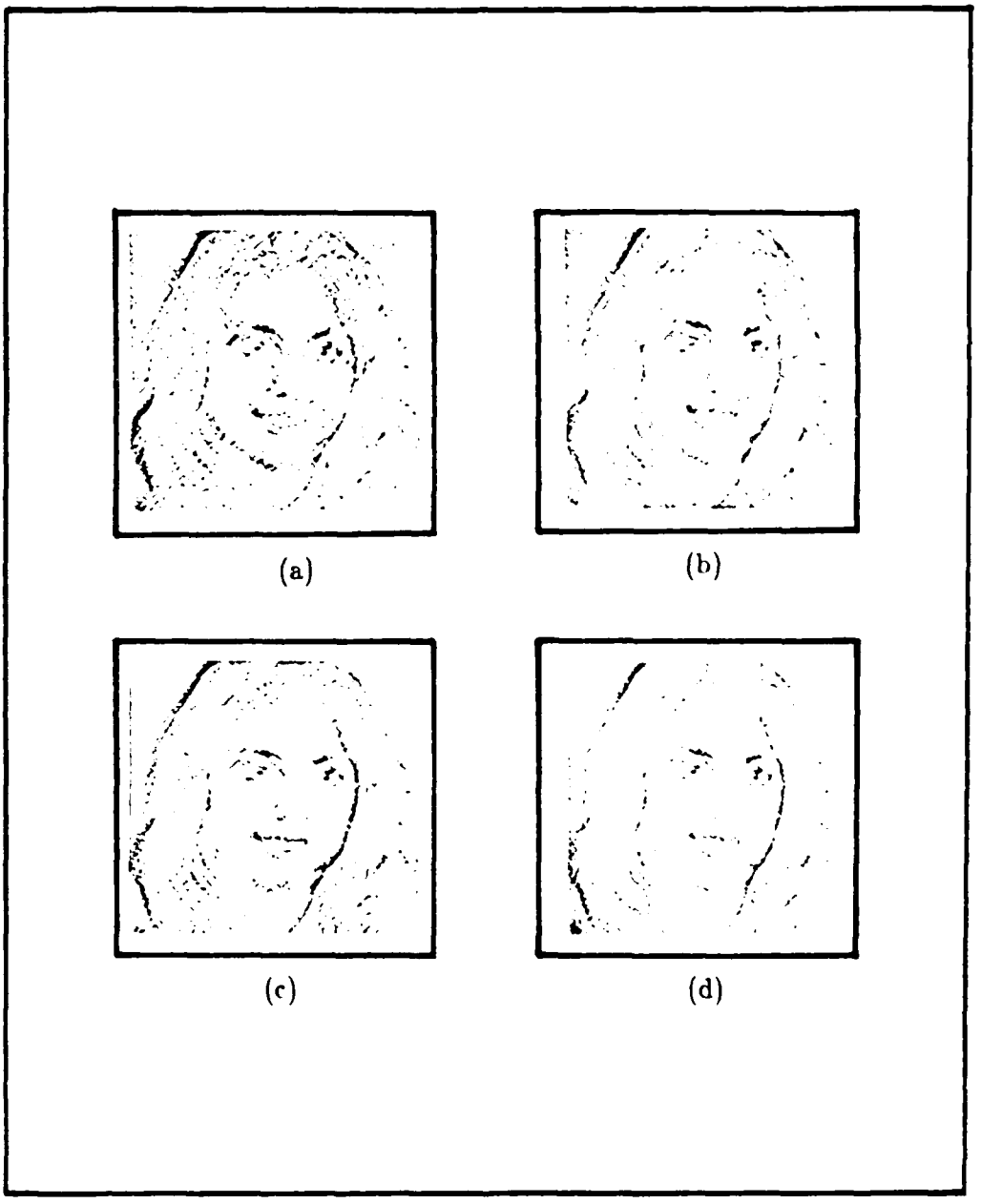

Fig. 6.9 Quantized error images $(\gamma = 1.5)$.
(a) First procedure (b) Second procedure
(c) Third procedure (d) Fourth procedure

to each other. The highest SNR values are obtained for the first procedure but there is only about a 0.5 dB improvement.

As a second simulation for this example, the step size is given a smaller value ($\gamma = 0.7979$). This value is taken from the Max table for the Gaussian distribution. Fig. 6.10 shows the corresponding results using the same four procedures. Good results are obtained for non-edge regions and good sharp edges are also obtained. The SNR results, which measure the performance of the reconstructed pictures, are given in Table 6.2. The first procedure gave an improvement of 0.5 dB while the third and fourth procedures lost 0.5 dB with respect to the second procedure.

Fig. 6.11 and Table 6.3 show the results of choosing γ corresponding to a Laplacian distribution ($\gamma = 0.7071$). Qualitatively we get the same results as in the reconstructed pictures as for Gaussian distribution. However there is a 1 dB improvement in the SNR.

Finally the results of the last simulation for this experiment are given in Fig. 6.12 and Table 6.4. In this case a smaller step size is used ($\gamma = 0.5$). In this case the predictive coding system provides good results in the non-edge regions but the edges are blurred out as we expect. At the same time there is an improvement of approximately 3 dB in the SNR over the Laplacian case.

To complete this experiment and to check the performance of the new procedures on a picture that was not in the set used to derive average parameters, the jelly bean picture (Fig. 6.6c) was tested. For this case a two-level quantizer with $\gamma = 0.7071$ was used. Fig. 6.13 shows the quality of the picture obtained by applying the four different procedures. It is clear that the quality of the reconstructed picture for procedures three and four is similar to that for the first and second procedures. Table 6.5 shows the SNR results. The highest SNR appeared for the picture coded by applying the first procedure. The second, third, and fourth procedures yielded SNR results that are very close.

The foregoing results show that using a fixed set of prediction parameters yields good image reconstructions which are close to the results of using real-time computed filter parameters. Also the variation of the SNR from one procedure to the other is small. The new procedures can be applied to any image outside the training set.

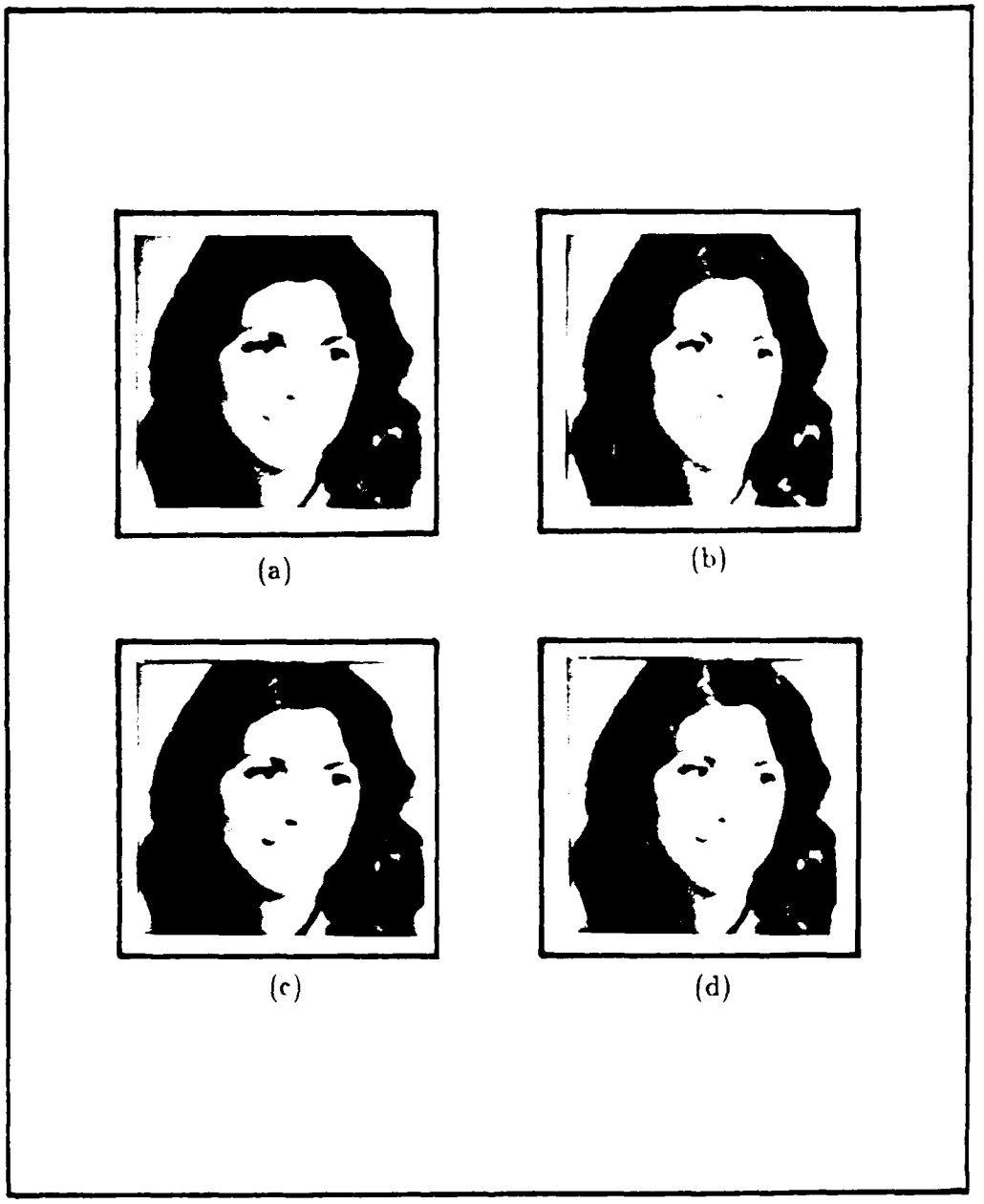

Fig. 6.10 Coded images ($\gamma = 0.7979$).
(a) First procedure (b) Second procedure
(c) Third procedure (d) Fourth procedure

TABLE 6.1 SNR FOR CODED IMAGES USING 2-LEVEL QUANTIZER WITH $\gamma = 1.5$

Procedure	Red	Green	Blue
First Procedure	16.37	13.44	11.28
Second Procedure	15.78	13.40	10.61
Third Procedure	15.39	13.20	9.86
Fourth Procedure	15.38	13.20	9.86

TABLE 6.2 SNR FOR CODED IMAGES USING 2-LEVEL QUANTIZER WITH $\gamma = 0.7979$

Procedure	Red	Green	Blue
First Procedure	21.85	18.93	16.77
Second Procedure	21.26	18.88	16.09
Third Procedure	20.87	18.68	15.35
Fourth Procedure	20.87	18.68	15.35

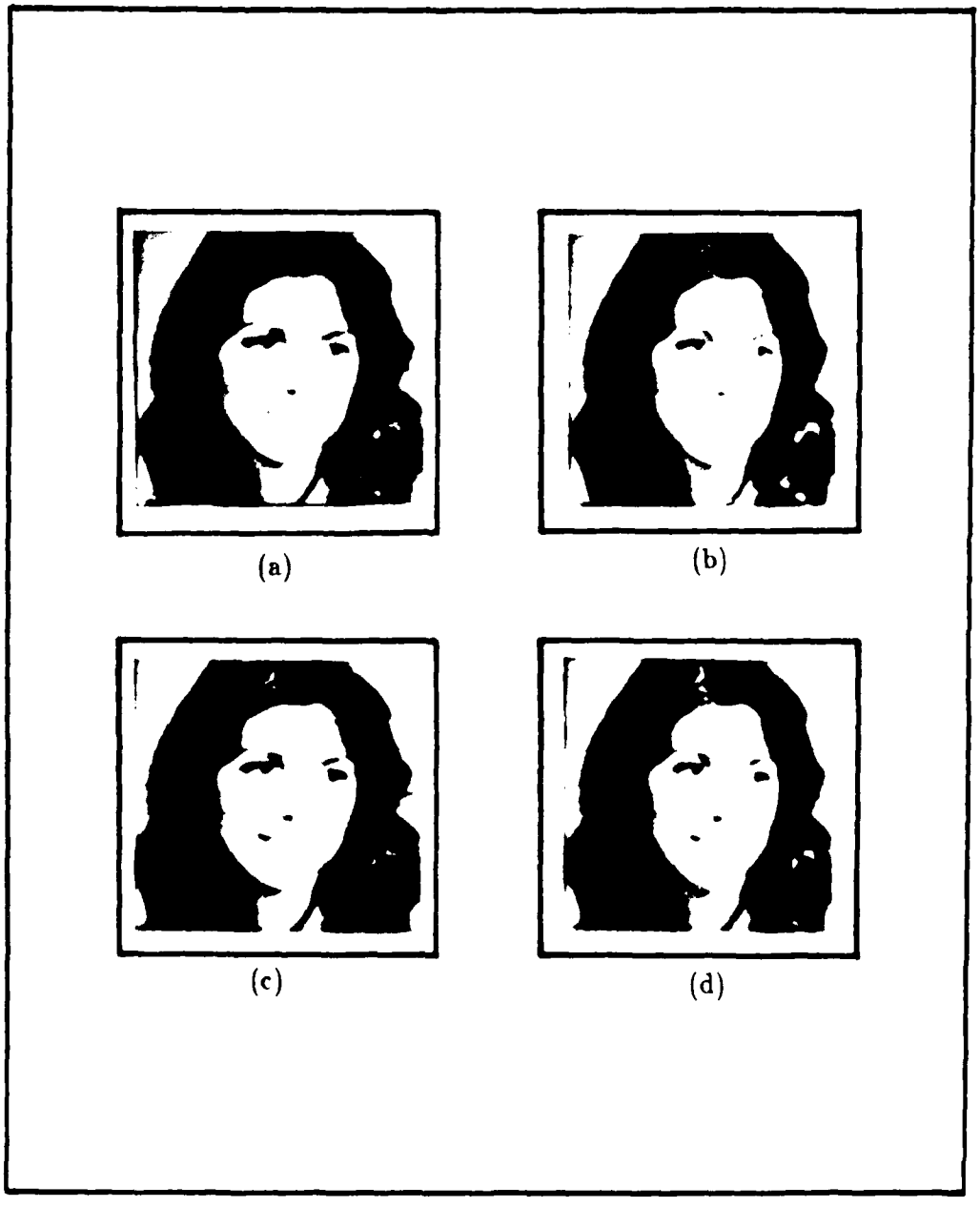

Fig. 6.11 Coded images ($\gamma = 0.7071$).
(a) First procedure (b) Second procedure
(c) Third procedure (d) Fourth procedure

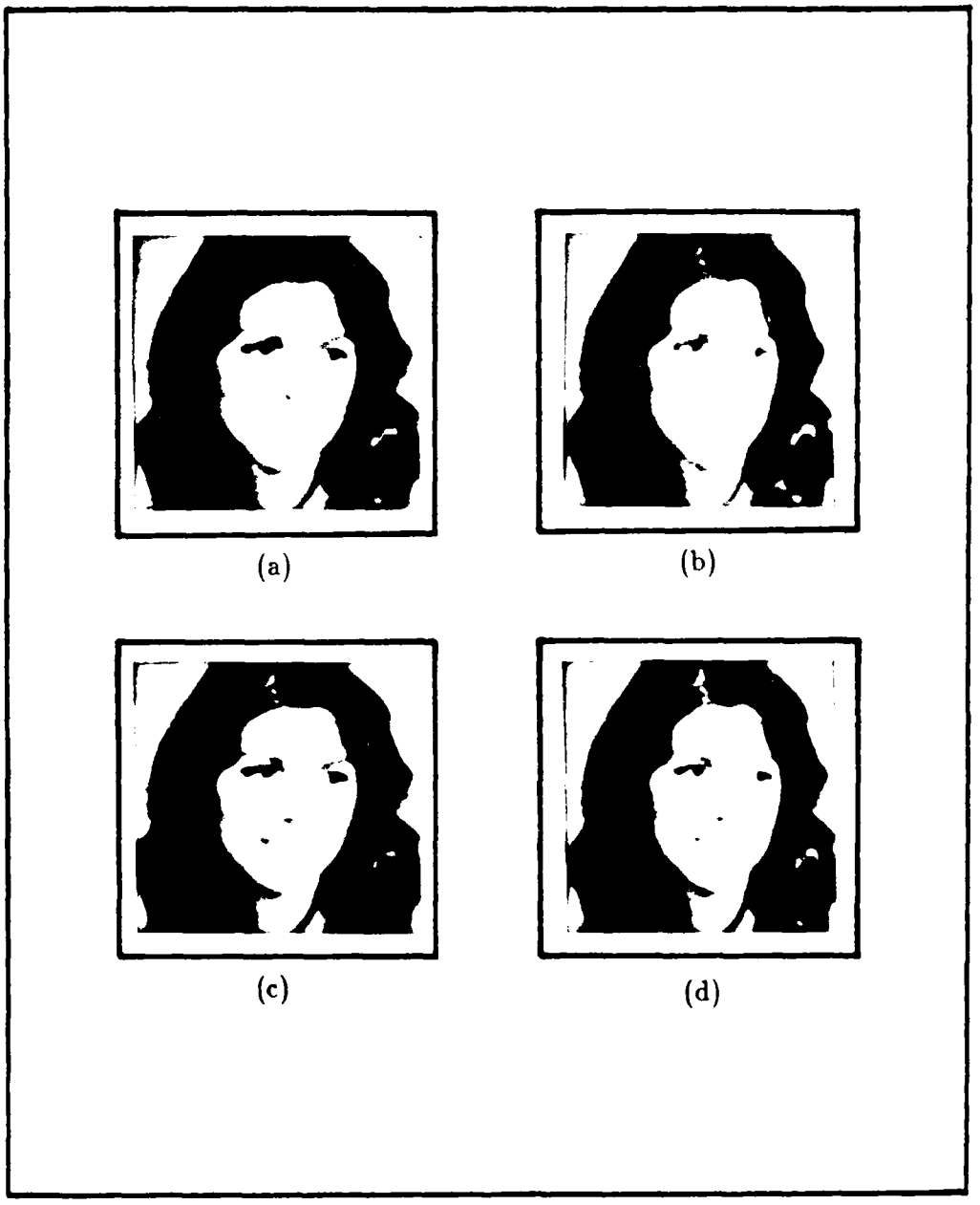

Fig. 6.12 Coded images ($\gamma = 0.5$).
(a) First procedure (b) Second procedure
(c) Third procedure (d) Fourth procedure

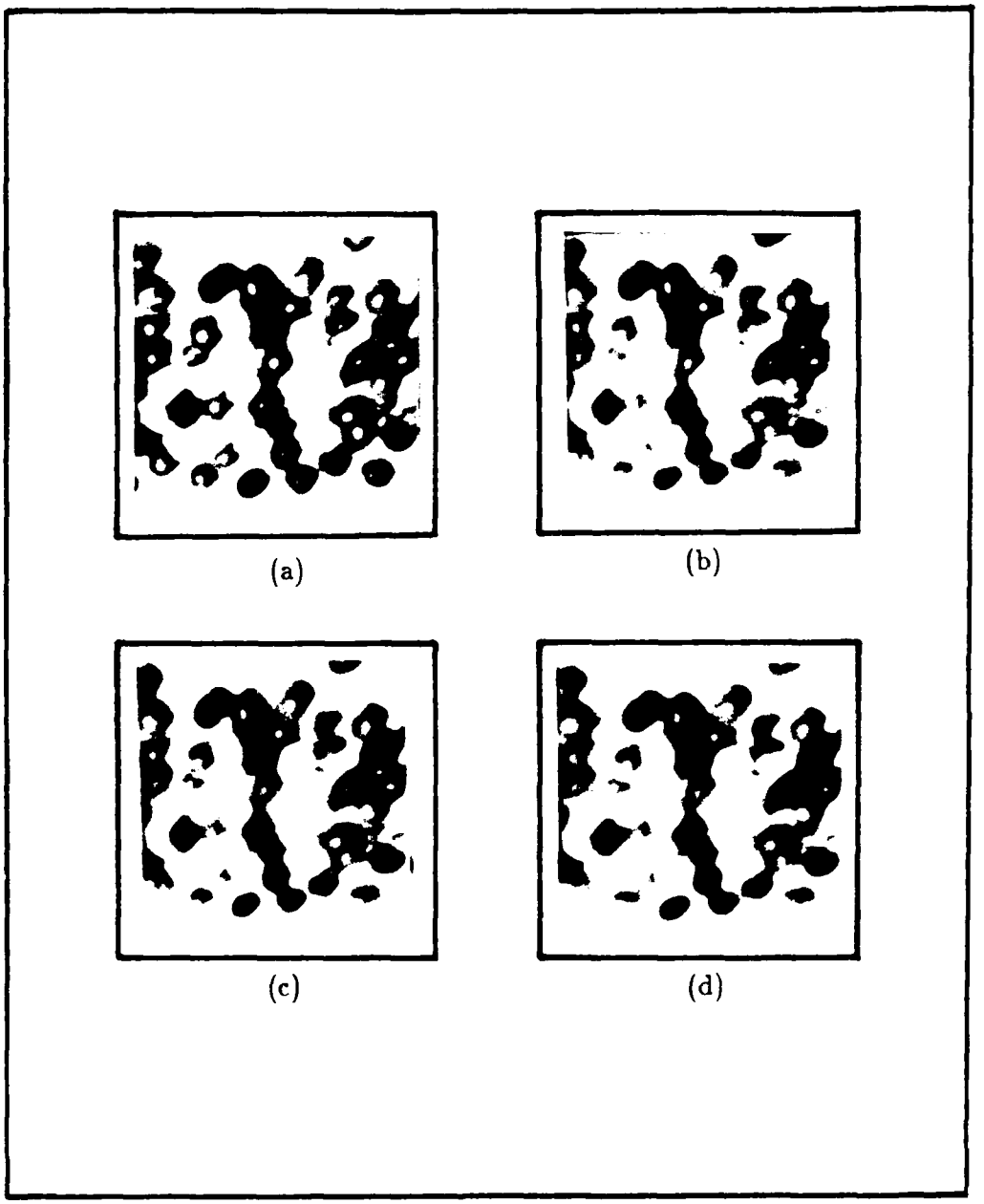

Fig. 6.13 Coded jelly bean images ($\gamma = 0.7071$).
(a) First procedure (b) Second procedure
(c) Third procedure (d) Fourth procedure

TABLE 6.3 SNR FOR CODED IMAGES USING 2-LEVEL QUANTIZER WITH $\gamma = 0.7071$

Procedure	Red	Green	Blue
First Procedure	22.90	19.98	17.82
Second Procedure	22.30	19.93	17.14
Third Procedure	21.92	19.73	16.45
Fourth Procedure	21.90	19.73	16.44

TABLE 6.4 SNR FOR CODED IMAGES USING 2-LEVEL QUANTIZER WITH $\gamma = 0.5$

Procedure	Red	Green	Blue
First Procedure	25.91	22.99	20.83
Second Procedure	25.32	22.94	20.15
Third Procedure	24.93	22.74	19.41
Fourth Procedure	24.93	22.74	19.41

TABLE 6.5 SNR FOR BEAN CODED PICTURE USING 2-LEVEL QUANTIZER WITH $\gamma = 0.7071$

Procedure	Red	Green	Blue
First Procedure	22.87	21.98	20.00
Second Procedure	22.48	21.90	19.86
Third Procedure	21.35	21.76	19.05
Fourth Procedure	21.35	21.76	19.05

In addition a 2-level quantizer is sufficient for these pictures. The bit rate in this case is reduced from 8 bits to 1 bit per pixel for each color component.

The step size of the quantizer is very important as we mentioned before. A small step size gave good non-edge results with poor edge sharpness. A large step size provided sharp edges but granular noise in the non-edge areas. Practically the step size should depend on the application. Small step sizes can be used when sharp edges are not important. For sharp edge requirements a large step size should be used.

2. Predictive Coding with a Three-Level Quantizer

The dynamic range of the residual signal may sometimes be too large to be well handled by a 2-level quantizer. This can lead to excessively large distortion in the reconstructed pictures. Also in the case of a two-level quantizer it is difficult to control the granular noise and at the same time keep sharp detail in the edges. Three-level quantizers attempt to overcome this problem by providing a zero level for small amplitudes of the residual signal and two other side levels for large amplitudes.

The performance of the color image coding algorithms described earlier has been studied using a three-level quantizer with input-output characteristics given in Fig. 6.4b. In this figure, let $r(1)=\Delta$, $r(3)=-\Delta$, $d(1)=-d$, and $d(2)=d$. In this case the quantized residual signal can be written in the form

$$e_q(n_1,n_2)=\begin{cases}\Delta & e(n_1,n_2)\geq d\\ 0 & -d<e(n_1,n_2)<d\\ -\Delta & e(n_1,n_2)\leq -d\end{cases} \tag{6.19}$$

where the reconstruction and decision levels control the dynamic range of the residual signal.

Two different examples are considered here. In the first example we assume that Δ is constant and $d=\frac{\Delta}{2}$. Fig. 6.14 shows the results of the simulated reconstructed images using a linear predictive model of the second order and a uniform fixed three-level quantizer with $\Delta=6$ and $d=3$. As in the previous section the four different procedures for determining linear prediction parameters are applied in this example. The SNR results are shown in Table 6.6. In the second example we assume a uniform three-

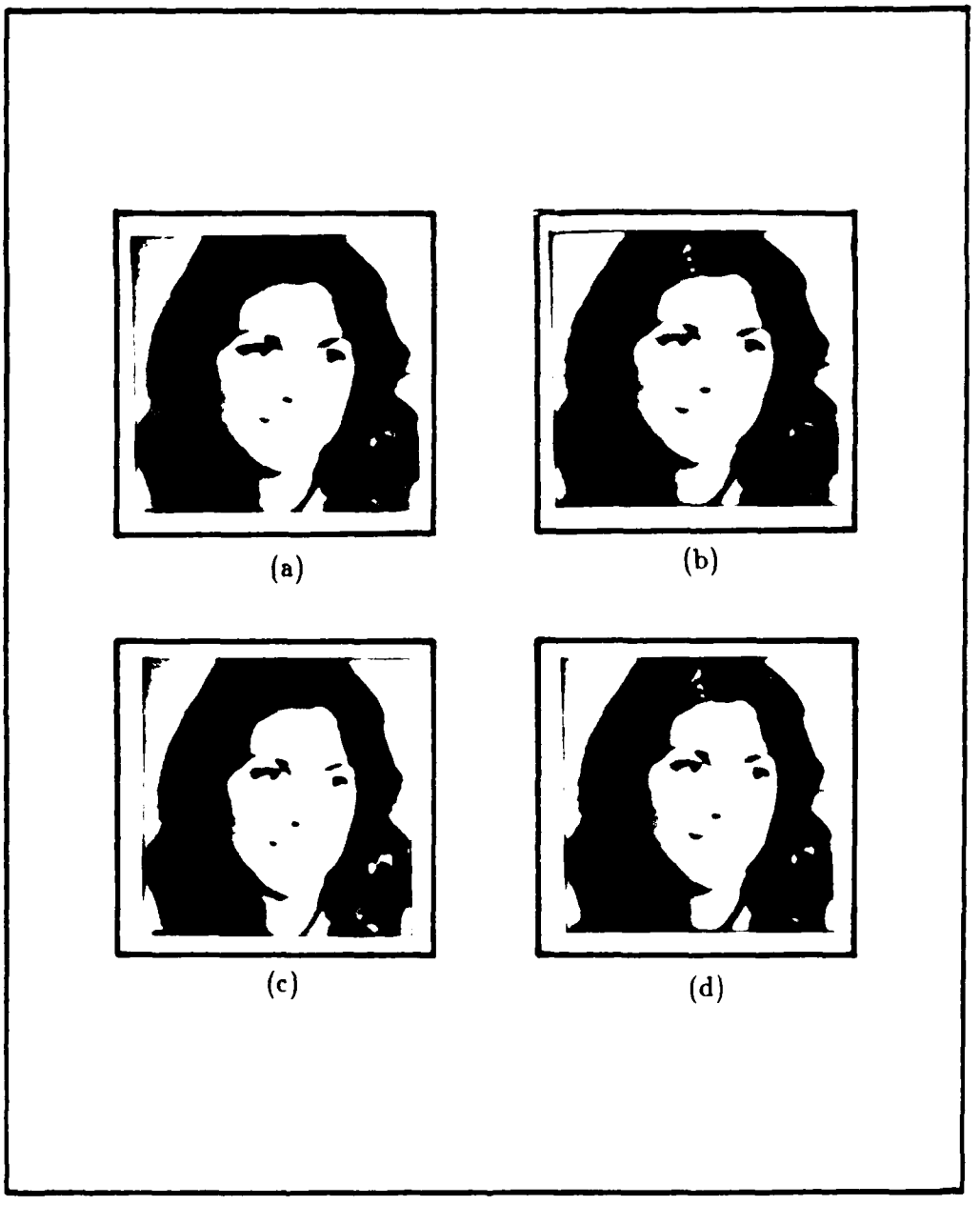

Fig. 6.14 Coded images $(\Delta = 6,\ d = 3)$.
(a) First procedure (b) Second procedure
(c) Third procedure (d) Fourth procedure

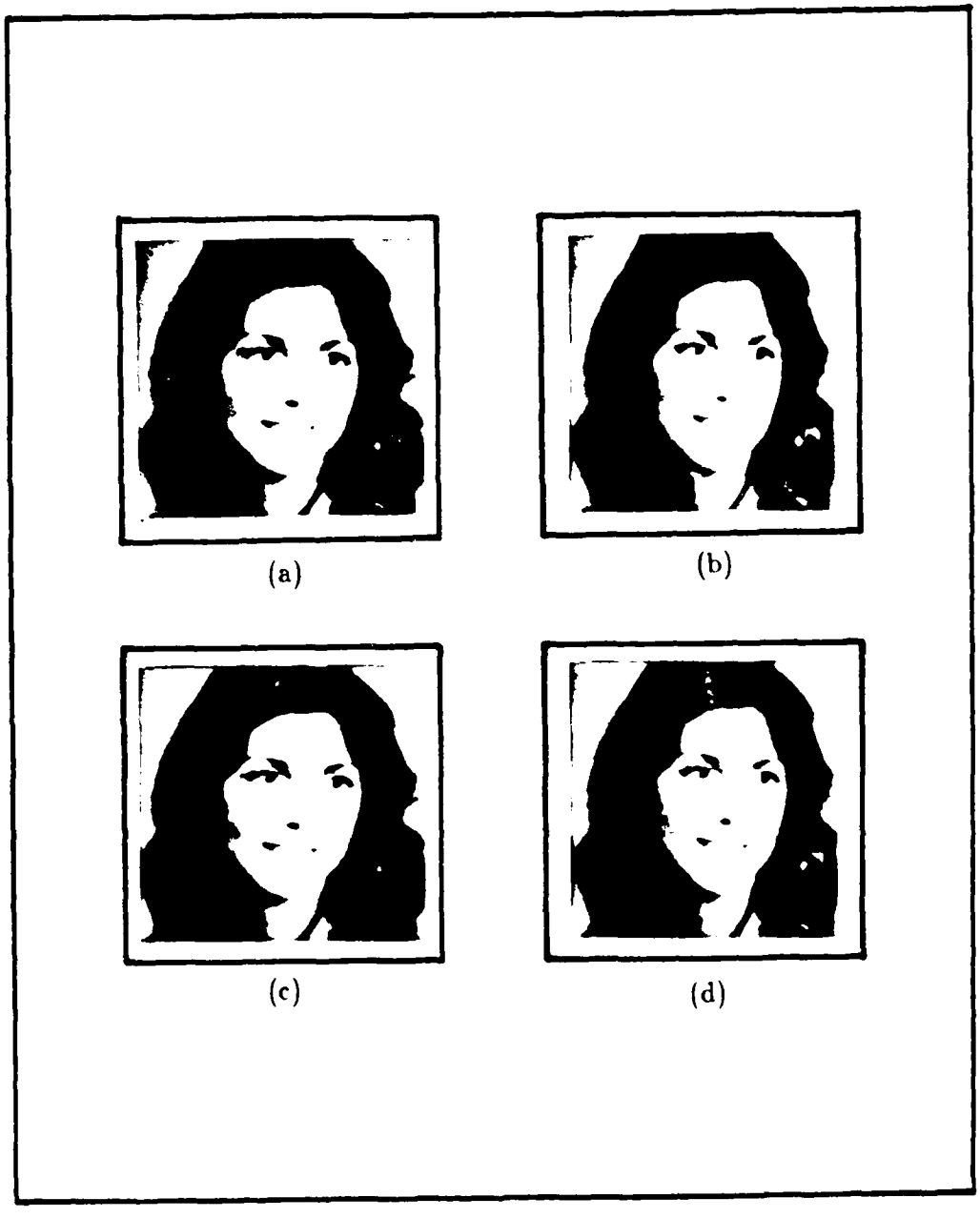

Fig. 6.15 Coded images using 3-level quantizer and second order linear predictive model $(\gamma = 3,\ \rho = 1.3)$.
(a) First procedure (b) Second procedure
(c) Third procedure (d) Fourth procedure

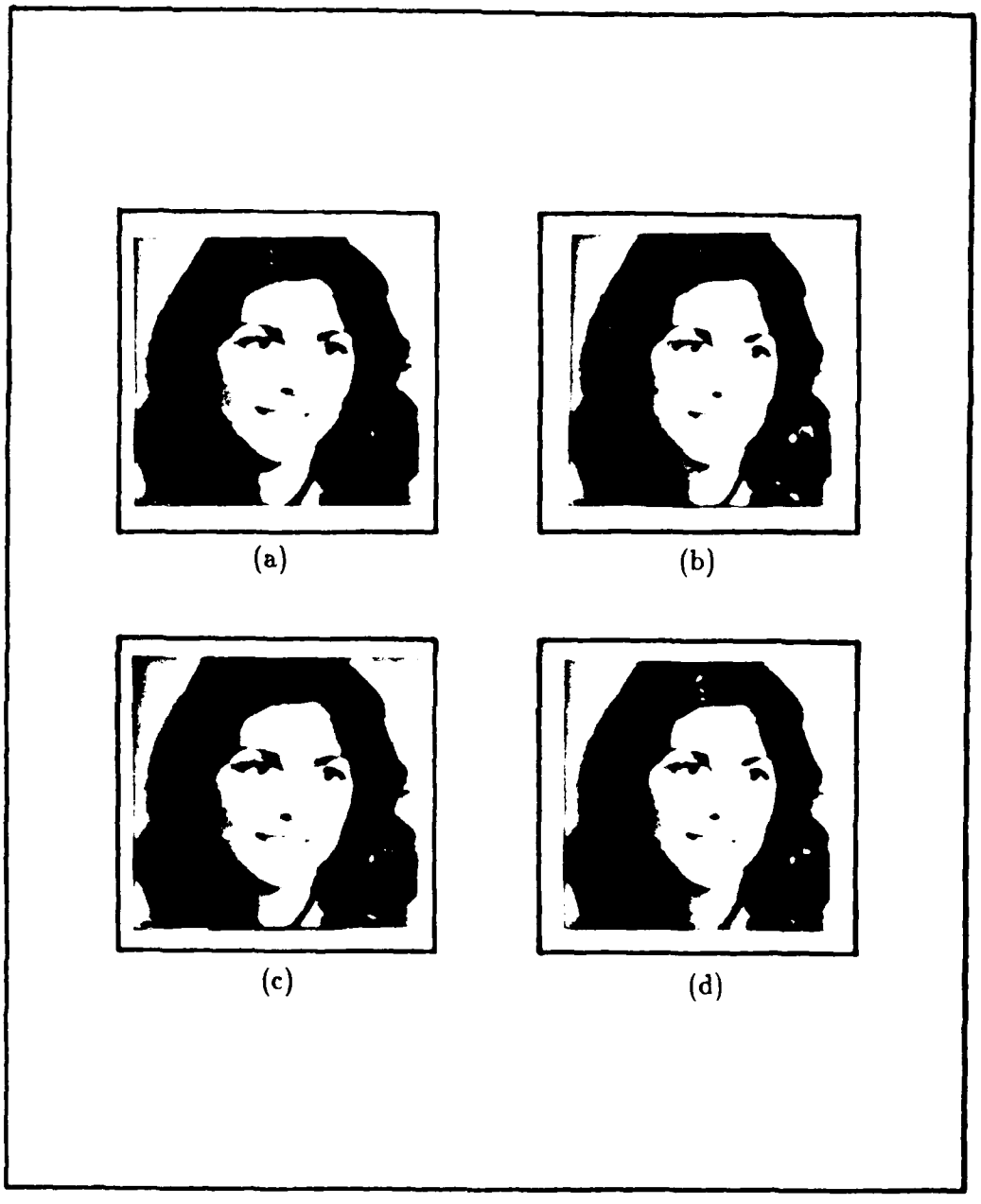

Fig. 6.16 Coded images using 3-level quantizer and third order linear predictive model $(\gamma = 2,\ \rho = 1.3)$.
(a) First procedure (b) Second procedure
(c) Third procedure (d) Fourth procedure

TABLE 6.6 SNR FOR CODED IMAGES USING 3-LEVEL QUANTIZER WITH $\Delta=6, d=3$

Procedure	Red	Green	Blue
First Procedure	22.97	22.23	18.32
Second Procedure	22.64	21.16	17.92
Third Procedure	22.54	21.25	17.74
Fourth Procedure	22.50	21.15	17.68

TABLE 6.7 SNR FOR CODED IMAGES USING 3-LEVEL QUANTIZER AND SECOND ORDER PREDICTIVE MODEL WITH $\gamma=2, \rho=1.3$

Procedure	Red	Green	Blue
First Procedure	19.73	18.07	16.02
Second Procedure	19.72	17.16	15.40
Third Procedure	19.45	17.43	15.02
Fourth Procedure	19.38	17.35	14.64

TABLE 6.8 SNR FOR CODED IMAGE USING 3-LEVEL QUANTIZER AND THIRD ORDER PREDICTIVE MODEL WITH $\gamma=2, \rho=1.3$

Procedure	Red	Green	Blue
First Procedure	19.79	18.16	16.39
Second Procedure	19.76	17.11	15.33
Third Procedure	19.51	17.43	14.98
Fourth Procedure	19.35	17.39	14.38

VII. CONCLUSIONS

This thesis described model-based methods for spectral estimation of multiple 2-D signals. Multichannel 2-D power spectral estimation based on AR modeling was studied extensively. We presented the multichannel models and gave an extension of the Jackson-Chien procedure for combining two quadrant-based estimates into a single combined estimate for the spectral matrix. The latter was called the combined quadrant(CQ) method. We further presented a method for estimation of the model parameters directly from the data. We also proposed a measure for comparing the closeness of two spectral estimates based on the divergence. Forward and backward NSHP models were shown to produce *different* estimates for the spectral matrix but the estimates were observed to get close to each other as the order of the model increased. Both the maximum likelihood method (MLM) of spectral estimation and the Improved MLM were extended to estimate the spectral matrix of auto- and cross-spectra for multiple 2-D random processes. Finally the multichannel 2-D spectral analysis models were applied to the problem of image coding.

Several examples were given of computed spectra and extensive experimental studies of performance were carried out. Phase estimates of the cross spectra for all of the methods were consistently accurate and were relatively insensitive to noise. Peak location for narrowband cases of sinusoids in noise was however noise sensitive and showed more bias with increased noise level.

In comparing the methods presented, the CQ spectral estimate compared favorably with the NSHP estimates and typically required less computation. Comparisons between the NSHP and CQ methods were made both qualitatively and quantitatively using a variety of test cases. The multichannel MLM was found experimentally to give better results than those obtained when the auto- and cross-spectra are estimated separately by MLM. Experimental results show that MLM has generally poorer resolution than AR based methods. However the IMLM appears to have almost comparable resolution to the AR. Finally, the application of spectral analysis models to color image coding shows

that we can overcome the real time computational problem involved in computing the predictive coefficients by using fixed coefficient matrices derived from a representative set of training images. This reduces complexity of the coding and eliminates the need to transmit side information.

This thesis can be considered as a first attempt at spectral analysis of multichannel two-dimensional random processes. More experience needs to be gathered in application of these methods to practical problems involving measured data. Further, other methods of spectral analysis such as the signal and noise subspace methods were not studied in this work and could be explored. In addition further application of multichannel models to image coding should be looked at. The latter topic was dealt with only as a brief excursion here but the results obtained are quite encouraging.

APPENDIX (A)

2--D BURG ALGORITHM

As mentioned in Chapter II, Burg developed an algorithm for estimating 1-D linear prediction parameters directly from the data. No estimation of the autocorrelation function is required in this algorithm. Given the 2-D reflection coefficient representation developed by Marzetta, the 1-D Burg algorithm can be straightforwardly extended to the 2-D case as follows. Given a wide sense stationary 2-D random process with zero mean $x(n_1,n_2)$, the idea of forward linear prediction is to estimate the "present" sample from a weighted sum of the "past" samples.

$$\hat{x}(n_1,n_2) = - \sum_{\substack{(i_1,i_2)\varepsilon\alpha \\ (i_1,i_2)\neq(0,0)}} a_{i_1 i_2} x(n_1-i_1,n_2-i_2) \tag{A.1}$$

where α represents the filter region of support and $a_{i_1 i_2}$ represent the filter coefficients. Similarly, the estimated value of the sample using backward linear prediction can be written as

$$\hat{x}'(n_1,n_2) = - \sum_{\substack{(i_1,i_2)\varepsilon\alpha \\ (i_1,i_2)\neq(0,0)}} a_{i_1 i_2} x(n_1+i_1,n_2+i_2) \tag{A.2}$$

where we have taken account of the fact that the single channel forward and backward linear predictive filters parameters are the same. Then the forward and the backward error signals $\varepsilon(n_1,n_2)$ and $\varepsilon'(n_1,n_2)$ can be expressed by

$$\varepsilon(n_1,n_2) = \sum_{(i_1,i_2)\varepsilon\alpha} a_{i_1 i_2} x(n_1-i_1,n_2-i_2) \tag{A.3}$$

$$\varepsilon'(n_1,n_2) = \sum_{(i_1,i_2)\varepsilon\alpha} a_{i_1 i_2} x(n_1+i_1,n_2+i_2) \tag{A.4}$$

where $a_{00} = 1$. These values of the error signals for order (p_1,p_2) can be written recursively as

$$\varepsilon^{(p_1,p_2)}(n_1,n_2) = \varepsilon^{(p_1,p_2-1)}(n_1,n_2) - K^{(p_1,p_2)}\,\varepsilon'^{(p_1,p_2-1)}(n_1-p_1,n_2-p_2) \tag{A.5}$$

$$\varepsilon'^{(p_1,p_2)}(n_1,n_2) = \varepsilon'^{(p_1,p_2-1)}(n_1,n_2) - K'^{(p_1,p_2)}\,\varepsilon^{(p_1,p_2-1)}(n_1+p_1,n_2+p_2) \tag{A.6}$$

where $K^{(p_1,p_2)}$ and $K'^{(p_1,p_2)}$ represent the forward and backward reflection coefficients respectively. Then the corresponding forward and backward filter of order (p_1,p_2) can be recursively estimated as

$$H^{(p_1,p_2)}(z_1,z_2) = H^{(p_1,p_2-1)}(z_1,z_2) - z_1^{-p_1}\,z_2^{-p_2}\,K^{(p_1,p_2)}\,H'^{(p_1,p_2-1)}(z_1^{-1},z_2^{-1}) \tag{A.7}$$

$$H'^{(p_1,p_2)}(z_1,z_2) = H'^{(p_1,p_2-1)}(z_1,z_2) - z_1^{p_1}\,z_2^{p_2}\,K'^{(p_1,p_2)}\,H^{(p_1,p_2-1)}(z_1^{-1},z_2^{-1}) \tag{A.8}$$

Defining the total estimated error power P as the average of all possible computed forward and backward squared error signals for the data results in

$$P = E\left\{\left[\varepsilon(n_1,n_2)\right]^2 + \left[\varepsilon'(n_1,n_2)\right]^2\right\} \tag{A.9}$$

By substituting Eqns. (A.5) and (A.6) into Eqn. (A.9), the power $P^{(p_1,p_2)}$ can be expressed as

$$\begin{aligned} P^{(p_1,p_2)} = E\ &\left[\varepsilon^{(p_1,p_2-1)}(n_1,n_2) - K^{(p_1,p_2)}\varepsilon'^{(p_1,p_2-1)}(n_1-p_1,n_2-p_2)\right]^2 \\ &+ \left[\varepsilon'^{(p_1,p_2-1)}(n_1,n_2) - K'^{(p_1,p_2)}\varepsilon^{(p_1,p_2-1)}(n_1+p_1,n_2+p_2)\right]^2 \end{aligned} \tag{A.10}$$

To find the best least square estimate, the total power is minimized with respect to the reflection coefficient parameter i.e.

$$\frac{\partial P^{(p_1,p_2)}}{\partial K^{(p_1,p_2)}} = 0 \tag{A.11}$$

The solution of Eqn. (A.11) is found to be

$$K^{(p_1,p_2)} = \frac{2 \sum_{(n_1,n_2)\in\alpha} \left[\varepsilon^{(p_1,p_2-1)}(n_1,n_2)\, \varepsilon'^{(p_1,p_2-1)}(n_1-p_1,n_2-p_2) \right]}{\sum_{(n_1,n_2)\in\alpha} \left[\left[\varepsilon^{(p_1,p_2-1)}(n_1,n_2) \right]^2 + \left[\varepsilon'^{(p_1,p_2-1)}(n_1-p_1,n_2-p_2) \right]^2 \right]} \quad \text{(A.12)}$$

Then the average power can take the form (Marzetta,1978)

$$P^{(p_1,p_2)} = P^{(p_1,p_2-1)} \left[1 - \left[K^{(p_1,p_2)} \right]^2 \right] \quad \text{(A.13)}$$

Now, to begin the computation, the order (p_1,p_2) is set to (0,0) with the initial conditions:

$$H^{(0,0)}(z_1,z_2) = 1 \quad \text{(A.14a)}$$

$$\varepsilon^{(0,0)}(n_1,n_2) = x(n_1,n_2) \quad \text{(A.14b)}$$

$$\varepsilon'^{(0,0)}(n_1,n_2) = x(n_1,n_2) \quad \text{(A.14c)}$$

and

$$P^{(0,0)} = E\left[\left[\varepsilon^{(0,0)}(n_1,n_2) \right]^2 + \varepsilon'^{(0,0)} \left[(n_1,n_2) \right]^2 \right] \quad \text{(A.14d)}$$

For p_1=0 and $(1 \le p_2 < P_2)$ or for $(1 \le p_1 < P_1)$ and $(-P_2 < p_2 < P_2)$, $H^{(p_1,p_2)}(z_1,z_2)$ is computed recursively from Eqn. (A.7). Also the forward and backward error signals are computed recursively from Eqns. (A.5) and (A.6). Between adjacent columns the following relations are used for the transition of the recursion:

$$H^{(p_1,-p_2-1)}(z_1,z_2) = H^{(p_1-1,p_2)}(z_1,z_2) \quad \text{(A.15a)}$$

$$P^{(p_1,-p_2-1)} = P^{(p_1-1,p_2)} \quad \text{(A.15b)}$$

$$\varepsilon^{(p_1,-p_2-1)}(n_1,n_2) = \varepsilon^{(p_1-1,p_2)}(n_1,n_2) \quad \text{(A.15c)}$$

$$\varepsilon'^{(p_1,-p_2-1)}(n_1,n_2) = \varepsilon'^{(p_1-1,p_2)}(n_1,n_2) \quad \text{(A.15d)}$$

The latter equations also appear in Marzetta's 2-D Levinson recursion and give a true minimum phase filter when the order parameter P_2 is infinity.

APPENDIX (B)

LEVINSON WIGGINS ROBINSON (LWR) ALGORITHM

In this appendix the computational procedure of 1-D multichannel Levinson recursion known as the LWR algorithm is described. Let $\mathbf{x}(n)$ be a wide sense stationary M-channel 1-D random process.

$$\mathbf{x}(n) = \begin{bmatrix} x_1(n) \\ x_2(n) \\ \cdot \\ \cdot \\ \cdot \\ x_M(n) \end{bmatrix} \tag{B.1}$$

Then the forward linear predictive filter of order P applied to the data can be expressed as

$$\varepsilon(n) = \sum_{i=0}^{P_1-1} \left[\alpha^{(i)}\right]^T \mathbf{x}(n-i) \tag{B.2}$$

or

$$\varepsilon(n) = \alpha^T \mathbf{x}_n \tag{B.3}$$

where α represents the block matrix of the filter coefficients.

$$\alpha = \begin{bmatrix} \mathbf{I} \\ \alpha^{(1)} \\ \cdot \\ \cdot \\ \cdot \\ \alpha^{(P-1)} \end{bmatrix} \tag{B.4}$$

where

$$\alpha^{(i)} = \begin{bmatrix} \alpha_{00}^{(i)} & \alpha_{01}^{(i)} & \cdots & \alpha_{0,P-1}^{(i)} \\ \alpha_{10}^{(i)} & \alpha_{11}^{(i)} & \cdots & \alpha_{1,P-1}^{(i)} \\ \cdot & \cdot & & \cdot \\ \cdot & \cdot & & \cdot \\ \cdot & \cdot & & \cdot \\ \alpha_{p-1,0}^{(i)} & \alpha_{p-1,1}^{(i)} & \cdots & \alpha_{p-1,P-1}^{(i)} \end{bmatrix} \tag{B.5}$$

and $\mathbf{x}_n$ is an vector of the ordered values $\mathbf{x}(n-i)$

$$\mathbf{x}_n = \begin{bmatrix} \mathbf{x}(n) \\ \mathbf{x}(n-1) \\ \cdot \\ \cdot \\ \cdot \\ \mathbf{x}(n-P) \end{bmatrix} \tag{B.6}$$

The corresponding Normal equations are

$$\mathbf{R}\,\boldsymbol{\alpha} = \mathbf{E} \tag{B.7}$$

or

$$\begin{bmatrix} \mathbf{R}(0) & \mathbf{R}(-1) & \cdots & \mathbf{R}(-P+1) \\ \mathbf{R}(1) & \mathbf{R}(0) & \cdots & \mathbf{R}(-P+2) \\ \cdot & \cdot & & \cdot \\ \cdot & \cdot & & \cdot \\ \cdot & \cdot & & \cdot \\ \mathbf{R}(P-1) & \mathbf{R}(P-2) & \cdots & \mathbf{R}(0) \end{bmatrix} \begin{bmatrix} \mathbf{I} \\ \boldsymbol{\alpha}^{(1)} \\ \cdot \\ \cdot \\ \cdot \\ \boldsymbol{\alpha}^{(P-1)} \end{bmatrix} = \begin{bmatrix} \mathbf{E}^{(P)} \\ \mathbf{0} \\ \cdot \\ \cdot \\ \cdot \\ \mathbf{0} \end{bmatrix} \tag{B.8}$$

where

$$\mathbf{R}(k) = E\left[\mathbf{x}(n)\,\mathbf{x}^T(n-k)\right] \tag{B.9}$$

and $\mathbf{E}^{(P)}$ is the error covariance of the optimal estimate.

$$\mathbf{E}^{(P)} = E\left[(\mathbf{x}_n - \hat{\mathbf{x}}_n)(\mathbf{x}_n - \hat{\mathbf{x}}_n)^T\right] \tag{B.10}$$

Similarly the backward linear predictive filter can be written in the following form

$$\varepsilon'(n-P+1) = \sum_{i=0}^{P-1} \left[\beta^{(i)}\right]^T \mathbf{x}(n-P+1+i) \tag{B.11}$$

where $\beta^{(i)}$ are the backward multichannel 1-D filter coefficient matrices. The corresponding Normal equations are

$$\mathbf{R}\,\beta = \mathbf{E}' \tag{B.12}$$

or

$$\begin{bmatrix} \mathbf{R}(0) & \mathbf{R}(1) & \ldots & \mathbf{R}(P-1) \\ \mathbf{R}(-1) & \mathbf{R}(0) & \ldots & \mathbf{R}(P-2) \\ . & . & & . \\ . & . & & . \\ . & . & & . \\ \mathbf{R}(-P+1) & \mathbf{R}(-P+2) & \ldots & \mathbf{R}(0) \end{bmatrix} \begin{bmatrix} \mathbf{I} \\ \beta^{(1)} \\ . \\ . \\ . \\ \beta^{(P-1)} \end{bmatrix} = \begin{bmatrix} \mathbf{E}'^{(P)} \\ \mathbf{0} \\ . \\ . \\ . \\ \mathbf{0} \end{bmatrix} \tag{B.13}$$

where $\mathbf{E}'^{(P)}$ represents the backward error covariance matrix.

$$\mathbf{E}'^{(P)} = E\left[\varepsilon'(n)\,\varepsilon'^{T}(n)\right] \tag{B.14}$$

Note that since from Eqn. (B.9) we have

$$\mathbf{R}(k) = \mathbf{R}^T(-k) \tag{B.15}$$

and the blocks of the correlation matrix in (B.13) are the transposes of the blocks of the matrix in (B.8). The solution of Equations (B.8) and (B.13) for forward and backward filter coefficients can be done recursively by relating the order (p) to the order (p-1) as follows

$$\alpha^{(p)} = \begin{bmatrix} \alpha^{(p-1)} \\ ..... \\ \mathbf{0} \end{bmatrix} - \begin{bmatrix} \mathbf{0} \\ ..... \\ \tilde{\beta}^{(p-1)} \end{bmatrix} \mathbf{K}^{(p)} \tag{B.16a}$$

$$\beta^{(p)} = \begin{bmatrix} \beta^{(p-1)} \\ \cdots\cdots \\ 0 \end{bmatrix} - \begin{bmatrix} 0 \\ \cdots\cdots \\ \tilde{\alpha}^{(p-1)} \end{bmatrix} K'^{(p)} \qquad \textbf{(B.16b)}$$

where $\tilde{\alpha}^{(p-1)}$ and $\tilde{\beta}^{(p-1)}$ are the block reverses of $\alpha^{(p-1)}$ and $\beta^{(p-1)}$ respectively, and $K^{(p)}$ and $K'^{(p)}$ represent the forward and backward reflection coefficient (or partial correlation) matrices of order (p) respectively. These can also be computed recursively as follows

$$K^{(p)} = \left[E'^{(p-1)} \right]^{-1} \Delta^{(p)} \qquad \text{(B.17a)}$$

$$K'^{(p)} = \left[E^{(p-1)} \right]^{-1} \left[\Delta^{(p)} \right]^{T} \qquad \text{(B.17b)}$$

where

$$\Delta^{(p)} = \left[R^{T}(1) \;\; R^{T}(2) \;\; \ldots \;\; R^{T}(p) \right] \tilde{\alpha}^{(p-1)} \qquad \text{(B.18)}$$

$$E^{(p)} = E^{(p-1)} \left[I - K'^{(p)} K^{(p)} \right] \qquad \text{(B.19a)}$$

and

$$E'^{(p)} = E'^{(p-1)} \left[I - K^{(p)} K'^{(p)} \right] \qquad \text{(B.19b)}$$

Details of the derivation of these results can be found in (Strand,1977).

APPENDIX (C)

MULTICHANNEL 1–D BURG ALGORITHM

A multichannel 1-D Burg algorithm was first developed by Nuttall (1976) and Strand (1977) independently. The idea is to compute the reflection coefficients matrices directly from the data instead of estimating the autocorrelation function and from these compute the filter parameters. Thus the multichannel 1-D Burg algorithm uses the LWR algorithm (Appendix B), except that the reflection coefficient matrices are computed from the available data.

Assume we have M-channels with N samples and define the following terms

$$F = \frac{1}{N_P} \sum_{n=1}^{N_P} \varepsilon^{(p)}(n) \left[\varepsilon^{(p)}(n) \right]^T \tag{C.1a}$$

$$B = \frac{1}{N_P} \sum_{n=1}^{N_P} \varepsilon'^{(p)}(n) \left[\varepsilon'^{(p)}(n) \right]^T \tag{C.1b}$$

$$G = \frac{1}{N_P} \sum_{n=1}^{N_P} \varepsilon'^{(p)}(n) \left[\varepsilon^{(p)}(n) \right]^T \tag{C.1c}$$

where $N_P = N - P$ (P represents the order of the filter), and $\varepsilon^{(p)}(n)$ and $\varepsilon'^{(p)}(n)$ represents the forward and backward error signals respectively. Then the matrix $\Delta^{(p)}$ defined in Appendix B is obtained as the solution of the bilinear equation

$$C_1 \Delta^{(p)} + \Delta^{(p)} C_2 = C_3 \tag{C.2}$$

where

$$C_1 = \left[\mathbf{E}'^{(p-1)} \right]^{-1} B \tag{C.3a}$$

$$C_2 = \left[\mathbf{E}^{(p-1)} \right]^{-1} F \tag{C.3b}$$

$$C_3 = -2G \tag{C.3c}$$

and where $\mathbf{E}^{(p-1)}$ and $\mathbf{E}'^{(p-1)}$ represent the error covariance matrices of the forward and backward linear predictive filters respectively.

There are several approaches that can be used to obtain explicit solutions to Equation (C.2). One form of the solution is given by Pease (1965) (Kucera,1974; Hartwig,1972,1975). The basic idea of this method is to transform Eqn. (C.2) into an equivalent vector form

$$Q\left[c_s\ \Delta^{(p)}\right] = \left[c_s\ C_3\right] \tag{C.4}$$

where $\left[c_s\ \Delta^{(p)}\right]$ represents the column string of $\Delta^{(p)}$

$$c_s\ \Delta^{(p)} = \left[\Delta_{11}^{(p)} \cdots \Delta_{M1}^{(p)}\ \Delta_{12}^{(p)} \cdots \Delta_{M2}^{(p)} \cdots \Delta_{MM}^{(p)}\right]^T \tag{C.5}$$

and $\left[c_s\ C_3\right]$ represents the column string of C_3 and where

$$Q = C_1 \otimes I_M + I_M \otimes C_2^T \tag{C.6}$$

where I_M is an $(M \times M)$ identity matrix. Thus having solved Eqn. (C.4) for $\Delta^{(p)}$, the reflection coefficient matrices $\mathbf{K}^{(p)}$ and $\mathbf{K}'^{(p)}$ can be found from (B.17) and the forward and backward error can be written recursively in the form

$$\boldsymbol{\varepsilon}^{(p)}(n) = \boldsymbol{\varepsilon}^{(p-1)}(n) - \left[\mathbf{K}^{(p)}\right]^T \boldsymbol{\varepsilon}'^{(p-1)}(n) \tag{C.7a}$$

$$\boldsymbol{\varepsilon}'^{(p)}(n) = \boldsymbol{\varepsilon}'^{(p-1)}(n+1) - \left[\mathbf{K}'^{(p)}\right]^T \boldsymbol{\varepsilon}^{(p-1)}(n+1) \tag{C.7b}$$

Now, assuming $\mathbf{x}(n)$ is a an M-channel random process, the recursive algorithm can start with the following initial conditions:

$$\alpha^{(0)} = \beta^{(0)} = \mathbf{I}_M$$

$$\varepsilon^{(0)}(n) = \mathbf{x}(n)$$

$$\varepsilon'^{(0)}(n) = \mathbf{x}(n)$$

$$\mathbf{E}^{(0)} = \mathbf{E}'^{(0)} = \frac{1}{N} \sum_{n=1}^{N} \varepsilon^{(0)}(n) \left[\mathbf{e}'^{(0)}(n) \right]^T$$

where $\alpha^{(0)}$ and $\beta^{(0)}$ are the forward and backward filter coefficients respectively, of order zero. Using Eqn. (C.1) the values F, B, and G can be computed which are used for solving Eqn. (C.4) to obtain $\Delta^{(p)}$. The reflection coefficient matrices are then computed from (B.17), and (B.16) and (B.19) of the LWR algorithm are used for computing the next order filter coefficients and error covariances.

APPENDIX (D)

MULTICHANNEL 2–D BURG ALGORITHM

As we mentioned in Chapter III section G a 2-D multichannel Burg algorithm can be developed as a straightforward combination of the 2-D Burg algorithm (Appendix A), and the 1-D multichannel Burg algorithm (Appendix C). Assume that the multichannel 2-D random process $\mathbf{x}(n_1,n_2)$ generating the (N_1,N_2) M-channel data points is zero mean and wide sense stationary. The present value $\mathbf{x}(n_1,n_2)$ can be predicted approximately from a linear weighted sum of the past values.

$$\hat{\mathbf{x}}(n_1,n_2) = -\sum_{\substack{(i_1,i_2)\in\alpha \\ (i_1,i_2)\neq(0,0)}} \mathbf{A}_{i_1i_2}^T \mathbf{x}(n_1-i_1,n_2-i_2) \tag{D.1a}$$

This is called a forward prediction, because $\mathbf{x}(n_1,n_2)$ is predicted ahead, in terms of "previous" values. Similarly we consider the backward prediction

$$\hat{\mathbf{x}}'(n_1,n_2) = -\sum_{\substack{(i_1,i_2)\in\alpha \\ (i_1,i_2)\neq(0,0)}} \mathbf{B}_{i_1i_2}^T \mathbf{x}(n_1+i_1,n_2+i_2) \tag{D.1b}$$

where the $\mathbf{B}_{i_1i_2}$ represent the backward filter coefficients. (Note that the region α is the same although the prediction matrices are not). Thus the forward and backward prediction errors can be written as

$$\boldsymbol{\varepsilon}(n_1,n_2) = \sum_{(i_1,i_2)\in\alpha} \mathbf{A}_{i_1i_2}^T \mathbf{x}(n_1-i_1,n_2-i_2) \tag{D.2a}$$

$$\boldsymbol{\varepsilon}'(n_1,n_2) = \sum_{(i_1,i_2)\in\alpha} \mathbf{B}_{i_1i_2}^T \mathbf{x}(n_1+i_1,n_2+i_2) \tag{D.2b}$$

where $\mathbf{A}_{00} = \mathbf{B}_{00} = I$. The forward and backward filter of the order (p_1,p_2) can be recursively estimated from

$$\mathbf{H}^{(p_1,p_2)}(z_1,z_2) = \mathbf{H}^{(p_1,p_2-1)}(z_1,z_2) - z_1^{-p_1}\, z_2^{-p_2}\, \mathbf{K}^{(p_1,p_2)^T}\, \mathbf{H}^{\wedge(p_1,p_2-1)}(z_1^{-1},z_2^{-1})$$

(D.3a)

$$\mathbf{H}^{\wedge(p_1,p_2)}(z_1,z_2) = \mathbf{H}^{\wedge(p_1,p_2-1)}(z_1,z_2) - z_1^{p_1}\, z_2^{p_2}\, \mathbf{K}^{\wedge(p_1,p_2)^T}\, \mathbf{H}^{(p_1,p_2-1)}(z_1^{-1},z_2^{-1})$$

(D.3b)

where $\mathbf{K}^{(p_1,p_2)}$ and $\mathbf{K}^{\wedge(p_1,p_2)}$ are the forward and backward reflection coefficient matrices of order (p_1,p_2) with dimension $(M\times M)$. The forward prediction error $\boldsymbol{\varepsilon}^{(p_1,p_2)}(n_1,n_2)$ and the backward prediction error $\boldsymbol{\varepsilon}^{\wedge(p_1,p_2)}(n_1,n_2)$ of order (p_1,p_2) can be written recursively in the following forms

$$\boldsymbol{\varepsilon}^{(p_1,p_2)}(n_1,n_2) = \boldsymbol{\varepsilon}^{(p_1,p_2-1)}(n_1,n_2) - \mathbf{K}^{(p_1,p_2)^T}\, \boldsymbol{\varepsilon}^{\wedge(p_1,p_2-1)}(n_1-p_1,n_2-p_2)$$

(D.4a)

$$\boldsymbol{\varepsilon}^{\wedge(p_1,p_2)}(n_1,n_2) = \boldsymbol{\varepsilon}^{\wedge(p_1,p_2-1)}(n_1,n_2) - \mathbf{K}^{\wedge(p_1,p_2)^T}\, \boldsymbol{\varepsilon}^{(p_1,p_2-1)}(n_1+p_1,n_2+p_2)$$

(D.4b)

The reflection coefficients are estimated by straightforward extension of the procedures for 1-D multichannel Burg algorithm (see Appendix C Eqns. (C.2)-(C.5)) and will not be detailed here.

APPENDIX (E)

MULTICHANNEL 2–D INCREMENTAL DIVERGENCE MEASUREMENT

The incremental divergence $\Delta J(1,2)$ between two multichannel random processes used in Chapter III can be expressed in terms of filter parameters or in terms of spectral estimates as follows.

1. In Terms of Filter Parameters

$$\Delta J(1,2) = -M + \frac{1}{2}\left\{ tr\ \mathbf{A}_2\mathbf{R}_1\mathbf{A}_2^T\boldsymbol{\Sigma}_2^{-1} + tr\ \mathbf{A}_1\mathbf{R}_2\mathbf{A}_1^T\boldsymbol{\Sigma}_1^{-1} \right\} \tag{E.1}$$

where M represents the number of channels, $\mathbf{A}_k$ (k=1,2) represents the set of filter coefficients of the process k, $\mathbf{R}_k$ is the entire covariance matrix of the process k, and finally $\boldsymbol{\Sigma}_k$ is the error covariance matrix of process k.

2. In Terms of Spectral Estimates

$$\Delta J(1,2) = -M + \frac{1}{8\pi^2} \int_{-\pi}^{\pi}\int_{-\pi}^{\pi} tr\ \mathbf{S}_1(\omega_1,\omega_2)\mathbf{S}_2^{-1}(\omega_1,\omega_2)d\omega_1 d\omega_2 \tag{E.2}$$

$$+ \int_{-\pi}^{\pi}\int_{-\pi}^{\pi} tr\ \mathbf{S}_2(\omega_1,\omega_2)\mathbf{S}_1^{-1}(\omega_1,\omega_2)d\omega_1 d\omega_2$$

where $\mathbf{S}_1$ and $\mathbf{S}_2$ are the $M \times M$ spectral matrices of the modeled random processes.

Proof

For this proof it is important to note that we regard the two linear predictive filters as fixed and that $\varepsilon_k(n_1,n_2)$ k=1,2 represents the output of the corresponding filter regardless of the input. Therefore when the input to the first linear predictive filter is the

process to which it is matched the output $\varepsilon_1(n_1,n_2)$ will be the minimum mean-square prediction error process. Where the input is the other random process will still call the output $\varepsilon_1(n_1,n_2)$ but in this case it will *not* be a minimum mean-square prediction error process.

1. In Terms of Filter Parameters

When the input to a linear predictive filter matched to a random process k is $\mathbf{x}(n_1,n_2)$ the output $\varepsilon_k(n_1,n_2)$ is given by

$$\varepsilon_k(n_1,n_2) = \mathbf{x}(n_1,n_2) - \hat{\mathbf{x}}(n_1,n_2) \tag{E.3}$$

where

$$\hat{\mathbf{x}}(n_1,n_2) = - \sum_{\substack{(i_1,i_2)\in\alpha \\ (i_1,i_2)\neq(0,0)}} \mathbf{A}_k(i_1,i_2)^T \mathbf{x}(n_1-i_1,n_2-i_2) \tag{E.4}$$

and where α represents the filter region of support.

When the input is the random process k to which the filter is matched, the output is the minimum mean-square prediction error for random process k. In this case the error covariance matrix of the output can be defined by

$$\Sigma_k = E_k\left[\varepsilon_k(n_1,n_2)\,\varepsilon_k^T(n_1,n_2)\right] \tag{E.5}$$

where E_k denotes expectation under the hypothesis that the input $\mathbf{x}(n_1,n_2)$ is random process k. If the input is Gaussian then the density function for the prediction error process is

$$f_k\left[\varepsilon_k(n_1,n_2)\right] = \frac{1}{(2\pi)^{\frac{M}{2}}\,|\Sigma_k|^{\frac{1}{2}}} \exp\left\{\frac{-1}{2}\left[\varepsilon_k^T(n_1,n_2)\,\Sigma_k^{-1}\,\varepsilon_k(n_1,n_2)\right]\right\} \tag{E.6}$$

The direct divergence or the mean information $I_\varepsilon(1,2)$ corresponding to the error process ε_1 and ε_2 is defined as

$$I_\varepsilon(1,2) = E_1\left[\Lambda_{1,2}\right] \tag{E.7}$$

where $\Lambda_{1,2}$ is the logarithm of the likelihood ratio

$$\Lambda_{1,2} = \log \frac{f_1\left[\varepsilon_1(n_1,n_2)\right]}{f_2\left[\varepsilon_2(n_1,n_2)\right]} \tag{E.8}$$

Note that since $\varepsilon_k(n_1,n_2)$ is uncorrelated with observations of the random process that appear on the right side of (E.4), $I_\varepsilon(1,2)$ represents the change in mean information that occurs when a new observation $\mathbf{x}(n_1,n_2)$ of the original random process is taken. If we substitute (E.6) and (E.8) in (E.7) then after some algebraic manipulation the direct divergence can be written in the form

$$I_\varepsilon(1,2) = \frac{1}{2} E_1\left[\varepsilon_2^T \Sigma_2^{-1} \varepsilon_2 - \varepsilon_1^T \Sigma_1^{-1} \varepsilon_1 - \log \frac{|\Sigma_1|}{|\Sigma_2|}\right] \tag{E.9}$$

Now observe that

$$E_1\left[\varepsilon_1^T \Sigma_1^{-1} \varepsilon_1\right] = tr\ \Sigma_1^{-1}\left[\varepsilon_1^T \varepsilon_1\right] = M \tag{E.10}$$

Thus Eqn. (E.9) takes the form

$$I_\varepsilon(1,2) = -\frac{M}{2} - \frac{1}{2}\log \frac{|\Sigma_1|}{|\Sigma_2|} + \frac{1}{2} E_1\left[\varepsilon_2^T \Sigma_2^{-1} \varepsilon_2\right] \tag{E.11}$$

If we rewrite Eqn. (E.3) as

$$\varepsilon_k(n_1,n_2) = \mathbf{A}_k^T \mathbf{x} \tag{E.12}$$

where $\mathbf{A}_k$ is a matrix of the filter coefficients (as defined in Chapter III section D) and $\mathbf{x}$ is a vector of the corresponding samples of the random process, then the final expression for the direct divergence can be obtained by substituting Eqn. (E.12) in the last term of Eqn. (E.11)

$$I_\varepsilon(1,2) = -\frac{M}{2} - \frac{1}{2}\log \frac{|\Sigma_1|}{|\Sigma_2|} + \frac{1}{2} tr\left[\mathbf{A}_2 \mathbf{R}_1 \mathbf{A}_2^T \Sigma_2^{-1}\right] \tag{E.13}$$

where

$$\mathbf{R}_1 = E_1\left[\mathbf{x}\,\mathbf{x}^T\right] \tag{E.14}$$

Similarly the mean information $I_\varepsilon(2,1)$ can be expressed by

$$I_\varepsilon(2,1) = -E_2\left[\Lambda_{1,2}\right] \tag{E.15}$$

where $E_2[\ .\ ]$ represents the expectation under f_2 and this leads to

$$I_\varepsilon(2,1) = -\frac{M}{2} - \frac{1}{2}\log\frac{|\Sigma_2|}{|\Sigma_1|} + \frac{1}{2}\,tr\left[\mathbf{A}_1\,\mathbf{R}_2\,\mathbf{A}_1^T\,\Sigma_1^{-1}\right] \tag{E.16}$$

The incremental divergence as we mentioned in Chapter II can be defined as

$$\Delta J(1,2) = I_\varepsilon(1,2) + I_\varepsilon(2,1) \tag{E.17}$$

Using Eqns. (E.13), (E.16) and (E.17) the incremental divergence measurement in terms of the filter parameters can finally be expressed in the form of (E.1).

2. In Terms of Spectral Estimates

The estimated power spectrum for a random process k using an autoregressive model can be expressed as (see Chapter IV):

$$\mathbf{S}_k(\omega_1,\omega_2) = \frac{1}{4\pi^2}\left[\mathbf{H}_k^{-1}(\omega_1,\omega_2)\,\Sigma_k\,\mathbf{H}_k^{H^{-1}}(\omega_1,\omega_2)\right] \tag{E.18}$$

and

$$\mathbf{H}_k(\omega_1,\omega_2) = \sum_{(n_1,n_2)\varepsilon\alpha}\mathbf{A}_k^T(n_1,n_2)e^{-j(\omega_1 n_1+\omega_2 n_2)} \tag{E.19}$$

where α is some chosen region of support and $\mathbf{A}_k(0,0)$ is the identity matrix. Now suppose $\mathbf{x}(n_1,n_2)$ represent either process 1 or 2 with zero mean and spectrum $\mathbf{S}_x(\omega_1,\omega_2)$, and let $\varepsilon_k(n_1,n_2)$ be defined by

$$\varepsilon_k(n_1,n_2) = \sum_{(i_1,i_2)\varepsilon\alpha} \mathbf{A}_k^T(i_1,i_2)\mathbf{x}(n_1-i_1,n_2-i_2) \tag{E.20}$$

Then

$$\mathbf{S}_{\varepsilon_k}(\omega_1,\omega_2) = \mathbf{H}_k(\omega_1,\omega_2)\,\mathbf{S}_x(\omega_1,\omega_2)\,\mathbf{H}_k^H(\omega_1,\omega_2) \tag{E.21}$$

By applying Parseval's theorem and using Eqn. (E.17) and the commutative properties of the trace we can take the expectation with respect to the random process **x** and write

$$E\left[\varepsilon_k^T(n_1,n_2)\,\Sigma_k^{-1}\,\varepsilon_k(n_1,n_2)\right] = tr\;\Sigma_k^{-1}\,E\left[\varepsilon_k(n_1,n_2)\,\varepsilon_k^T(n_1,n_2)\right]$$

$$= tr\int_{-\pi-\pi}^{\pi\,\pi}\Sigma_k^{-1}\,\mathbf{S}_{\varepsilon_k}(\omega_1,\omega_2)\,d\omega_1 d\omega_2$$

$$= tr\int_{-\pi-\pi}^{\pi\,\pi}\Sigma_k^{-1}\,\mathbf{H}_k(\omega_1,\omega_2)\,\mathbf{S}_x(\omega_1,\omega_2)\,\mathbf{H}_k^H(\omega_1,\omega_2)\,d\omega_1 d\omega_2$$

$$= tr\int_{-\pi-\pi}^{\pi\,\pi}\left[\Sigma_k^{-1}\,\mathbf{H}_k(\omega_1,\omega_2)\,\mathbf{S}_k(\omega_1,\omega_2)\,\mathbf{H}_k^H(\omega_1,\omega_2)\right]\left[\mathbf{S}_x(\omega_1,\omega_2)\,\mathbf{S}_k^{-1}(\omega_1,\omega_2)\right]d\omega_1 d\omega_2$$

$$= \frac{1}{4\pi^2}\,tr\int_{-\pi-\pi}^{\pi\,\pi}\left[\mathbf{S}_x(\omega_1,\omega_2)\,\mathbf{S}_k^{-1}(\omega_1,\omega_2)\right]d\omega_1 d\omega_2 \tag{E.22}$$

Now suppose that our input random process **x** is the random process 1. Then from Equation (E.22) we can say that

$$E_1\left[\varepsilon_1^T(n_1,n_2)\,\Sigma_1^{-1}\,\varepsilon_1(n_1,n_2)\right] = \frac{1}{4\pi^2}\,tr\int_{-\pi-\pi}^{\pi\,\pi}\left[\mathbf{S}_1(\omega_1,\omega_2)\,\mathbf{S}_1^{-1}(\omega_1,\omega_2)\right]d\omega_1 d\omega_2$$

$$= M \tag{E.23}$$

and

$$E_1\left[\varepsilon_2^T(n_1,n_2)\,\Sigma_2^{-1}\,\varepsilon_2(n_1,n_2)\right] = \frac{1}{4\pi^2}\,tr\int_{-\pi-\pi}^{\pi\,\pi}\left[\mathbf{S}_1(\omega_1,\omega_2)\,\mathbf{S}_2^{-1}(\omega_1,\omega_2)\right]d\omega_1 d\omega_2 \tag{E.24}$$

Substituting (E.23) and (E.24) into the expression for the direct divergence given by Eqn. (E.9) we have

$$I_{\varepsilon}(1,2) = -\frac{M}{2} - \frac{1}{2}\log\frac{|\Sigma_1|}{|\Sigma_2|} + \frac{1}{8\pi^2}\int_{-\pi}^{\pi}\int_{-\pi}^{\pi} tr\left[S_1(\omega_1,\omega_2)\, S_2^{-1}(\omega_1,\omega_2)\right] d\omega_1 d\omega_2 \tag{E.25}$$

Similarly we can show that

$$I_{\varepsilon}(2,1) = -\frac{M}{2} - \frac{1}{2}\log\frac{|\Sigma_2|}{|\Sigma_1|} + \frac{1}{8\pi^2}\int_{-\pi}^{\pi}\int_{-\pi}^{\pi} tr\left[S_2(\omega_1,\omega_2)\, S_1^{-1}(\omega_1,\omega_2)\right] d\omega_1 d\omega_2 \tag{E.26}$$

Substituting (E.25) and (E.26) into (E.17), we get the final expression of the incremental divergence given by (E.2).

APPENDIX (F)

APPLICATIONS TO IMAGE SPECTRAL ANALYSIS

In this appendix we developed an experiment to study the spectra of data corresponding to a color image shown in Figure F.1a. The figure represents an aerial photograph of a ground area, (data courtesy of Rome Air Development Center, Griffiss AFB, N.Y.), with size 128×128-pixel. Figures F.1b, c, and d represent the red, green, and blue components of the color image.

Two portions of this image of size 64×64-pixels are taken. The first part corresponds to the lower-left corner which represents the field, while the second portion lies in the upper-right corner and represents the trees.

Fig. F.2a shows a 2-D plot of the intensity variation of the green component in the field image. The index n_1 is taken as the horizontal direction, and index n_2 as the vertical direction. Figure F.2b represents the one dimensional plot of Fig. F.2a. Different slices of the green component of the color image in the horizontal and vertical directions are shown. It is clear that the variation of the intensity in the horizontal direction is very high while in the vertical direction the intensity variation is very low. This implies that the spectral energy is concentrated around $\omega_2 = 0$.

In a similar manner Fig. F.3 shows a two-dimensional plot of intensity variation of the green component of the trees portion of the color image, in the horizontal and vertical directions. Rapid variations of intensity appear in the n_1- direction and very slow variations appear in the n_2-direction. Fig. F.2 and Fig. F.3 are taken here only as an example showing the intensity variation. We could also show the intensity variation of the other color image components, but the plots are quite similar.

The color image is considered here as a 3-channel 2-D random process, where each color component (red, green, and blue) represents a separate channel. In this example only red and green components are analyzed, where the red component is designated as channel 1 and the green component as channel 2.

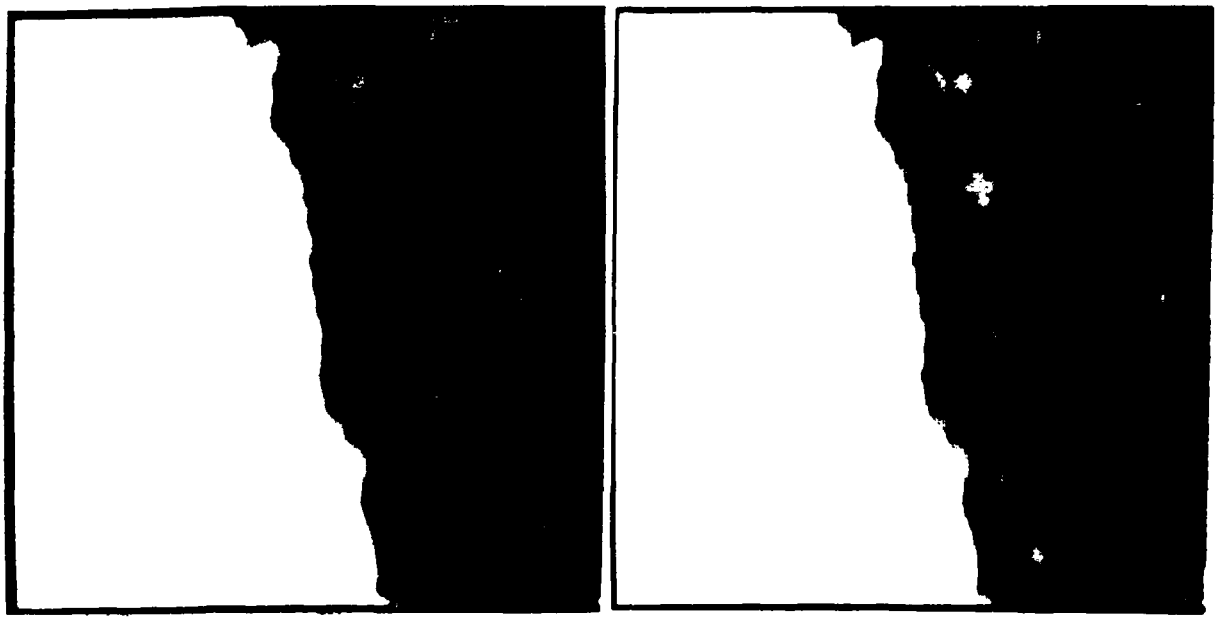

(a) Color image (b) Red component

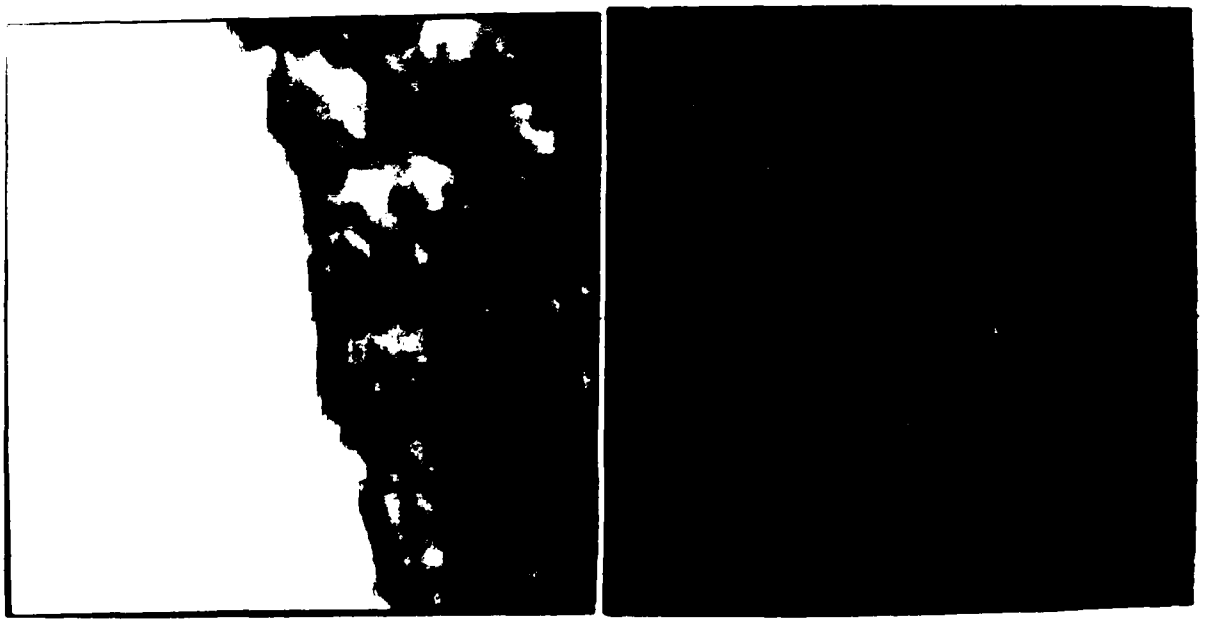

(c) Green component (d) Blue component

Fig. F.1 Color image of trees and field.

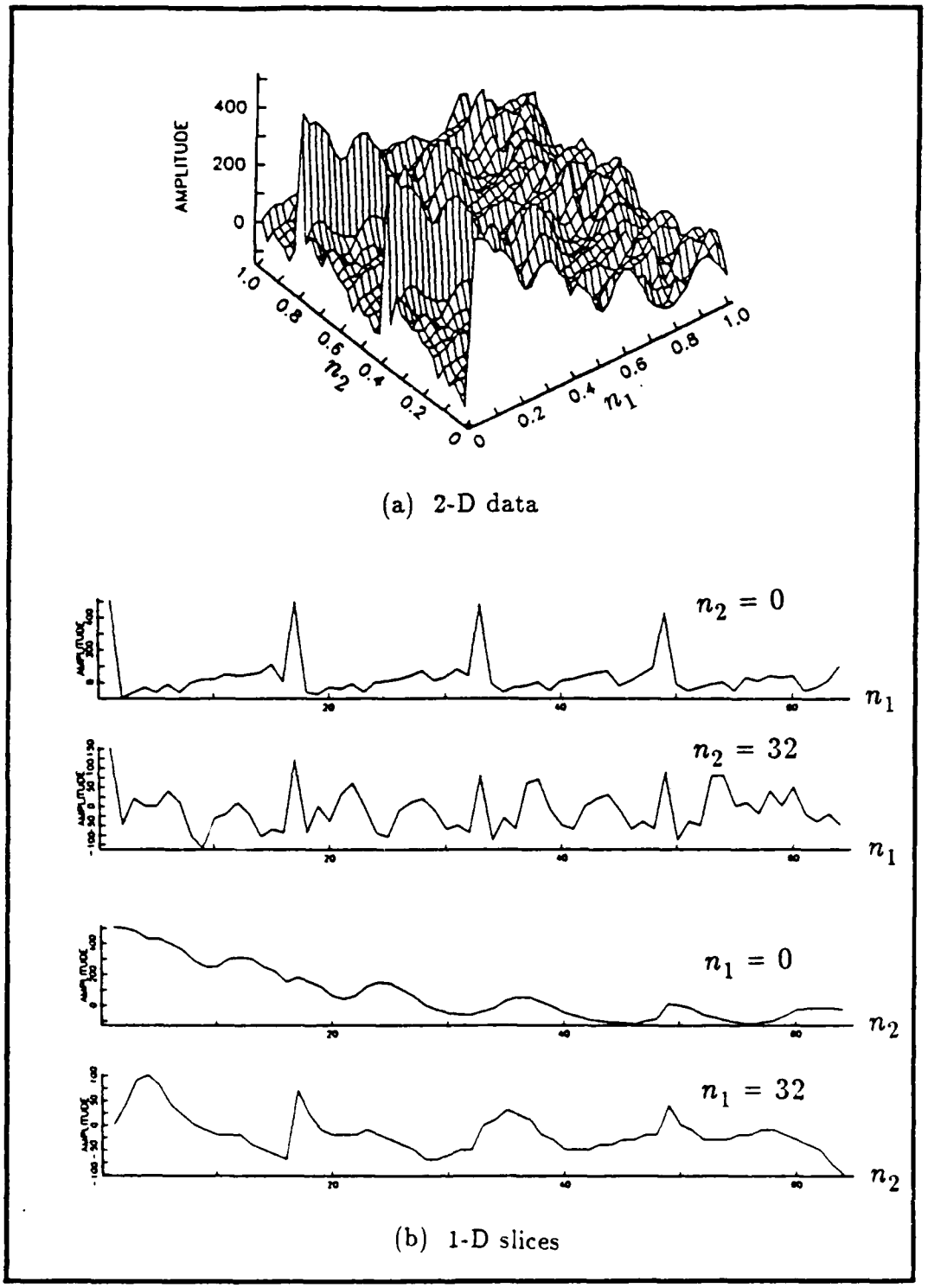

Fig. F.2 Spatial variation of green component intensity in the field image.

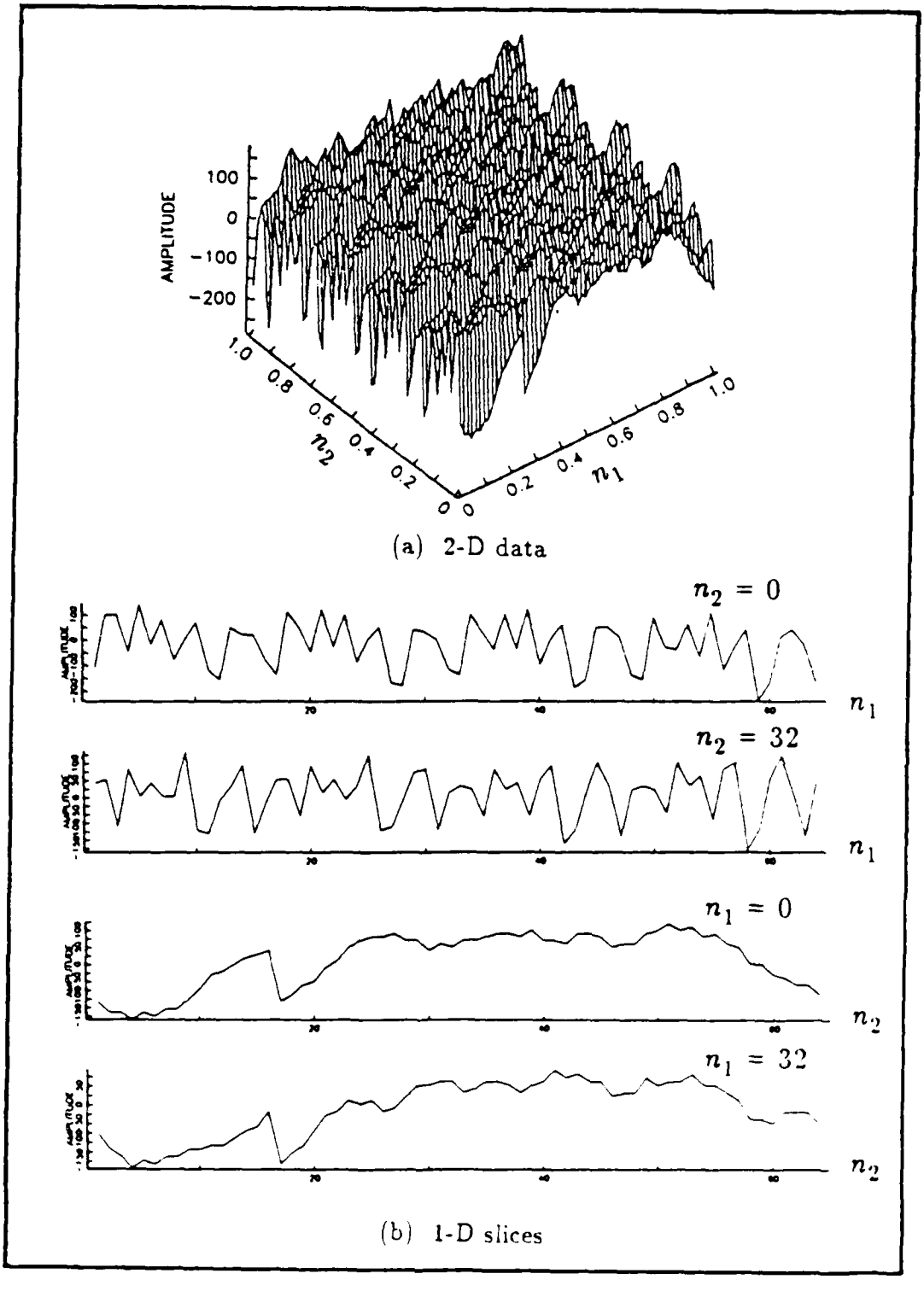

Fig. F.3 Spatial variation of green component intensity in the trees image.

The blue component for this image was very dark showing very low signal strength in this channel. A sixth order NSHP model was used to estimate the spectral matrix.

Fig. F.4 shows the components of the estimated spectral matrix for the field portion. The spectrum of the red component is shown in Fig. F.4a, while the spectrum of the green component is shown in Fig. F.4b. Figure F.4c shows the cross spectrum amplitude and phase. The red, green and magnitude of the cross spectrum appear to be very similar. The power distribution is concentrated around $\omega_2 = 0$ and the middle and higher frequencies of the ω_1 direction. This distribution of power is due to the appearance of regularly spaced lines in the image corresponding to the rows of plants occurring in the field image. The estimated phase of the cross spectrum component varies between $+10^0$ and -40^0.

Fig. F.5 shows the spectral estimate of the trees portion of the color image. Again we considered the red component as channel 1 and the green component as channel 2. The spectra of red and green components are shown in Fig. F.5a and b respectively. Figure F.5c shows the amplitude and phase of the cross spectrum component. As in the field portion, the autospectra (red and green) components and the magnitude of the cross spectra are similar. The power is also distributed around zero frequency in ω_2 direction, but occur at lower frequencies in the ω_1 direction than in case of the field portion. This results agrees with the intensity variation plot shown in Fig. F.3, which indicates that the intensity variations are not the same in horizontal and vertical directions. The phase of the cross spectrum for the trees image is also between 10^0 and -40^0.

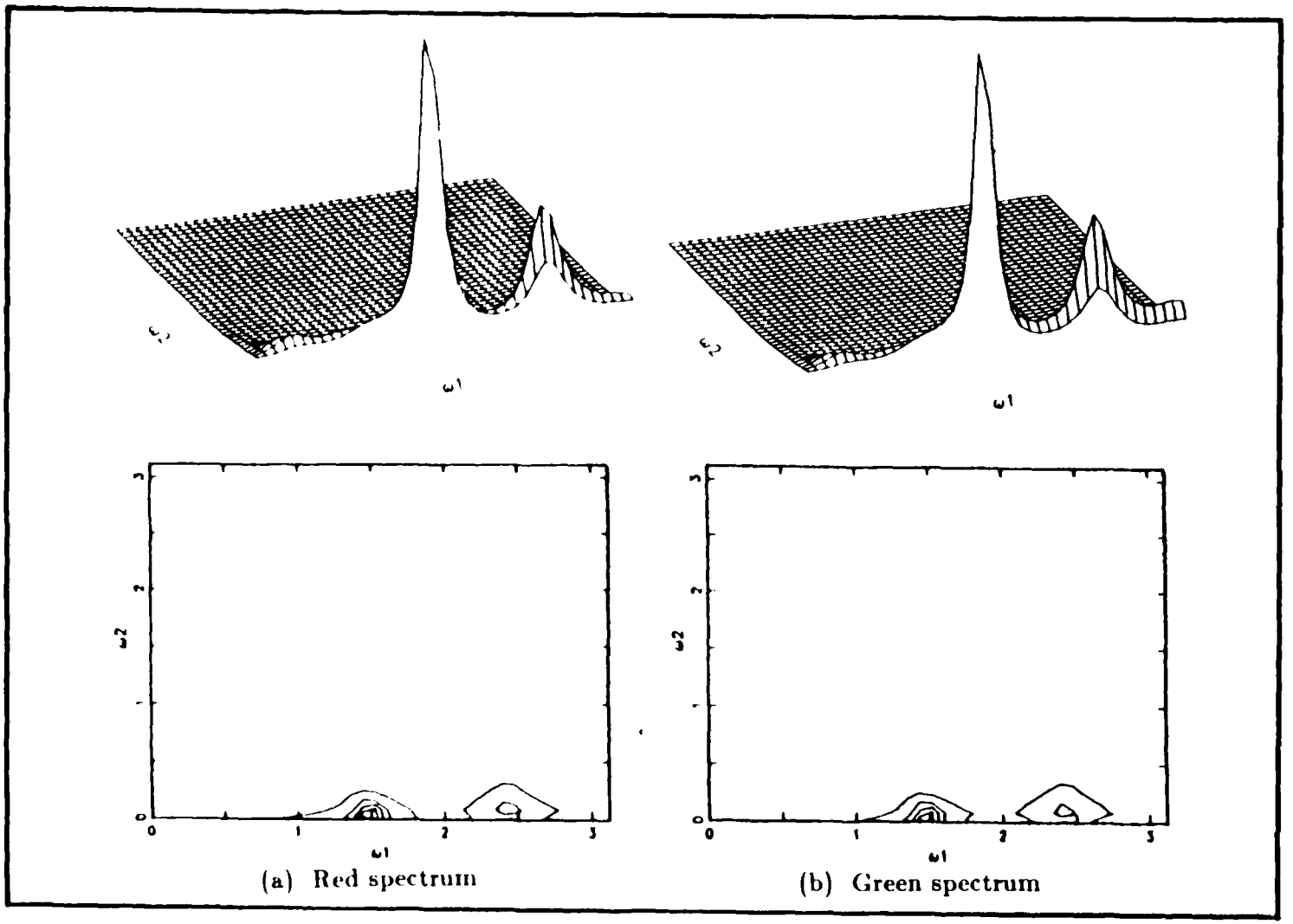

(a) Red spectrum (b) Green spectrum

Fig. F.4 Spectra for red and green components of the field image.

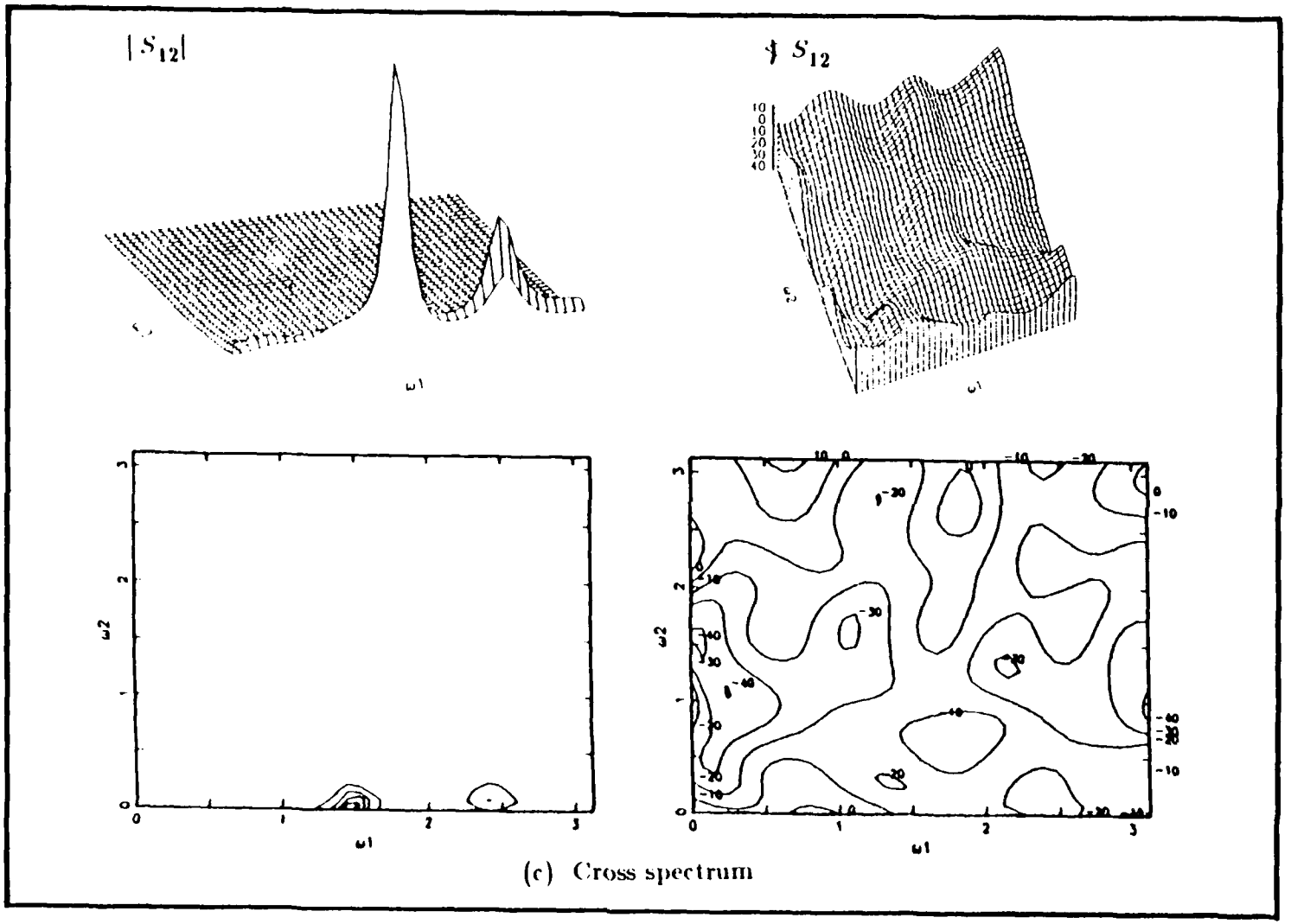

(c) Cross spectrum

Fig. F.4 Spectra for red and green components of the field image. (cont'd)

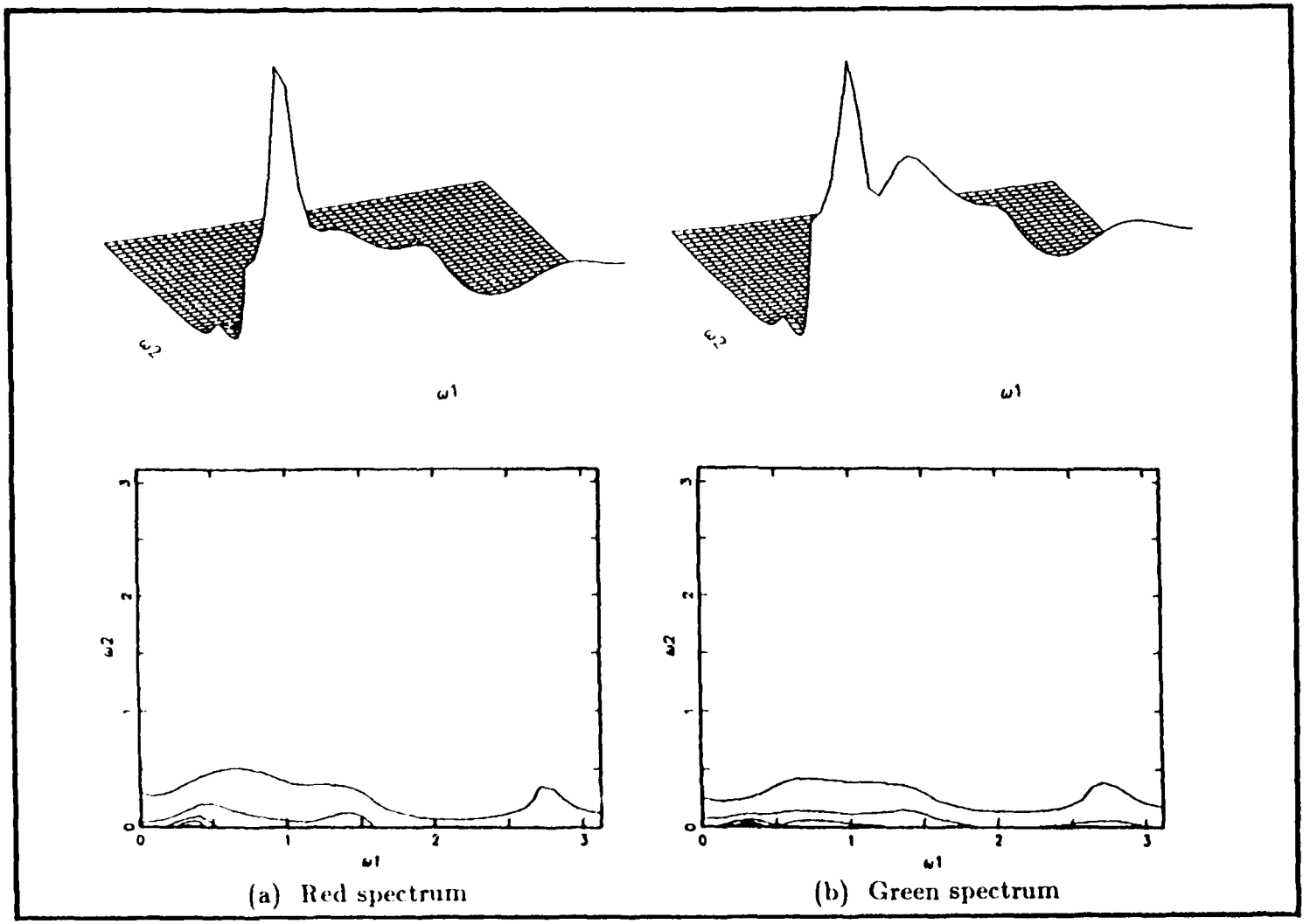

Fig. F.5 Spectra for red and green components of the trees image.

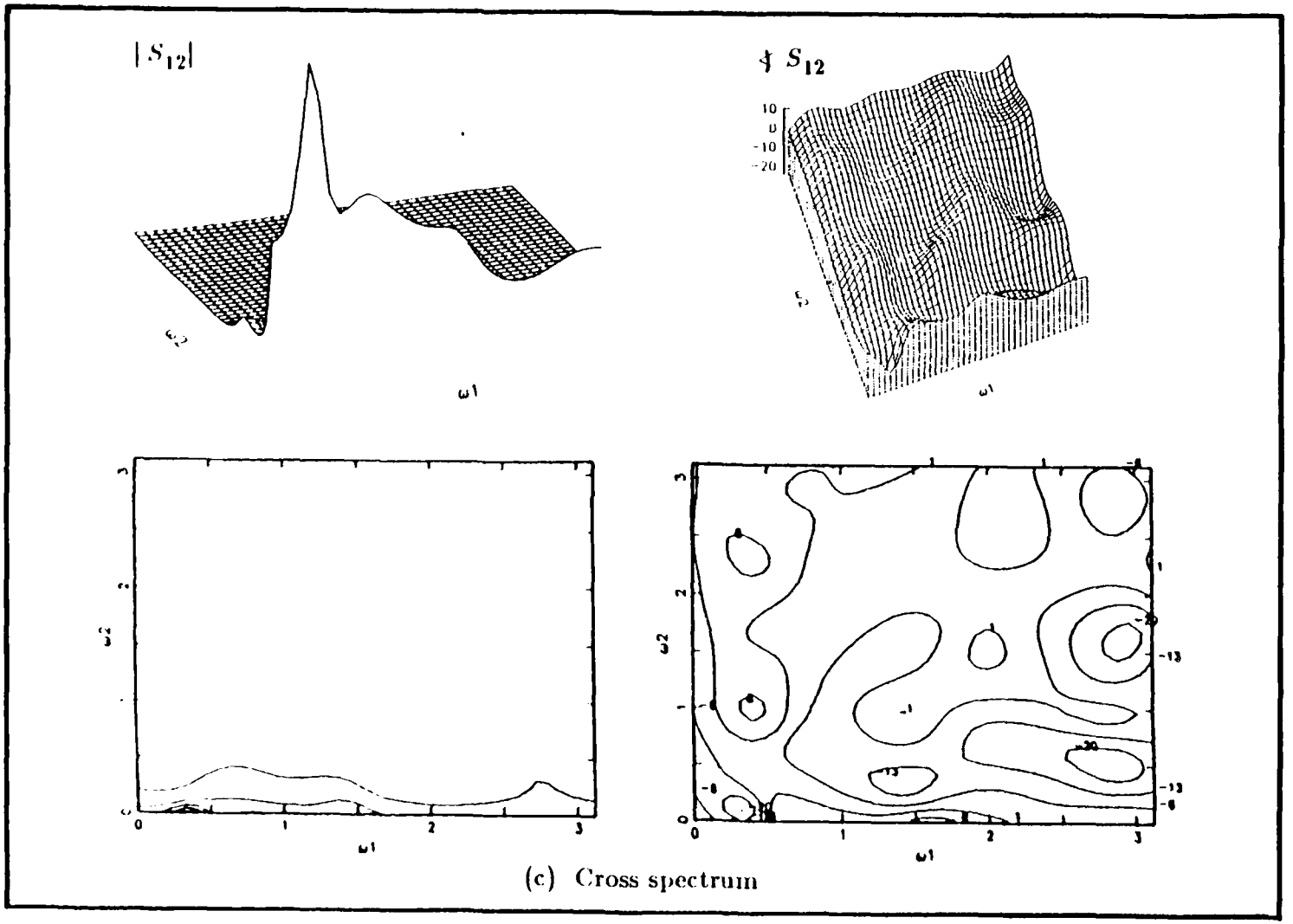

(c) Cross spectrum

Fig. F.5 Spectra for red and green components of the trees image. (cont'd)

APPENDIX (G)
VECTOR QUANTIZATION

In Chapter VI we discussed scalar quantization and showed that a two or three level uniform quantizer is sufficient to achieve good quality in the reconstructed coded images using multichannel predictive coding techniques.

Vector quantization is another approach to quantization which is used for coding a vector source. The data required to be coded are divided into blocks which are then sequentially encoded block by block. It is the vector generalization of the usual PCM system. (Linde et al,1980; Gray and Linde,1982; Gray,1984; Cuperman,1985; Hang and Woods,1985; Makhoul,1985; Goldberg,1986)

Let the image be divided into N blocks of pixels and let these pixels be formed into a k-dimensional vector $\mathbf{x}_i$. Then the total image can be represented by the larger vector

$$\mathbf{x} = \begin{bmatrix} \mathbf{x}_1 \\ \mathbf{x}_2 \\ \cdot \\ \cdot \\ \cdot \\ \mathbf{x}_N \end{bmatrix} \tag{G.1}$$

where

$$\mathbf{x}_i = \begin{bmatrix} x_{i1} \\ x_{i2} \\ \cdot \\ \cdot \\ \cdot \\ x_{ik} \end{bmatrix} \tag{G.2}$$

In vector quantization the vector $\mathbf{x}_i$ is mapped into another k-dimensional vector $\hat{\mathbf{x}}_i$ which is close to it in k-dimensional space. The vector $\hat{\mathbf{x}}$ which is transmitted is then composed of the individual $\hat{\mathbf{x}}_i$ value. We call this the *quantized* value of $\mathbf{x}$.

$$\hat{\mathbf{x}} = \begin{bmatrix} \hat{\mathbf{x}}_1 \\ \hat{\mathbf{x}}_2 \\ \cdot \\ \cdot \\ \cdot \\ \hat{\mathbf{x}}_N \end{bmatrix} = q\ (\mathbf{x}) \tag{G.3}$$

The vectors $\hat{\mathbf{x}}_i$ are drawn from a reproduction alphabet (or codebook) $\mathbf{y}$.

A major issue for vector quantization is codebook design. The VQ algorithm most frequently used is called Linde-Buzo-Gray (LBG) vector quantizer algorithm (Linde et al,1980) and involves a clustering of the data in k-dimensional space. A codebook $\mathbf{y}$ with length (i.e. number of quantization levels) J can be written in the following form

$$\mathbf{y} = \begin{bmatrix} \mathbf{y}_1 \\ \mathbf{y}_2 \\ \cdot \\ \cdot \\ \cdot \\ \mathbf{y}_J \end{bmatrix} \tag{G.4}$$

where

$$\mathbf{y}_i = \begin{bmatrix} y_{i1} \\ y_{i2} \\ \cdot \\ \cdot \\ \cdot \\ y_{ik} \end{bmatrix} \tag{G.5}$$

In this case the bit rate can be defined by

$$R = \log_2 J \quad \text{bits per vector} \tag{G.6}$$

or

$$r = \frac{R}{k} \quad \text{bits per sample} \tag{G.7}$$

Note that the number of quantization levels is usually restricted to be a binary number for digital coding applications.

Observe that VQ can allow fractional rates in bits per sample while this is not the case in scalar quantization. The minimum bit rate of a scalar quantizer is 1 bit per sample while a k-dimensional VQ can theoretically achieve a bit rate of 1/k bits per sample.

The distortion caused by replacing the original input vector $\mathbf{x}$ by the new vector $\hat{\mathbf{x}}$ is given by the distortion measurement $d(\mathbf{x},\hat{\mathbf{x}})$. The most widely used type of distortion measurement is the squared-error-distortion (Gray,1984; Makhoul,1985).

$$d(\mathbf{x},\hat{\mathbf{x}}) = \| \mathbf{x} - \hat{\mathbf{x}} \|^2$$

$$= \sum_{i=1}^{k} | x_i - \hat{x}_i |^2 \qquad \text{(G.8)}$$

To quantitatively measure the performance of the coding system we could use the average distortion $E\left[d(\mathbf{x},\hat{\mathbf{x}}) \right]$. In practice however, normalized average distortion is used instead of the actual value of the average distortion. We refer to this normalized average distortion as the SNR measurement and it can be defined by

$$SNR = 10 \log_{10} \frac{E\left[\| \mathbf{x} \|^2 \right]}{E\left[d(\mathbf{x},\hat{\mathbf{x}}) \right]} \qquad \text{(G.9)}$$

The performance of the color image predictive coding technique using VQ and applying the multichannel linear predictive models described in Chapter VI has been studied through the following simulation experiment. The original pictures used in this experiment are shown in Fig. 6.6. The simulations were run on 128×128 pixel images with 8 bits per color component (i.e. 24 bits per color pixel).

We started the simulation with the lady's face given in Fig. 6.6a. The predictive filter coefficients of the second order model for the whole image were obtained by solving a set of Normal equations. The corresponding codebook of the residual signal was obtained using the LBG codebook design algorithm with the following parameters. The codebook size is J=64. The vectors of dimension k ($k=3\times P_1\times P_2$) where 3 represents the

AD-A191 273 MULTICHANNEL 2-D POWER SPECTRAL ESTIMATION AND APPLICATIONS(U) NAVAL POSTGRADUATE SCHOOL MONTEREY CA H T EL-SHAER DEC 87 4/4

UNCLASSIFIED F/G 12/3 NL

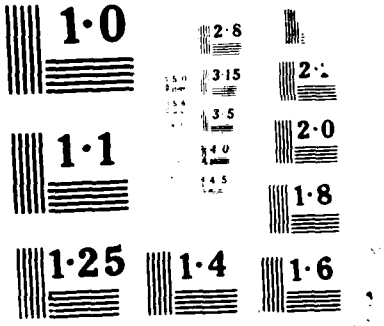
1·0
1·1
1·25
1·4
1·6
1·8
2·0
2·2
2·5
3·15
3·5
4·0
4·5

number of the color components were then obtained by vectoring a block of dimension $(P_1 \times P_2)$ of the picture. Specifically in this experiment we assumed that $P_1=P_2=2$.

The reconstructed coded lady's face image using this designed codebook is shown in Fig. G.1a and the corresponding residual is shown in Fig. G.1b. Note that we are using here the prediction error coder system described in Chapter VI (see Fig. 6.3), which is not as good in quality as the predictive coding system (Fig. 6.2) but it is easier to construct. The bit rate in this specific example is 0.5 bit per sample and the corresponding SNR measurement values are 20.198 dB for the red component, 17.506 dB for the green component, and 14.879 dB for the blue component.

Now, several filter coefficient matrices were designed for different images by solving a set of Normal equations corresponding to each image. Specifically we used the all images given in Fig. 6.6 except Fig. 6.6h. Applying the third procedure described in Chapter VI, we obtained a fixed filter coefficient matrix. Using the same codebook designed before, the corresponding reconstructed image of the lady's face is shown in Fig. G.1c. The corresponding SNR for the red component is 20.026 dB, for the green component is 17.406 dB, and for the blue component is 14.688 dB.

Comparing Fig. G.1a with Fig. G.1c we see that approximately the same quality of pictures are obtained. In addition, the SNR values are very close to each other. Note that the reconstructed pictures are not of the same quality as in case of scalar quantization because we used here the prediction error coder system which accumulates noise at the receiver. Also the block size used is very small ((2×2) for each color component) and the size of the training data was not very large.

To check the efficiency of the third procedure using the VQ technique the fixed set of filter coefficients and the designed codebook were used to reconstruct an image that was not part of the training data. (The house picture shown in Fig. 6.6h). The reconstructed house picture is shown in Fig. G.1d and the corresponding SNR in dB are 16.730, 18.647, and 19.604 for the red, green, and blue components, respectively.

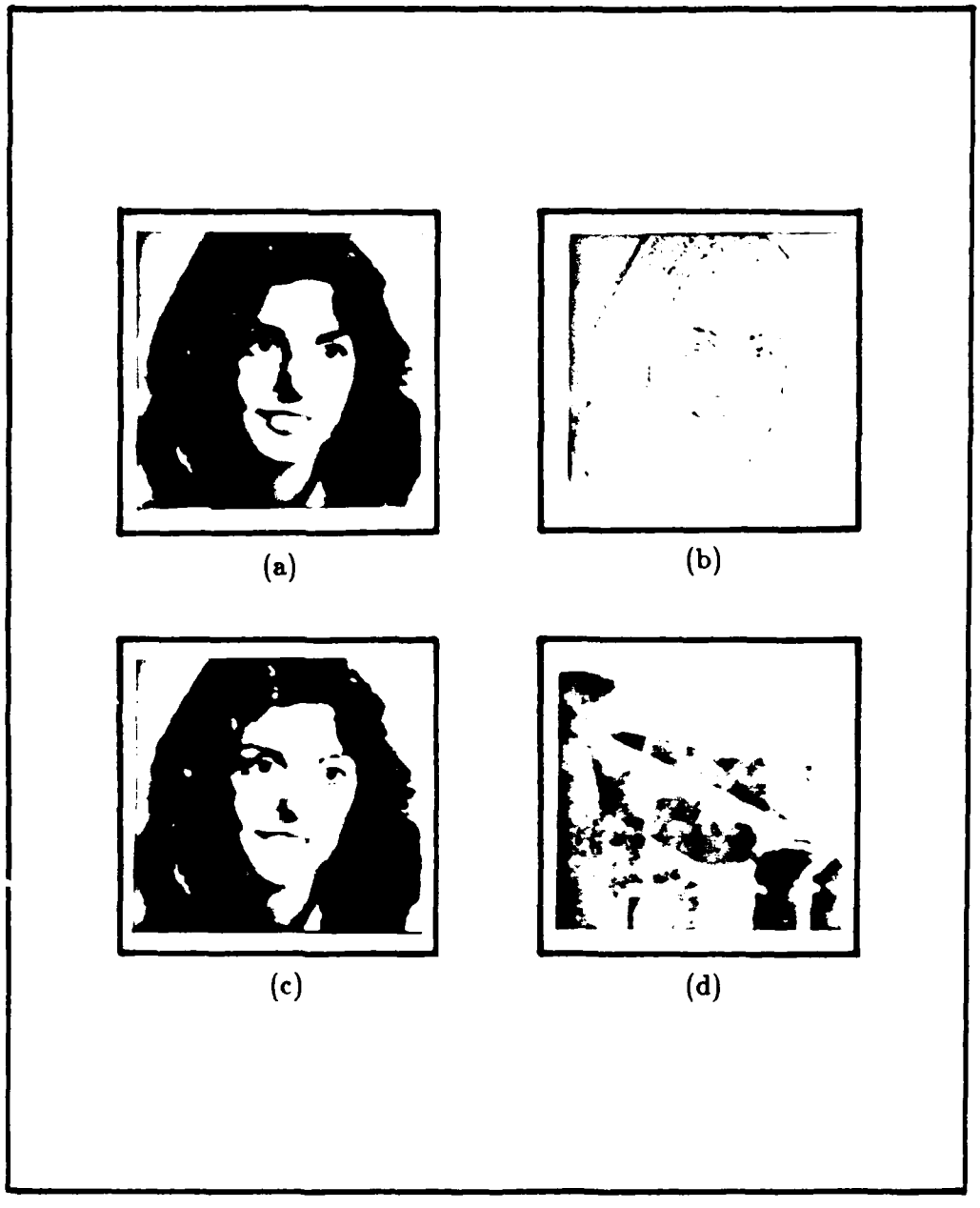

Fig. G.1 Reconstructed images using VQ.
(a) Reconstructed lady's face image (using second procedure)
(b) Error image
(c) Reconstructed lady's face image (using third procedure)
(d) Reconstructed house image

LIST OF REFERENCES

T.J. Abatzoglou, "A Fast Local Maximum Likelihood Estimator for Time Delay Estimation", *Proc. of IEEE Int. Conf. on Acoustics, Speech, and Signal Processing*, pp. 1773-1776, Florida, March 1985.

T.J. Abatzoglou, "A Fast Maximum Likelihood Algorithm for Frequency Estimation of a Sinusoid Based on Newton's Method", *IEEE Trans. on Acoustics, Speech, and Signal Processing*, Vol. ASSP-33, No. 1, pp. 77-89, February 1985.

N. Andersen, "On the Calculation of Filter Coefficients for Maximum Entropy Spectral Analysis", *Geophysics*, Vol. 39, No. 1, pp. 69-72, February 1974.

B. S. Atal and M. R. Schroeder, "Adaptive Predictive Coding of Speech Signals", *The Bell System Technical Journal*, pp. 1973-1986, October 1970.

A.B. Baggeroer, "Maximum Likelihood Estimation of Cross Spectral", MIT Lincoln Laboratory, Project Report PA-343, 13 January 1975.

R. L. Baker, "Vector Quantization of Digital Images", Ph.D. Dissertation, Stanford University, 1984.

A.A. Beex and M.A. Rahman, "On Averaging Burg Spectral Estimators for Segments", *IEEE Trans. on Acoustics, Speech, and Signal Processing*, Vol. ASSP-34, No. 6, pp. 1473-1484, December 1986.

V.D. Bos," Alternative interpretation of Maximum Entropy Spectral analysis", *IEEE Trans. Inform. Theory*, IT-17, pp. 493-494, 1971.

Y. Bresler and A. Macovski, "Exact Maximum Likelihood Estimation of Superimposed Exponential Signals in Noise", *Proc. of IEEE Int. Conf. on Acoustics, Speech, and Signal Processing*, pp. 1824-1827, Florida, March 1985.

J. P. Burg, "Three-Dimensional Filtering With an Array of Seismometers", *Geophysics*, Vol. XXIX, No. 5, pp. 693-713, October 1964.

J. P. Burg, "Maximum Entropy Spectral Analysis", Proc. of the 37th Meeting of the Society of Exploration *Geophysicists*, 1967.

J. P. Burg, "A New Analysis Technique for Time Series Data", Paper presented at Advanced Study Institute on Signal Processing, Nato, Enschede, Netherlands, 1968.

J.P. Burg, "Maximum Entropy Analysis", Ph.D. Dissertation *Stanford University,* Standford, CA, 1975.

J. P. Burg, "The Relationship Between Maximum Entropy Spectra and Maximum Likelihood Spectra", *Geophysics,* Vol. 37, No. 2, pp. 375-376, April 1972.

P. Burrascano, G. Martinelli, and G. Orlandi, "Identification of Truncated Narrow-Band Autoregressive Processes", *Proc. of the IEEE,* Vol. 74, No. 8, pp. 1164-1165, August 1986.

A. Buzo, A. H. Gray, R. M. Gray, and J. D. Markel, "Speech Coding Based Upon Vector Quantization", *IEEE Trans. on Acoustics, Speech, and Signal Processing,* Vol. ASSP-28, No. 5, October 1980.

S.D. Cabrera and T.W. Parks, "Deterministic Estimation of Two-Dimensional Signals", *Proc. of IEEE Int. Conf. on Acoustics, Speech, and Signal Processing,* pp. 867-870, Boston, April 1983.

J.A. Cadzow and K. Ogino, "Two-Dimensional Spectral Estimation", *IEEE Trans. on Acoustics, Speech, and Signal Processing,* Vol. ASSP-29, No. 3, pp. 396-400, June 1981.

J.A. Cadzow, "Autoregressive Moving Average Spectral Estimation: A Model Equation Error Procedure", *IEEE Trans. on Geoscience and Remote Sensing,* Vol. GE-19, No. 1, pp. 24-28, January 1981.

J. Capon, R. J. Greenfield, and R. J. Kolker, "Multidimensional Maximum-Likelihood Processing of a Large Aperture Seismic Array", *Proc. of the IEEE,* Vol. 55, No. 2, pp. 192-211, February 1967.

J. Capon, "High Resolution Frequency-Wavenumber Spectral Analysis", *Proc. of the IEEE,* Vol.57, No.8, pp. 1408-1418, August 1969.

R. Chellappa, Y. Hu, and S. Kung, "On Two-Dimensional Markov Spectral Estimation", *IEEE Trans. on Acoustics, Speech, and Signal Processing,* Vol. ASSP-31, No.4, pp. 836-841, August 1983.

J. H. Chen, and A. Gersho, "Vector Adaptive Predictive Coding of Speech at 9.6 kb/s", *Proc. of IEEE Int. Conf. on Acoustics, Speech, and Signal Processing, ICASSP,* pp. 1693-1696, Tokyo, 1986.

D.G. Childers, "Modern Spectrum Analysis", IEEE Press, John Wiley & sons, INC., NY, 1978.

C. F. Cowan and P. M. Grant, "Adaptive Filters", Prentice-Hall, Inc. Englewood Cliffs, New Jersey 07632, 1985.

V. Cuperman, and A. Gersho, "Vector Predictive Coding of Speech at 16 kbits/s", *IEEE Trans. on Communications,* Vol. COM-33, No. 7, pp. 685-696, July 1985.

L. D. Davisson, R. M. Gray, "Data Compression", Dowden, Hutchinson & Ross, Inc. 1976.

B. W. Dickinson, "Two-Dimensional Markov Spectrum Estimates Need Not Exist", *IEEE Trans. Information Theory,* Vol. IT-26, No. 1, pp. 120-121, January 1980.

F.U. Dowla and J.S. Lim, "Improved Maximum Likelihood Method for Two-Dimensional Spectral Estimation", *Proc. of IEEE Int. Conf. on Acoustics, Speech, and Signal Processing,* pp. 851-854, Boston, April 1983.

F.U. Dowla and J.S. Lim, "Relationship Between Maximum Likelihood Method and Autoregressive Modeling in Multidimensional Power Spectrum Estimation", *IEEE Trans. on Acoustics, Speech, and Signal Processing,* Vol. ASSP-32, No. 5, pp. 1083-1087, October 1984.

F.U. Dowla and J.S. Lim, "Resolution Property of the Improved Maximum Likelihood Method", *Proc. of IEEE Int. Conf. on Acoustics, Speech, and Signal Processing,* pp. 820-822, Florida, March 1985.

D.E. Dudgeon, "Fundamentals of Digital Array Processing", *Proc. of the IEEE,* Vol. 65, No. 6, pp. 898-904, June 1977.

D.E. Dudgeon and R.M. Mersereau ,"Multidimensional Digital Signal Processing", Prentice-Hall, 1984.

T.S. Durrani and R. Chapman, "Eigenfilter Methods for 2-D Spectral Estimation", *Proc. of IEEE Int. Conf. on Acoustics, Speech, and Signal Processing, ICASSP,* pp. 863-866, Boston, 1983.

A. Efron and D.W. Tufts, "Estimation of Frequencies of Multiple Two-Dimensional Sinusoids: Improved Methods of Linear Prediction", *Proc. of the IEEE,* Vol. 74, No. 2, February 1986.

M.P. Ekstrom, "Digital Image Processing Techniques", Academic Press Inc., 1984.

M.P. Ekstrom and J.W. Woods, "Two-Dimensional Spectral Factorization with Applications in Recursive Digital Filtering", *IEEE Trans. Acoustics, Speech, and Signal Processing,* Vol. ASSP-24, No. 2, pp. 115-128, April 1976.

L.J. Faber, "Commentary on the Denominator Recursion for Burg's Block Algorithm", *Proc. of the IEEE,* Vol. 74, No. 7, pp. 1046-1047, July 1986.

P.M. Fishman, L.K. Jones, and C.W. Therrien, "The Minimal Divergence Solution to the Gaussian Masking Problem", Lincoln Laboratory, MIT, Technical Report 569, May 1981.

P.M. Fishman, L.K. Jones, and C.W. Therrien, "The Design of Masking Processes by the Method of Minimal Divergence", *IEEE Trans. on Information Theory*, Vol. IT-29, No. 2, pp. 245-255, March 1983.

B. Friedlander, "Lattice Methods for Spectral Estimation", *Proceeding of the IEEE*, Vol. 70, No. 9, pp. 990-1017, September 1982.

O. L. Frost, T. M. Sullivan, "High-Resolution Two-Dimensional Spectral Analysis", *Proc. of IEEE Int. Conf. on Acoustics, Speech, and Signal Processing, ICASSP*, pp. 673-676, Washington, D.C., April 1979.

J. D. Gibson, "Adaptive Prediction in Speech Differential Encoding Systems", *Proc. of the IEEE*, Vol. 68, No. 4, pp. 488-523, April 1980.

A.A. Giordano, F.M. Hsu, "Least Square Estimation with Applications to Digital Signal Processing", John Wiley & Sons.

M. Goldberg, P. R. Boucher, S. Shilien, "Image Compression Using Adaptive Vector Quantization", *IEEE Trans. on Communications*, Vol. COM-34, No. 2, pp. 180-187, February 1986.

D. J. Goodman, and A. Gersho, "Theory of an Adaptive Quantizer", *IEEE Trans. on Communications*, Vol. COM-22, No. 8, pp. 1037-1045, August 1974.

R. M. Gray, "Vector Quantization", *IEEE ASSP Magazine*, pp. 4-29, April 1984.

R. M. Gray, and Y. Linde, "Vector Quantizers and Predictive Quantizers for Gauss-Markov Sources", *IEEE Trans. on Communications*, Vol. COM-30, No. 2, pp. 381-389, February 1982.

T.L. Grettenberg, "Signal Selection in Communication and Radar Systems", *IEEE Trans. on Information Theory*, pp. 265-275, October 1963.

Gutowski P.R., Robinson E.A., Treitel S., "Spectral Estimation: Fact or Fiction", *IEEE Trans. Geosci. Electron.*, Vol. GE-16, pp. 80-84, April 1978.

H. Hang, and J. W. Woods, "Predictive Vector Quantization of Images", *IEEE Trans. on Communications*, Vol. COM-33, No. 11, pp. 1208-1219, November 1985.

F.J. Harris, "On the Use of Windows for Harmonic Analysis with the Discrete Fourier Transform", *Proc. IEEE*, Vol. 66, pp. 51-85, January 1978.

R.E. Hartwig, "Resultants and the Solution of *AX - XB = -C*", *SIAM J. Appl. Math*, Vol. 23, No. 1, pp. 104-117, July 1972.

R.E. Hartwig, "*AX - XB = C*, Resultants and Generalized Inverses", *SIAM J. Appl. Math*, Vol. 28, No. 1, pp. 154-182, January 1975.

T.L. Henderson, "Geometric Methods for Determining System Poles from Transient Response", *IEEE Trans. on Acoustics, Speech, and Signal Processing*, Vol. ASSP-29, No. 5, pp. 982-988, October 1981.

G.D. Hingorani and J.C. Hancock, "A Transmitted Reference System for Communication in Random or Unknown Channels", *IEEE Trans. on Communication Technology*, Vol. 13, No. 3, pp. 293-301, September 1965.

S. Y. Hwang, "Computation of Correlations in 1-D and 2-D Digital Signals and Systems", *Proc. of IEEE Int. Conf. on Acoustics, Speech, and Signal Processing, ICASSP*, pp. 766-768, Denver, April 1980.

L. B. Jackson and H. C. Chien, "Frequency and Bearing Estimation by Two-Dimensional Linear Prediction", *Proc. Int. Conf. Acoustic, Speech, and Signal Processing*, pp. 665-668, Washington, D.C., April 1979.

A.K. Jain, "Partial Differential Equations and Finite-Difference Methods in Image Processing, Part 1: Image Representation", *J. of Optimization Theory and Applications*, Vol. 23, No. 1, pp.65-90, September 1977.

A.K. Jain and J.R. Jain, "Partial Differential Equations and Finite Difference Methods in Image Processing- Part II: Image Restoration", *IEEE Trans. on Automatic Control*, Vol. AC-23, No. 5, October 1978.

A. K. Jain, "Image Data Compression: A Review", *Proc. of the IEEE*, Vol. 69, No. 3, March 1981.

A.K. Jain, "Advances in Mathematical Models for Image Processing", *Proc. of the IEEE*, Vol. 69, No. 5, pp. 502-528, May 1981.

N. S. Jayant, "Digital Coding of Speech Waveforms: PCM, DPCM, and DM Quantizers", *Proc. of the IEEE*, Vol. 62, No. 5, pp. 611-630, May 1974.

N. S. Jayant, "Waveform Quantization and Coding", IEEE Press, New York, 1976.

N. S. Jayant, and P. Noll, "Digital Coding of Waveforms", Prentice-Hall, Inc. Englewood Cliffs, New Jersey, 1984.

H. Jeffreys, "An Invariant Form for the Prior Probability in Estimation Problems", *Proc. Roy. Soc. A.*, Vol. 186, pp. 453-461, 1946.

G. M. Jenkins and D. G. Watts, "Spectral Analysis and its Applications", Holden-Day, Oakland, California, 1968.

R. W. Johnson, J. E. Shore, and J. P. Burg, "Multisignal Minimum-Cross-Entropy Spectrum Analysis with Weighted Initial Estimates", *IEEE Trans. on Acoustics, Speech, and Signal Processing*, Vol. ASSP-32, No. 3, pp. 531-539, June 1984.

T. Kailath, "The Divergence and Bhattacharyya Distance Measure in Signal Selection", *IEEE Trans. on Communication Technology*, Vol. COM-15, No. 1, pp. 52-60, February 1967.

T. Kailath, "A View of Three Decades of Linear Filtering Theory", *IEEE Trans. on Information Theory*, Vol. IT-20, No. 2, pp. 146-178, March 1974.

Y. Kamp, "Some Results on Constrained Maximum Likelihood Estimation", *Proc. of IEEE Int. Conf. on Acoustics, Speech, and Signal Processing*, pp. 1405-1407, Tokyo, Japan, April 1986.

R.L. Kashyap, "Characterization and Estimation of Two-Dimensional ARMA Models", *IEEE Trans. on Information Theory*, Vol. IT-30, No. 5, pp. 736-745, September 1984.

S.M. Kay, "Recursive Maximum Likelihood Estimation of Autoregressive Processes", *IEEE Trans. on Acoustics, Speech, and Signal Processing*, Vol. ASSP-31, No. 1, pp. 56-65, February 1983.

S. M. Kay, and S. L. Marple, "Spectrum Analysis-A Modern Perspective", *Proc. of the IEEE*, Vol. 69, No. 11, pp. 1380-1419, November 1981.

D. Kazakos and P. Papantoni-Kazakos, "Spectral Distance Measures Between Gaussian Processes", *IEEE Trans. on Automatic Control*, Vol. AC-25, No. 5, pp. 950-959, October 1980.

S. B. Kesler, ed., "Modern Spectrum Analysis II ", *IEEE Press*, New York, 1986.

V. Kucera, "The Matrix Equation $AX + XB = C$", *SIAM J. Appl. Math.*, Vol. 26, No.1, pp. 15-25, January 1974.

R. Kumaresan and D.W. Tufts, "Improved Spectral Resolution III: Efficient Realization", *Proc. of the IEEE*, Vol. 68, No. 10, pp. 1354-1355, October 1980.

R.T. Lacoss," Data Adaptive Spectral Analysis Methods", *Geophysics*, Vol. 36, No. 4, pp. 661-675, August 1971.

J.L. Lacoume, C. Latombe, N. Martin, M. Gharbi, and R. Lidin, "AR and ARMA Models in Spectral and Multispectral Analysis", *Proc. of IEEE Int. Conf. on Acoustics, Speech, and Signal Processing*, pp. 240-244, Boston, April 1983.

M.A. Lagunas, M.E. Santamaria, A. Gasull, and A. Moreno, "Cross Spectrum ML Estimate", *Proc. of IEEE Int. Conf. on Acoustics, Speech, and Signal Processing*, pp 77-80, Florida, March 1985.

S. W. Lang, and J. H. McClellan, "Multidimensional MEM Spectral Estimation", *IEEE Trans. on Acoustics, Speech, and Signal Processing*, Vol. ASSP-30, No. 6, pp. 880-887, December 1982.

S. W. Lang, and J. H. McClellan, "Spectral Estimation for Sensor Arrays", *IEEE Trans. on Acoustics, Speech, and Signal Processing*, Vol. ASSP-31, No. 2, pp. 349-358, April 1983.

S.W. Lang and J.H. McClellan, "Frequency Estimation with Maximum Entropy Spectral Estimators", *IEEE Trans. on Acoustics, Speech, and Signal Processing*, Vol. ASSP-28, No. 6, pp. 716-724, December 1980.

Y. C. Lim and S. R. Parker, "On the Synthesis of Lattice Parameter Digital Filters", *IEEE Trans. on Circuits and Systems*, Vol. CAS-31, No. 7, pp. 593-601, July 1984.

J. S. Lim and N. A. Malik, "A New Algorithm for Two-Dimensional Maximum Entropy Power Spectrum Estimation", *IEEE Trans. on Acoustics, Speech, and Signal Processing*, Vol. ASSP-29, No. 3, pp. 401-413, June 1981.

Y. Linde, A. Buzo, and R. M. Gray, "An Algorithm for Vector Quantizer Design", *IEEE Trans. on Communications*, Vol. COM-28, No. 1, pp. 84-95, January 1980.

J.Makhoul, "Linear Prediction: A Tutorial Review", *Proc. IEEE*, Vol.63, pp.561-580, April 1975.

J. Makhoul, "Stable and Efficient Lattice Methods for Linear Prediction", *IEEE Trans. on Acoustics, Speech, and Signal Processing*, Vol. ASSP-25, No.5, pp. 423-428, October 1977.

J. Makhoul, S. Roucos, and H. Gish, "Vector Quantization in Speech Coding", *Proc. of the IEEE*, Vol. 73, No. 11, pp. 1551-1588, November 1985.

P. A. Margos, R. W. Schafer, and R. M. Mersereau, "Two-Dimensional Linear Prediction and Its Application to Adaptive Predictive Coding of Images", *IEEE Trans. on Acoustics, Speech, and Signal Processing*, Vol. ASSP-32, No. 6, pp. 1213-1229, December 1984.

N. A. Malik, and J. S. Lim, "Properties of Two-Dimensional Maximum Entropy Power Spectrum Estimates", *IEEE Trans. on Acoustics, Speech, and Signal Processing*, Vol. ASSP-30, No. 5, pp. 788-798, October 1982.

T. Marill and D.M. Green, "On the Effectiveness of Receptors in Recognition Systems", *IEEE Trans. on Information Theory*, pp. 11-17, January 1963.

J. D. Markel, and A. H. Gray, "Linear Prediction of Speech", Springer-Verlag, Berlin Heidelberg, NewYork, 1976.

G. Martinelli, G. Orlandi, and P. Burrascano, "Pole Identification of ARMA Processes by Extended Levinson Recursion", *IEEE Trans. on Circuits and Systems*, Vol. CAS-33, No. 3, pp. 348-350, March 1986.

S.L. Marple Jr. and A.H. Nuttall, "Experimental Comparison of Three Multichannel Linear Prediction Spectral Estimators", *IEE Proc.*, Vol. 130,Pt. F, No. 3, pp. 218-229, April 1983.

Lawrence Marple Jr., "Digital Spectral Analysis with Applications", Prentice Hall, 1987.

T. L. Marzetta, "A Linear Prediction Approach to Two-Dimensional Spectral Factorization and Spectral Estimation", *Ph.D. dissertation*, Dep. Elec. Eng. & Comput. Sci., Mass. Inst. Technol., Cambridge, MA, February 1978.

T. L. Marzetta, "The Design of 2-D Recursive Filters in the 2-D Reflection Coefficient Domain", *Proc. of IEEE Int. Conf. Acoustics, Speech, and Signal Processing*, pp. 32-35, 1979.

T.L. Marzetta," Two-Dimensional Linear Prediction: Autocorrelation Arrays, Minimum Phase Prediction Error Filters, and Reflection Coefficient Arrays", *IEEE Trans. on Acoustics Speech and Signal Processing*, Vol. ASSP-28, No. 6, pp. 725-733, December 1980.

T.L. Marzetta and S.W. Lang, "New Interpretations for the MLM and DASE Spectral Estimators", *Proc. of IEEE Int. Conf. on Acoustics, Speech, and Signal Processing*, pp. 844-846, Boston, April 1983.

T.L. Marzetta, "A New Interpretation for Capon's Maximum Likelihood Method of Frequency-Wavenumber Spectral Estimation", *IEEE Trans. on Acoustics, Speech, and Signal Processing*, Vol. ASSP-31, No. 2, pp. 445-449, April 1983.

J. Max, "Quantization for Minimum Distortion", *IEEE Trans. Information Theory*, Vol. IT-6, pp. 7-12, March 1960.

K. Minami and N. Schlumberger, "Prony's Method Based on Eigenanalysis and Over-determined System Approach", *Proc. of IEEE Int. Conf. on Acoustics, Speech, and Signal Processing, ICASSP*, pp. 27.13.1-27.13.4, Tokyo, April 1986.

N. Mohanty, "Random Signals Estimation and Identification Analysis and Applications", Van Nostrand Reinhold Company, New York.

M. Morf, A. Vieirn, D.T.L. Lee and T. Kailath, "Recursive Multichannel Maximum Entropy Spectral Estimation", *IEEE Trans. Geosci. Electron.*, Vol. GE-16, pp. 85-94, April 1978.

B.R. Musicus, "Fast MLM Power Spectrum Estimation from Uniformly Spaced Correlations", *Proc. of IEEE Int. Conf. on Acoustics, Speech, and Signal Processing*, pp. 1333-1335, Florida, March 1985.

J. H. McClellan, "Multidimensional Spectral Estimation", *Proc. of IEEE*, Vol. 70, No. 9, pp. 1029-1039, September 1982.

A. N. Netravali, "Picture Coding: A Review", *Proc. of the IEEE*, Vol. 68, No. 3, pp. 366-406, March 1980.

C.L. Nikias and M.R. Raghuveer, "Multi-Dimensional Spectral Estimation via Parametric Models", *Proc. of IEEE Int. Conf. on Acoustics, Speech, and Signal Processing*, pp. 213-218, Boston, April 1983.

C.L. Nikias and M.R. Raghuveer, "A New Class of High-Resolution and Robust Multi-Dimensional Spectral Estimation Algorithms", *Proc. of IEEE Int. Conf. on Acoustics, Speech, and Signal Processing*, pp. 859-862, Boston, April 1983.

T. Ning and C.L. Nikias, "The Optimum Approach to Multichannel AR Spectrum Estimation", *Proc. of IEEE Int. Conf. on Acoustics, Speech, and Signal Processing, ICASSP*, pp. 800-803, Florida, March 1985.

A. H. Nuttall, "Multivariate Linear Predictive Spectral Analysis Employing Weighted Forward and Backward Averaging: A Generalization of Burg's Algorithm", *Naval Underwater System Center*, New London, CT, NUSC Tech. Rep. 5501, October 1976.

S.J. Orfanidis, "Optimum Signal Processing, An Introduction", Macmillan, Inc. New York, 1985.

Oppenheim A.V., and Schafer R.W., " Digital Signal Processing", pp. 532-571, 1975.

A. Papoulis," Maximum Entropy and Spectral Estimation:A Review", *IEEE Trans. on Acoustics, Speech, and Signal Proc.*, Vol. ASSP-29, No. 6, December 1981.

W. K. Pratt, "Digital Image Processing", John Wiley & Sons, Inc. 1978.

M. B. Priestley, "Spectral Analysis and Time Series", Academic Press, Inc. 1981.

S.R. Parker, and A.H. Kayran, " Lattice Parameter Autoregressive Modeling of Two-Dimensional Fields-Part I: The Quarter-Plane Case", *IEEE Trans. on Acoustics, Speech and Signal Processing,* Vol. 4, pp. 872-885, August 1984.

Proc. of RADC Spectrum Estimation Workshop, Rome Air Development Center, Griffiss Air Force Base, NY 1978, 77. (Later ASSP Workshop on Spectrum Estimation (1981-1986)).

E. A. Robinson, "A Historical Perspective of Spectrum Estimation", *Proc. of the IEEE,* Vol. 70, No. 9, pp. 885-907, September 1982.

S. Roucos, and D.G. Childers, "A Two-Dimensional Maximum Entropy Spectral Estimator", *Proc. of IEEE Int. Conf. on Acoustics, Speech, and Signal Processing, ICASSP,* pp. 669-672, Washington, D.C., April 1979.

S. Roucos, D.G. Childers, "A Two-Dimensional Maximum Entropy Spectral Estimator", *IEEE Trans. on Information Theory,* Vol. IT-26, No. 5, pp. 554-560, September 1980.

F.C. Schweppe, "On the Bhattacharyya Distance and the Divergence Between Gaussian Processes", *Information and Control,* Vol. 11, pp. 373-395, 1967.

G. Sharma and R. Chellappa, "Two-Dimensional Spectrum Estimation Using Noncausal Autoregressive Models", *IEEE Trans. on Information Theory,* Vol. IT-32, No. 2, pp. 268-275, March 1986.

O.N.Strand ," Multichannel Complex Maximum Entropy (Autoregressive) Spectral Analysis", *IEEE Trans. on Automatic Control,* Vol. AC-22, No. 4, pp. 634-640, August 1977.

D.N. Swingler, "Burg's Maximum Entropy Algorithm Versus the Discrete Fourier Transform as a Frequency Estimator for Truncated Real Sinusoids", *J. of Geophysics Research,* Vol. 85, No. B2, pp. 1435-1438, March 1980.

C.W.Therrien," The Application of Linear Prediction to Sequential Classification of Radar Target Signatures", *MIT Lincoln Laboratory,* Technical Report 517,25 March 1976.

C.W. Therrien and K. Fukunaga, "Properties of Separable Covariance Matrices and Their Associated Gaussian Random Processes", *IEEE Trans. on Pattern Analysis and Machine Intel.,* Vol. PAMI-6, No. 5, pp. 652-656, September 1984.

C.W. Therrien, "The Analysis of Multichannel Two-Dimensional Random Signals", *Technical Report,* Naval Postgraduate School, NPS62-87-002, Monterey, CA, October 1986.

C.W. Therrien and H.T. El-Shaer, "2-D Multichannel Autoregressive Spectral Estimation", *Proc. 20th Asilomar Conference on Signals, Systems, and Computers*, November 1986, Pacific Grove, CA.

C.W. Therrien and H.T. El-Shaer, "Methods for Multichannel 2-D Spectrum Analysis: Description and Comparison", *Proc. of IEEE Int. Conf. on Acoustics, Speech, Signal Processing, ICASSP*, April 1987, Dallas, TX.

C.W. Therrien and H.T. El-Shaer, "Maximum Likelihood Multichannel Multidimensional Spectrum Estimation", *International Society for Optical Engineering, SPIE*, San Diego, CA, August 1987.

C.W. Therrien and H.T. El-Shaer, "Methods for Multichannel 2-D Spectrum Estimation Part I", Submitted to *IEEE Trans. on Acoustics, Speech, and Signal Processing*.

C. W. Therrien, "Relations Between 2-D and Multichannel Linear Prediction", *IEEE Trans. on Acoustics, Speech, and Signal Processing*, Vol. ASSP-29, No. 3, pp. 454-456, June 1981.

C. W. Therrien, "Linear Prediction for 2-D Vector Random Fields", *Proc. 19 th Asilomar Conference on Circuits, Systems, and Computers*, November 1985, Pacific Grove, CA.

D. Tjostheim, "Autoregressive Modeling and Spectral Analysis of Array Data in the Plane", *IEEE Trans. on Geoscience and Remote Sensing*, Vol. GE-19, No. 1, pp. 15-24, January 1981.

D.W. Tufts and R. Kumaresan, "Improved Spectral Resolution", *Proc. of the IEEE*, Vol. 68, No. 3, pp. 419-420, March 1980.

D.W. Tufts and R. Kumaresan, "Improved Spectral Resolution II", *Proc. of IEEE Int. Conf. on Acoustics, Speech, and Signal Processing, ICASSP*, pp. 592-597, Denver, April 1980.

D.W. Tufts and R. Kumaresan, "Estimation of Frequencies of Multiple Sinusoids: Making Linear Prediction Perform Like Maximum Likelihood", *Proc. of the IEEE*, Vol. 70, No. 9, pp. 975-989, September 1982.

T.J. Ulrych and R.W. Clayton, "Time Series Modelling and Maximum Entropy", *Physics of the Earth and Planetary Interiors*, 12, pp. 188-200, 1976.

H. L. Van Trees, "Detection Estimation, and Modulation Theory Part I", John Wiley & Sons, 1968.

P.D. Welch, "The Use of FFT for the Estimation of Power Spectra: A Method Based on Time Average over Short Modified Periodograms", *IEEE Trans. Audio Electroacoust.*, Vol. AU-15, pp. 70-73, June 1967.

S.J. Wernecke, and L.R. D'Addario, "Maximum Entropy Image Reconstruction", *IEEE Trans. on Copmuters*, Vol. C-26, No. 4, April 1977.

P. Whittle, "On the Fitting of Multivariate Autoregressions, and the Approximate Canonical Factorization of a Spectral Density Matrix", *Biometrika*, 50, 1 and 2, pp. 129-134, 1963.

R.A. Wiggins and E.A. Robinson, " Recursive Solution to the Multichannel Problem", *J. Geophysical Research*, Vol. 70, pp. 1885-1891, 1965.

J.W. Woods, " Two-Dimensional Discrete Markovian Fields", *IEEE Trans. on Inform. Theory*, Vol. IT-18, No. 2, pp. 232-240, March 1972.

J.W. Woods, "Two Dimensional Markov Spectral Estimation", *IEEE Trans. on Inform. theory*, Vol. IT-22, No. 5, pp. 552-559, 1976.

T. Yokota, and T. Sato, "2-D spectral Estimation Combining Parametric Estimation of Background and Maximum Entropy Estimation", *IEEE Trans. on Acoustics, Speech, and Signal Processing*, Vol. ASSP-32, No. 2, pp. 220-223, April 1984.

L. H. Zetterberg, S. Ericsson, and H. Brusewitz, "Interframe DPCM with Adaptive Quantization and Entropy Coding", *IEEE Trans. on Communications*, Vol. COM-30, No. 8, pp. 1888-1899, August 1982.

INITIAL DISTRIBUTION LIST

		No. Copies
1.	Defense Technical Information Center Cameron Station Alexandria, VA 23304-6145	2
2.	Research Administration Code 012 Naval Postgraduate School Monterey, CA 93943	1
3.	Library, Code 0142 Code 0142 Naval Postgraduate School Monterey, CA 93943-5002	2
4.	Chairman, Department of Electrical and Computer Engineering Code 62 Naval Postgraduate School Monterey, CA 93943	1
5.	Dr. Tom Kerr Group 95 MIT Lincoln Laboratory 244 Wood St. Lexington, MA 02173-0073	1
6.	Dr. Steve Sacks Naval Research Laboratory Code 61R (Nat'l. Ctr. 1) Space & Naval Warfare Sys. Command Washington, D.C. 20363	1
7.	Prof. C.W. Therrien Code 62Ti Naval Postgraduate School Monterey, CA 93943	4

8. Prof. H. Fredricksen
Code 53Fs
Naval Postgraduate School
Monterey, CA 93943 — 1

9. Prof. P.A.W. Lewis
Code 55Lw
Naval Postgraduate School
Monterey, CA 93943 — 1

10. Prof. P.H. Moose
Code 62Me
Naval Postgraduate School
Monterey, CA 93943 — 1

11. Prof. L.J. Ziomek
Code 62Zm
Naval Postgraduate School
Monterey, CA 93943 — 1

12. Hamdy Taha El-Shaer
12 Mohamed Wagih Khaliel Street, #5
Sant Fatima, Heliopolies
Cairo, Egypt — 7

13. Prof. Ramzy El-Shaer, Vice President
Ain Shams University
Al-Abbasia
Cairo Egypt — 2

14. Prof. Helmy El-Shaer
80 Amar ben Yaser Street
Heliopolis
Cairo, Egypt — 1

15. Dr. P.D. Welch
T.J. Watson Research Center
P.O. Box 704
Yorktown Heights
N.Y. 10598 — 1

16. Library, Military Technical College
Kobry El-Koba, Abbasia
Cairo, Egypt — 1

END

DATE

FILMED

5-88

DTIC